MAGNETIC SUSCEPTIBILITY, PETROLOGY AND GEOCHEMSITRY OF GRANITOIDS IN PARTS OF KARBI ANGLONG HILLS, ASSAM

by

ANETTSUNGLA

Submitted

In partial fulfilment of the requirement of the Degree of

Doctor of Philosophy in Geology

Nagaland University

NAGALAND UNIVERSITY

December 2022

DECLARATION

I, Anettsungla, hereby declare that the subject matter of this thesis is the record of work done by me, during the period May 2014 to December 2022. That the content of this thesis has not provided the basis for the award of any previous degree to me, or to the best of my knowledge, to anybody else, and that the thesis has not been submitted by me for any research degree in any other University/Institute.

This thesis is submitted to the Nagaland University in partial fulfilment for the degree of Doctorate in Philosophy in Geology under the supervision of Dr. (Mrs.) Vikoleno Rino of Nagaland University.

<table>
<tr><td>Date:</td><td>ANETTSUNGLA</td></tr>
<tr><td>Place: Department of Geology</td><td>Ph.D. Scholar</td></tr>
<tr><td>Nagaland University</td><td>Department of Geology</td></tr>
<tr><td>Kohima Campus, Meriema</td><td>Reg. No. 586/2014 (20th May, 2014)</td></tr>
</table>

<table>
<tr><td>Head</td><td>Supervisor</td></tr>
<tr><td>Prof. S. K. Singh</td><td>Dr. Vikoleno Rino</td></tr>
<tr><td>Department of Geology</td><td>Department of Geology</td></tr>
<tr><td>Nagaland University</td><td>Nagaland University</td></tr>
<tr><td>Kohima Campus, Meriema</td><td>Kohima Campus, Meriema</td></tr>
</table>

NAGALAND UNIVERSITY

Dr. (Mrs.) Vikoleno Rino
Associate Professor
Department of Geology
Kohima Campus
Meriema -797 004

Mobile : 8787467916
E-mail : vikolenorino@nagalanduniversity.ac.in

CERTIFICATE

The thesis presented by Mrs. Anettsungla, Ph.D. research scholar of the Department of Geology, Nagaland University, Kohima Campus, Meriema bearing registration No. 586/2014, dated 20th May 2014 embodies the results of investigations carried by her under my supervision.

I, certify that this work has not been presented for any degree elsewhere and that the candidate has fulfilled all conditions laid down by the University.

Dated: (Dr. VIKOLENO RINO)
                                                                                                 Supervisor

PLAGIARISM-FREE UNDERTAKING

Name of Research Scholar	Anettsungla
Ph.D. Registration Number	No. 586/2014
Title of Ph.D. thesis	Magnetic Susceptibility, petrology and geochemistry of granitoids in parts of Karbi Anglong Hills, Assam
Name & Institutional Address of the Supervisor / Co-Supervisor	Dr. Vikoleno Rino Associate Professor Department of Geology, Nagaland University Kohima Campus, Meriema
Name of the Department & School	Department of Geology / School of Sciences
Date of submission	
Date of plagiarism check	30.12.2022
Percentage of similarity detected by the **URKUND** software	1%

I hereby declare/ certify that the Ph.D. thesis submitted by me is complete in all respects, as per the guidelines of the Nagaland University for this purpose. I also certify that the thesis (soft copy) has been checked for plagiarism using URKUND similarity-check software. It is also certified that the contents of the electronic version of the thesis are the same as the final hard copy of the thesis. A copy of the report generated by the URKUND software is also enclosed.

(Name & Signature of the Scholar)

Date:

Place:

Name & Signature of the Supervisor with seal:

ACKNOWLEDGEMENT

I could not have undertaken this journey without the support of certain people, so I take the pleasure of acknowledging them in this section.

This impossible task came to fruition only through the grace of the Almighty God with His wisdom and divine intervention. Giving all praises to Him.

Some individuals I cannot refrain from thanking them are mentioned in random order.

My utmost gratefulness goes to my Supervisor Dr. Vikoleno Rino for her faith in me. The level of patience, consideration and continual support you have shown to me is astounding. I will be forever indebted to you for mentoring me with your knowledge and constructive feedbacks throughout the entire work. As if it were not enough, I have been so blessed to have met Shri Vizhoto Hibo, Supervisor's spouse who left no stones unturned to ease my fieldwork. Thank you so much.

Words are inadequate to express my thankfulness to my loving parents, wonderful sisters (Oya Aren, Oya Bendang, Oya Jathy, Oya Yanger, my dearest Moaso) and my husband Nungshi who have all gone above and beyond to help me come this far. This work is a harvest of your indomitable belief in me that kept me going even during my most difficult days. Your immense encouragement, the unceasing prayers, your indefatigable support and the like got me thus far. I never could have reached this point in life without you all. I also want to thank my precious daughter Shisa for being an angel, I am in awe with your being and patience. I am so blessed to be your Oja.

Also, I'd like to extend my gratitude to my in-laws and relatives for the relentless support till completion of this work.

My dear friends and colleagues - Mrs. Aienla Ozukum, Dr. Moalong Kichu and Dr. Moiya for their friendship, constant encouragements, valuable feedbacks and help till the final editing. Your presence has impacted and inspired my life let alone the course of this work. The contributions and help in different forms by Miss Dieze Meyase and Dr. Sanen during the course of this work is also acknowledged.

PARTICULARS OF THE CANDIDATE

NAME OF THE CANDIDATE   : Anettsungla

DEGREE   : Ph.D.

DEPARTMENT   : Geology

TITLE OF THE THESIS   : **Magnetic susceptibility, petrology and geochemistry of granitoids in parts of Karbi Anglong Hills, Assam**

DATE OF ADMISSION   : 2nd September, 2013

APPROVAL OF RESEARCH PROPOSAL   : 16th June, 2014

REGISTRATION NUMBER & DATE   : 586/2014 (20th May, 2014)

Head of the Department

Biodata of the Candidate

I. PAPERS PUBLISHED

1. Anettsungla.; Rino, V. and Kumar, S. (2018): Redox Condition, Nature and Tectono-magmatic Environment of Granitoids and Granite gneisses from the Karbi Anglong Hills, Northeast India: Constraints from Magnetic Susceptibility and Biotite Geochemistry, *Jour. Geol. Soc. India,* **91***: 601-612.*

2. Kumar, S.; Pundir, S.; Rino, V.; Bora, S.; Pathak, M.; Anettsungla.; Joshi, H.; Rawat, M.S.; Pieru, T. and Singh, K. M. (2022): Geochemistry of Proterozoic and Cambrian granites from Meghalaya Plateau, Northeast India: Implication on petrogenesis of post-collisional, transitional from I-type to A-type felsic magmatism. *Geol. Jour.* **57**(Issue 4): 1476-1510.

II. ABSTRACT PUBLISHED/ORAL PRESENTATION

1. Petrography and Geochemistry of Granitoids of Karbi Anglong Hills, Northeast India. National Seminar on Geology, Geochemistry, Tectonics, Energy and Mineral Resources of Northeast India & AGM of Indian Society of Applied Geochemists, Department of Chemistry, Nagaland University (9-11th November 2016). Oral presentation.

2. Magnetic susceptibility, major oxide and trace elemental studies of granitoids in parts of Kaziranga area, Karbi Anglong Hills, Assam. National Seminar on Chemistry in Interdisciplinary Research, Department of Chemistry, Nagaland University (9 – 10th November, 2018). Oral presentation.

III. WORKSHOP/TRAINING ATTENDED

1. National Seminar on the theme 'Science & Technology for Human Development' in Manipur University organized by Indian Science Congress Association, during 21st-23rd January 2015.

2. Regional workshop for Young Earth Scientists on 'Tectonics, Sedimentation and

Geohazards with special reference to NE India' organized by the Department of Geology, Nagaland University (16-21 November, 2015)

3. National Seminar on Interdisciplinary Research in Chemical Sciences, NSIRCS-2016, organized by Department of Chemistry, Kohima Science College (Autonomous), Jotsoma Kohima Nagaland in collaboration with Directorate of Higher Education, Government of Nagaland (28th-29th September, 2016)

4. One week Workshop on "Advanced Petrography" organized by Department of Geological Sciences, Gauhati University, (26th of June- 1st of July, 2018)

5. National Webinar on Landslide susceptibility of Kohima Town, Nagaland Organized by Department of Geology, Model Christian College, Kohima, Nagaland on 26th March, 2021.

IV. CSIR-JRF NET 2011

Preface

The study has been undertaken to understand the petrogenetic and evolutionary history of granitoids in parts of Karbi Anglong Hills, Assam. The outcomes of the study are compiled and accessible in 7 chapters, each of which deals with different aspects of the study.

The compilation commences with the **first chapter** familiarizing the study area, the objectives and scope of the research. The **second chapter** discusses the stratigraphic and tectonic framework of the study area. It includes the regional stratigraphy, geologic setting and the distribution of the lithologic units. The Magnetic susceptibility factors related to the study area and the inference discussed systematically.

Third Chapter deals with the methodology adopted. **Chapter 4** covers the petrography and mineralogical studies of the different rock units encountered in the study area. Modal analysis and textural features have also been discussed here. **Chapter 5** deals with the detailed mineralogy with special emphasis on biotite mineral chemistry to decipher the redox conditions of felsic magmas. Suitable interpretations are drawn in this chapter concerning the oxygen fugacity, magmatic temperatures and pressure at the time of emplacement of the granitoids.

In **Chapter 6** the geochemical aspects of the rocks are discussed to identify the processes of magma evolution. Such inferences aids in approximating the tectonic discrimination and the protolith evolution. **Chapter 7** summarizes the study and presents the conclusions.

All chapters are organized with all texts appearing first followed subsequently by the related plates, figures and tables.

An attempt has been made for the first time to study the magnetic susceptibility, chemistry of plagioclase- biotite database of Karbi Anglong Hills. This work presents a complete set of petrological, mineralogical (EPMA) and bulk geochemical (major, trace and rare earth elements) database. This work would further the knowledge about the petrogenetic history and the geochemical studies to infer the tectonic history of the region. It is hoped that this thesis will provide a source of information and offer new insights for further understanding and future research works.

CONTENTS

Chapter 6: Geochemistry

Chapter 7: Discussion and Conclusion

References

Published Papers

LIST OF TABLES

LIST OF FIGURES

CHAPTER I

INTRODUCTION

The state of Assam is situated in the Northeastern part of India, between the latitudes 24° and 28° North and longitudes 90° and 96°. Having an area of 78,523 sq. km, it is the largest of the eight Northeast sister states. Geographically, Assam state connects the other six Northeastern states to the main India, hence also referred to as the "gateway to Northeastern region". It is bounded by the states of Nagaland and Manipur on the eastern border; Arunachal Pradesh and Bhutan to the North; Meghalaya, Bangladesh, Tripura and Mizoram on its South and the western border by the West Bengal.

Physiographically, Assam is comprised of the vast alluvial plains of the Brahmaputra River and Barak River valleys; the central part of the state is marked by hilly terrains consisting of the Karbi Anglong Hills and the North Cachar Hills. Having an elevation of 50-120m above m.s.l the wide Brahmaputra Valley is considered to be the Eastern continuation of the Indo-Gangetic trough of the Northern part of the country; the hills on the other hand is an extension of the Meghalaya Plateau corresponding to the Peninsular rock masses of India.

The Karbi Anglong Hills (erstwhile Mikir Hills) is situated in the innermost part of Assam, standing at an elevation of approximately 1000 m extending within 25.5°-27° N latitude and 92.5°-94 ° E longitudes. The Hills are considered to be an eastern extension of the Shillong plateau being separated from each other by the alluvium tract of the Kopili river and the NE-SW Kopili lineament (Nandy, 1980), later identified as the Kopili Fault (Das Gupta & Nandy, 1982).

The Karbi Anglong hills characterize a peneplained surface, composed of Archaean Gneissic complex as the oldest rock unit represented by gneisses, schist and granites, which was overlain by the metasediments of the Shillong Series (Krishnan, 1960). Granitoid intrusions occur within the basement gneisses and enclaves of the latter and basic rocks are found within the granitoids.

1.1   LOCATION AND ACCESSIBILITY

The studied area falls between latitudes 25.5° to 27°N and longitude of 92.5° and 94°E (Fig. 1) and occupies the central part of Assam. Covering an area of about 7000km2, the Karbi Anglong Hills of Assam is part of the Survey of India Toposheet Nos. 83F/2 to 83F/12. Karbi Anglong Hills is accessible through land routes and National Frontier Railways which passes through the district along its boundary in some towns. Two major roads cover the North (NH-37) and East (NH-39). The interior hilly parts of the district are sparsely connected by mud-roads and foot-tracks. The nearest airport (Dimapur, Nagaland) is 54 Kms away from Diphu town (head-quarter of Karbi Anglong district).

1.2   PHYSIOGRAPHY AND DRAINAGE

The study area generally shows a hilly terrain at its central segment, along with valleys of the Brahmaputra and Barak rivers. The Brahmaputra Valley is said to be Quaternary fill and the drainage pattern appears that of antecedent type. The Surma River Valley occupies a triangular area surrounded by the North Cachar and Manipur Hills in the east, Meghalaya in the northwest and Mizoram and Tripura Hills in the south. The valleys are low-lying with swamps. The Singhason peak standing at an altitude of about 1600 m above sea level is noteworthy for being the highest peak in the Karbi Anglong Hills.

Comparatively Assam receives more rainfall than most parts of India; this rain feeds the Brahmaputra River. Two major rivers of the state are Brahmaputra and the Surma (or Barak). Kaliani, Kopili, Jamuna, Deopani and Dhansiri are some main rivers in the Karbi Anglong Hills, which are joined by some streams like Tarapung, Janghanri, Junjan, Rangoli, Bajajuri, Tarapung, Lohajuri, Bar Longsu, Deuri and Berjan. Dendritic drainage pattern is shown by the rivers and streamlets in the Karbi Hills. The drainage system could be indicative of being both topography and structurally controlled.

1.3   CLIMATE AND RAINFALL

Assam is a state, where monsoon months predominate summer and winter months. The climate falls under "Tropical Monsoon Rainforest Climate". Monsoon sets in the month of May, which is often marked by strong winds, heavy clouded skies and sometimes accompanied by showers and hailstorms. Heavy downpours are experienced in the months of June and it continues till the month of October. Cyclones have also been reported once in a while during this period of

time. Annually, the average rainfall of the state is between 220-290 cm. Winter is pleasant and remains dry and starts from the month of November and it continues till February, when the temperature falls down till 277.15K (4˚C). Summer months are March and April, when the temperature goes up to 310˚K (37˚C). During summer, the climate of Assam is marked by high humidity.

1.4   FLORA, FAUNA AND CULTIVATION

The landscape of the state is covered by deciduous and evergreen mixed dense forests which comprise varieties of trees; important floras are bamboos, shrubs, herbs and Sal tree. Orchids, epiphytes and parasites are usually sheltered by the forests.

The forested area in the state provides home for a diverse population of wildlife such as elephant, buffalo, pig, gaur, bison, panther, deer, tiger, bear and the district have the largest population of Hoolock gibbons in Assam. The single horned Indian Rhino (Rhinoceros unicornis) is considered the significant fauna from the rest of wildlife. Also, birds such as pelican and storks are found in the Kaziranga wild life sanctuary along with varieties of Asiatic bird species in the wild.

Among the many agricultural products of the region, the main produces are tea, rice, mustard, jute, coconut, betels, pulses, sugarcane, potatoes, citrus fruits and bananas. Assam state ranks as one of the major tea producers within the country.

1.5   HUMAN HABITATION

A wide diversity of tribal communities resides in the Karbi Anglong Hills. It is said that the Karbi tribes were the original settlers. Also, influx of people is observed both along the valleys as well as across the hills; ethnic people of mongoloid groups and mainland Indian tribals are brought in by the Tea Industry. The other indigenous people are Kacharis, Bodo. Lalung (Tiwas), Dimasa, Rengma Nagas, Kukis, Garos, Khasis and Shyams. The different tribes maintain and practice their own ethnic rituals. Main source of income is shifting cultivation, also locally called 'Jhum', along with the Tea Industry. Assamese is the local dialect.

1.6   PREVIOUS WORK

The initial record of geological interest in respect of Assam state was contributed by H.B. Medlicott (1865) and Mallet (1876), published in G.S.I Memoirs with the information on geological mapping of Upper Assam Coal Belts. Geological reports were subsequently

contributed by the premier Assam Oil Company of Digboi (1912) in Upper Assam. Stratigraphy of the Tertiary sediments of Assam has been recorded by Evans (1932).

The pioneering works in the Karbi Anglong Hills dated back to as early as 1896, when F.H. Smith reported gneisses, traps, shales and sandstone series; mention has been made that the sandstones were equivalent to the Siwalik. H.H Hayden (1909) and M. Vinayak Rao (1914) also worked on the limestone deposits of the Hills. Systematic geological mapping of the Hills initiated with the Geological Survey of India (GSI) in the pre independence, more intense surveys however followed post the independence; the geologists involved with the surveys are Mukherjee and Khedkar (1938-39; 1940-41); K.K. Sengupta and J. Sengupta, 1943; D.K. Chandra, 1949 or D.R. Chandra (1947-48).; D.K. Chandra, M.M. Munshi and V.K. Raina, 1959; M.B. Pawde Powde and Banerjee, 1961; M.M. Munshi, 1961; Munshi and Duara (1962-63); B.K. Duara, B.D. Adhikari Duara and Debadhikari (1964-66); A.C. Bhattacharya and G. Burman or Barman, 1966; M.D. Limaye (1966-67); K.K.Sengupta and R.N. Mukhopadhyay (1971-72); R.N.Mukhopadhyay and A. Dutta (1972-73); A.R.Nambiar and R.N.Mukhopadhyay (1973-74); A. Dutta and Muralidharan (1974-75); P.K.Muralidharan and Des Raj (1975-76; 1982); G.K. Pancholi, Des Raj and K.Chandrashekar (1978-79); A.K. Buragohain, J.C.Dutta, V.N. Bajpai, Y. Kumar, D.P. Das and H.S. Shrivastava during 1982-83 and 1983-84 field season; Dutta and Das (1984-85); J.C. Dutta, Venkata Subramanium, S.K. Das and B. Chatterjee (1985-86); J.C. Dutta and M. Surendranath and A.K. Buragohain (1988-89), Bora and Roy (1999).

Krishnan (1968) correlated the Precambrian rocks of the Shillong Plateau with the Archaean complex of the Peninsular India. Stratigraphy of Assam Valley has been discussed by Bhandari et at., (1973). Ghosh et al., (1991, 1994 and 2005) compiled a comparative geochemistry and geochronology of granitoids of Meghalaya; an age range of 881- 479 Ma for the granitoids and 1714-1150 Ma for the basement gneisses has been deduced from the Rb-Sr isotopic ages relating to final amalgamation events of the Gondwana Supercontinent. Bhattacharyya (1998) experimented with the granitic plutons of Assam Meghalaya Plateau and gave age range from 479 ±26 Ma to 690 ± 19 Ma indicative of late Proterozoic period. Sarma & Dey (1996, 1997, 1998 and 1999) worked at different parts of the Assam-Meghalaya plateau in the basement gneissic complex and migmatitic terrain.

Alkaline rocks have been reported at the Samchampi- Samteran district of the Hills by Nag et al., (1999). Works of Nandy (2005) are the pioneering studies on the geodynamic evolution of the Northeastern India including the Mikir Hills.

Detailed petrography and geochemical studies of Mikir Hills are numerable and research literatures were not available till the recent decades; Rajaraman et al (2008) pointed that evolutionary trend of the Hills granitoids are co-relatable with that of Mylliem granite in Meghalaya. Hussain & Ahmad (2009) worked on the geochemical signatures of the Mikir Hills Massif (MHM) granitoids. Their findings opined towards subduction related magmatism in a convergent plate scenario. With the granitoids emplaced during Neoproterozoic times, the study connotes to the construction of the Gondwana Supercontinent.

Majumdar and Dutta (2006, 2007, 2014, 2015), Majumdar (2010) worked on the NW of the Karbi Hills; A-type granitoids of the Dizo Valley have been credited to a post Collisional setting. The area has been predicted to be a potential resource of rare earth metals. Parameters such as zircon age dating and geochemical studies indicated late Pan-African granitoid magmatism with an age of 515.1 ± 3.3 to 515 ± 2.7 Ma old. The oldest rocks i.e., Gneissic Complex has been dated to be 2.67 Ga (Majumdar & Dutta, 2016; Kumar et al., 2017). Comprehensive works on the magnetic susceptibility and biotite geochemistry of granitoids and granite gneisses from the Karbi Anglong Hills with emphasis on the redox condition, nature and tectono-magmatic environment has been given by Anettsungla et al., 2018 (present work). U/Pb zircon geochronology indicates that the late stage porphyritic granitoids were emplaced over a span of about 94 Ma, subsequent to the emplacement of mafic dykes, sills and stocks in a post collision rift basin, now represented by the 'Shillong Basin' (Gogoi et al., 2019). Metallogenic appraisals of the Mesoproterozoic (1599 ± 17 Ma) Kuthori porphyry granitoids for porphyry-type copper mineralization was carried out in northern Karbi Hills by Mazumdar & Gogoi (2020). Based on field relationship and mineral chemical analyses mafic-felsic magma mixing model was inferred for the generation of mafic magmatic enclaves and felsic granites in Kathalguri pluton of Karbi Anglong massif (Hazarika et al., 2021). Recent studies on prospect for porphyry copper mineralization in A-type granitoids from the Precambrian shield of the Karbi Anglong Hills was carried out and inferred that the Kuthori-Bagori of Kaziranga granitoid of the Karbi Hills (Mikir Hills) in NE India is an ideal location for porphyry copper mineralization (Mazumdar et al., 2021, 2022). In a recent study, geochemical studies of the Proterozoic and Cambrian granites from Meghalaya Plateau including Karbi

Anglong Hills are carried out to assess the nature, origin and tectono-evolution of felsic magmatism in relation with the supercontinent cycles. (Kumar et al., 2022).

There are both challenges and opportunities of mineral exploration as the geology of this tiny craton has been poorly understood; mineral exploration works is mostly confined to reporting of occurrences; metallogenic analysis hardly receives attention (Majumdar, 2017). Due to poor accessibility, thick tropical forests and geopolitical reasons, there are constraints to further the research works in the study area.

1.7   AIM AND SCOPE OF WORK

Granitoid rocks represent one of the integral parts of the continental crust and merit tremendous attention owing to their variant nature, source materials, their origin and geotectonic settings. Also, processes that give rise to granitoids are inconsistent, with the resultant rocks differing in composition and ore-prospecting both in time and space. This variability has given rise to a diverse classification scheme for granitoids. About thirty schemes of granite classification have been reviewed and proposed (Barbarin 1990, 1999). Among which I-, S-, M- and A- types (Chappel & White, 1974; Loiselle & Wones, 1979; Collins et al., 1982; Pitcher, 1983) of genetic and geodynamic classification of granitoids received much attention. The incidence of enclave types in granitoids has formed a strong basis for the proposal of hybrid-type granitoids (Castro et al., 1991).

Taking the magnetic property of granitoids as standpoint, magnetic susceptibility (MS) studies ($\times$10-3 SI) classify the granitoids into magnetite-series granites (MS>3$\times$10-3 SI unit) and ilmenite series (MS$\leq$3$\times$10-3 SI) granites (Kanaya & Ishihara, 1973; Ishihara, 1977; Ishihara et al., 2002; Takagi, 2004) corresponding to oxidized-type and reduced-type granites respectively (Takagi and Tsukimura, 1997). This form a powerful tool in field study of granite (sensu lato) terrane as the MS values can be measured directly from the field. The magnetite contents have an important bearing on the redox state and hence potential to generate the barren or mineralized pegmatite system could be determined.

Whole rock geochemical database and chemistry of plagioclase-biotite of granitoids from Karbi (Mikir) hills are sporadic and sparse, further there is data gap on the magnetic susceptibility studies. Therefore, the present research work has been formulated to generate a complete set of petrographical, mineralogical and bulk geochemical data base which can help to understand the geodynamics and potential of mineralization (if any) of the region. In this

context, to throw light on the petrogenesis and geodynamics of the Karbi Anglong Hills Granitoids (KAHG) a viable model will be the ultimate output of the present investigation.

The following aims and objectives were framed and achieved systematically through field and laboratory investigations of granitoids from the Karbi Anglong district of Assam as a part of research works leading to Ph.D. degree.

- The well-exposed granitoid localities of the area are carefully chosen and the contact relationship between the KAHG and other genetically important features recognized are documented.

- Fresh rock samples of KAHG are collected in the field based on mineral content, grain size and other megascopic characters at outcrop level and located on traverse map.

- Magnetic susceptibility measurements are recorded in the field on smooth rock surfaces of KAHG to further classify the granite series and redox condition.

- The respective granitoids are classified (typology) and their macro- and micro-structures were documented.

- Rock thin sections are prepared to account the modal mineral data for IUGS nomenclature and recognition of igneous series and to document microstructural features.

- Electron microprobe analysis (EPMA) of selected representative samples of KAHG are carried out to categorize the composition of plagioclase and biotite, followed by estimation of the redox condition based on biotite equilibria.

- Analyses of representative samples of KAHG carried out for major, trace including rare earth elements (REE) by means of suitable analytical instruments to generate geochemical data

- Mineralogical and geochemical database are deciphered using modern petrologic methods.

- Built on the stated lines of evidences, a viable petrogenetic and geodynamic model responsible for the evolution of Karbi Hills granitoids (KHG) is proposed.

***
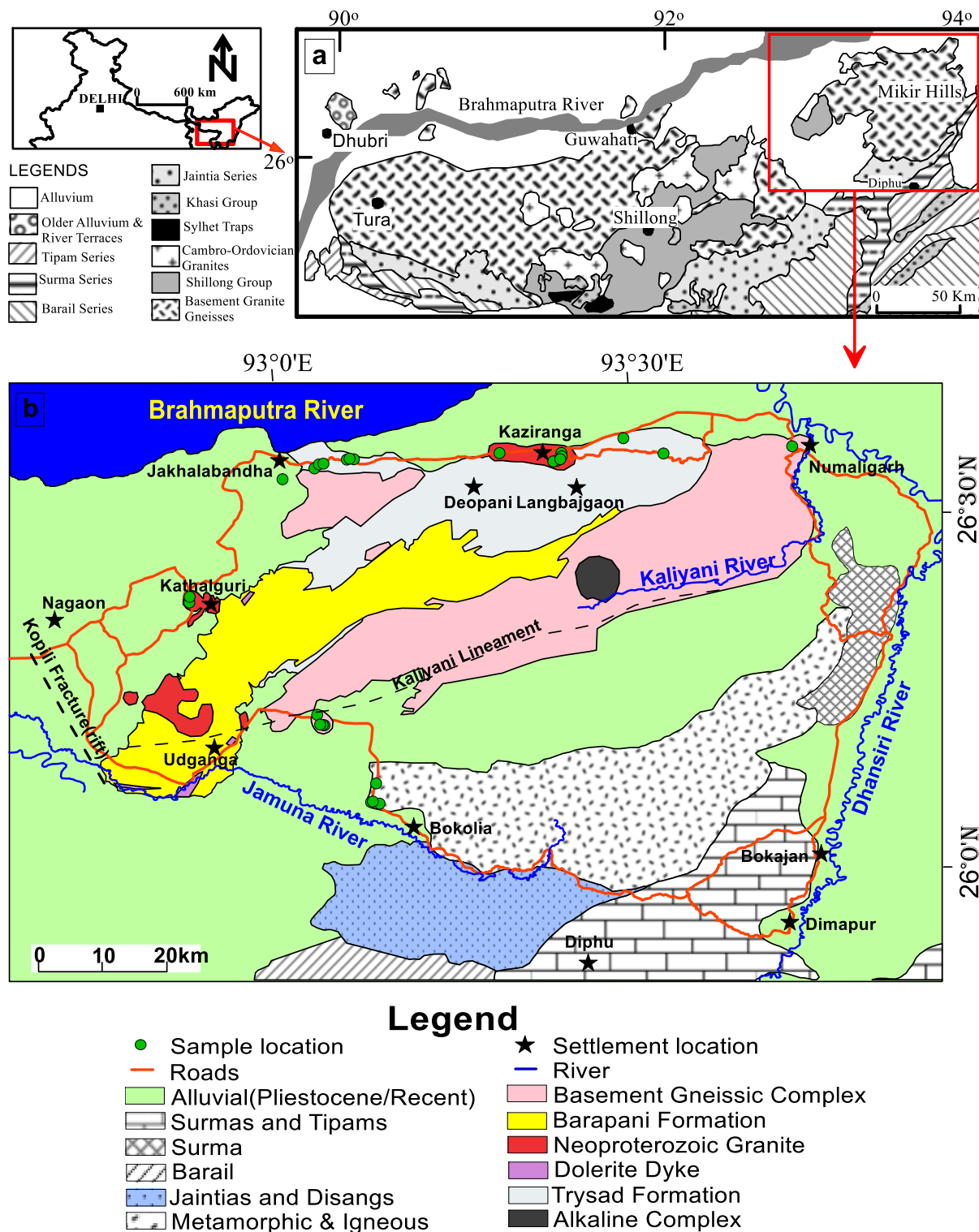
Figure:1 (a) Geological map of the Meghalaya plateau and Mikir Hills (*Kumar et al., 2017a*) (b) Geological map of the study area showing the sample locations of Karbi Anglong Hills, Assam (Modified after *Das Gupta,1977; Dhurandhar et al. 2019*).

CHAPTER II

GEOLOGICAL SETTING OF THE AREA

2.1   REGIONAL GEOLOGY AND TECTONICS

The Shillong plateau (Meghalaya) and Karbi Hills (Assam) together represent the Shillong-Meghalaya Gneissic Complex (SMGC) of Proterozoic age (Chatterjee, 2017). The Karbi Hills existing at the eastern side of the former is divided by the dextral strike-slip Kopili fault (Chatterjee, 2017). The plateau is in turn considered as the northeastern extension of the Indian peninsular shield and is a product of Indo- Eurasian collision and its related contractional deformation. The plateau is thus standing amongst several crisscross faults. (Chatterjee et al., 2007) considered the Meghalaya plateau as remnant of the Indian shield (Mesoproterozoic) and was in close association with Australo-Antarctica block as demonstrated by Neoproterozoic-Cambrian paleomagnetic reconstruction of the Rodinia Supercontinent. The Prydz Bay suture has been proposed to surpass through SMGC with the western fringe of said suture amid Sonapahar and Garo-Goalpara.

Chatterjee et al., (2007) co-related the Shillong-Meghalaya Gneissic Complex (SMGC) to the global event of magmatism, considered it as result of Pan-African and Antarctic amalgamation with east coast of India with an age of 1596±15 Ma (Mesoproterizoic).

The plateau is covered by a predominance of the Basement Gneissic complex along with Shillong group of meta-sedimentary rocks belonging to Proterozoic. Previous works on the granite plutons and data of ages (Isotopic) of the plateau is analogous to tectono- thermal plutonism across many parts of the country, southwest Australia which links to periods of final amalgamation of Gondwana Supercontinent (Ghosh et al., 2005). Early Cretaceous Period saw some rock forming events which must have stimulated fractures that later gave way for eruption of lava; Sylhet Traps are typical and links genetically to the Kerguelen hotspot of the Indian Ocean (Ghatak and Basu,

2011). Ensuing this event was the marine transgression along the Plateau's southern margin and the resultant sedimentary deposition of Upper Cretaceous-Cenozoic period. There have been events of continuous upheaval of the Plateau since Cretaceous accompanied by the submergence of the area in its vicinity, particularly towards the south and north.

Assam had gone through a number of significant phases in its geological evolutionary history. Initially it was a constituent of the Gondwana Supercontinent. Ensuing stage was the deposition of the coal-bearing Gondwana during the Permo-carboniferous when the area in its vicinity was rifted from the landmass. It was associated with few local volcanic activities. It was followed by the marine sedimentation in the Northern edge of India when the Southern Tibet drifted apart from the former. Assam also experienced late Triassic or early Jurassic marine sedimentation, during which the carbonatite intrusion of Sung Valley occurred. In the late Jurassic to early Cretaceous, eastern and southern shores of Assam started the marine sedimentation which correlates to the time when the eastern edge of India separated. This phase experienced the outpouring of few igneous activities like the Sylhet and Mikir Hills Traps, also some intrusions of basic and ultrabasic rocks. Early Eocene age saw the collision with Tibet on its North and to its East with Myanmar. The entire land was wedged in between the mentioned colliding zones with additional compression from the Mishmi Hills on its Northeast direction which marks the final phase. Consequently, the Shillong- Karbi Hills plateaux got uplifted.

Assam plateau consisting the Garo, Khasi and Jaintia Hills, also isolated Mikir Hills in its Northeast direction is considered the prolongation of Archaean rocks of Bihar detached from each other by Ganges, Brahmaputra valley. Bulk of the plateau including the valley and the hills show a predominance of Precambrian rocks- gneisses and granites. The Brahmaputra valley marks the eastern extension of the Indo-Gangetic trough of North India; furthermore, the Peninsular rock mass of Karbi Anglong Hills is also the continuation of Shillong Plateau. Brahmaputra has gone through upliftment and subsidence of the varying Precambrian crystalline blocks indicated by its present configuration- remnant observed at Karbi Hills and Shillong plateau. Overthrusted by the Mishmi Hills on the Northeast and Naga- Patkai range on its Southeast at the Tertiary period, a "foreland spur" has appeared.

The Shillong plateau and Karbi Anglong Hills represents the north-eastern extension of the Precambrian Indian Shield, bounded by the Brahmaputra Fault to its north, the northerly dipping E-W trending Dauki Fault to the south, to the west by the Jamuna lineament and to its east, the Belt of Schuppen.

Major fracture running in between the Shillong Plateau and Karbi Anglong Hills is the Kopili lineament. Trending in a NW-SE direction, this lineament is less prominent in comparison with NE-SW trending Kaliyani lineament. These major features are spatially close, with the latter cutting through the Karbi Anglong Hills and demarcate the Western edge of the Shillong group outcrop. Karbi Hills have a NE-SW strike foliation direction which is akin to the continuation of the Eastern Ghats of Orissa.

Geologically, the state of Assam is comprised of a variety of rocks belonging to different ages. The Stratigraphic succession and general geology of Assam is provided in Table-1, also a comprehensive stratigraphic succession of the Karbi Anglong Hills provided in Table-2. The following paragraphs will shed some light upon the characteristic lithology of each of the groups and formations exposed in the state in general:

GNEISSIC COMPLEX: Proterozoic Gneissic Complex of Meghalaya Plateau continues to be exposed in Assam which is in its Northwest direction. A better part of the Central Assam is occupied by the Gneissic Complex and in western Brahmaputra basins isolated inselbergs are sporadically projecting within Quarternary plains. Lithologically, it consists of gneiss, schist, migmatites hosting enclaves of amphibolite, also high grade supracrustal rocks (Nandy, 2001; Ghosh et al., 2005a). Intrusions by younger acidic rocks as aplite, granite and pegmatites is observed in the migmatitic granitoids and the basic rocks ranges from amphibolites, metadolerite and epidiorite. Most dominant rock type however is gneiss, the biotite- bearing quartzofeldspathic variety in particular, are exposed sparsely in the districts of Kamrup, Goalpara, Nagaon and North Cachar Hills. Minor occurrence of magnetite-hematite quartzite bands (meta-sedimentary) are seen within the gneiss in the Goalpara district (Bilasipara, Chandardinga and Abhayapuri).

The Basement complex is intricate considering the structural as well as the evolutionary history in addition to the intrusive associations. The terrain has been proposed to be a mosaic of varied tectonic blocks which is indicated by polyphase deformations (at least

two) and intrusions at various places. Syntectonic granitization related to an earlier E-W axis folding is assumed as the contributing agent for the formation of gneissic granites and associated migmatitic rocks. The emplacement of porphyritic granites and its subsequent deformation to augen-gneisses could be due to the later NE-SW axis phase of folding. Regional metamorphic facies of amphibolite-granulite have given rise respectively to gneisses, schists and the granulites. Quartz vein intrusions within the schist are co-folded together with the host. The veins which appear unaffected by fold movements are older than those that cut across the overlying Shillong group.

SHILLONG GROUP: The Shillong Group overlies the Gneissic Complex comprising predominantly of conglomerate and metasediments (Quartzite-phyllite-schist association). The Meso-Palaeo Proterozoic age rocks shares an unconformable relationship with the Gneissic complex. The metasediments have intrusive relationship with several younger granitic bodies exhibiting age range of 885-480 Ma (Mitra and Mitra, 2001). In the Northern and western portions of Karbi Anglong Hills across the Kopili Valley and in the northern side of North Cachar Hills, the Shillong group of rocks are encountered. The rocks trend in a NE-SW direction with low to high angled dips. Relict sedimentary structures such as ripple marks, current and graded bedding are often preserved within the quartzites. The rocks have undergone low greenschist facies metamorphism. Development of garnet, staurolite and andalusite at the intrusions zones by granite plutons depicts contact metamorphism. Across the Kopili valley, Shillong Group and the Gneissic Complex strike continues in an almost collinear trend which could be suggestive of the continuation of the Meghalaya Massif rocks with Kopili graben being the divider.

The Shillong group is further comprised of two Formations: The older Tyrsad Formation and younger Barapani Formation. The older formation is comprised of volcanics like rhyolite and Tuff, also metasediments (Quartzite-phyllite-schist association) and often have banded ferruginous rocks. Barapani Formation is composed dominantly of sandstones with magnetite; also, Oligomictric conglomerates.

GRANITE PLUTON: A group of batholithic dimension granite bodies intrude both the basement and the Shillong group. The Neo-Proterozoic-Lower Palaeozoic age types of granite bodies encountered within Karbi Anglong Hills are mainly of two varieties; non-porphyritic granite with medium to coarse grains, occasionally foliated occurring

in the central part of the batholithic mass and porphyritic granite encircling the former variety. However, conclusive evidence showing the granite types to be of separate intrusion phases is yet to be established. It may be representative of differences in crystallization phases from same magma. Pink granite having slight foliation could be migmatization products of biotite schist country rock. Small bodies of metadolerites and amphibolites also occurrs within the metasediments of Shillong group around the Siliguri region of Karbi Anglong Hills. The same intrusions are seen within the granite bodies by the Luhajuri- Bajajuri- Tarapung- Barapung nala sections and Samchampi.

LOWER GONDWANA GROUP: Fox (1934) was the pioneer reporter of the existence of Lower Gondwana rocks in the state. The rocks are seen at the farthest edge of western Assam along the Meghalaya border. Gondwana rocks shares unconformity with the underlying and overlying Granite plutons and Sylhet Traps respectively. The whole assemblage is named as Kaharbari (Permian) initially by Acharyya and Ghosh (1968b) with an age comparable to lower Barakar Banerjee et.al, 1977. Gondwana rocks are divided into Talchir and Karharbari formations.

Talchir Formation is the older sequence where the lithology consists of alternating conglomerate and shales. Boulder conglomerates occupy the basal section which varies from grey to brown having subangular to rounded clasts within silty matrix. Quartz, quartzite, gneisses and pegmatites comprise the clasts having a size variation of 12 to 15 cm diameter. Khaki green colored shale is of silty and micaceous nature which is unsorted and lack stratification.

Karharbari Formation comprises thin, sandstone and carbonaceous shale beds and thicker conglomerate bed. Shales have good preservation of plant impressions and have high mica content. Spheroidal clast of quartz veins within sandy matrix is characteristic of the brownish to greenish grey conglomerates. This younger Formation is however scantily exposed.

ALKALI COMPLEX OF SAMCHAMPI: The Alkali- complex which occurs hosted within the granitic rocks covers a vast part of Samchampi. The mafic-ultramafic-carbonatite complex consists of a range of syenites, mafics (biotite or alkaline pyroxenites, shonkinite), also ultramafics including melteigite and ijolite, carbonatites, apatite-hematite-magnetite rock and cherty rocks. Carbonatite dykes occupying mostly the eastern and northern boundary of the complex are often embedded with partially

digested xenoliths of syenites and ultramafics, and occasionally grades into mafic-ultramafic rocks. In Karbi Anglong Hills along the south of Matikhola Parbat, they are found associated with rhyolite flows. Magnetite-hematite rocks bearing apatite is found along the core of the complex. Resemblance is noted between this occurrence and the Sung valley carbonatite complex of Meghalaya.

SYLHET TRAP: Sylhet trap outcrops are sporadic in Assam with its aerial extent insignificant to plot within the map of desired scale. Extremely weathered exposures have been reported from the vicinity of Selvetta, Koilajan and some localities of Karbi Anglong Hills. The outcrop includes altered chert or olive-green trap rocks which overlain the gneisses. An early cretaceous age can be deduced from the palynofossils occurring within the trap.

TERTIARIES: The Tertiary rocks overlies the Precambrian rocks. Tertiary rocks include shelf and geosynclinals facies sediments where Jaintias and Disangs are the older groups. Succeeding group of rocks are Barail, Surma, Tipam, Dupitila and Dihing. History about Assam's tertiary sediments is greatly controlled by the 'Brahmaputra Arch' falling parallel to Brahmaputra River.

JAINTIA GROUP: Jaintia Group represents a shelf facies. The Eocene sediments contain abundant fossils and are calcareous. The Jaintias are subdivided into Langpar, Shella and Kopili Formation. However, the older Langpar is exposed in Meghalaya. Meanwhile the younger formations are exposed in North Cachar Hills (Garampani) and in Karbi Anglong Hills along the eastern and southern.

Shella Formation, consists of three units of limestone bands and clastic sandstone existing one after the other, in a sequence, the basal part is called the Lower Sylhet Sandstone Member. The sandstones representing lower Sylhet member in Assam are relatable with the units found in the southern scarp of Meghalaya i.e., Khasi and Jaintia Hills. Shales and marl bands are also found in minute quantities. Presence of micro fossils indicate Middle to Upper Eocene age.

The Shella Formation and the Kopili Formation have conformable contact. The younger formation comprising of grey splintery shales are ferruginous and interstratified with sandstone with calcareous marl. The Surma group overlaps the Kopili Formation in the

northeast of Lumding. Fossil content suggests Upper Eocene age for the Kopili Formation.

DISANG GROUP: Splintery shales with thin interbands of sandstone represent the Disang Group of Assam. The dark grey shale is often layered with limonite. In Upper Assam, Disangs consists of alternating thick beds of splintery shale and thinner hard flaggy grey sandstone as well as sandy shales. The rocks are grey, iron stained with carbonaceous streaks.

BARAIL GROUP: Conformably overlying the Disangs, the Barail Group represents a geosynclinal facies. Lithologically, the Barails are made up of coarse sandstone, shale and carbonaceous shale. Some meager streaks of coal have been encountered within the carbonaceous shales. Outcrops of Barail Group are seen in portions north of the Cachar and Karbi Anglong Hills and in the south-eastern portion of North Cachar Hills. In Surma valley and North Cachar Hills, the Laisong, Jenam and Renji Formations represents the Barail Group of rocks and in upper Assam as Nagaon, Bargolai and Tikak Parbat Formation.

The Laisong Formation includes grey, thin beds of sandstone interbedded thin sandy and carbonaceous shales, streaks of coal and infrequent massive sandstone. Formation thickness ranges between 2000 to 2500 m.

Jenam Formation has gradational relations with the underlying and overlying Laisong and Renji Formations respectively. They are argillaceous consisting dominantly of shale, sandy and carbonaceous shale with coal streaks accompanied by hard sandstone. Typical of this formation is the abundance of Pteridophytic flora.

Having a thickness of 600 to 1000 metres, Renji Formation consists of hard massive sandstone with minor shale and sandy shale. Upper Assam have different terminology of Barail group as Nagaon sandstone formation, Bargolai and Tikak Parbat Formation.

SURMA GROUP: The Surma Group of Lower Miocene unconformably overlain the Barail Group covering a vast areal extend in parts of North Cachar and Surma Valley. Narrow exposure of the rocks is exposed in the south-eastern part of the Karbi Anglong Hills. Bhuban Formation of lower arenaceous facies and Bokabil Formation of upper argillaceous facies are the divisions within the group. Fossilized spores and pollens within the Shale indicate age range of Oligocene to Miocene.

TIPAM GROUP: Tipam Group represent an arenaceous facies older Tipam Sandstone Formation and an argillaceous facies younger Girujan Clay Formation. The group of rocks are encountered in many parts of Surma Valley. Both formations are noted to wane out in a north-west direction at the South eastern valley of upper Assam.

Tipam Sandstone is dominantly coarse-grained ferruginous sandstone with gritty false beds alternated with shale, clay, sandy shale and conglomerates. A Miocene age and a Pliocene to Pliestocene age has been given based on the palynogical contents within the rocks. Mottled clay, sand and shale with ferruginous, coarse to gritty sandstone is noted in the Lacustrine Girujan Clay Formation.

DUPITILA GROUP: Tipam Group is followed by the Dupitila Group. The Mio-Pliocene age rocks share an unconformity with the older group. Lithologically made up of ferruginous loose, poorly consolidated coarse sand, clay and with mottled nature observed in both which are layered with pockets of pebbles. Sporadic but good characteristic exposures are seen in Cachar and Karimganj districts.

Namsang Formation represents the group in Upper Assam. The fluviatile formation follows the same lithology with reasonable increase in conglomerate. The Formation overlain the Girujan Clays with an unconformable relationship.

DIHING GROUP: The fluvial Dihing Group of Pliocene age succeeds the Dupitila Group. The lithology includes thick beds of pebble which alternate with coarse grained sandstone, conglomerate also with clay and grit. An unconformity separates Namsang and the overlying Dihing which is witnessed near Jaipur, Upper Assam.

SIWALIK GROUP: Subansiri and Kimin Formations are named respectively for the Middle and Upper Siwalik rocks. Fine to medium grained sandstone, massive with enhanced mica are characteristic of the Subansiri Formation while soft sandstones including bands of claystone represents the Kimin Formation.

QUATERNARY SEDIMENTS: The Quaternary sequence unconformably overlains the Dihing Group. Its sequence is dominantly sand and indurated clays of variable colors with deposits of boulder and gravel. The deposits are suggested to be altered derivatives of the previous rocks and does not link to a fluvial origin. The Older Alluvium resides by the southern side in the locality of the granite hills (Precambrian)

also as river terrace (northern region) close to the Himalayan foothills, whilst the newer Alluvium is visible in the current route of Brahmaputra River.

2.2   GEOLOGY AND FIELD RELATIONSHIP

In the midst of the vast alluvial tract of the central part of Assam, the Karbi (Mikir) Hills stand out and represent a horst-like feature and face the Brahmaputra lineament on its North and to the south the Indo Burma Range (IBR). The hills are raised, portraying an oblong configuration engraved with close spaced linear and criss crossing drainage.

The Karbi Anglong Hills, Assam uplifted to a height of about 1359m are widespread over an area of about 7000km^2. The geological relationship and stratigraphy of Karbi Anglong Hills corresponds to that of Shillong plateau, and is regarded as the Eastern continuation of the latter separated by an alluvium tract of the Kopili river along the major NW-SE trending fracture zone namely the Kopili rift. The Shillong plateau and KAH represents the north-eastern extension of the Precambrian Indian Shield, bounded by the Brahmaputra Fault to its north, the northerly dipping E-W trending Dauki Fault to the south, to the west by the Jamuna lineament and to its east, the Belt of Schuppen.

Precambrian Gneissic terrain stands as the base for the overlying assemblages of rock units in the Karbi Hills. The Basement complex is predominant of gneiss, chiefly the biotite-bearing quartzofeldspathic gneiss; schist, migmatites with younger acidic to basic intrusions. Succeeding the basement unit is the Shillong Groups comprising of metasedimentaries like quartzite-phyllite-schist association. The Shillong Group occurs along the South-western part and along the eastern boundary of Nogaon district where they reportedly include quartzites, muscovite-biotite- sericite schists and locally, phyllites. The rocks in this area have apparently reached a slightly higher grade of metamorphism as compared to those in Meghalaya Plateau. The structural trends of these rocks are NE-SW with dip varying from low to high angles. Quartzites, which are the dominant rocks of the group, are generally grey, white or buff coloured, fairly compact and fine to medium grained. They are made up of quartz grains embedded in a sericitic matrix. Dolamara and nearby area displays such exposures.

Intermittent intrusions of magmas of diverse nature are initiated since the Proterozoic in both the earlier rock units. The Gneissic terrain and the overlying metasedimentary

rocks are exposed in the north and northwestern region of the Hills. Towards the south, the Hills coalesce with the Barails of North Cachar Hills which are post Oligocene sediments; the Karbi Hills extends further Southeast till the Naga Hills.

Granitoids show intrusive relation into the Basement gneissic bodies, metasedimentaries of Shillong Group and amphibolites. They occur by the fringes of the Karbi Anglong Hills and also host enclaves of the gneiss and basic rocks and aplites which endured the metamorphism.

2.2.1   GRANITOIDS OF KARBI ANGLONG HILLS (KAHG)

Batholithic dimension granite plutons are generally observed. Based on field observation, mode of occurrence and megascopic characters, the Karbi Anglong Hills Granitoids (KAHG) shows heterogeneity in nature from coarse grained porphyritic granitoid to medium grained massive non-porphyritic and foliated biotite enriched granite gneiss; the rock outcrops vary from grey to pink hues with variable textures. Associations with schists, foliated gneisses, granulites with intrusive pegmatites are noted.

The Granitoids shows intrusive relation into the basement units and contain enclaves of the Basement gneisses and basic rocks. Undeformed manner of the granitoids could suggest there were no preceding events of orogenic movements after their emplacement and subsequent attainment of stability.

PORPHYRITIC GRANITOIDS (PGN): Porphyritic granitoids (PGN) depicts a medium to coarse grained texture, grey and pink varieties are recognised. The porphyritic rocks are emplaced as isolated plutons in different parts of the Hills. Northern region of the Hills has shown intrusions of porphyritic granitoids, mostly in the vicinity of Kaziranga (KZ). Randomly oriented tabular to subrounded K-feldspar (up to 8cm) megacrysts is characteristic of the porphyritic granitoids (Fig. 2.1a). At places the K-feldspars are affected by potash metasomatic fluids thus showing a characteristic pinkish look.

Variables sizes of mafic enclaves are commonly observed in the porphyritic variety which can be subrounded to semi-elliptical (Fig. 2.1b&c). Kaziranga picnic spot outcrops are pink in colour often show pegmatitic and aplitic veins (Fig. 2.1d), however the rocks in general were moderately foliated with medium to coarse grains. (Fig. 2.1e).

NON-PORPHYRITIC GRANITOIDS (NPG): Non- porphyritic granitoids (NPG) have been encountered in western and central regions of the KAH. Rocks units are grey (salt-pepper), pink and medium grained, free of phenocrysts. Mahamaya, Amguri (AR), Seconee, Kathalguri (KH) and Numaligarh (NL) are the sample locations. Leucocratic, grey coloured granitoids are exposed in Kathalguri (KH) and Numaligarh (NL).

Texture is medium grained, massive with the outcrop (Fig. 2.2a) color varying from grey to pink and are rather phenocryst free (Fig. 2.2b). Small rounded or lenticular microgranular enclaves are hosted sparingly in the non- porphyritic rocks (Fig. 2.2c). Pronounced quartzo-feldspathic veins are common throughout the locality (Fig.2.2d) Pegmatites, quartz veins traversing through the outcrops are ever-present.

BASEMENT GNEISSIC GRANITE (BGN): Coarse grained, massive gneissic pink outcrops often occur as isolated inselbergs projecting out of the Quaternary plains in the Southernwestern part of the Hills (Centre Bazaar Fig. 2.3a). Intrusive nature of coarser grained random bands of pink granites seen cross cutting both along and across gneissocity of the grey granite gneiss/ migmatites, the bands are lesser than 6-8cms in thickness which could be suggestive of a younger granite activity, noted at Centre Bazaar (Fig. 2.3b). Howraghat (HW) granitoids show contacts of host rock with large enclaves which are sporadically edged by thick quartz bands (Fig. 2.3c). BGN show high migmatization displaying biotite-rich melanosome in the Karkok and Loringthepi areas. Felsic minerals display pinching and swell structures and mafic clots which are aggregates of biotite leads to augen-like gneissic structure are typical of the BGN.

GRANITE GNEISS (GGN): The granite-gneisses and migmatites are the most extensively developed rock, occupying large part of the central and southern Mikir Hills. GGN is phenocryst free and mesocratic (Fig. 2.4a). Granitoids of Gajraj area (GG) are moderately foliated, there is a random allignment of the ferromagnesian minerals giving rise to slight gneissosity, distinct alternating bands of coarse grained quartzo-feldspathic minerals and the darker mafic bands of biotite and magnetite.

Outcrops vary from grey or pink in colour (Fig. 2.4b), exhibit well defined to irregular foliations which locally grade into non-foliated, augen bearing, banded and migmatitic varieties. The darker nature of the rock units could be attributed to more content of ferromagnesium minerals biotite (Fig. 2.4c).

2.2.2 SAMPLE AND LOCATION

Locations of representative samples collected along the study area are indicated in (Fig. 1, Chapter-1). The geographic co-ordinates of the sample locations are given in Appendix 1.

2.3 MAGNETIC SUSCEPTIBILITY OF KARBI ANGLONG HILLS GRANITOIDS (KAHG)

A huge benefit of the Magnetic Susceptibility (MS) method is that we obtain first-hand knowledge of the magnetic state of any granite outcrop at the site itself employing the hand held Kappameter. It is the quickest way of classifying the granitoids into Ilmenite and magnetite-series granitoids as each granite rock exposure depicts its distinguishing range of values. The boundary between the two series has been defined by the MS value of 3×10^{-3} SI unit.

Ishihara (1977) proposed two classes of granites according to their mineral content: The Magnetite and llmenite series granites respectively. The oxygen fugacity of the crystallizing magma is considered a controlling factor about the opaque oxide mineralogy and so, oxidized and reduced nature indicates magnetite and ilmenite series granites respectively. Ishihara suggested that ilmenite series granites were comparable to the S-type granites of Chappell & White (1974) and the magnetite series granites to be equivalent to the I-types. The system principally is an advantage to mineral exploration for the reason that magnetite series granites occur in association with copper-base metals and ilmenite series granites are associated with tin-tungsten mineralization.

MS measurements were taken along the traverse from Dimapur-Dokmoka (southwest), Dokmoka-Jakhalabanda (northwest), Jakhalabandha-Kaziranga (north) and Kaziranga-Nummaligarh (northeast) for the Karbi Anglong Hills Granitoids (KAHG).

In KAHG the highest value of MS is about 51.182×10^{-3} SI unit which is of gneissic variety and corresponds to the magnetite Series. Measurement can be as low as 0.044×10^{-3} SI unit correlating to Ilmenite granitoid Series. The Magnetic Susceptibility (MS) values ($\times 10^{-3}$SI) of the KAHG along with corrected values, range and average values are given in Table 3.

PORPHYRITIC GRANITOIDS (PGN): Magnetic Susceptibility (MS) values for the porphyritic varieties at Kaziranga are comparatively less, corresponding both to Ilmenite and the magnetite series granitoids. Values range from 1.684 to 10.466×10^{-3} SI unit (n=106; av=3.651) for the pink variety and $2.144-5.53 \times 10^{-3}$ SI unit (n=18; av= 3.573) for the grey variety found near Kaziranga tourist lodge. Pink Coarse grained porphyritic granitoids near Bagoria shows lesser MS values of 1.744 to 2.703×10^{-3} SI unit correlating to the Ilmenite series.

NON-PORPHYRITIC GRANITOIDS (NPG): Non-porphyritic Kathalguri and Amguri granitoids have huge variations in the MS values varying between $1.831-25.734 \times 10^{-3}$ SI unit (n=26; av= 12.461) and $2.308-14.231 \times 10^{-3}$ SI unit (n=55; av= 5.641) respectively. The granitoids belong to both the Ilmenite and Magnetite series. Also, Krist Jyoti and Seconee granitoids corresponds to both ilmenite and magnetite series based on values ranging from $0.215-3.306 \times 10^{-3}$ SI units (n=13; av=1.677) and $2.664-6.301 \times 10^{-3}$ SI units (n=11; av=4.471). However, there is less variation in the MS readings. Granitoids exposed around Mahamaya shows the lowest values ($0.044-2.306 \times 10^{-3}$ SI unit), corresponding to ilmenite series.

GNEISSIC VARIETY: The gneissic Granites are exclusively of Magnetite series with Dolomara showing the highest range of MS values ($20.33-36.09 \times 10^{-3}$ SI unit). The measured MS values of Gajraj area (GG) granitoids range between 3.976 to 12.321×10^{-3} SI unit (n=48; av= 7.410) corresponding entirely to magnetite series granitoids. Panbari has values from $7.197-25.616 \times 10^{-3}$ SI unit.

Basement Gneissic Granites (BGN): Loringthepi Granitoids (LG) show enormous disparity of MS values between 4.122 to 51.182×10^{-3} SI unit. The MS values of Howraghat area granitoids range between 4.171 to 17.270×10^{-3} SI unit (n=18; av=11.873). Karkok Granitoids (KG) range between 4.329 to 21.575×10^{-3} SI unit corresponding to magnetite series granitoids apart from an erroneous value of 2.752×10^{-3} SI unit.

Figure 2.1: Field photograph of PGN showing (A) Randomly oriented euhedral to subhedral K-feldspars phenocrysts in porphyritic granitoid (B)&(C) Porphyritic granitoid encompassing small semi-rounded, semi-elliptical microgranular enclaves (D) Kaziranga picnic spot outcrops frequently show pegmatitic/ aplitic veins (E) moderately foliated with more ferromagnesian minerals.

Figure 2.2 Field photograph of NPG showing (A) Massive outcrop of Kathalguri pluton (B) Medium grained grey phenocryst free granite outcrops (C) Small rounded microgranular enclaves hosted sparingly in NPG (D) Quartzo-feldspathic veins in Kathalguri and (E) Pink medium grained NPG of Mahamaya with intrusive pegmatitic veins and aplitic veins.

Figure 2.3: Field photograph of BGN showing (A) Isolated inselbergs of Basement granite gneiss at Centre Bazaar (B) Batches of coarser grained pink granite cross cuts both along, across gneissocity of the grey granite gneiss/ migmatites at Centre Bazar (C) The contacts of host rocks and enclaves sporadically edged by thick quartz (D) Moderately banded biotite-rich melanosome in the basement granite gneiss.
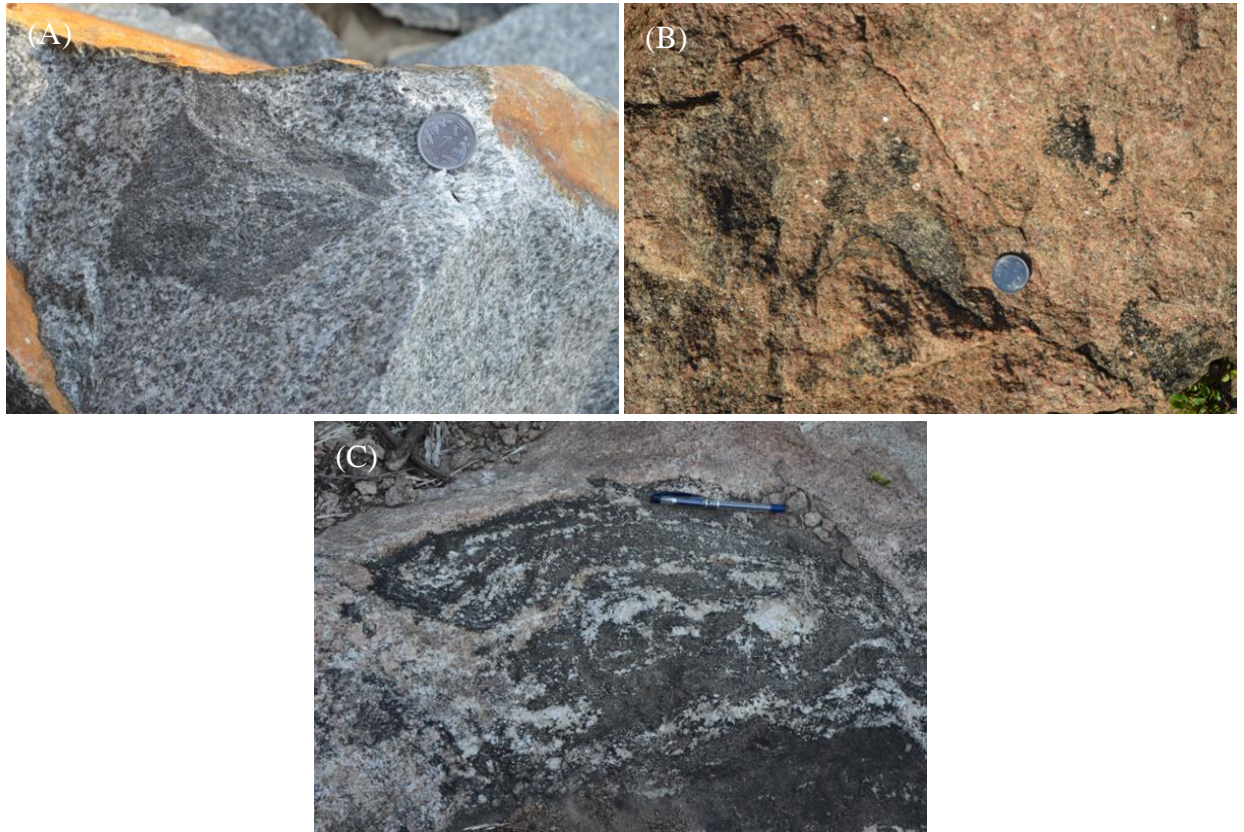
Figure 2.4: Field photograph of GGN showing (A) phenocryst free and mesocratic outcrop (B) outcrops vary from grey or pink (C) the rock units with random alignment of the ferromagnesian minerals.

TABLE- 1: GENERAL STRATIGRAPHIC SET UP AND GEOLOGY OF ASSAM

Age	Group Name	Formation	Lithology
Holocene	Unclassified	**Newer or Low-Level Alluvium**	Sand, Silt and clay
Middle to Upper Pleistocene	Unclassified	**Older Alluvium**	Sand, clay, pebble, gravel and boulder deposit
-- *Unconformity/Tectonic* ----------------------------------			
Pliocene-Pleistocene	**Siwalik Group**	**Kimin Formation**	Sandstone with clay stone
		Subansiri Formation	Micaceous sandstone
Pliocene	**Dihing Group**	**Dihing Formation** (900m)	Pebble beds, soft sandy clay, clay, conglomerates, grit and sandstone
-- *Unconformity*--			
Mio-Pliocene	**Dupitila Group**	**Dupitila Formation** (Surma Valley: 3000m)	Sandstone, mottled clay, grit and conglomerate; locally with beds of coal, conglomerate and poorly consolidated sandstone with layers and pockets of pebbles
		Namsang Formation (Upper Assam: 800m)	Coarse, gritty, poorly consolidated sandstone and conglomerate of coal pebbles
-- *Unconformity*--			
Mio-Pliocene	**Tipam Group**	**Girujan Clay Formation** (1800m)	Mottled clays, sandy shale and subordinate mottled, coarse to gritty sandstone
		Tipam Sandstone Formation (2300m)	Bluish grey to greenish, coarse to gritty, false bedded, ferruginous sandstone, clays, shales and conglomerates
-- *Unconformity*--			
Miocene	**Surma Group**	**Bokabil Formation** (900 to 1800m)	Shale, sandy shale, siltstone, mudstone and lenticular, coarse ferruginous sandstone
		Bhuban Formation (1400 to 2400m)	Alternations of sandstone and sandy shale and thin conglomerate, argillaceous in middle part
-- *Unconformity*--			
Eocene- Oligocene	**Barail Group**	**Renji Formation** (600 to 1000m)	Massive bedded sandstone; its equivalent - the Tikak Parbat Formation in the Upper Assam is marked by thick coal seam in basal part
		Jenam Formation (1000 to 3300m)	Shale, sandy shale, and carbonaceous shales with interbedded hard sandstone; its equivalent the Bargolai Formation in Upper Assam is marked by thin coal seams
		Laisong Formation (2000 to 2500m)	Well bedded compact flaggy sandstone and subordinate shale; its equivalent- the Nagaon Formation in Upper Assam is marked by thin bedded, hard sandstone and interbedded shale.
	Disang Group		Splintery dark grey shale and thin sandstone
		Kopili Formation	Shale, sandstone and marl.

Palaeocene-Eocene	**Jaintia Group**	**Shella Formation**	Sylhet Limestone (Fossiliferous Limestone) Sylhet sandstone, clay and thin coal seam
		Langpar Formation (Exposed in Meghalaya)	Calcareous shale, sandstone-limestone
-- *Unconformity*---			
Cretaceous	**Alkali Complex of Samchampi**		Pyroxenite-Serpentinite with abundant development of melilite pyroxene rock, ijolite, syenite and carbonatite
-- *Unconformity*---			
Cretaceous		**Sylhet Trap** (600m) (Exposed in Meghalaya)	Basalt, alkali basalt, rhyolite acid tuff
-- *Unconformity*---			
Permo-Carboniferous	**Lower Gondwana**	**Kaharbari Formation**	Very coarse to coarse grained sandstone with conglomerate lense, shale, carbonaceous shale and coal
		Talchir Formation	Basal tillite, conglomerate with sandstone bands, siltstone and shale
-- *Unconformity*---			
Neo-Proterozoic-early Palaeozoic	**Granite Plutons**	…………………	Porphyritic coarse granite, pegmatite, aplite, quartz vein traversed by epidiorite, dolerite
-- *Intrusive contact* ---			
Palaeo-Meso Proterozoic	**Shillong Group**	……………………...	Quartzite, phyllite, quartz- sericite schist, conglomerate
-- *Unconformity* ---			
Archaean (?) Proterozoic	**Gneissic Complex**	……………………...	Complex metamorphic group comprising ortho and para gneisses and schists, migmatites granulites etc. Later intruded by acidic and basic intrusives.

(After G.S. I, Miscellaneous Publication No. 30. Part IV Vol: 2 (i), 2009)

TABLE-2: A GENERALIZED STRATIGRAPHIC SUCCESSION OF THE KARBI ANGLONG HILLS

(Modified after Mazumdar, 1986; Dhurandhar et al 2019)

Geological Age	Group	Formation	Lithology
Tertiary			Thin bedded low dipping sandstone
---Unconformity---			
Cretaceous			Basaltic magmatism, dykes, carbonatite complexes
-- Intrusive contact--			
Cambro-Ordovician		Non- porphyritic granitoids	Medium-fine grained, salt and pepper textured
-- Intrusive contact--			
Mesoproterozoic		Porphyritic granitoids	Fine-grained porphyry granite, light to dark grey, pink
-- Intrusive contact--			
		Mafic intrusives	Metamorphosed basalts (amphibolites)
Mesoproterozoic			
-- Intrusive contact--			
Paleo-Mesoproterozoic	Shillong Group	Barapani Formation (Arenaceous)	Sandstone with magnetite Oligomictic conglomerate
		Tyrsad Formation (Argillaceous)	Volcanics: Rhyolite, Tuffaceous/volcanoclastics bands+ magnetite Quartzite, Schists, Phyllites
---Unconformity---			
		Basement Complex	Granite Gneiss, Porphyritic granite and Migmatite

TABLE 3: MAGNETIC SUSCEPTIBILITY (MS) VALUES (X10^{-3}SI) OF KARBI ANGLONG HILLS GRANITOIDS (KAHG)

PORPHYRITIC GRANITOIDS (PGN)

Location Coordinates	Location Name	Field description	MS measurement (x10^{-3}SI units)	Average MS	Range MS
26º34'41.5" 93º24'26.4"	**Kaziranga**	Pink, Coarse grained porphyritic	3.201, 2.296, 2.461	2.719 (n=3)	2.296-3.201
26º34'40.6" 93º24'26.4"	**Kaziranga**	Pink, Coarse grained porphyritic	1.906, 2.014, 1.964, 2.033, 2.052	1.994 (n=5)	1.906-2.052
26º34'40.6" 93º24'26.6"	**Kaziranga**	Pink, Coarse grained porphyritic	2.848, 3.111, 3.211, 3.395	3.141 (n=4)	2.848-3.395
26º34'24.1" 93º24'09.0"	**Kaziranga**	Pink, Coarse grained porphyritic	4.747, 1.957, 2.919, 4.288, 3.423	3.467 (n=5)	1.957-4.747

Location Coordinates	Location Name	Field description	MS measurement (x10⁻³SI units)	Average MS	Range MS
26°34'24.1" 93°24'09.5"	**Kaziranga**	Pink, Coarse grained porphyritic	4.58, 3.455	4.018 (n=2)	3.455-4.58
26°34'26.0" 93°24'16.1"	**Kaziranga**	Pink, Coarse grained porphyritic	3.394, 2.898, 3.763, 4.319, 4.116	3.698 (n=5)	2.898-4.319
26°34'28.5" 93°24'18.3"	**Kaziranga**	Pink, Coarse grained porphyritic	3.246, 2.962, 4.539, 4.813, 3.025	3.717 (n=5)	2.962-4.813
26°34'31.5" 93°24'21.0"	**Kaziranga**	Pink, Coarse grained porphyritic	3.982, 4.298, 5.683, 3.438, 3.345	4.149 (n=5)	3.345-5.683
26°34'37.9" 93°24'24.6"	**Kaziranga**	Pink, Coarse grained porphyritic	3.87, 4.226, 5.096, 3.559, 3.806, 4.403, 4.661, 5.029, 3.792, 2.389	4.083 (n=10)	2.389-5.096
26°34'42.4" 93°24'25.9"	**Kaziranga**	Pink, Coarse grained porphyritic	8.435, 10.024, 10.466, 5.968, 9.635	8.906 (n=5)	5.968-10.466
26°34'47.2" 93°24'57.5"	**Kaziranga**	Porphyritic pink Granite	2.109, 8.599, 3.145, 2.371, 3.671, 4.528, 1.684, 1.849, 2.292, 4.788, 4.101	3.558 (n=11)	1.684-8.599
26°34'18.4" 93°23'45.0"	**Kaziranga**	Porphyritic pink Granite	7.886, 4.619, 6.678, 6.289, 6.564, 8.122, 8.048, 7.951	7.020(n=8)	4.619-8.122
26°34'22.0" 93°24'00.8"	**Kaziranga**	pink Granite	8.385, 10.132, 10.021, 10.065, 7.663, 9.064, 5.944	8.753 (n=7)	5.944-10.132
26°34'42.2" 93°24'26.6"	**Kaziranga**	Porphyritic pink Granite	5.124, 5.548, 6.189, 7.365, 5.390, 6.169, 5.990	5.628(n=7)	5.124-7.365
26°35'01.8" 93°24'21.8"	**Kaziranga**	Porphyritic grey Granite	5.044, 2.144, 4.491, 4.733, 2.281, 2.174, 4.936, 5.530, 2.418, 2.700, 3.216, 3.501, 2.893, 4.675, 3.811, 4.675, 2.788, 2.299	3.573(n=18)	2.144-5.53
26°35'06.9" 93°19'07.9"	**Near Bagoria**	Coarse grained porphyritic pink	1.974, 2.444	2.209 (n=2)	1.974-2.444
26°35'06.9" 93°19'08.5"	**Near Bagoria**	Coarse grained porphyritic pink	2.133, 2.245	2.189 (n=2)	2.133-2.245
26°35'06.9" 93°19'07.9"	**Near Bagoria**	Coarse grained porphyritic pink	1.837, 2.24, 2.651, 2.114, 2.067	2.182 (n=5)	1.837-2.651
26°35'70.0" 93°19'09.7"	**Near Bagoria**	Coarse grained porphyritic pink	2.032, 2.281, 1.975	2.096 (n=3)	1.975-2.281
26°35'06.5" 93°19'07.7"	**Near Bagoria**	Coarse grained porphyritic pink	2.606, 1.947	2.277 (n=2)	1.947-2.606
26°35'07.0" 93°19'07.9"	**Near Bagoria**	Coarse grained porphyritic pink	2.703, 2.059	2.381 (n=2)	2.059-2.703
26°35'06.06" 93°19'07.9"	**Near Bagoria**	Coarse grained porphyritic pink	1.744, 1.915, 1.988, 1.837	1.830 (n=4)	1.744-1.988
26°35'06.0" 93°19'09.8"	**Near Bagoria**	Coarse grained porphyritic pink	1.988, 1.837	1.913 (n=2)	1.837-1.988
26°35'06.7" 93°19'10.2"	**Near Bagoria**	Coarse grained porphyritic pink	1.796, 2.281	2.039 (n=2)	1.796-2.281

NON-PORPHYRITIC GRANITOIDS (NPG)

Location Coordinates	Location Name	Field description	MS measurement (x10⁻³SI units)	Average MS	Range MS
26°22'19.8" 93°53'01.9"	**Kathalguri**	Grey Granite	7.826, 6.985, 8.556, 6.887, 6.012, 7.468,	5.013(n=10)	1.831-8.556

			7.312, 1.831, 1.947, 2.774		
26°22'17.1" 93°53'01.4"	**Kathalguri**	Grey Granite	10.515, 9.440, 11.781, 13.632, 12.070, 15.173, 13.45, 13.878	12.492(n=8)	9.44-15.173
26°22'44.5" 93°52'58.5"	**Kathalguri**	Grey Granite	17.60, 13.878, 15.793, 20.854, 22.063, 24.460, 25.734, 18.639	19.878(n=8)	13.878-25.734
26°12'50.0" 93°03'42.9"	**Krist Jyoti**	Pink Granite	1.077, 0.707, 2.535, 2.965, 0.215, 1.058, 3.306, 2.217, 2.140, 2.578, 2.025, 0.350, 0.629	1.677(n=13)	0.215-3.306
26°32'48.11" 93°00'46.6"	**Seconee Tea Estate**	Pink Granite	4.501, 5.035, 4.632, 4.897, 6.301, 4.423, 5.009, 5.015, 3.954, 2.664, 2.745	4.471 (n=11)	2.664-6.301
26°35'32.4" 93°43'58.4"	**Numaligarh Tea Garden**	Grey Granite	12.230, 13.803, 9.804, 9.898, 9.430, 8.044, 10.409, 8.429, 8.849, 9.328, 8.623	9.895 (n=11)	8.044-13.803
26°35'35.5" 93°43'57.6"	**Numaligarh Tea Garden**	Grey Granite	8.563, 9.461, 11.87, 12.380, 11.931, 14.26, 10.871	11.334 (n=7)	8.563-14.26
26°11'59.5" 93°04'17.0"	**Mahamaya**	Pink Granite	2.306, 0.988, 0.574, 0.832, 1.507, 1.422, 0.977	1.229(n=7)	0.574-2.306
26°12'01.4" 93°04'09.5"	**Mahamaya**	Pink Granite	0.151, 0.125, 0.148, 0.265 ,0.326, 0.240, 0.089, 0.262	0.201 (n=8)	0.089-0.326
26°12'00.7" 93°04'00.2"	**Mahamaya**	Pink Granite	0.139 ,0.122, 0.044, 0.135	0.11 (n=4)	0.044-0.139
26°12'28.4" 93°04'12.8"	**Mahamaya Sing Teron village**	Granite; Pink, med-fine grained, mafic minerals are <5 %, massive	0.234, 0.285, 0.484, 0.271, 0.232, 0.389, 0.448, 0.289, 0.351, 0.333, 0.357, 0.401, 0.243, 0.410, 0.343, 0.272, 0.223, 0.351, 0.247	0.324 (n=19)	0.223-0.484
26°34'03.9" 93°03'51.1"	**Amguri**	Fine grained pink	4.171, 2.308, 3.878, 4.382, 4.669, 4.818	4.038 (n=6)	2.308-4.818
26°34'03.9" 93°03'51.4"	**Amguri**	Fine grained pink	5.222, 4.89, 4.408, 4.17, 3.913, 5.15	4.626 (n=6)	3.913-5.222
26°34'03.9" 93°03'51.6"	**Amguri**	Fine grained pink	3.735, 3.64, 4.057, 5.04, 5.103, 5.086	4.444(n=6)	3.64-5.103
26°34'03.9" 93°03'51.8"	**Amguri**	Fine grained pink	4.722, 4.213, 5.27, 5.894, 6.422	5.304 (n=5)	4.213-6.422
26°34'07.1" 93°04'13.8"	**Amguri**	Fine grained pink	5.001, 4.249, 7.982, 4.008, 4.004, 4.05, 5.928	5.032 (n=7)	4.004-7.982
26°34'8.2" 93°04'13.9"	**Amguri**	Fine grained pink	5.699, 5.546, 5.632	5.626 (n=3)	5.546-5.699
26°34'26.2" 93°06'16.1"	**Amguri**	Fine grained pink	4.49, 4.124, 4.383, 3.717, 4.521, 3.833, 4.756	4.261 (n=7)	3.717-4.756
26°34'26.9" 93°06'15.0"	**Amguri**	Coarse grained grey	7.467, 5.784, 6.507, 6.328	6.522 (n=4)	5.784-7.467
26°34'26.4" 93°06'15.1"	**Amguri**	Medium grained pink	6.114, 4.765, 3.796, 4.811, 4.128	4.723 (n=5)	3.796-6.114

26°33'41.8" 93°03'29.0"	**Amguri**	Pink Granite	10.16, 13.22, 11.235, 11.738, 14.231, 10.440	11.837(n=6)	10.16-14.231

GRANITE GNEISS (GGN)

Location Coordinates	Location Name	Field description	MS measurement (x10⁻³SI units)	Average MS	Range MS
26°34'57.6" 93°33'01.8"	**Dolomara**	Grey Gneissic Granite	26.98, 25.552, 21.83, 26.19, 26.632, 24.546, 20.33, 36.09, 24.931	25.898 (n=9)	20.33-36.09
26°36'13.5" 93°29'40.7"	**Panbari**	Grey Granite, Gneissic	24.26, 22.44, 24.02, 23.112, 20.96, 17.377, 20.97, 19.453, 23.87, 12.647, 21.70	20.983 (n=11)	12.647-24.26
26°36'11.1" 93°29'42.0"	**Panbari**	Grey Granite, Gneissic	25.616, 21.83, 23.957, 15.001, 21.956, 18.468, 18.650	20.783 (n=7)	15.001-25.616
26°36'13.1" 93°29'36.0"	**Panbari**	Grey Granite, Gneissic	8.938, 8.030, 8.867, 8.158, 7.197, 7.735	8.154 (n=6)	7.197-8.938
26°34'28.3" 93°06'40.8"	**Gajraj**	Coarse grained pink	6.538, 6.776, 7.403, 6.682, 6.15	6.71 (n=5)	6.15-7.403
26°34'28.5" 93°06'41.3"	**Gajraj**	Coarse grained grey	5.641, 6.28	5.961 (n=2)	5.641-6.28
26°34'28.6" 93°06'41.3"	**Gajraj**	Coarse grained pink	5.875, 5.829, 6.919	6.208 (n=3)	5.875-6.919
26°34'28.7" 93°06'42.3"	**Gajraj**	Coarse grained pink	6.956, 6.411, 6.165, 6.437, 7.164	6.627 (n=5)	6.165-7.164
26°34'28.8" 93°06'42.3"	**Gajraj**	Coarse grained pink	10.813, 7.762, 9.838, 7.092	8.876 (n=4)	7.092-10.813
26°34'27.4" 93°06'42.1"	**Gajraj**	Coarse grained pink	8.244, 6.606, 7.081, 6.616, 6.362	6.982 (n=5)	6.362-8.244
26°34'27.6" 93°06'43.4"	**Gajraj**	Coarse grained pink	9.042, 5.933, 5.802, 5.932, 6.572, 5.138, 5.974	6.342 (n=7)	5.138-9.042
26°34'29.1" 93°06'44.5"	**Gajraj**	Coarse grained pink	8.944, 9.032, 8.688, 9.354, 9.415	9.087 (n=5)	8.688-9.415
26°34'29.2" 93°06'46.4"	**Gajraj**	Coarse grained pink	9.926, 12.321	11.124 (n=2)	9.926-12.321
26°34'29.5" 93°06'38.6"	**Gajraj**	Pink Granite	4.067, 6.081, 3.976, 6.237, 7.816, 7.123, 7.541, 6.483, 8.222, 4.102	6.165 (n=10)	3.976-8.222

BASEMENT GRANITE GNEISS (BGN)

Location Coordinates	Location Name	Field description	MS measurement (x10⁻³SI units)	Average MS	Range MS
26°05'20.6" 93°08'59.3"	**Howraghat**	Pink Granite	8.085, 5.300, 13.653, 7.601, 9.985, 4.171, 7.254, 7.440, 10.060, 6.220, 10.673, 13.150, 7.738, 10.871	8.729(n=14)	4.171–13.653
26°05'20.9" 93°08'59.3"	**Howraghat**	Pink Granite	12.391, 17.270, 15.03, 15.376	15.017 (n=4)	12.391-17.270

25º59'51.7" 93º18'33.7"	**Karkok**	Fine-grained pink	4.798, 4.329	4.564 (n=2)	4.329-4.798
25º59'51.1" 93º18'33.9"	**Karkok**	Fine-grained pink	4.375, 4.776	4.576(n=2)	4.375-4.776
26º05'32.7" 93º08'24.2"	**Karkok**	Medium-grained pink	9.705, 13.607, 11.378, 10.235	11.231(n=4)	9.705-13.607
26º05'32.6" 93º08'24.1"	**Karkok**	Medium-grained pink	8.047, 4.064, 4.637, 4.239	5.247 (n=4)	4.064-8.047
26º05'33.9" 93º08'24.5"	**Karkok**	Medium-grained grey	11.903, 10.802, 9.246	10.584 (n=3)	9.246-11.903
26º05'32.3" 93º08'24.9"	**Karkok**	Gneissic granite	16.067, 13.047, 11.446	13.52 (n=3)	11.446-16.067
26º05'32.2" 93º08'24.8"	**Karkok**	Gneissic granite	21.575, 12.719, 5.036	13.11 (n=3)	5.036-21.575
26º05'31.3" 93º08'18.3"	**Karkok**	Pink Granite	6.581, 7.303, 5.836, 5.698, 2.752, 7.105	5.879 (n=6)	2.752-7.303
26º07'05.7" 93º08'41.7"	**Loringthepi**	Medium grained pink	16.382, 11.167, 12.675, 9.632	12.464 (n=4)	9.632-16.382
26º07'04.9" 93º08'41.8"	**Loringthepi**	Medium grained pink	18.193, 16.344, 6.485, 13.681, 19.251, 19.189	15.5224 (n=6)	6.485-19.251
26º07'06.1" 93º08'42.8"	**Loringthepi**	Medium grained grey	14.718, 13.552, 17.738, 9.956, 11.562, 15.43, 16.627, 15.027, 11.221, 11.578, 10.807, 9.549, 15.384, 14.194, 13.692	13.402 (n=15)	9.549-17.738
26º07'05.6" 93º08'42.8"	**Loringthepi**	Medium grained grey to pinkish (gneissic)	11.402, 9.034, 8.685	9.707 (n=3)	8.685-11.402
26º07'05.3" 93º08'43.0"	**Loringthepi**	Medium grained grey to pinkish (gneissic)	38.717, 36.643, 44.232, 51.182, 44.945	43.144 (n=5)	36.643-51.182
26º07'05.2" 93º08'43.1"	**Loringthepi**	Medium grained grey to pinkish (gneissic)	40.308, 37.123, 37.466, 42.51, 39.497, 41.354, 34.94, 33.703, 43.31, 35.035	38.525 (n=10)	33.703-43.31
26º07'04.1" 93º08'41.0"	**Loringthepi**	Fine grained grey (gneissic)	4.684, 8.611, 10.903, 10.175, 9.222, 9.891, 9.812, 8.903, 6.709, 10.985	8.990 (n=10)	4.684-10.985
26º07'04.9" 93º08'43.7"	**Loringthepi**	Pink Granite	17.206, 18.351, 6.574, 8.362, 9.887, 18.126, 4.700, 4.122, 8.740, 10.05, 9.480, 4.511, 7.983, 4.198, 5.404, 8.383	9.755(n=16)	4.122-18.351

CHAPTER III

METHODOLOGY

3. 1   INTRODUCTION

In the present study, sufficient time was invested for consulting the available knowledge in the literatures and work was initiated with dedicated observation in the field employing the traditional geological tools (clinometer compass, hand lens, hammer, magnetic susceptibility meter and notebook etc.). Proceeding step was entering the laboratory and analytical dominion. With the advent of analytical and modern petrological methods, a variety of intensive parameters are available for estimation of bulk chemical, physical and optical properties of the granitoids. The methodology and instrumentation techniques employed are briefly described in this chapter.

3. 2   FIELD TECHNIQUES

Detailed fieldwork was carried out and planned traverses were made along the National Highway 37 & 39. Representative rock samples were collected in the areas of Karkok, Mahamaya, Amguri, Kathalguri, Kaziranga, Dolomara and Numaligarh in Karbi Anglong District during the periods 2013-2014 and 2018. Sample location areas and path of traverse were traced and marked through GPS.

Structures, textures and inter-relationships of various litho-types observed in the field were photographed and supplementary sketches wherever required for documentation were collected. Magnetic susceptibility (MS) measurements have been done on the surfaces of rock outcrops using a Kappameter. Sufficient number of fresh representative samples of the Karbi Anglong granitoids was collected for further laboratory and geochemical investigations.

3. 3   MAGNETIC SUSCEPTIBILITY (MS)

The Magnetic Susceptibility (MS) measurement was obtained using a portable MS meter (KM-7). Measurements were obtained directly from fresh rock outcrop in the field and laboratory. The meter operates at a frequency of 10 kHz, with a sensitivity of 1×10^{-6} SI units and can be operated within 10˚ to 60˚C temperature ranges. Measurement of MS values can be obtained by placing the instrument on the rock surface and pressing the 'measure button' for a short time. Afterwards, the meter was immediately lifted away from the measured surface into the open air (more than 30 cm) followed by pressing the measure bottom shortly again with the meter indicating the actual MS values. Measurements can be taken in less than 3 seconds per sample. Smooth rock surfaces in the dimensions >100x100mm were preferred for the measurement. Whenever the outcrop surfaces were uneven the measured MS values were normalized based on correction factor given in Table 4.

3. 3   LABORATORY STUDIES

After completion of the field study, preparation of rock thin sections and powder for optical studies and geochemical analyses respectively were adopted in the Laboratory. Optical studies were done at the Department of Geology, Nagaland University with a LEICA Polarizing Microscope (Model DM 750P). Geochemical studies were carried out at Wadia Institute of Himalayan Geology (WIHG), Dehradun. It includes the X-Ray Fluorescence (XRF) Spectroscopy and Inductively Coupled Plasma-Mass Spectrometry methods (ICP-MS) for determining the major, trace and rare earth elements composition. Measurement of the fractional concentration of representative elements was also undertaken with the help of Electron Probe Micro-Analysis (EPMA).

3.3.1   SAMPLE PREPARATION FOR THIN SECTIONS

In order to proceed with the petrographical studies, thin sections of the representative rock samples were prepared. Selection was made based on the distribution of rock types, physical properties and the freshness of the rock samples. Rock chips were cut by means of conventional methods of rock cutting; it was later polished with different sizes of carborundum powder.

3.3.2   PREPARATION OF POWDER FOR GEOCHEMICAL ANALYSES

Representative rock samples were grinded to prepare the powdered form for chemical analysis treatment. Rock pieces (1 to 2 cm) were chipped off on a steel anvil with the help of hammer, each sample were then cleaned in acetone and dried. Subsequently, the dried samples were grounded and pulverized in a Disk mill pulverizing machine. Samples of about 100g can be pulverized at a time and the process can get over in few seconds upto 5 minutes depending upon the hardness of the samples. Desirable grain size of the powder after pulverization is less than 50μm and should not feel rough on the fingers such that it passes through a -300 mesh. While preparing the sample, precaution was given in order to avoid any possible contamination of each successive sample by cleaning thoroughly with acetone before proceeding to the next sample.

3.4   OPTICAL STUDIES

Optical studies are vital for identification of the mineral assemblages and to classify rocks. Rock thin sections were studied using LEICA Polarizing Microscope (Model DM 750P). About 22 thin sections of the samples were studied. The desired and important textural features and the relationships between minerals were photographed and the various optical properties of each mineral, such as color, habit, textures, relationships with each other etc were studied both under the plane polarized light and through crossed nicols. Modal mineral analysis of representative samples was carried out. Minimum of 1000 points were counted for each thin section and the percentages of the individual minerals were determined.

3.5   ANALYTICAL METHODS

Thin sections and pulverized samples prepared of the representative rock samples were used for the different geochemical analyses. Estimation of the major, trace and rare earth elements is discussed in the following paragraphs.

3.5.1   X-RAY FLUORESCENCE (XRF) SPECTROSCOPY

The phenomenon of emission of photons due to transfer of electrons from outer to inner orbital is called fluorescence. X-Ray Fluorescence (XRF) spectroscopy is a method widely used for identifying and seldom quantifying elements present in a substance. In this

method, a high energy x-ray photon is emitted from an x-ray source and strikes the sample for identification. These emitted rays termed as primary x-ray photons possess energy enough to displace the innermost electrons from K or L orbital. This removal of electrons disturbs the stability of the atom of the sample as its atoms become ions which are unstable. In order to acquire a stable electronic arrangement, electrons from an outer shell, like L or M, move into void spot of the inner orbital. This entire process leads to emission of an x-ray photon and is termed as "secondary x-ray photon". It must be noted that the secondary x-ray photon is quite different from the primary x-ray photon on the fact that the former is characteristic of a specific element whose presence in a given sample is identified by analyzing the energy of the secondary x-ray photons.

This method finds wide use in field applications and industrial production for control of materials because it is fast and does not destroy the sample. One major drawback is that it is neither suitable for identifying light elements with atomic number 19(K) and below; nor can it identify species like acetate. However, a positive factor is that many sample holders that are generally organic polymers consisting of C, H, O will be transparent for both primary and secondary x-ray photons.

As long as the sample is placed in a material (such as a plastic bag) transparent to x-rays, it can be conveniently analyzed. A total of 27 rock samples were grounded into fine powder using Jaw Crusher and Pulverizer. They were then subjected to analysis using Pressed Pellets (Briquette). To make one pressed pellet, a collapsible Al cup was filled with a binding aid as boric acid and 1 gm of the powdered sample on top. A pressure of 20 tons was applied to the cup using the help of a hydraulic press. Binders were mixed thoroughly with the powdered rock sample before subjecting to pressure in order to reinforce its stability and durability.

3.5.2   INDUCTIVELY- COUPLED PLASMA MASS SPECTROMETRY (ICP-MS)

Inductively- Coupled Plasma Mass Spectrometry (ICP-MS) is a modern analytical technique, which has been developed and successfully used as a powerful tool for fast, multi element analysis since 1983. Out of the different types of laboratories, Geochemical analysis laboratories were the pioneers to have adopted this technique i.e., ICP-MS,

because of its monitoring capabilities of trace and rare earth elements (ppm) with more sensitivity and increased data output per unit time.

Plasma may be defined as a cloud of highly ionized gas, composing ions, electrons and neutral particles. The flame for this technique consists of incandescent plasma (ionized gas) of Ar heated inductively by radio frequency energy at 4-50 MHz. whereby a temperature of about 10,000K is attained. Since plasma sources operate at higher temperatures, sample atoms are subjected to temperatures around 7000K, which is about twice of that obtained in techniques like in Atomic Absorption Spectrophotometry (AAS) where flame temperature is 3200K.

ICP-MS is considered superior to other analytical techniques because the high temperatures of the plasma source which produces greater number of excited atoms than obtained by Flame Emission Spectroscopy (FES) or AAS. The plasma source in ICP-MS is also capable of providing data or spectra for a large number of elements which makes this technique suitable for simultaneous elemental determinations, unlike in AAS, where only one or two elements can be measured at a time. Also, due o the high temperature of its plasma source, ICP-MS has the potential to deal with both simple and complex matrices with minimal matrix interferences.

As a result of these advantages, ICP-MS can be used for simultaneous elemental determinations of trace and rare earth elements (REE) in various geochemical materials. These elements are analyzed using an ICP-MS Model ELAN DRC-II (Perkin Elmer instrument, US) and the analysis is carried out by the open acid digestion method as follows:

1. Samples are powdered beforehand and 50mg of the powdered samples are taken in Polytetrafluoroethylene (PTFE) or Teflon beakers.
2. Each sample is moistened with few drops of water.
3. 20 ml of a mixture solution of HF, HNO_3, $HClO_4$ or HCl in the ratio of 7:3:1 respectively is added to each beaker containing different samples and the beakers are swirled to achieve complete mixture of the sample with the solution.

4. The beakers are then covered with lids and are kept for overnight when digestion occurs.

5. The beakers are heated on the following day, over hot plates at a temperature between 200-250°C for about 60 minutes.

6. The lids are then removed and the contents are heated continuously until it evaporates to almost dryness.

7. The evaporation process is repeated twice after adding 5ml of the mixture solution of 7:3:1.

8. The contents are then dissolved using 20ml of 1:1 distilled water and HNO_3 solution and 5ml of Rhodium solution.

9. The volume is then made up to 250 ml by diluting with distilled water and stored in reagent bottles (polythene).

10. Clear solutions are obtained which is a dilution of 1:1000. These solutions are used for the elemental determination of trace and rare earths.

3.5.3 ELECTRON PROBE MICRO-ANALYSIS (EPMA)

Electron Probe Micro-Analysis (EPMA) is a micro analytical technique in which a small target area of the sample is pin pointed for examination. EPMA works on the principle that when high- speed electrons collide with a solid target i.e., the polish surface of the sample, energy is emitted in the form of X-rays, which are characteristic of the sample element. These emitted X-rays are detected by a detector and shown as emission peaks in a read-out and wave length of these emission peak can be related to the atomic number of the elements contained in the sample and hence, element present in the sample can be identified. In addition, EPMA not only provides identity of a sample but also, concentration of the element in a given sample can be determined as the intensity of the emission peaks provide information of the amounts of the various elements contained in the sample.

Since, EMPA is the study of solid samples involving X-rays, this technique follows Bragg's equation (given by W. L. Bragg), which is given as, $2d \sin\Theta = n\lambda$

Where, d is the spacing between successive lattice planes

Θ is the glancing angle

n is an integer (1,2,3....etc) know as order of refection

λ is the wavelength of the x-rays

The sample to be studied by EMPA should be polished and in the form of either standard thin sections or solid blocks. Standard polish thin sections need to be epoxy mounted and dimensions should be 45-47 mm length, 25mm width and 1mm thick. While polished solid block needs to be Bakelite or polyvinyl chloride (PVC) mounted, and have to be perfectly rounded whose diameter should be 25mm and thickness should be equal to or less than 15mm. Smoothening of the sample is done by using 1000 mesh carborundum (SiC) powder and then polishing is done by a series of steps, the details of which are given below. It is important to note that, after each step of polishing, the slide should be washed thoroughly using a separate cloth for each step.

1. Polishing was done using chrome oxide (Cr_2O_3) for about 30 minutes.
2. Followed by polishing using 6-micron diamond paste (D.P.) for about 20 minutes.
3. Next polishing was done using 3-micron diamond paste (D.P.) for about 20 minutes.
4. Further polishing using 1-micron diamond paste (D.P.) for about 20 minutes.
5. Final polishing using 1/4-micron diamond paste (D.P.) for 5 minutes.

Depending on the requirement of the area of research, detailed petrographic analysis is done.

3.5.4   PETROCHEMICAL CALCULATIONS AND GRAPHICAL DIAGRAMS

The results and database acquired from the various chemical analyses mentioned have been processed further, which includes a number of petrochemical calculations and graphical illustrations i.e., bivariate, triangular and spidergraph plotting of the bulk major oxides, trace and rare earth elements. Tectonic environment and petrogenesis of the granitoids can be inferred through such discriminant diagrams.

From the analytical data of Biotite mineral chemistry, chemical structural formula was calculated based on 11 oxygen atoms. Microprobe data determine the total Fe content as FeO. normalization process was used for the partitioning of Fe^{3+} and Fe^{2+} from Iron as

FeO^t, the Cation-based partitioning scheme take into account vacancies associated with Al-substitution by means of the dioctahedral component as given in equation:

Total cations - (K+Na+Ca+Ba) + Ti+1/2Al ^{VI} xc= 7.0   (1)

Where, Al^{VI} Xc= (Al+Cr) ^{VI}-Al+ (K+Na+2Ca+Ba)   (2)

Biotite analytical results were normalized with reference to equation (1) during which the calculated excess charge is removed to permit Fe^{3+} content evaluations. MS-DOS based bioterm programme operates for the structural formulae calculations of Fe^{3+} as well for the intensive graphical representations and parameters.

3.6   SOFTWARE AND ROCKWARE

All the Geochemical database tables were entered and processed for various purposes making use of the spreadsheet (MS Excel 2007). Also, database handling and processing have been facilitated with the help of a range of softwares. ARC GIS was utilized in preparing the geological map and a better portion of the figures were digitized with Surfer 11.0 version and CorelDRAW 12. Bioterm was used for presenting the EPMA analyses of rock-forming minerals. Spidergraphs, binary, ternary and tectonic discrimination plots have been generated with Geochemical Data (GCD) Kit 4.00 version, the system is useful in recalculation and handling of the whole-rock geochemical data analyzed. The CIPW normative minerals were also calculated using the same.

TABLE-4: CORRECTION FACTORS USED TO NORMALIZE THE MEASURED MS VALUES

Surface Unevenness (mm)	Correction Factor
1	1.07
2	1.15
3	1.23
4	1.32
5	1.41
6	1.51
7	1.61
8	1.72
9	1.84
10	1.96

CHAPTER IV

PETROGRAPHY AND MODAL MINERALOGY

4.1   INTRODUCTION

Petrographical studies encompass systematic description and interpretation of rock textures in field and in hand specimen along with the mineral content which render invaluable information about the petrogenesis of igneous rocks. The elemental building units of all magmatic rocks are the Minerals. The minerals store within them different petrogenetic records which can be decoded by their morphologies (shape and sizes), chemical compositions, and their mutual interrelationships with each other and also in the enclosed minerals. Proper petrographic study under microscope therefore is a must to furnish important geological information that is concealed within their minute domain.

Hibbard (1995) considered textures developed in rock are the evidences of rock forming processes 'written in stone'. Textures are invaluable in indicating the cooling and crystallization rates of magma and also the phase relations during crystallization between the crystallized minerals and the parent magma.

Based on the macroscopic features observed in field in view of the mode of occurrences, the different litho-units and their associations accompanied by the microscopic observations, classifications of Karbi Anglong Hills Granitoids have been made.

4.2   PETROGRAPHY

Megascopically the Karbi Anglong Hills Granitoids (KAHG) are leucocratic to mesocratic and classifies as (i) fine to coarse grained and distinctly porphyritic, (ii) medium grained massive

nonporphyritic granitoids and (iii) moderately foliated granite gneiss. The granitoids mostly vary from grey to pink in color, usually massive and compact in nature, and are phaneritic.

In the porphyritic variety the phenocrysts are normally white-pinkish-brown feldspar within a greyish matrix consisting of quartz, plagioclase, biotite, hornblende and accessory minerals. The phenocrysts are of different sizes (upto 8 cm) while their nature ranges from sub spherical-elliptical to lenticular. Random and isolated, elliptical to tabular shaped mafic enclaves are not uncommon within the porphyritic granites.

The non-porphyritic variety are medium to coarse grained, appear in general as salt and pepper nature, and randomly host mafic clots of xenoliths, and frequently cut through by veins of coarser grained quartzo-feldspathic minerals.

Gneissic variant of KAHG is generally medium grained, foliated and sheared. The characteristic foliation is noted by the alternating lenses of leucocratic and mafic minerals in a preferred orientation. Slightly coarser interlocking granular minerals and darker lengthened minerals are perceptible.

The petrographic observations of granitoids and related rocks of Karbi Anglong hills have been documented in order to establish phase relationships and their genetic significance.

The Karbi Anglong Hills Granitoids in general shows a hypidiomorphic equigranular to inequigranular texture. Exsolution textures as myrmeckite, perthite and graphic are well noted. Major mineral phases of KAHG are quartz, alkali feldspar and plagioclase in varied proportion together with biotite. Accessory phases include titanite, apatite, zircon, epidote, and iron oxides; the mineral assemblages vary within the different types of granitoids. Magnetite with sub-cubic to rhombic shape, zircon with prismatic forms and apatite with spike structure occurs as inclusion in the larger feldspars and biotite crystals. The granitoids indicates erratic alterations which include replacement of biotite and plagioclase by chlorite and sericite respectively. Fractures are normally filled by secondary alteration minerals as magnetite, apatite, chlorite and epidote.

4.2.1 PORPHYRITIC GRANITOIDS (PGN)

The Porphyritic Granitoids vary from medium to coarse grained, grey to pink in colour. Kaziranga and Bagoria area granitoids (KZ) are porphyritic with subhedral phenocrysts basically

of K-feldspar, plagioclase and quartz. The finer grained groundmass consists of an assemblage of feldspars, quartz, biotite, and muscovite. Accessory minerals include apatite, zircon, titanite and opaques (Fe-Ti oxides).

Alkali-feldspars develop distinct cross-hatched texture with the bigger grains poikilitically enclosing finer plagioclase feldspars, quartz and few zircon minerals (Fig. 4.1a). The K-feldspar phenocrysts are subhedral and randomly oriented. Plagioclase minerals commonly exhibit simple twinning and show porphyritic texture. Cluster of subhedral phenocryst of plagioclase set in a finer matrix is also observed. Discrete zoning is observed within plagioclase porphyries, some display sieve-textured center (Fig. 4.1b) with colour variation from light to dark grey in the segmented zones of the grain under cross nicols. Sericitisation of the subhedral plagioclase feldspars are frequent (Fig. 4.1c). Myrmekite intergrowth at the boundary of graphic and perthitic textures are developed recurrently in the feldspar crystals (Fig. 4.1d&e). Quartz grains are frequently intergrown within alkali feldspar giving rise to graphic texture.

Biotites are anhedral to subhedral, flaky with one-set cleavage as well as massive. Flaky biotites are pale green while those of massive habit are commonly dark brown in color. Later crystals are anhedral and also interstitial in nature filling the cracks and rims within larger feldspar grains (Fig. 4.1f). Kaziranga Resort Picnic spot pink granitoids sporadically exhibit moderate bending of the subhedral tabular and flaky biotite along the cleavages (Fig. 4.2a). Bending of cleavages must have formed due to ductile deformation of flaky nature, and are commonly found proximal to subhedral Fe-Ti oxides. Such grains regularly exhibit typical 'bird's eye' extinction with variation from pink, blue, straw yellow to light green interference color (Fig. 4.2b). Primary as well as secondary biotites are distinctly seen. Greenish biotite is often accompanied by anhedral sphenes and Fe-oxides. Porphyritic granitoids however has comparatively less content of biotites compared with the gneissic varieties.

Amphiboles are rare, biotization of the hornblende is common; anhedral Fe-oxide grains are abundant, weathered (Fig. 4.2c&d) and sometimes develop a reddish-brown colour. Fine, euhedral acicular apatites are randomly dispersed as inclusions in larger quartz, biotite and plagioclase minerals. Titanite and Fe-ti oxides are poikilitically included within the biotite grains (Fig. 4.3a). Accessory grains of epidote frequently develop along the fractures of larger feldspar and biotite grains (Fig. 4.3.b). Grains of subhedral Fe oxides, minute zircon with pleochroic

haloes is associated as inclusions within biotite, growth of accessory titanite and epidote also seen at the peripheries (Fig. 4.3 c).

4.2.2 NON-PORPHYRITIC GRANITOIDS (NPG)

Non-porphyritic granitoids of Kathalguri (KH) and Numaligarh (NL) display an interlocking hypidiomorphic texture to equigranular texture (Fig. 4.4a) of medium grained mineral assemblages of potash-feldspar, quartz, plagioclase, and biotite. Zircons, opaques as magnetite, apatite ± amphibole are the main accessory phase in these granitoids. Contact of constituent minerals is sharp, exhibiting the characteristic of the individual minerals.

Quartz crystals are anhedral to subhedral with low relief, can be interlocking polycrystalline (Fig. 4.4 b) sometimes demonstrate undulose extinction which may suggest deformation. Quartz shows interference first order grey and pale-yellow color and are frequently intergrown within feldspar as vermicular forms depicting myrmeckite texture (Fig. 4.4 c). Perthite intergrowths in the form of string and flame type within the adjoining boundaries of alkali-feldspar and plagioclase grains are also observed (Fig. 4.4 d). Feldspars are sporadically sericitised along the cleavages giving it a hazy appearance; grain boundaries are irregular and highly corroded now and then. Subhedral microcline grains often show characteristic cross-hatched twinning. Zoning is occasionally observed in plagioclase feldspar. Plagioclase with secondary set of twinning, including albite twining (Fig. 4.4 e).

There are abundant greenish brown biotite grains and insignificant quantity of iron oxides in the NPG. Biotite is subhedral; generally, occur in close proximity to quartz and K-feldspar. Biotites show association with subhedral to euhedral rhombic crystals of sphene, though such crystals are less abundant. Minor inclusions of zircon (elongated/ sub-spherical) and apatite needles are observed frequently within the biotites (Fig. 4.4f) and dark brown massive biotite is lacking any cleavage while the flaky biotites shows development of cleavage (Fig. 4.4g). The latter with strongly pleochroic Bird's eye extinction under XPL exhibiting second order interference colours varying from blue, green, straw yellow to pink and under the plain polarised view it can be pale green to dark brown.

4.2.3 GRANITE GNEISS (GGN)

Granite gneiss outcrops are both in pink and grey varieties, darker coloured even in hand specimen as ferromagnesian minerals are easily recognized. GGN rocks are fine-medium subhedral grained, weakly foliated indicated by the alternation of thin melanocratic layers with leucocratic quartzofeldpathic bands. Lighter bands are thicker and more recurrent in comparison to the presence of mafic bands.

The granite gneiss dominantly contains coarser grains of quartz, feldspars within matrix of fine-medium crystals of biotite, quartz and feldspars. Fine grains of opaques are randomly dispersed besides other accessories as acicular apatite, subhedral titanite, pleochroic laths of zircon and hornblende.

Medium grained quartz displays a poikilitic texture enclosing finer grained quartz, biotite and scanty feldspars. Quartz shows anhedral to subhedral texture.

Cross hatching subhedral microclines crystals are less common. Perthite exsolution of microcline within plagioclase appear to be on the initial development phase on some grains. K-feldspar and plagioclase grains have myrmekitic natured contacts. Recrystallized finer crystals of plagioclase within larger grains of microcline grains are observed in Gajraj granitoids (Fig. 4.5a). Plagioclase and alkali feldspar develops sericitization in granite gneiss.

Biotite is the main mafic mineral in the granite gneiss. The crystal is finer and more copious in comparison with PG and NPG. Nature of the grain is subhedral slender, platy, pleochroic from dark brown to yellowish, pink, blue, and frequently elongated exhibiting preferred orientation along the schistosity of the rock (Fig. 4.5b). Biotites are also present as interstitial grains (Fig. 4.5c) and are frequently transformed to chlorite. Fragments of sphene and iron oxides are closely associated with biotite.

Subhedral to sub rhombic Fe-Ti oxides generally lie adjacent to the biotite grains or within cleavages and borders of grains like biotite and feldspar. Fe-Ti oxides are medium to occasionally broad in width and spread randomly (Fig. 4.5d). Zircon exhibit the characteristic pleochroic halo and develop adjacent to the biotite margins. Accessory epidote is seen within the cluster of biotite grains in Gajraj granite gneiss (Fig. 4.5e).

4.2.4   BASEMENT GRANITE GNEISS (BGN)

Basement granite gneiss represented by Karkok (KG), Centre Bazaar (CB) and Loringthepi granitoids (LG) are mesocratic with faint gneissosity. Mineralogically, the rocks do not hold much difference from the granite gneiss, therefore only the obvious characters are illustrated; Presence of amphibole is characteristic of BGN (Fig. 4.6a), while its presence is very erratic in GGN.

Sericitisation of the subhedral feldspars are frequent. Feldspar hold exsolved growths like perthites and have myrmekitic natured contacts. Quartz grains are subhedral medium grained, show color variation from pale yellow to dark gray in cross polars. Some crystals are broader with serrated anhedral outline.

Bioitites are anhedral to subhedral, fine to medium grained and interstitial. It represents the majority of the ferromagnesian minerals and show color alteration with varying intensities from green to brown. The stretched biotites accompanied by slightly flattened quartz and feldspars exhibits the schistose nature of the rock. Biotite is commonly associated with hornblende and titanite (Fig. 4.6b). Subhedral Fe-Ti oxides (mainly magnetite) in close contact with greenish brown biotite is common. Slender apatite spikes and zircon laths represent the majority of the accessory minerals.

Subhedral rhombic brown titanite are observed having association with biotites. They appear moderately fractured and display high relief (Fig. 4.6c). Anhedral grains of accessory Amphiboles are noted with color variation from yellowish brown to olive green under cross nicols. Mostly the amphiboles have undergone chloritization (Fig. 4.6 d) and biotitization.

4.3   MODAL MINERALOGY AND IUGS CLASSIFICATION

Based on the results of the petrographic study, modal analyses (volume percentage of the mineral constituents) of 22 thin section samples of KAHG which is representative of PGN, NPG, GGN and BGN were carried out. Results acquired are represented in Table 5. Recalculated Q (quartz) - A (alkali feldspar) - P (plagioclase) are plotted according to International Union of Geological Sciences (IUGS) recommendations (Streckeisen, 1976; Fig. 4.7). Modal percentages of NPG correspond to monzogranite with a few exceptions of syenogranite and quartz monzonite. The

modal composition of PGN correspond to monzogranite and syenogranite. GGN occupy the field of monzogranite while BGN belong both to syenogranite and monzogranite.
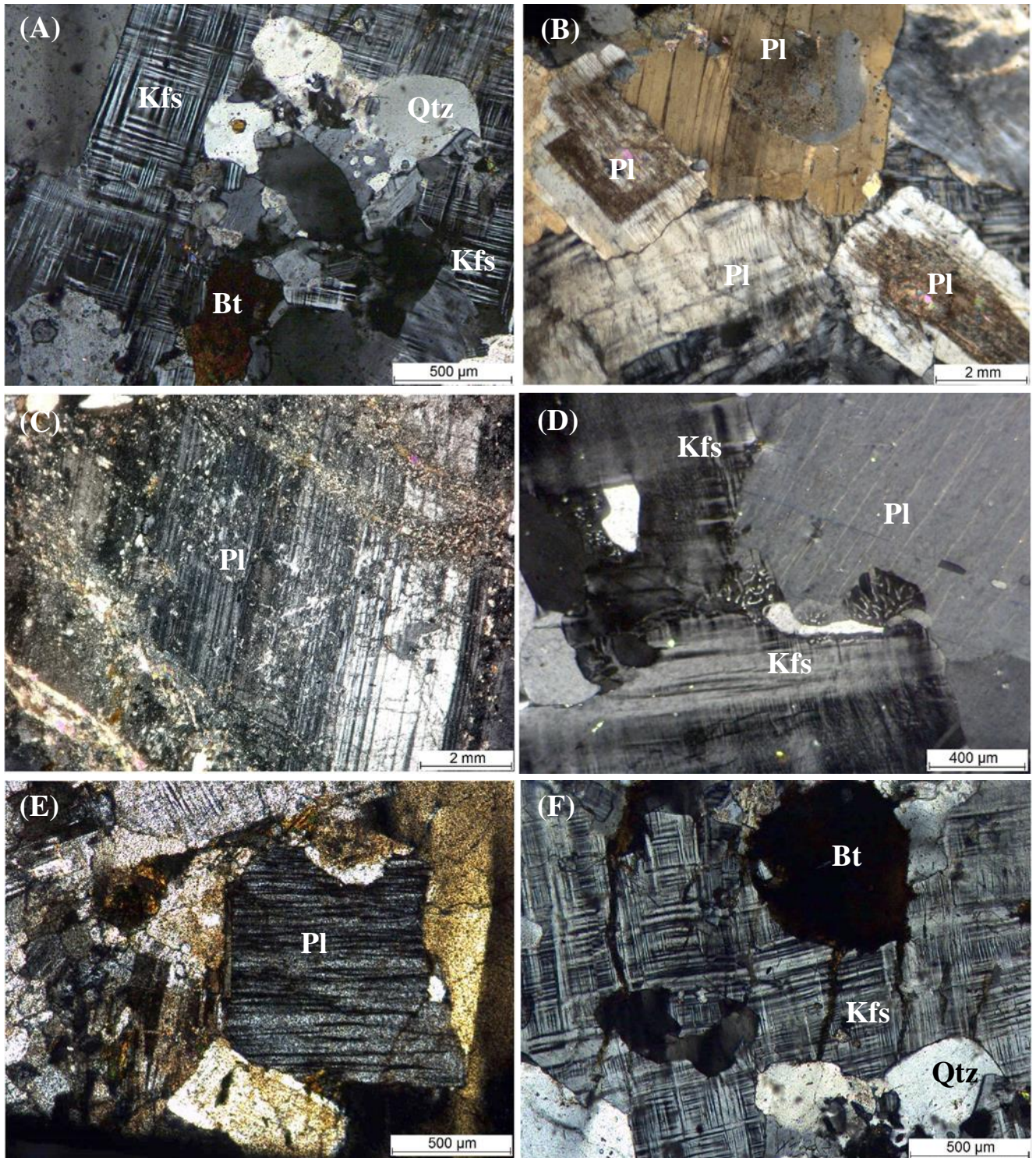
Figure 4.1: Photomicrograph of feldspar in porphyritic granitoids of KAHG showing (A) well developed cross-hatched texture in microcline grains poikilitically enclosing finer grained plagioclase; quartz and zircon (B) discrete zoning within plagioclase porphyries which displays sieve-textured center (C) sericitisation of plagiocalse feldspars (D) myrmeckite texture developed at feldspar grain outline, perthitic and graphic texture also preserved (E) perthitic intergrowth developed in feldspars crystals (F) Interstitial biotite fills the cracks and rims within larger feldspar grains.
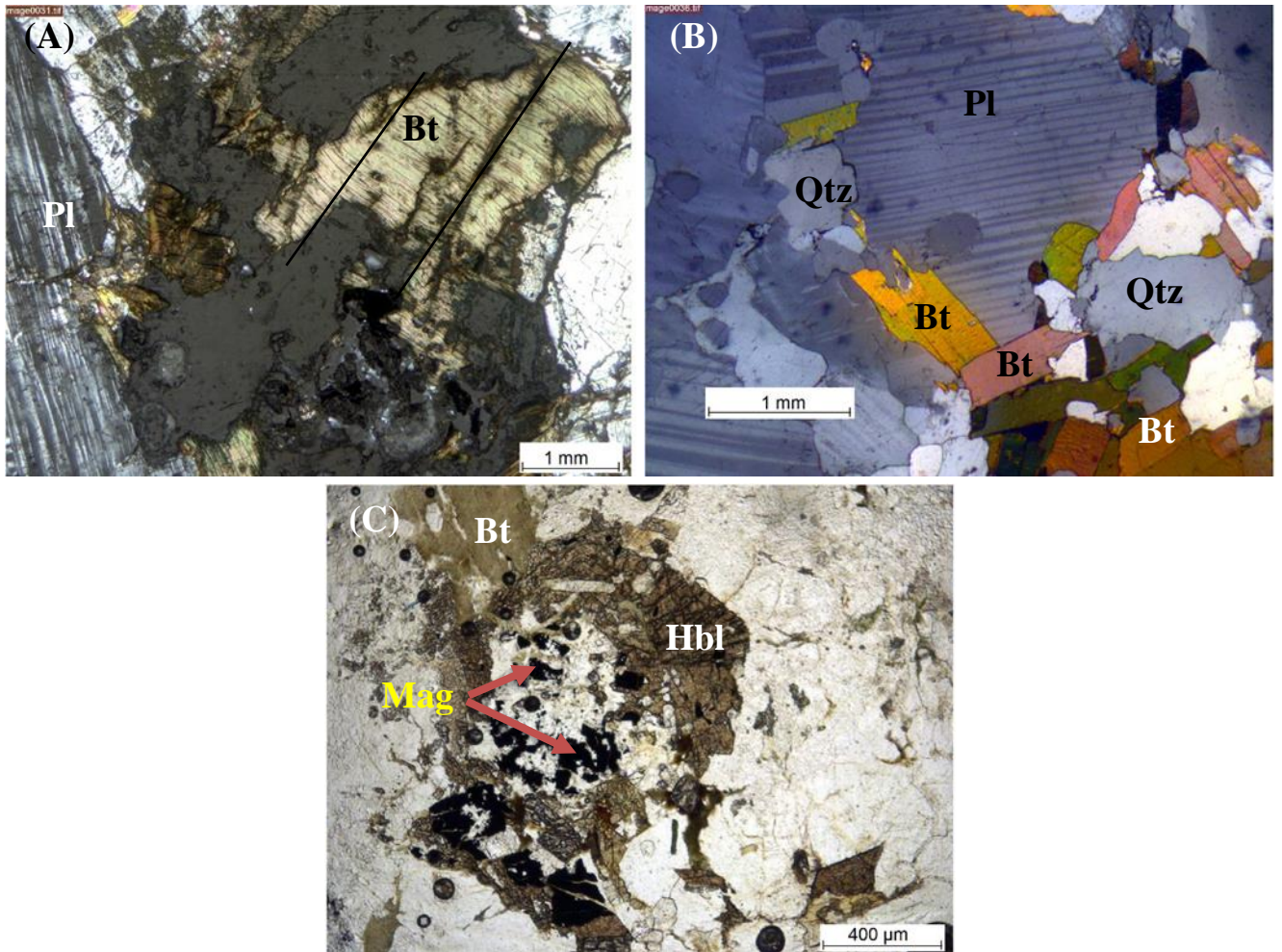
Figure 4.2: Photomicrograph of biotite and amphibole in porphyritic granitoids of KAHG showing (A) kink bands by subhedral flaky biotite along the cleavages (B) biotites exhibiting typical 'bird's eye' extinction with variation from pink, blue, straw yellow to light green interference colors (C) biotitization of hornblende under plane polarized light; note the random abundance of Fe oxides
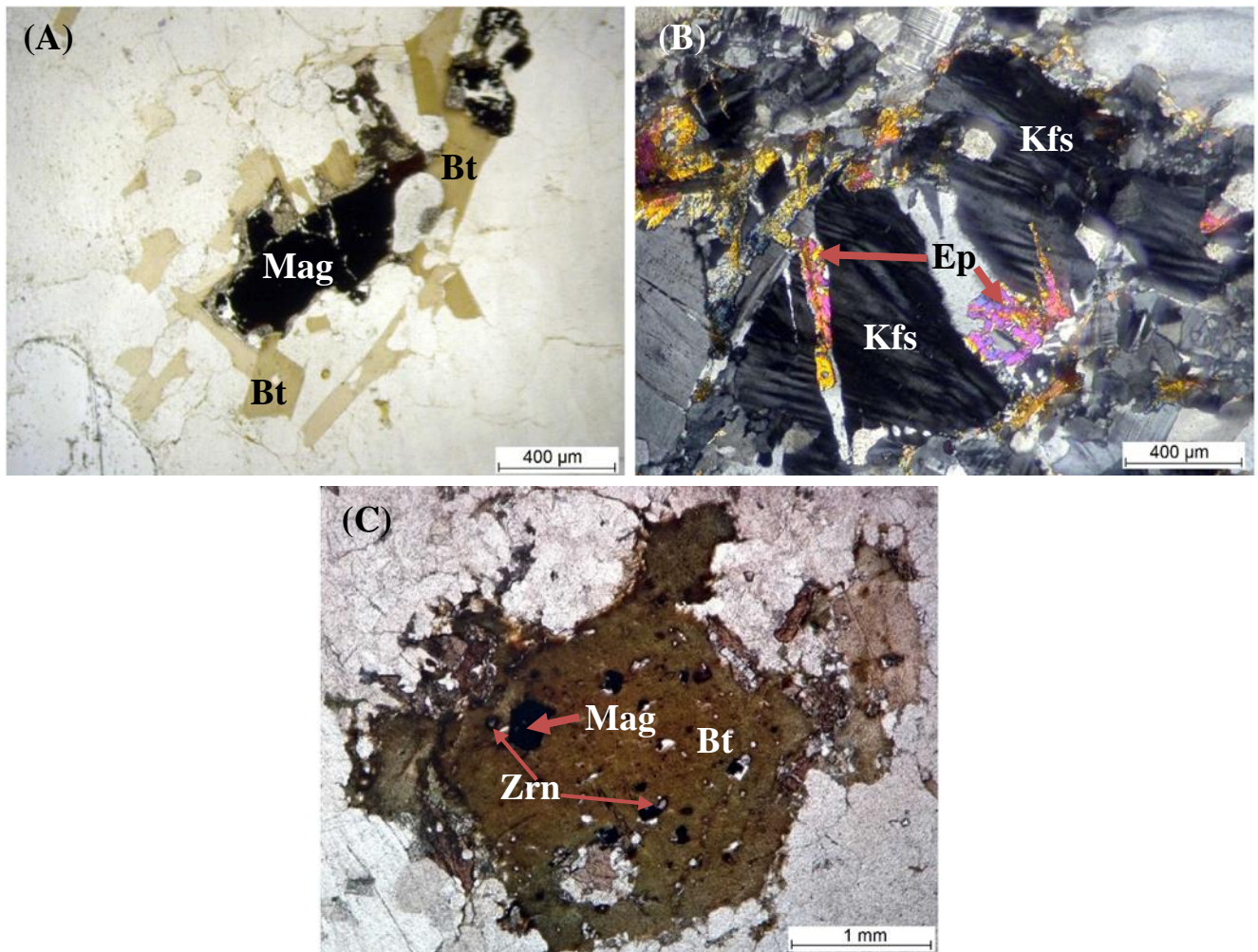
Figure 4.3: Photomicrograph of common accessory minerals in porphyritic granitoids of KAHG (A) poikilitic inclusions of titanite and Fe oxides within the biotite (B) development of epidote along the fractures of feldspar grains (C) biotites showing inclusions of zircon under plane polarized light; note the development of resorption texture along the margin.
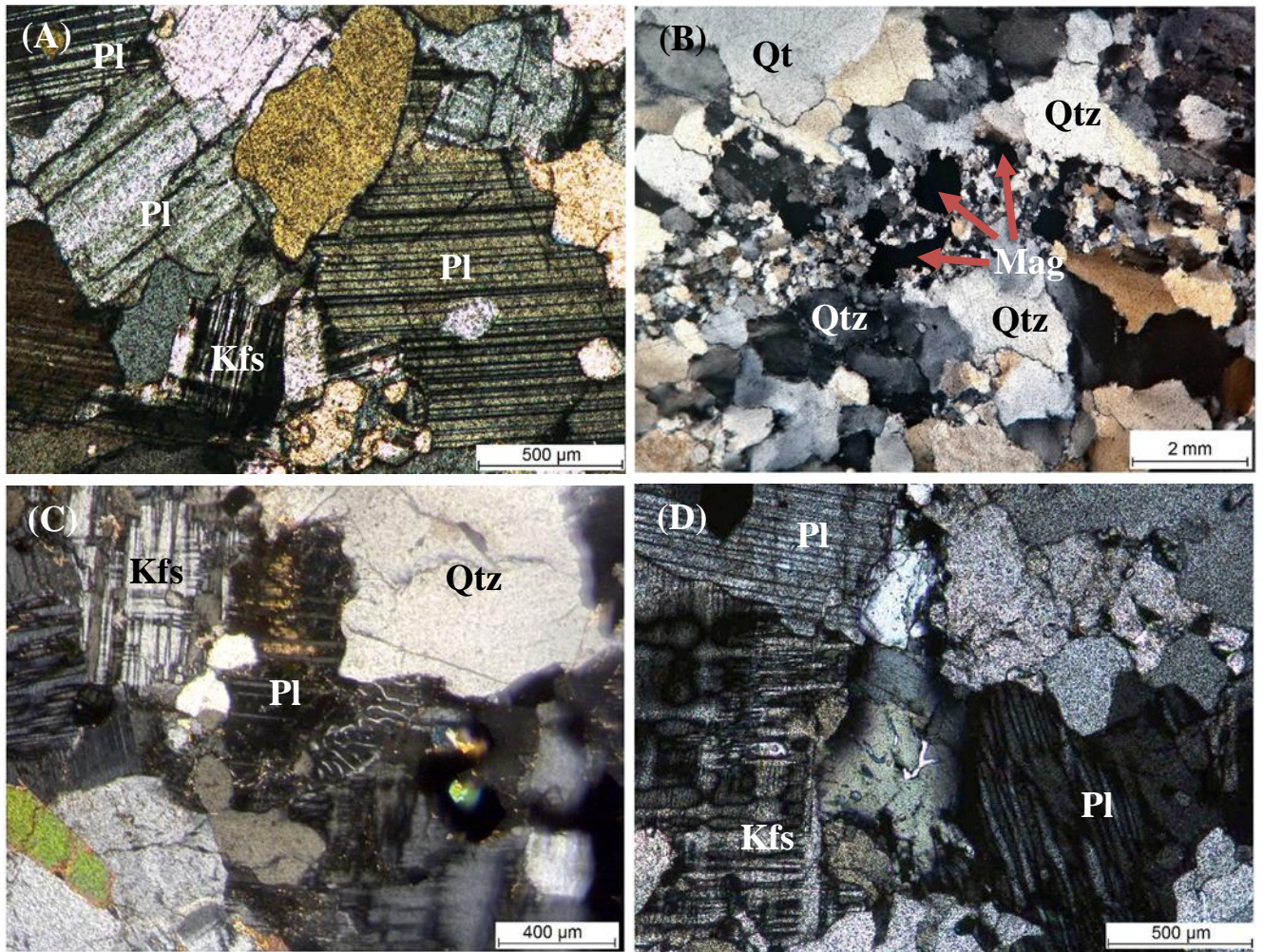
Figure 4.4: Photomicrograph of non-porphyritic granitoids of KAHG showing (A) hypidiomorphic, equigranular to interlocking texture (B) anhedral to subhedral interlocking polycrystalline quartz crystals are with low relief (C) myrmekite texture and (D) perthite intergrowths at the adjoining area of alkali-feldspar and plagioclase.
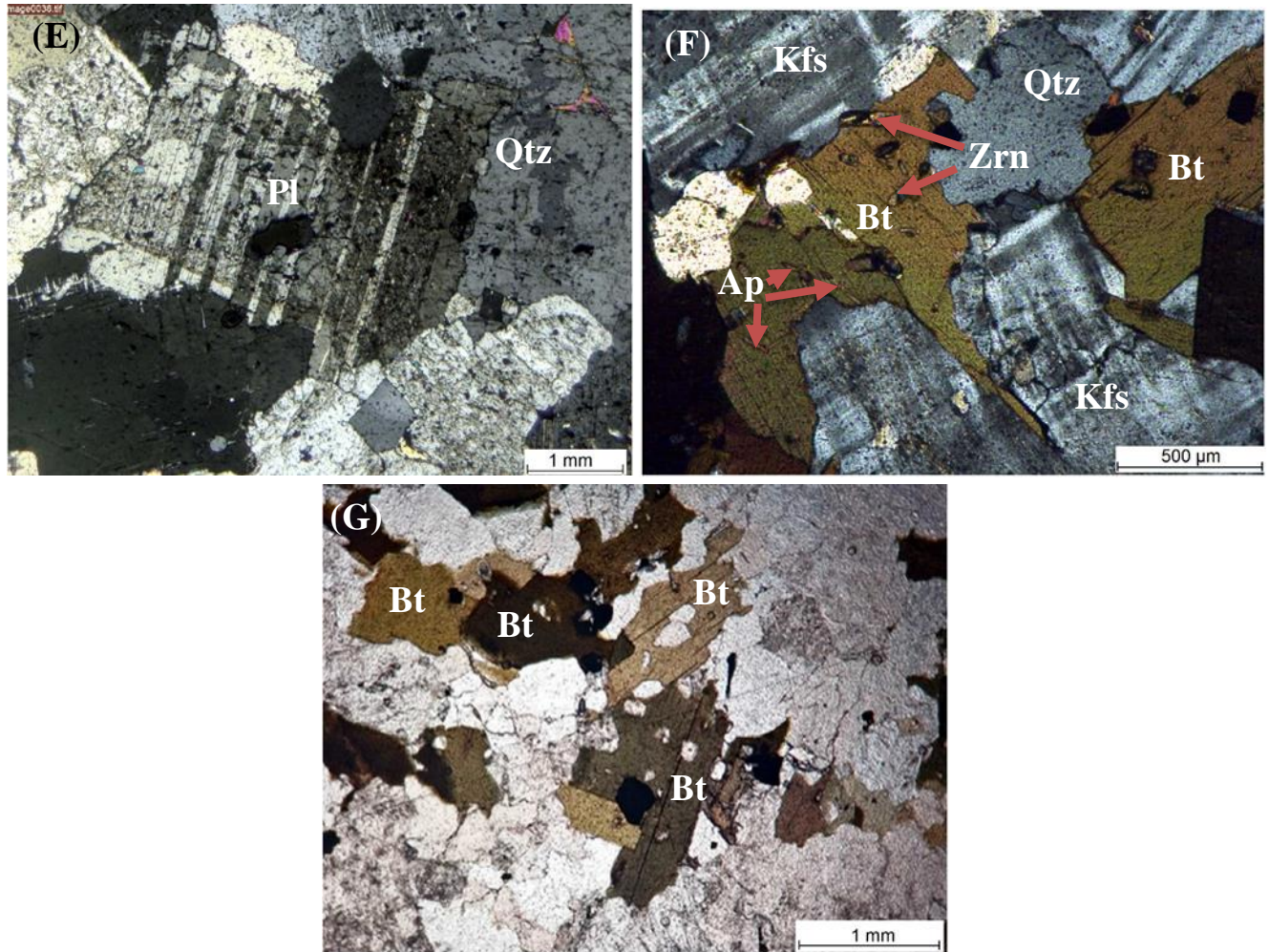
Figure 4.4: (E) albite twinning exhibited by plagioclase feldspar (F) inclusions of zircon and apatite needles observed within the biotites (G) massive nature of biotite without cleavage and platy nature with cleavage
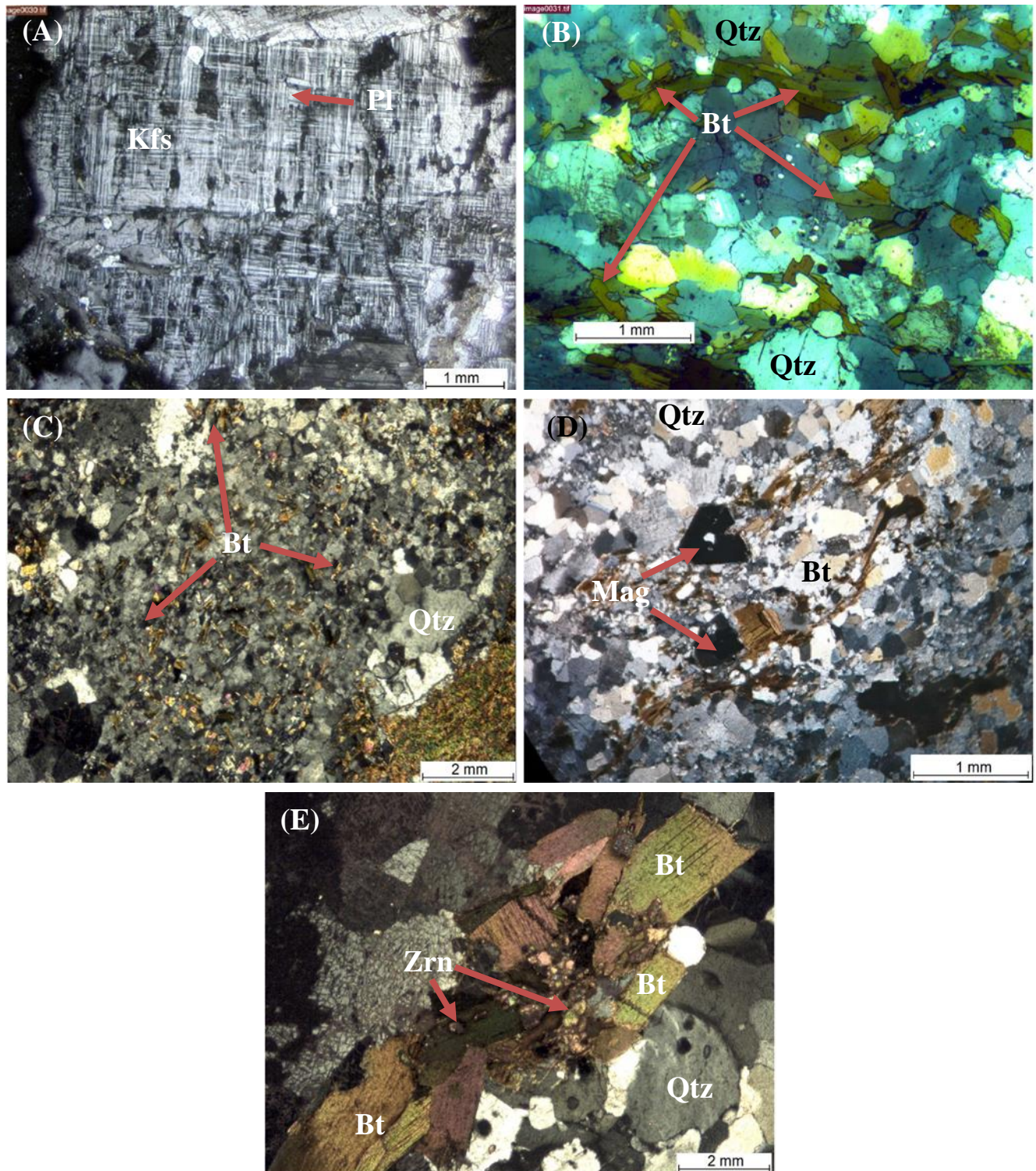
Figure 4.5: Photomicrograph of granite gneiss of KAHG showing (A) recrystallized crystals of plagioclase within larger microcline laths grains (B) subhedral, platy, lenticular pleochroic biotites are elongated displaying preferred orientation (C) interstitial grains of chloritized biotite (D) subhedral to sub-rhombic iron oxides in close proximity to biotite (E) accessory epidote within the cluster of biotite grains. Note the preferred orientation of biotites.
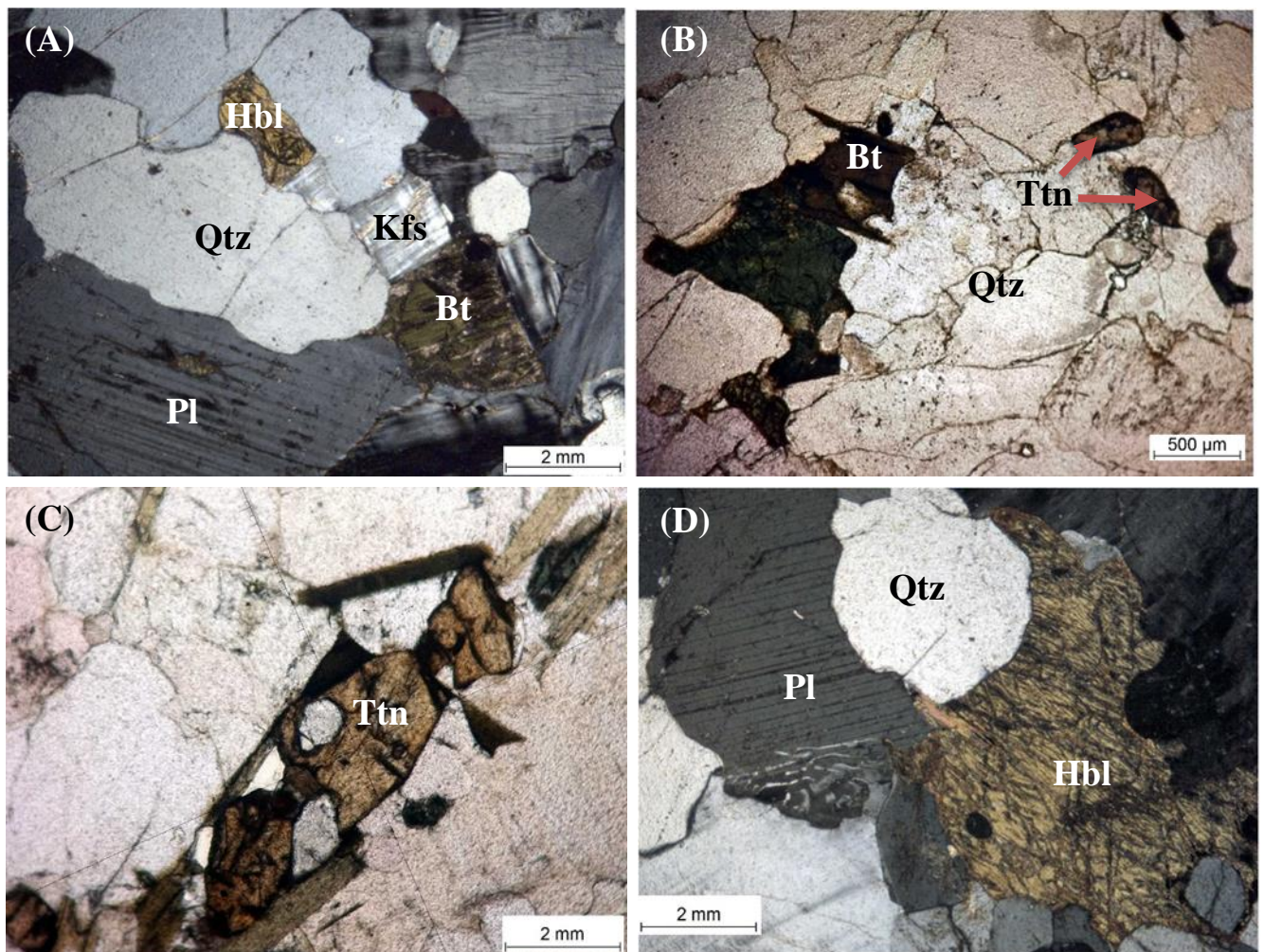
Figure 4.6: Photomicrograph of basement granite gneiss showing (A) pale olive green- brownish amphibole grain near feldspars (B) close association of biotite with hornblende and titanite (C) moderately fractured rhombic titanite crystal with high relief (D) chlorititization and biotitization of amphibole.
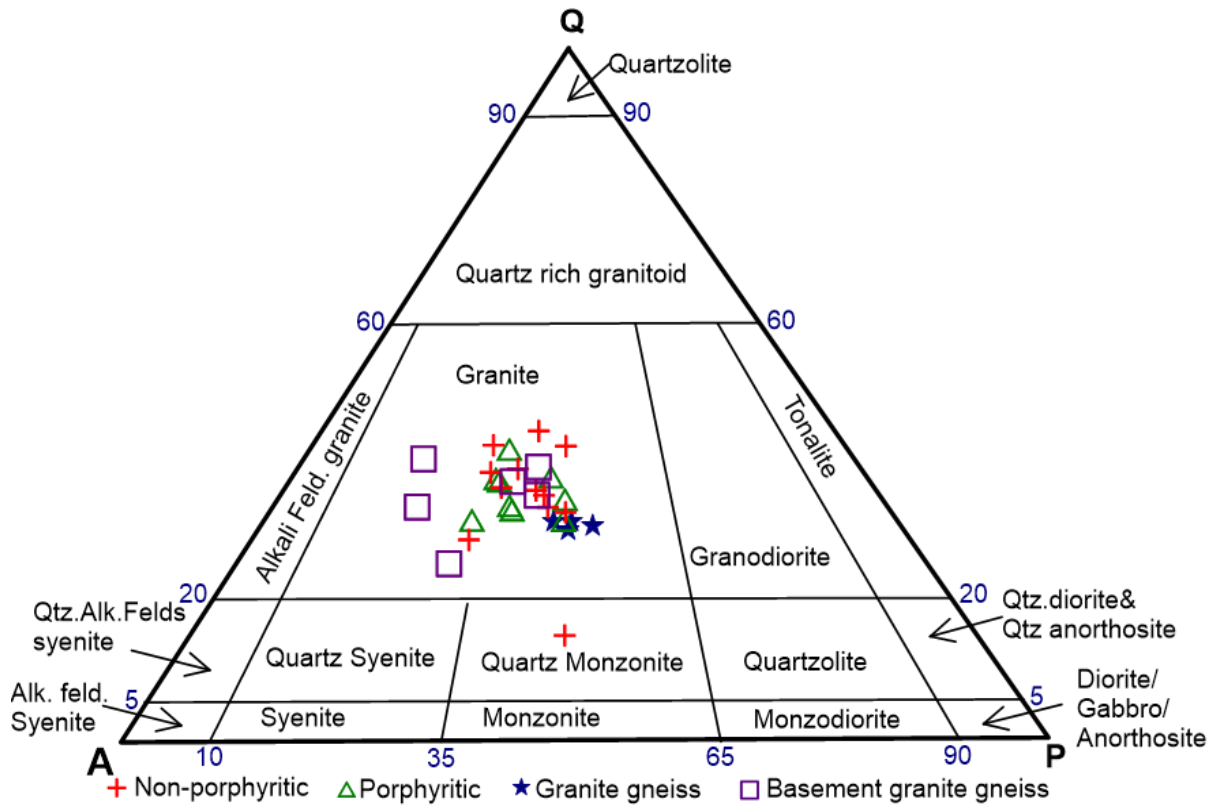
Figure 4.7: Quartz (Q)-Alkali-feldspar (A)-Plagioclase (P) triangular plot representing the modal composition of porphyritic granitoids (PG), non-porphyritic (NPG), granite gneiss (GGN) and basement granite gneiss (BGN) (after Streckeinsen, 1973; Le Maitre, 2002). Index: Red Cross= NPG, Green triangle= PGN, Blue star= GGN, Purple square= BGN

TABLE 5: MODAL MINERAL CONSTITUENTS (VOLUME PERCENTAGE) OF
REPRESENTATIVE SAMPLES OF KAHG

PORPHYRITIC GRANITOIDS (PGN)

Sl. No	Sample No	Quartz	K-feldspar	Plagioclase	Biotite	Accessories*	Total
1	KZ-14	29.3	33.7	28	1.7	7.3	100
2	KZ-15	36.6	34.4	20	0.2	8.8	100
3	KZ-17	26.01	31.43	27.21	7.14	8.21	100
4	KZ-42	28.16	41.42	19.74	5.5	5.18	100
5	KZ-45	32.2	30.05	25.29	3.81	8.7	100.05

NON- PORPHYRITIC GRANITOIDS (NPG)

Sl. No	Sample No	Quartz	K-feldspar	Plagioclase	Biotite	Accessories*	Total
1	KZ-4	34.2	36	19.3	2.5	8	100
2	KZ-5	31.1	33	29.1	1.79	5.01	100
3	KZ-7B	28.5	29	24	8.9	9.6	100
4	KZ-9	28.1	29.7	23	7.8	11.4	100
5	KZ-10	38.03	27.3	25.8	0.97	7.91	100
6	KZ-11	24.1	36.8	19.3	7.8	12.5	100.5
7	KZ-19	41	22.5	20	7.3	9.2	100
8	KZ-22	38.2	34.4	18	1.9	7.5	100

GRANITE GNEISS (GGN)

Sl. No	Sample No	Quartz	K-feldspar	Plagioclase	Biotite	Accessories*	Total
1	AO2	29	31.3	18.5	7	14.2	100
2	KZ-18	24	29.7	27	10.1	9.9	100.7
3	KZ-21	27.3	33	21.2	11	7.5	100
4	KZ-27	23.3	29.7	31.8	6.5	8.7	100
5	KZ-29	25.7	35	29.5	2.1	7.4	99.7

BASEMENT GRANITE GNEISS (BGN)

Sl. No	Sample No	Quartz	K-feldspar	Plagioclase	Biotite	Accessories*	Total
1	KZ-1A	13.8	39.7	38	15	7.7	100.7
2	KZ-1C	25.9	35.7	29	2.7	6.8	100.1
3	KZ-3A	21	36.9	31.3	2.3	8.6	100.1
4	KZ-3	23	37.1	30	2.9	6.9	100

*Sphene, muscovite, hornblende, apatite, zircon, magnetite and ilmenite

CHAPTER V

MINERAL CHEMISTRY

5.1   INTRODUCTION

Minerals can be pictured by the recurring patterns of their fundamental crystal configuration, which can be protracted into three dimensional macroscopic crystals. Further, the chemical composition of the mineral is a more standard basis of classification or description. The majority of minerals are ionic compounds and comprises systematic arrangements of variable charge size anions and cations.

Mineral chemistry study is crucial to infer substitution relation and chemical variations. In an effort to decipher the physical condition and the evolution of KAHG, some important rock forming minerals of KAHG are studied. Maintaining the apparent limiting factors, empirical and experimental standardized geothermobarometers are employed whereby the EPMA database of biotite and feldspars were taken into consideration.

This chapter presents the chemical analyses of the feldspars and biotite present in KAHG. Electron probe micro analyses (EPMA) of rock-forming minerals (plagioclase and biotite) constituting these granitoids have been carried out from the representative samples of studied lithotypes, which help decipher mineral-chemical evolution, classification, elemental substitution relationship, nature and physical conditions of host magma evolution.

Electron Micro-Probe Analysis data on 37 plagioclases, 30 individual mineral grains of alkali feldspar, and 175 biotites are presented in Tables 6, 7 & (8-17) respectively.

5.2   FELDSPAR

Owing to the ubiquitous nature of feldspar minerals in majority of the igneous rocks in conjunction with the vast range of its members, the feldspars are inevitably fundamental in the categorization

of the igneous rocks. Chemically the feldspar family is divided within the ternary end members K-feldspars ($KAlSi_3O_8$) to Albite ($NaAlSi_3O_8$) to Anorthite ($CaAl_2Si_2O_8$). Constituents between the former end members and the later end members are referred to as alkali feldspar and plagioclase feldspar respectively.

5.2.1   COMPOSITION AND CLASSIFICATION OF FELDSPAR

Relatively fresh samples of feldspar from KAHG are selected and progressed with the electron microprobe analysis. The analytical result of plagioclase composition along with their calculated structural formulae based on 8 oxygen atoms and end-members are given in Table 6.

The general formula of plagioclase is XZ_4O_8 where X=Ca, Na, K and X=Si, Al.

The structural formula of the analyzed plagioclases parallels to the ideal formula. Other ions, which are present in very limited amount, include Fe. The feldspars are classified in terms of end-members Or-An-Ab (Fig. 5.1).

Composition of plagioclase in the PGN ($An_{7.18}Ab_{88.73}Or_{0.29}$-$An_{10.96}Ab_{92.48}Or_{0.59}$), NPG ($An_{10.86}Ab_{86.68}Or_{0.39}$-$An_{12.51}Ab_{88.76}Or_{2.04}$), GGN ($An_{14.28}Ab_{82.48}Or_{0.70}$-$An_{16.13}Ab_{84.48}Or_{1.80}$) and BGN ($An_{23.44}Ab_{70.70}Or_{0.69}$-$An_{27.50}Ab_{75.87}Or_{2.04}$) varies from albite to oligoclase with the exception of one albitic plagioclase (KH8). The plagioclase in albite field is more altered and sericitized compared to the plagioclase of oligoclase compositions.

Broadly, equivocal range of $An_{7.17}$ (albitic) to $An_{27.50}$ (oligoclase) was noted from all samples irrespective of the nature of granitoids except for an abnormal value of $An_{1.768}$ (NPG). Orthoclase component for all granite variant shows minor variation from $Or_{0.30}$-$Or_{2.04}$. Major distinction is recorded with respect to the ranges in anorthite and albite in all granite type.

Plagioclase of PGN is predominantly albitic in composition while GGN and BGN variety is entirely of oligoclase and BGN records the maximum value of anorthite ($An_{27.50}$) within the plagioclase (Fig. 5.1).

In the compositional variation of plagioclase from KAHG, in terms of Ab-An-Or components Fig. 5.1) two cluster is observed, where PGN, GGN and NPG (samples KH8, AR) are clustering closer to the sodic rich end while BGN (samples LG, KG) plots very close to the Oligoclase series.

PGN samples (KZ-33 and KZ-15) hosts a varying nature of plagioclase which are unaltered, along with zoned and sericitised plagioclases which probably caused the albitic composition. Boxy-cellular plagioclase is frequently observed in the NPG variety (sample KH-8). Such morphologies are suggestive of an active undercooling in a magma mixing situation where intrusion of a mafic magma happened as the plagioclases were crystallizing. GGN frequently shows resorbed plagioclase within larger microcline. Experimental works indicated that plagioclase having endured intense undercooling is most likely to show crystals which are more sodium rich than that which grows in equilibrium circumstances (Lofgren, 1974). Sodic growth is thus restricted in diffusion and exhibit crystals with more sodic composition. Plagioclase morphology and the enhanced sodic compositions are well clarified by the growth mechanisms (Bennett et al., 2019).

SiO_2 content in plagioclase ranges from (61.76-68.93 wt.%). The highest SiO_2 content (68.93 wt.%) is observed in NPG. The Al_2O_3 content of KAHG is moderate with values ranging from 19.37- 23.71 wt.%.

K-feldspars in almost all the samples of KAHG correspond to orthoclase ranging from $An_0Ab_{2.80}Or_{89.7}$-$An_{0.36}Ab_{10.20}Or_{96.76}$). BGN samples show the most significant difference in the orthoclase component with lower value $Or_{89.7}$ to higher value of $Or_{96.06}$ Table-7. Albite mole % ranges from $Ab_{2.80}$- $Ab_{10.20}$ along with very low anorthite component <0.36 mole %. Thus, entirely of the plagioclases remain poor in the orthoclase end-member while the alkali feldspars are deprived in the anorthite end-member.

5.3   BIOTITE

Biotite, a hydrous ferromagnesian mineral, is an abundant mineral within granitoids. It is an important component which is fit to indicate the redox conditions of felsic magmas (e.g., Wones & Eugster 1965; Czamanske et al., 1981; Burkhard 1991, 1993). Biotite have been proved effective in evaluating the redox state and nature of felsic melts (e.g., Kumar et al., 2005, 2006; Kumar & Singh, 2008; Kumar & Pathak, 2010, Ishihara & Imai, 2014; Bora & Kumar, 2015; Singh et al 2016). The general formula of biotite is $X_2Y_6Z_8O_{20}(OH)_4$ where, X=K, Na and Ca; Y=Al^{VI}, Mg, Fe, Mn, Cr and Ti; and Z=Si and Al^{IV}.

Biotite is the most widespread ferromagnesian mineral occurring in all types of granitoids rocks in Karbi Anglong Hills. The observed pleochroism within the biotite minerals varying from pale green to brownish green reflects chemical composition differences in the different granitoids.

Electron microprobe analysis of total 175 spot of biotites is obtained; 82 from NPG, 56 from PGN, 25 from BGN and 14 from GGN. Table 8-17 lists the structural formulae and chemical composition of the biotites analyzed and worked out on the basis of oxygen atoms.

5.3.1   COMPOSITION AND CLASSIFICATION

In accordance with the Foster (1960) method which deliberates on atoms per formula unit (apfu) occupied at T (Tetrahedral) and M (Octahedral) positions of chemical structure, the biotite minerals of KAHG were categorized.

The variations in X_{Mg} of biotites (Table 8-17) are prominent with BGN (KG, LG) (X_{Mg}= 0.59-0.71) showing the highest values, followed by KZ15-KZ17-NL-AR (X_{Mg}= 0.46-0.58), and KH-GG-KZ-33 (X_{Mg}=0.30-0.42) being the least range of X_{Mg}. Higher values of X_{Mg} (0.71) is recorded in gneissic variety while the lower X_{Mg} values of (0.30) in leucogranites. These differences in compositional groups with regard to the annite and phlogopite activity might be symptomatic of diverse nature of crystallization of the biotites from their primary melt.

According to Czamanske & Wones (1973) the X_{Mg} (Mg/Mg+Fe^t) of biotite is a sensitive and an ideal indicator for the redox conditions of the crystallizing magma. The higher X_{Mg} values can be conclusive of biotite minerals which has an oxidizing environment during their crystallization rather than a reducing condition (Ishihara et al., 2002, Kumar & Pathak, 2010, Bora & Kumar, 2015).

Ternary plot of the relative mole fraction of Mg^{+2}, Fe^{+2} and Fe^{+3} ions in biotite of KAHG after Beane, 1974 (Fig. 5.2a), mostly lie within or close to the field of primary biotite. An exception is the BGN (LG&KG) which falls close to the field of hydrothermally altered biotite being slightly enriched in phlogopite component.

Biotite compositions diagram (Fig. 5.2b) in terms of Mg-(Al^{VI}+Fe^{3+}+Ti) -(Fe^{2+}+Mn) after Foster (1960) affirms that the KG and LG biotites of BGN locates within the field of Mg- biotite, a little above the Fe^{2+} biotite field while biotites of NPG (NL, KH, AR), PGN and GGN have broad

compositional affinity with Fe^{2+} biotites having a minor difference in the contents of Mg, Fe^{2+}, and Mn. LG biotites are relatively enriched in magnesian as compared to KG biotites. The X_{Mg} (=Mg/Mg+Fe^t) of biotites of BGN (KG=0.59-0.63 and LG=0.65-0.71) are significantly higher than that of biotites of PGN (KZ=0.30-0.55), and NPG (KH=0.36-0.42, NL=0.50-0.53, AR=0.53-0.58) and GGN(GG=0.33-0.40).

In Fe^t/Fe^t+Mg vs Al ^{IV} (Fig.5.3), diagram of Deer et al., (1963) the biotites closely cluster mostly within eastonite to siderophyllite fields and near boundary separating these two end-members.

The biotites in general show significant variations in the X_{Fe}(=Fe^t/Fe^t+Mg) ratios (0.29-0.7) and Al^{IV} contents (0.66-1.25apfu). The PGN and NPG variety has higher Al^{IV} content i.e., NPG (NL=1.09-1.14 apfu; KH8A = 1.1-1.14 apfu; KH7A= 1.12-1.16 apfu; AR = 1-1.04 apfu) and PGN (KZ33= 1.09-1.15 apfu; KZ15= 1.11-1.25 apfu; KZ17= 0.99-1.1 apfu). However, the GGN (0.66-1.07 apfu) and BGN samples (KG=1.04-1.09 apfu; LG=0.82-1.09 apfu) has shown considerably less Al^{IV} content. The elevated Al^{IV} content in biotite could be suggestive of crystallization from a magma which was more saturated in aluminium derived from a crustal contaminated source and/or metapelitic (e.g., Batchelor, 2003). The biotites of BGN (LG-KG) have also shown a narrow range of X_{Fe} (=Fe^t/Fe^t+Mg=0.29-0.41) whereas biotites from the GGN (GG), PGN (KZ) and NPG (KH, NL, AR) reflect a wider variation with high content of X_{Fe} (Fe^t/Fe^t+Mg=0.42-0.7). Such disparity gives a hint of inclusion of different crustal matters during the genesis along with differentiation in the degree of fractionation (Kumar & Pathak, 2010; Bora & Kumar, 2015).

According to the ternary diagram of MgO-FeO^t-Al$_2$O$_3$ (Fig. 5.4) after Albuquerque (1973) which illustrates the compositional affinity of biotites in KAHG, samples KG, LG and AR trend in the direction of the field of biotite related with hornblende, pyroxene/ olivine, which are features of calc-alkaline, metaluminous (I-type) melts of subduction zone affinity, suggesting their relations with mantle components. Biotites from NL, KH, GG and KZ however shows a broader compositional affinity which resembles the biotites allied with and/or without the other ferromagnesium minerals and muscovite and alumina-silicates, which are characteristics of peraluminous (S-type) granitoid melts formed in syn-collisional environment.

The ternary diagram TiO$_2$–FeO*–MgO (FeO* = FeO + MnO) by Nachit et al., (2005), reflects that the KAHG have compositions that are more or less akin to hydrothermally re-equilibrated biotite

with few exceptions from (KH7 and KZ33) falling under the field of primary magmatic biotites (Fig. 5.5). The TiO_2–FeO–MgO parameter thus served as a quantitative tool to differentiate the biotites of primary magma from that of re equilibrated nature due to the actions of hydrothermal water.

5.3.2   NATURE OF HOST MAGMA

The major elemental composition of biotites crystallized in the primary rocks can be employed to reflect the nature of the host magma and the tectonic regime as well. Biotite show variation in silica content from (SiO_2= 34.46-39.31wt. %) which is relatively low. PGN rocks belonging to Kaziranga area (KZ-15) shows the least value of SiO_2 (34.46 wt.%). SiO_2 content of Amguri granites (AR) (38.24-39.31wt.%) of NPG variety shows the highest value, which does not vary substantially from that of biotites of BGN (KG-LG =37.95-39.28wt. %).

The Al_2O_3 content is rather high and fluctuate from 12.95 to 16.86 wt.% for the PGN and NPG which is slightly higher than the GGN and BGN (12.08 to 13.65 wt.%). The Al_2O_3 content exhibit negative correlation with silica.

The PGN (KZ) have the minimum TiO_2 range (TiO_2=0.95-2.87 wt.%), followed by the NPG i.e., KH, NL and AR (TiO_2=1.55-3.03 wt.%). GGN (GG TiO_2=2.01-2.41 wt.%) and BGN (LG and KG; TiO_2=1.96-3.5wt.%) have the maximum TiO_2 content.

Biotite from KG (FeO^t/MgO=1.06- 1.22; Table 7) and LG (FeO^t/MgO=0.73- 0.98, Table 8) plutons have the least value of FeO^t/MgO ratio (<1.22) and less aluminous (Al^t=1.09-1.21) components, which point to biotites crystallized in calc-alkaline subduction-related, metaluminous (I-type) granitoid melt (Abdel-Rahman, 1994). Biotites of AR (FeO^t/MgO=1.28-1.59), KZ-15& KZ-17 (FeO^t/MgO=1.47-2.09) and KH-NL (FeO^t/MgO= 1.57-3.22) show quite higher FeO^t/MgO ratios. The recommended FeO^t/MgO ratio of 3.48 for the biotites crystallized in a peraluminous suite (Abdel-Rahman, 1994) and consequently biotites of GG (FeO^t/MgO=2.64-3.59) and KZ-33 (FeO^t/MgO=3.29-4.11) are more aluminous, with low-Mg which must have been achieved in a typical syn-collisional, peraluminous (S-type) granitoid magma (Abdel-Rahman, 1994).

The chemical evaluates of the KAHG biotites when plotted in the tectonic discrimination diagrams of Abdel-Rahman (1994) in terms of Al_2O_3 Vs FeO^t, Al_2O_3 Vs MgO and MgO Vs FeO^t (Fig. 5.6a, b & c) suggests that there is a dominance of biotites having affinity for calc-alkaline I-type

orogenic suite with a few samples of PGN (KZ) and GGN (GG) having affinity with evolved peraluminous S-type suites (Fig 5.6a & c). MgO Vs FeO^t diagram show a negative correlation and non-porphyritic granitoid KH along with the former two samples cluster close to the calc-alkaline and peraluminous field boundary, suggesting dominance of Fe$\rightleftharpoons$Mg substitution during biotite evolution.

In terms of ternary oxide MgO- FeO^t- Al$_2$O$_3$ diagram of (Abdel-Rahman, 1994), however the analyzed biotites occupy a distinct plot within the compositional affinity of biotites in calc-alkaline suite (mostly orogenic subduction- related) I-type granitoids (Fig. 5.7). An exception is the porphyritic granitoids (KZ-33) which falls slightly within the field of biotite in peraluminous (including S- Type) Suites.

However, biotite classification diagram after Nachit (1985), based on Mg and Al components, majority of biotite crystals have affinity with peralkaline rocks. PGN (KZ17, KZ15) and NPG(NL) biotites show transitional alkaline and peralkaline nature though closer to the lower limit with the alkaline field. The plot exhibits an almost constant linear Al trend with variable Mg contents.

5.3.3   OXYGEN FUGACITY (fO$_2$)

Oxygen fugacity (fO$_2$) is vital for understanding the mechanisms that govern the creation of volcanic gases, in estimating the element partition processes, also to discern the phase relations in the magma generation and crystallization (Cottrell & Kelley, 2011). fO$_2$ show contrasting states within the different regions of the Earth i.e., it varies from the core where Fe can be stable in its metallic form to the surface where it is in stable oxide form Fe$_2$O$_3$ and it differs by order of magnitude (e.g., Frost&McCammon, 2008). In a system, it is analogous to the equilibrium partial pressure of oxygen gas.

The oxygen fugacity (fO$_2$) along with the water fugacity (f_{H2O}) are considered imperative parameters for hydrous minerals in granitoids and appear to have control on its composition far more than the other intensive parameters as temperature and pressure (Anderson, 1996). Based on the studies of Wones & Eugster (1965), in the system Fe^{2+}-Fe^{3+}-Mg, c axis of the unit cell of biotite contracts with increase in Fe^{3+}, and suggested positions of biotite which is now employed as a basic approximation of fO$_2$ if Fe^{3+}/Fe^{tot} ratios of the biotite is known.

Employing the primary and secondary biotite compositions of the primary rocks, one can hint about the maximum fO_2, temperature (T), also the minimum fH_2O or hydrogen fugacity (fH_2). Eugsters (1965) considered the relative proportions of Fe^{2+}(annite)- Mg(phlogopite)- Fe^{3+} (oxyannite) while estimating the fO_2 conditions that prevailed through the crystallization of biotite and following the same, together with fO_2 buffer limits after Wones & Eugster (1965), compositions of KAHG biotites are plotted in terms of mole percent annite, phlogopite and proton-deficient oxyannite (Fig. 5.9) The figure compares biotite compositions stabilized at different oxygen buffers FMQ (fayalite-magnetite- quartz), NNO (Nickel-nickel oxide), and HM (hematite-magnetite). It is evident from the plot that KAHG biotites stabilized broadly between FMQ and NNO buffer and also between NNO and HM buffer (Figure 5.9) and the trend exhibited by the biotite compositions is in accord with the presence of Fe-Ti oxides (magnetite, ilmenite) and absence of hematite in KAHG. The biotites broadly express a trend of iron enrichment beginning from NNO buffer and extends below FMQ.

The magmatic biotite annite activity gives idea about fO_2 and fH_2O in the magma. When the magma undergoes crystallization fH_2O is said to increase with falling temperature because of the crystallization of anhydrous phase. In conjunction with that, if fO_2 is buffered, the annite component intensify by the growth of $Fe^{2+}/(Fe^{2+}+Mg)$ ratio through the chemical reaction of K-feldspar and magnetite. Similarly, annite component increases when fO_2 drops (constant fH_2O and T) which can be due to a reduction of Fe^{3+}/Fe^t ratios or by the former process.

Thus, oxygen and water are the two-volatile equilibrium representative in the magmatic biotites. The process of dissociation of water corelate the activities of mentioned components to hydrogen. Once an estimation of temperature and fO_2 is carried out by means of biotite equilibria, and the K-feldspar and magnetite activities identified, then following (Wones, 1972; Czamanske & Wones 1973) the water fugacity (fH_2O) can be calculated by employing the annite activity in biotite as:

$$KFe_3AlSi_3O_{10}(OH)_2 + 0.5O_2 = \quad KAl\,Si_3O_8 + \quad Fe_3O_4 + \quad H_2O \quad\quad (1)$$
Annite $\qquad\qquad\qquad\qquad\qquad\qquad$ Sanidine $\quad$ magnetite $\quad$ Water
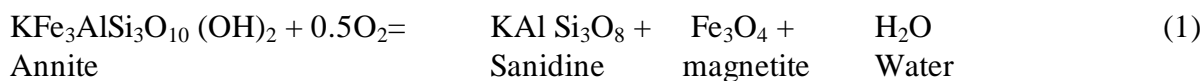
For this reaction (1) Wones (1972) gave that:

$$\log fH_2O = 7409/T + 4.25 + 0.5 \log fO_2 + 3 \log X_{annite} - \log a_{sanidine} + \log a_{Fe3O4} \quad\quad (2)$$

Where, T stands for absolute Temperature in Kelvin, X_{annite} is given as molar fractions of Fe^{2+} in the octahedral site not Fe/Fe+Mg, and $a_{sanidine}$ and a_{Fe3O4} respectively denotes the activities of K-feldspar and magnetite. Given relationship open ways to recount the physical and compositional variables (Speer, 1987), following the work of latter concerning the stability of annite constituent in biotite, Wones (1981) further revised it:

$$\log f_{H2O}=4819/T + 6.69 +3 \log X_{annite} + 0.5\log f_2O - 0.011 (P-1)/ T(°K) + \log a_{sanidine} + \log a_{Fe3O4} \quad (3)$$

which is valid at oxygen fugacities between NNO and HM buffers. Here the activity of magnetite is considered as 1.0 while the activity of sanidine is taken as 0.8.

Qualitative estimation of oxygen fugacity fO_2 have been made based on experimentally calibrated curves of Wones & Eugster (1965). A projection of constant $Fe^{2+}/(Fe^{2+}+Mg)$ ratio of biotite is delineated in the fO_2-T space at 2070 bars total pressure (Fig. 5.10). Biotites of KAHG display stability under moderately oxidizing conditions at FMQ and NNO buffers with fO_2 varying from 10^{-12} to $10^{-15.9}$ bars at temperatures between 733 and 881°C. PGN representative samples exhibit the most variable temperatures of 733 to 881°C within fO_2 limits of 10^{-12} to $10^{-15.7}$ bars very close to NNO buffer. GGN (NNO; fO_2 =10^{-15} to $10^{-15.5}$; T=750-780 °C), NPG samples represented by KH (FMQ- NNO; fO_2 =10^{-13} to $10^{-15.9}$; T=750-790 °C), NL (NNO; fO_2 =10^{-13} to 10^{-14}; T=820-850 °C), AR (FMQ-NNO; fO_2 =10^{-12} to 10^{-14}; T=835-868 °C). The inference of an oxidizing situation at the time of emplacement is also consistent with the modal abundance of Fe-Ti oxides in the samples together with higher MS values.

Ni-NiO buffer was employed for the estimation of water fugacity and temperature conditions. The calculated T°C-fH_2O curve was projected unto the binary diagram (Fig.5.11) and the intersecting points at the experimental curve noted. For PGN biotite, estimated conditions at around 1.9 Kbar at minimum temperature 684°C for WSG solidus curve, while the same biotite equilibrium intersects the WSQD solidus at around 3.1kbar at a temperature of about 740°C. GGN biotites display to some extent higher minimum temperatures of 700°C and 754°C and lower fH_2O values of 1.5 Kbar and 2.35 Kbar respectively for WSG and WSQD curves.

5.3.4   BIOTITE CRYSTALLIZATION TEMPERATURE AND PRESSURE ESTIMATES

Ilmenite and magnetite minerals tend to pair in general within silicic igneous rocks, the coupled minerals are engaged for approximating magmatic temperature of host rocks (Buddington & Lindsley, 1964; Ghiorso & Sack, 1991; Anderson et al., 1993). The KAHG are composed of plagioclase, K-feldspar, and quartz as the dominant phases yet, considerable amounts of accessory phases as biotite, hornblende, apatite and Fe-Ti oxide minerals (ilmenite, magnetite) are present (upto 10-15 vol.%).

Luhr et al, (1984) thermometer parameter has been applied for the calculation of temperatures for KAHG biotite crystallization (Table 18). The employed equation is:

$$T\,(K) = \frac{838}{1.0337 - Ti/Fe^{2+}}$$

Given equation is constructed on the coupled exchange of Ti and Fe^{2+} in biotite, as the said ions are temperature sensitive and so it is possible to acquire reliable data about temperature concerning igneous and metamorphic rocks Luhr et al, (1984). Consequently, the apparent temperature of biotite crystallization estimated for KAHG vary from 856.28 to 1061.03°C, with the lowest and highest temperature exhibited respectively by PGN (856.28- 943.27°C) and BGN (938.91- 1061.03°C).

Biotites aides further in approximating the emplacement depth of its hosting intrusive rock based on concentration of TiO_2 and Al^{VI}. Granites which consist of biotite with high TiO_2 and Al^{VI} values are suggestive of crystallization of deep-seated granites (Machev et al., 2004; Bora & Kumar, 2015) also, a low TiO_2 and a comparatively high Al^{VI} value is considered to indicate an abyssal depth of formation.

In this study, TiO_2 values are moderate ranging from 0.95 to 3.5 apfu and Al^{VI} varies from 0.03 to 0.84 apfu. BGN have TiO_2=1.96- 3.5 wt%, Al^{VI} = 0.03- 0.39 apfu, GGN=2.01- 2.41 wt%, Al^{VI} = 0.19- 0.84 apfu, PGN=0.95- 2.87 Al^{VI} = 0.22- 0.45 apfu, NPG=1.55- 3.03, Al^{VI} = 0.16- 0.32 apfu.

GGN exhibits comparatively high TiO_2 values coupled by highest Al^{VI}, potentially indicating a deeper mid- crustal crystallization depth. Relatively low TiO_2 and high Al^{VI} contents of PGN are supportive of an abyssal depth of formation.

It is established that total Al content of biotite get enhanced along with increase in pressure and that crystallization pressure of granitoids is supposedly constrained by the mentioned content Uchida et al, (2007). Therefore, the total Al in biotite of KAHG have been utilized as a geobarometry parameter following the given formula

$$P \text{ (kbar)} = 3.33A^T - 6.53 \text{ (0.33)}$$

Where Al^T refers to total number of Al atoms in biotite on the bases of 22 oxygen equivalents.

Following given equation, the estimated crystallization pressure range of KAHG biotite range from 0.73 to 3.79 kbars. The biotite crystallization pressure of BGN is lowest (0.73 to 1.53 kbars), GGN have variable average pressures (1.80 to 3.46 kbars) and PGN with the highest values (1.86 to 3.79 kbars) and data of NPG more restricted within (1.40 to 2.93 kbars).

Henry et al, (2005) predicts the biotite crystallization temperatures using the contents of Ti and X_{Mg}. Following his geothermometer parameter the KAHG indicate the near solidus crystallization temperature (~400-630°C approximately) (Fig. 5.12). Biotites of BGN supports a higher temperature of 550-630°C. PGN exhibits lowest biotite formation temperature i.e 400°C. BGN which hosts more and larger mafic enclaves displays higher crystallization temperatures.
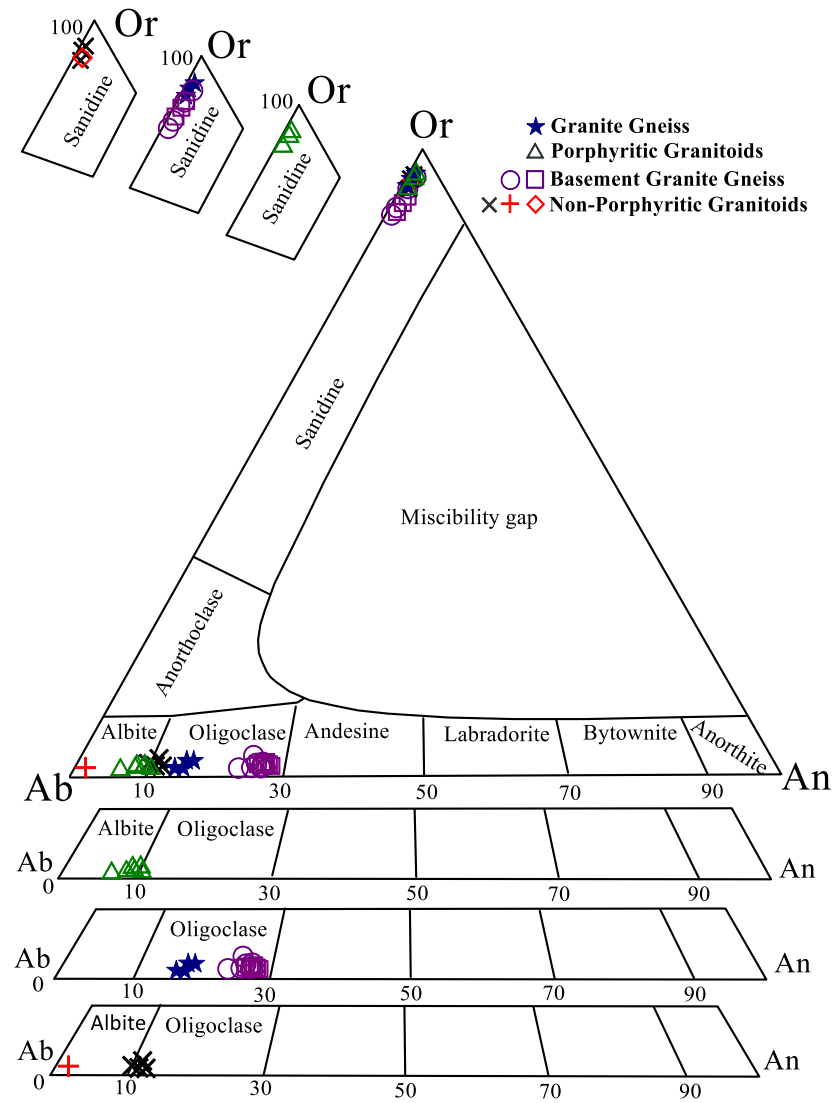
Fig. 5.1: Compositional variation of plagioclase from KAHG, in terms of Ab-An-Or components.
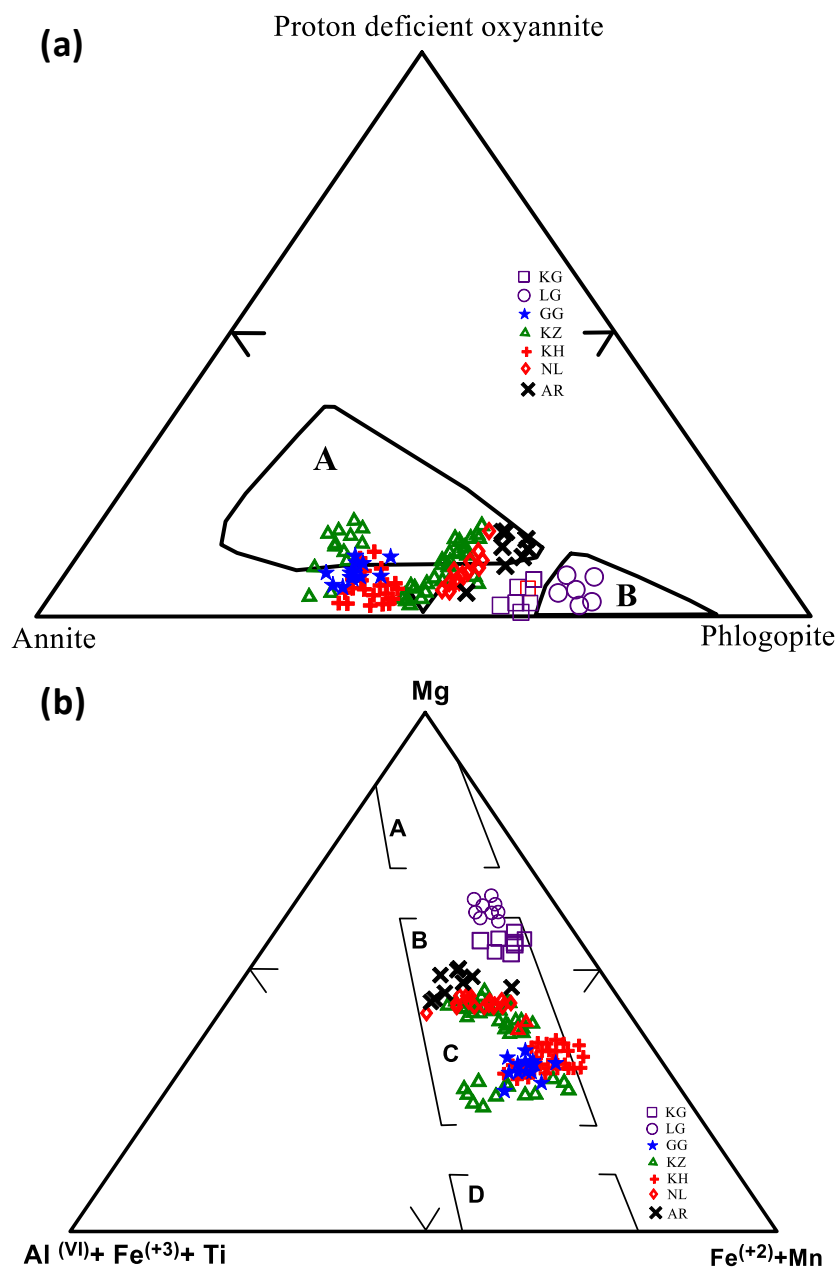
Figure 5.2: (a) Fe^{+2} - Fe^{+3} - Mg^{+2} ternary plot after Beane (1974).

A: Field of primary biotite B: Field of hydrothermal biotites (encircled after Foster,1960). Note that biotites of gneissic KG and LG lie close to the field of primary biotite.

(b). Mg-(Al^{VI}+Fe^{3+}+Ti) -(Fe^{2+}+Mn) ternary diagram. The Fields of A-Phlogopite, B-Mg-biotite, C-Fe^{2+} biotite, D-Siderophyllites and Lipdomelane after Foster (1960).

Symbols: Basement granite gneiss (KG, LG); granite gneiss (GG); porphyritic granite (KZ); non-porphyritic granite (KH, NL, AR).
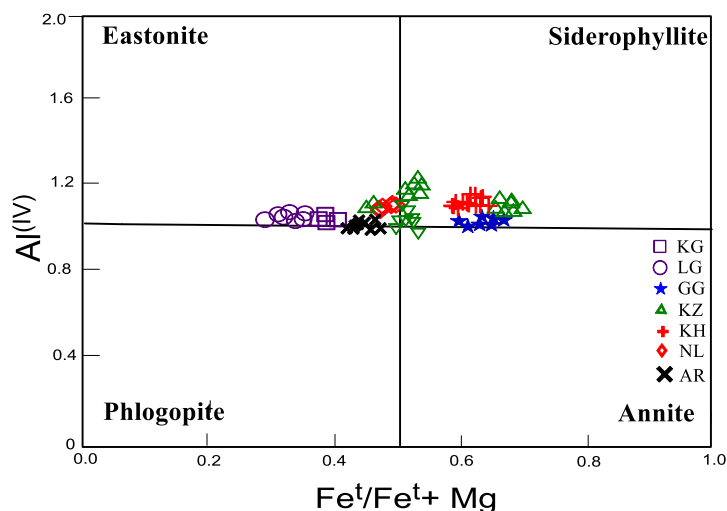
Fig. 5.3: Fe^t/Fe^t+Mg vs Al ^{IV} biotite classification diagram of KAHG after Deer et al, (1963). Symbols: Basement granite gneiss (KG, LG); granite gneiss (GG); porphyritic granite (KZ); non-porphyritic granite (KH, NL, AR).
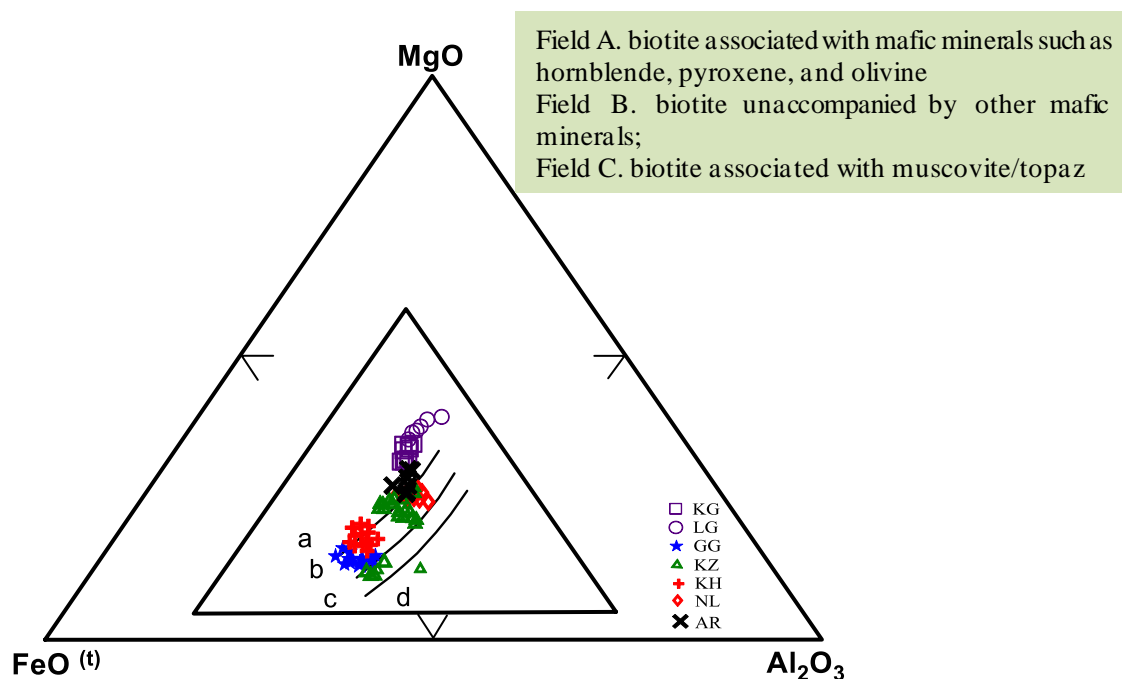
Figure 5.4: Ternary diagram of $MgO-FeO^t-Al_2O_3$ after Albuquerque (1973) (a) Biotite coexisting with amphibole (b) Biotite coexisting with ferro magnesian minerals (c) Biotite coexisting with muscovite (d) Biotite coexisting with aluminosilicate. Symbols: Basement granite gneiss (KG, LG); granite gneiss (GG); porphyritic granite (KZ); non-porphyritic granite (KH, NL, AR).
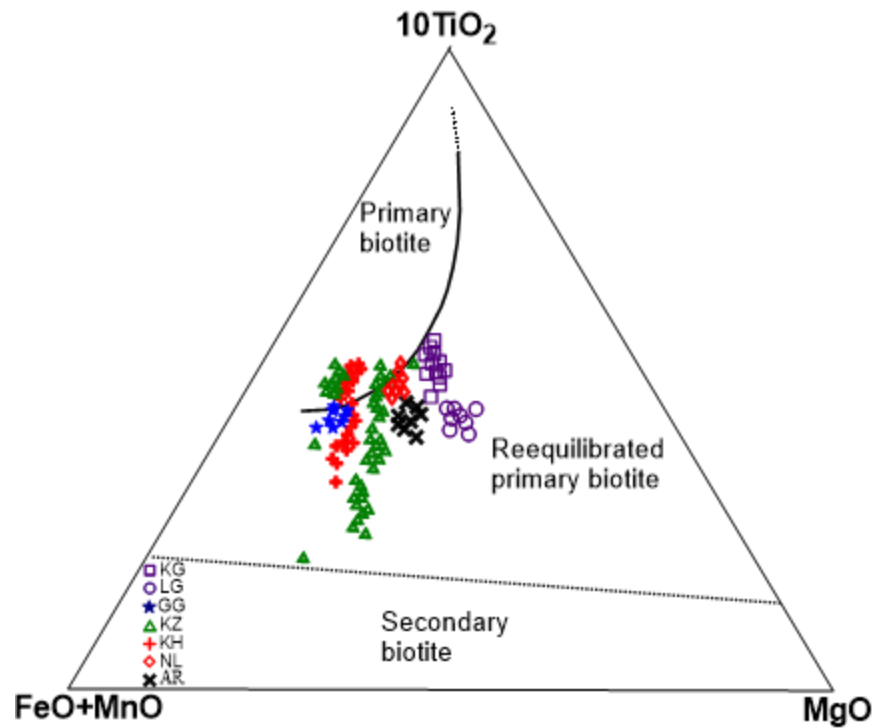
Fig. 5.5: TiO$_2$–FeO*–MgO (FeO* = FeO + MnO) ternary diagram after Nachit et al (2005). Symbols: Basement granite gneiss (KG, LG); granite gneiss (GG); porphyritic granite (KZ); non-porphyritic granite (KH, NL, AR).
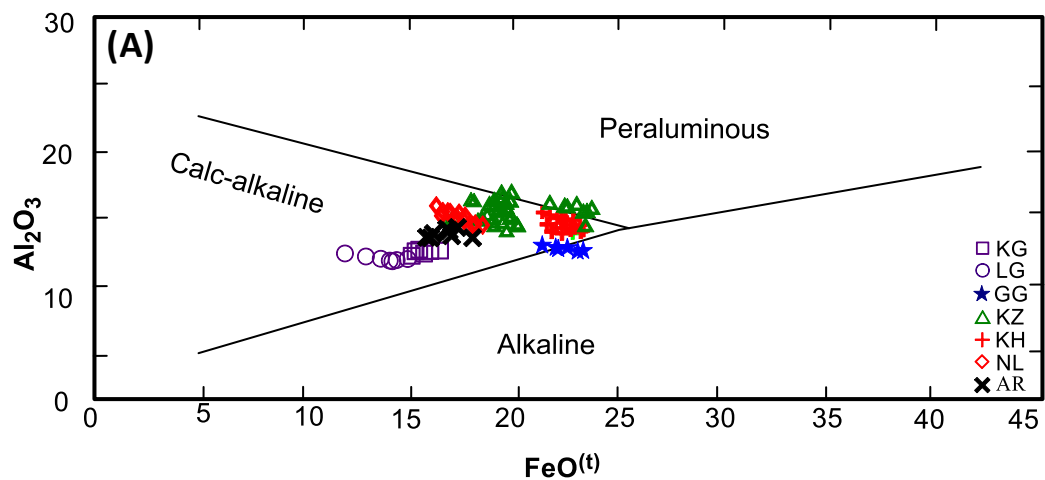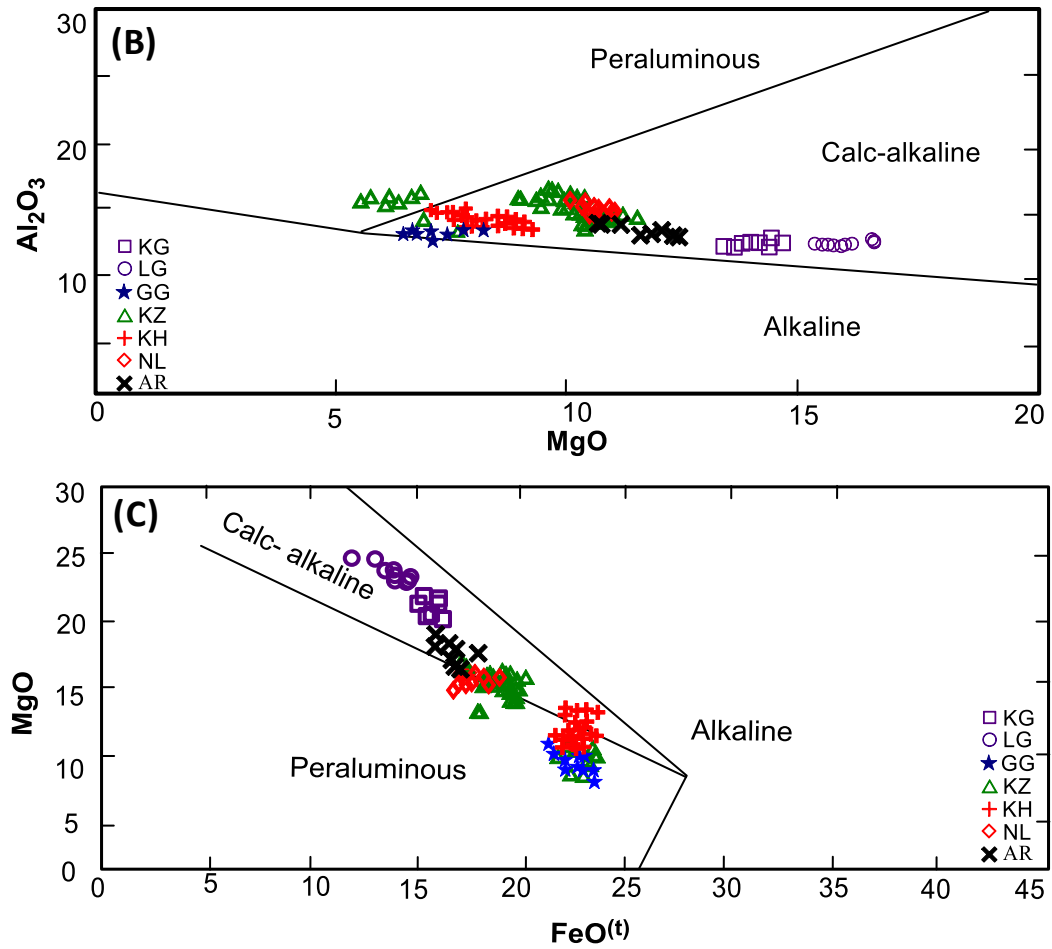
Fig.5.6: Tectonic discrimination diagrams of (Abdel-Rahman, 1994) a) FeO^t Vs Al$_2$O$_3$ b) MgO Vs Al$_2$O$_3$ c) FeO^t Vs MgO. Symbols: Basement granite gneiss (KG, LG); granite gneiss (GG); porphyritic granite (KZ); non-porphyritic granite (KH, NL, AR).
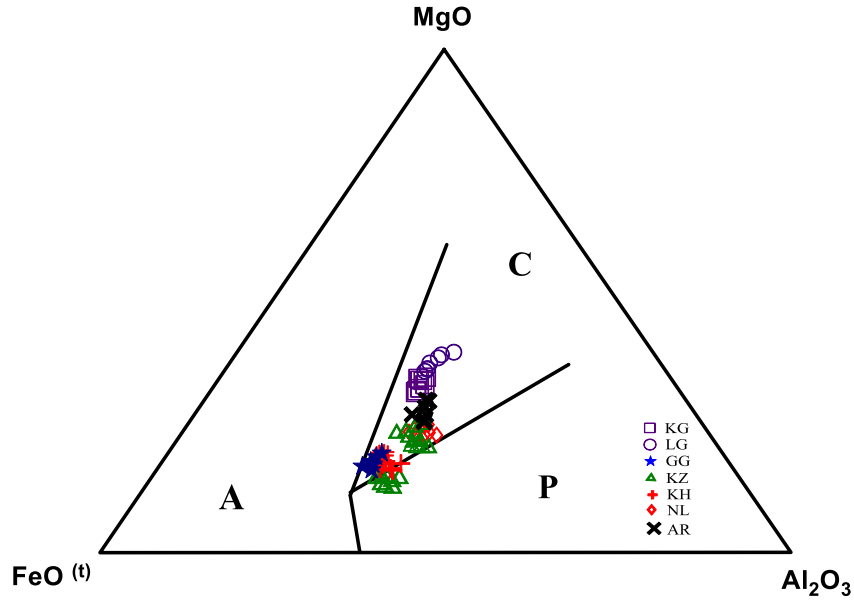
Fig. 5.7: Ternary MgO- FeO^t- Al$_2$O$_3$ diagram of biotites of KAHG, wherein the fields of biotite composition corresponding to various host magma types are taken after (Abdel-Rahman, 1994) A- Biotite in anorogenic suites, C- Biotite in calc-alkaline suites, P- Biotite in peraluminous (including S- Type) Suites. Symbols: Basement granite gneiss (KG, LG); granite gneiss (GG); porphyritic granite (KZ); non-porphyritic granite (KH, NL, AR).
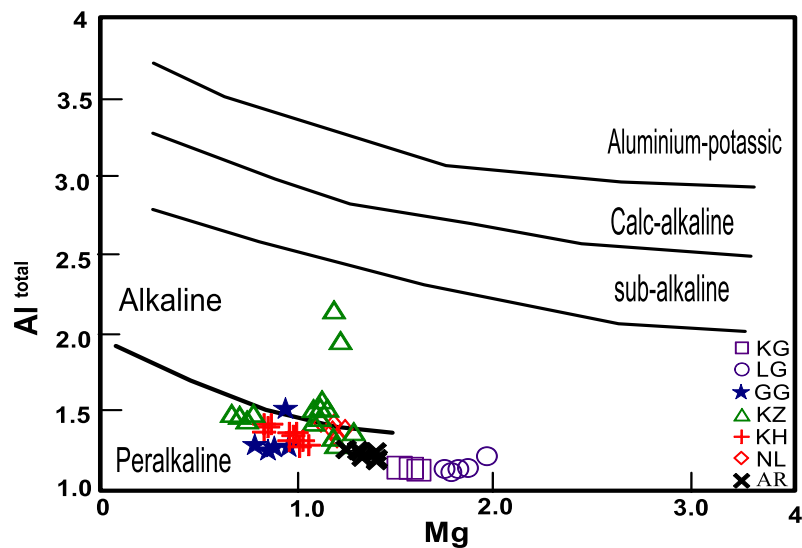
Fig. 5.8: Biotite classification diagram of KAHG after Nachit et al., (1985). Symbols: Basement granite gneiss (KG, LG); granite gneiss (GG); porphyritic granite (KZ); non-porphyritic granite (KH, NL, AR).
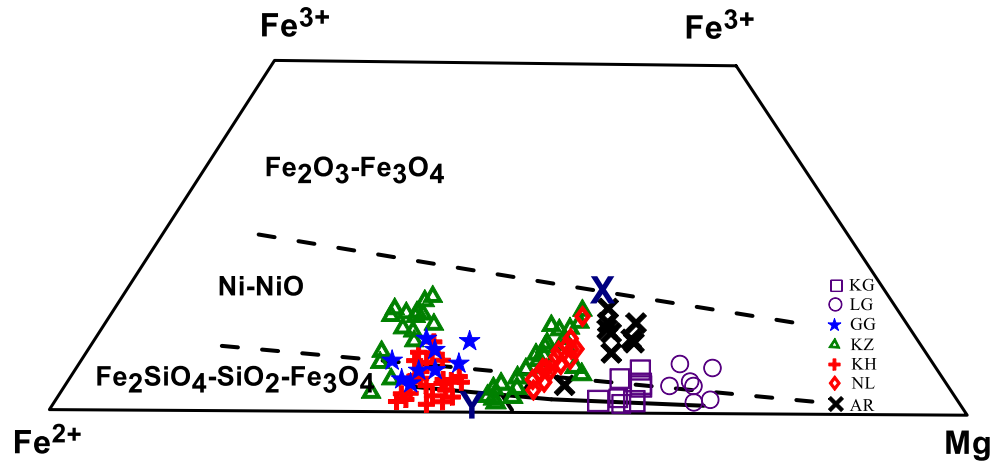
Fig. 5.9: Composition of biotites in terms of mole percent annite, phologopite and proton-deficient oxyannite. The buffer lines of biotite stability are shown after Wones & Eugsters (1965). Symbols: Basement granite gneiss (KG, LG); granite gneiss (GG); porphyritic granite (KZ); non-porphyritic granite (KH, NL, AR).
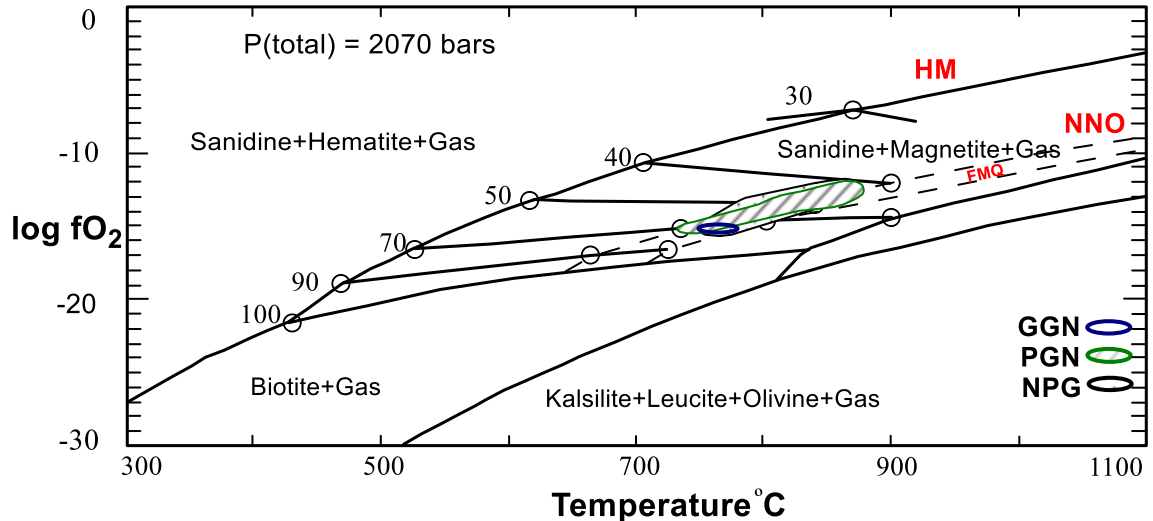
Fig. 5.10: Temperature vs fO_2 binary diagram of experimentally calibrated biotite equilibria at constant P=2070 bars (Wones & Eugster, 1965). Ranges of fO_2 and T°C for biotite crystallization respectively for PGN, NPG and GGN melts.
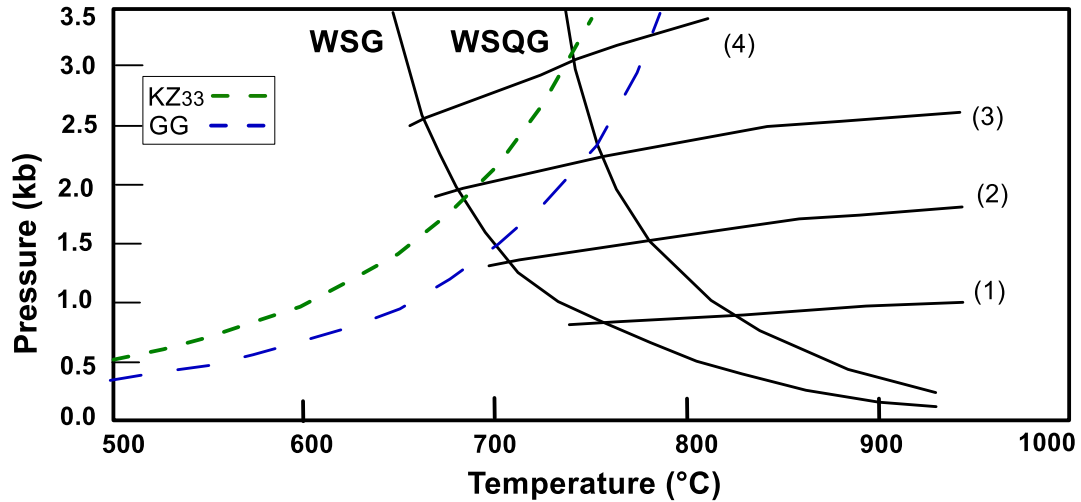
Fig. 5.11: Biotite equilibria in terms of f_{H2O} and temperature calculated for biotites of PGN (KZ33) and GGN, which intersect the water saturated granodiorite (WSG) and water saturated quartz diorite (WSQD) (After Piwinski, 1968). The lines labelled with 1,2,3 and 4 represent the water pressure.
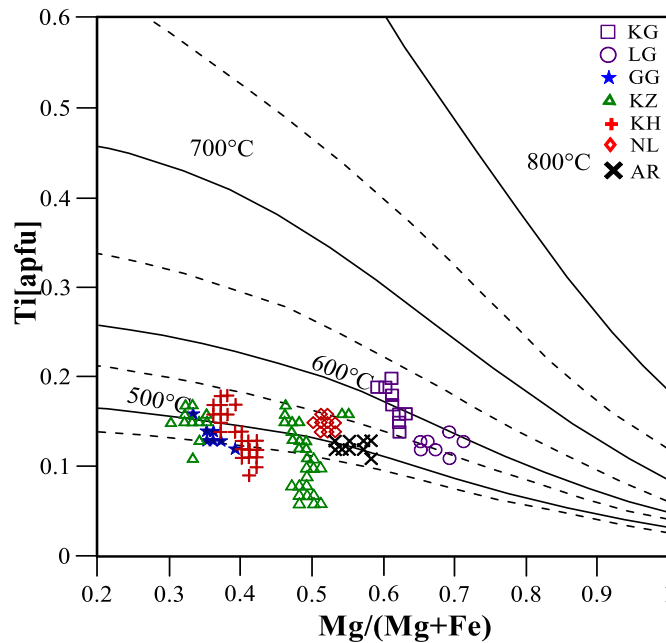
Fig. 5.12: Ti vs. Mg/ (Mg + Fe) plot of biotite from KAHG showing temperatures of biotite formation (after Henry et al., 2005).

TABLE-6: PLAGIOCLASE FELDSPAR STRUCTURAL FORMULA ON THE BASIS OF 8 O

Oxide (wt %)	KZ8A 1	KZ12 2	KZ12 3	KZ12 4	KZ12 5	KZ12 6	KZ12 7	KZ12 8	KZ12 9	KZ12 10	KZ22 11
				NON-PORPHYRITIC GRANITOIDS							
SiO_2	68.93	66.12	66.34	66.6	65.21	65.28	66.73	66.35	66.84	65.94	61.97
Al_2O_3	19.37	20.8	21.17	20.92	20.71	20.48	20.84	20.76	20.99	20.74	23.02
CaO	0.36	2.42	2.76	2.46	2.41	2.43	2.44	2.54	2.47	2.34	5.54
Na_2O	10.99	10.43	10.57	10.62	10.39	10.56	10.28	10.5	10.38	10.57	8.23
K_2O	0.1	0.25	0.15	0.26	0.37	0.26	0.35	0.15	0.26	0.07	0.24
FeO	0.06	0.1	0.08	0.02	0.09	0.1	0.08	0.15	0.08	0.11	0.05
total	99.81	100.12	101.07	100.88	99.19	99.11	100.72	100.45	101.02	99.77	99.05
Si	3.032	2.904	2.883	2.899	2.888	2.89	2.915	2.904	2.911	2.903	2.781
Al	1.004	1.077	1.084	1.073	1.081	1.069	1.073	1.071	1.078	1.076	1.218
Z	4.036	3.981	3.967	3.972	3.969	3.959	3.988	3.975	3.989	3.979	3.999
Ca	0.017	0.114	0.128	0.115	0.114	0.115	0.114	0.119	0.115	0.11	0.266
Na	0.937	0.888	0.89	0.896	0.892	0.906	0.871	0.891	0.877	0.902	0.716
K	0.006	0.014	0.008	0.014	0.021	0.015	0.02	0.008	0.014	0.004	0.014
X	0.96	1.016	1.026	1.025	1.027	1.036	1.005	1.018	1.006	1.016	0.996
An%	1.768	11.208	12.508	11.188	11.130	11.122	11.370	11.694	11.455	10.858	26.739
Ab%	97.648	87.414	86.683	87.404	86.835	87.461	86.688	87.483	87.110	88.755	71.882
Or%	0.585	1.379	0.809	1.408	2.035	1.417	1.942	0.822	1.436	0.387	1.379

TABLE-6 CONTINUED

Oxide (wt %)	KZ-2 12	KZ-2 13	KZ-2 14	KZ-2 15	KZ-2 16	KZ6 17	KZ6 18	KZ6 19	KZ6 20	KZ6 21	KZ6 22	KZ6 23	KZ6 24
						BASEMENT GRANITE GNEISS							
SiO2	62.46	62.35	63.24	62.65	62.76	62.24	61.90	62.10	62.29	62.03	62.45	61.76	62.87
Al2O3	23.38	23.63	23.71	23.64	23.56	23.19	23.19	22.96	23.15	22.90	23.24	23.38	23.00
CaO	5.48	5.64	5.48	5.57	5.66	5.42	5.22	5.38	5.32	5.28	5.53	5.28	4.87
Na2O	8.38	8.26	8.04	8.03	8.04	8.33	8.50	8.38	8.54	8.56	8.39	8.19	8.71
K2O	0.32	0.22	0.35	0.24	0.31	0.26	0.25	0.24	0.23	0.22	0.21	0.31	0.12
FeO	0.11	0.07	0.05	0.16	0.12	0.18	0.10	0.16	0.18	0.06	0.12	0.18	0.16
total	100.13	100.17	100.87	100.29	100.45	99.62	99.16	99.22	99.71	99.05	99.94	99.10	99.73
Si	2.772	2.767	2.793	2.783	2.784	2.778	2.768	2.782	2.773	2.779	2.778	2.771	2.797
Al	1.223	1.236	1.234	1.238	1.232	1.220	1.222	1.212	1.215	1.209	1.218	1.236	1.206
Z	3.995	4.003	4.027	4.021	4.016	3.998	3.990	3.994	3.99	3.988	3.996	4.007	4.003
Ca	0.261	0.268	0.259	0.265	0.269	0.259	0.250	0.258	0.254	0.253	0.264	0.254	0.232
Na	0.721	0.711	0.688	0.692	0.692	0.721	0.737	0.728	0.737	0.744	0.724	0.712	0.751
K	0.018	0.012	0.020	0.014	0.018	0.015	0.014	0.014	0.013	0.013	0.012	0.018	0.007
X	1.000	0.991	0.967	0.970	0.978	0.995	1.001	1.000	1.00	1.010	0.999	0.984	0.990
An%	26.063	27.051	26.802	27.321	27.504	26.053	24.977	25.828	25.275	25.104	26.380	25.794	23.442
Ab%	72.124	71.693	71.160	71.277	70.702	72.459	73.599	72.801	73.423	73.650	72.427	72.403	75.870
Or%	1.812	1.256	2.038	1.402	1.794	1.488	1.424	1.372	1.301	1.245	1.193	1.803	0.688

TABLE-6 CONTINUED

Oxide (wt %)	PORPHYRITIC GRANITOIDS					
	KZ15 32	KZ33 33	KZ33 34	KZ33 35	KZ33 36	KZ33 37
SiO_2	67.27	66.43	66.83	66.21	66.81	67.69
Al_2O_3	20.23	20.48	20.37	20.44	20.27	20.38
CaO	1.5	2.1	1.85	2.16	1.82	1.87
Na_2O	10.68	9.82	10.15	9.66	10.13	9.97
K_2O	0.06	0.05	0.08	0.05	0.1	0.07
FeO	0.04	0.1.	0.09	0.06	0.02	0.07
total	99.78	98.98	99.37	98.58	99.15	100.05
Si	2.962	2.965	2.964	2.969	2.969	2.988
Al	1.05	1.077	1.065	1.08	1.062	1.06
Z	4.012	4.042	4.029	4.049	4.03	4.048
Ca	0.071	0.1	0.088	0.104	0.087	0.088
Na	0.912	0.85	0.873	0.84	0.873	0.853
K	0.003	0.003	0.005	0.003	0.006	0.004
X	0.986	0.953	0.965	0.946	0.965	0.946
An%	7.178	10.537	9.107	10.964	8.979	9.352
Ab%	92.481	89.164	90.424	88.734	90.434	90.231
Or%	0.342	0.299	0.469	0.302	0.587	0.417

TABLE-7: ALKALI- FELDSPAR STRUCTURAL FORMULA

Oxide	NON-PORPHYRITIC								
	KZ12 1	KZ12 2	KZ12 3	KZ12 4	KZ12 5	KZ12 6	KZ12 7	KZ12 8	KZ12 9
SiO2	64.96	64.95	64.49	64.54	64.73	64.47	64.2	64.44	65.72
Al2O3	17.65	17.67	17.48	17.52	17.59	17.64	17.66	17.36	17.94
CaO	0	0	0.01	0	0.02	0	0.01	0.02	0.01
Na2O	0.38	0.52	0.55	0.52	0.57	0.62	0.54	0.36	0.91
K2O	15.96	15.67	15.74	15.87	15.8	15.86	15.59	15.81	15.21
FeO	0.04	0.01	0.03	0.04	0.03	0.08	0.07	0.07	0.05
total	98.99	98.82	98.3	98.49	98.74	98.67	98.07	98.06	99.84
Si	3.035	3.041	3.033	3.029	3.03	3.017	3.028	3.044	3.04
Al	0.972	0.975	0.969	0.969	0.971	0.973	0.982	0.966	0.978
Z	4.007	4.016	4.002	3.998	4.001	3.99	4.01	4.01	4.018
Ca	0	0	0.001	0	0.001	0	0.001	0.001	0
Na	0.034	0.047	0.05	0.047	0.052	0.056	0.049	0.033	0.082
K	0.951	0.936	0.945	0.95	0.944	0.947	0.938	0.953	0.898
X	0.985	0.983	0.996	0.997	0.997	1.003	0.988	0.987	0.98
An%	0.000	0.000	0.051	0.000	0.101	0.000	0.051	0.103	0.051
Ab%	3.492	4.801	5.040	4.744	5.193	5.608	4.998	3.341	8.331
Or%	96.508	95.199	94.909	95.256	94.707	94.392	94.950	96.556	91.619

TABLE-7 CONTINUED

Oxide	GRANITE GNEISS										
	KZ-6 10	KZ-6 11	KZ-6 12	KZ-6 13	KZ-6 14	KZ-6 15	KZ23 16	KZ23 17	KZ23 18	KZ23 19	KZ23 20
SiO2	64.46	64.04	65.11	64.7	64.51	64.82	64.42	64.55	64.11	64.02	64.31
Al2O3	18.06	17.92	18.04	17.89	17.97	17.92	17.54	17.58	17.63	17.66	17.42
CaO	0.02	0.04	0	0	0	0	0	0.02	0	0	0.02
Na2O	1.08	0.92	0.61	0.41	0.62	0.63	0.55	0.37	0.3	0.43	0.52
K2O	14.44	14.92	15.04	15.21	15	15.09	15.81	15.79	15.88	16.04	15.69
FeO	0.07	0.02	0.05	0.03	0.1	0.07	0.03	0.03	0.05	0.01	0.05
total	98.13	97.86	98.85	98.24	98.2	98.53	98.35	98.34	97.97	98.16	98.01
Si	3.029	3.016	3.048	3.051	3.038	3.041	3.028	3.038	3.028	3.015	3.034
Al	1.000	0.995	0.995	0.994	0.997	0.991	0.972	0.975	0.981	0.980	0.969
Z	4.029	4.010	4.043	4.045	4.036	4.032	4.000	4.013	4.010	3.996	4.003
Ca	0.001	0.002	0.000	0.000	0.000	0.000	0.000	0.001	0.000	0.000	0.001
Na	0.098	0.084	0.055	0.037	0.057	0.057	0.050	0.034	0.027	0.039	0.048
K	0.866	0.896	0.898	0.915	0.901	0.903	0.948	0.948	0.957	0.964	0.944
X	0.965	0.982	0.953	0.952	0.958	0.961	0.998	0.983	0.984	1.003	0.993
An%	0.104	0.205	0.000	0.000	0.000	0.000	0.000	0.103	0.000	0.000	0.102
Ab%	10.196	8.551	5.806	3.936	5.911	5.967	5.022	3.435	2.791	3.915	4.791
Or%	89.700	91.244	94.194	96.064	94.089	94.033	94.978	96.462	97.209	96.085	95.108

TABLE-7 CONTINUED

oxide	GRANITE GNEISS					PORPHYRITIC GRANITOIDS				
	KZ-2 21	KZ-2 22	KZ-2 23	KZ-2 24	KZ-2 25	KZ33 26	KZ33 27	KZ33 28	KZ33 29	KZ33 30
SiO2	65.08	65.13	65.33	65.96	65.5	65.13	64.62	65.1	64.22	64.62
Al2O3	17.9	18.01	18.07	18.09	18.14	17.73	17.68	17.76	17.84	17.89
CaO	0	0.07	0	0.02	0.04	0	0.01	0	0	0.02
Na2O	0.83	0.95	0.85	0.83	0.67	0.41	0.57	0.49	0.36	0.51
K2O	15.15	15.05	15.2	15.59	15.47	16.12	15.77	15.97	16.34	15.76
FeO	0.05	0.03	0.06	0.12	0.04	0.04	0.1	0.07	0	0.08
total	99.01	99.24	99.51	100.61	99.86	99.43	98.75	99.39	98.76	98.88
Si	3.036	3.025	3.031	3.028	3.032	3.031	3.025	3.029	3.003	3.021
Al	0.984	0.986	0.988	0.979	0.990	0.972	0.975	0.974	0.983	0.986
Z	4.020	4.011	4.019	4.007	4.021	4.003	4.000	4.004	3.987	4.006
Ca	0.000	0.003	0.000	0.001	0.002	0.000	0.001	0.000	0.000	0.001
Na	0.075	0.086	0.076	0.074	0.060	0.037	0.052	0.044	0.033	0.046
K	0.902	0.892	0.900	0.913	0.913	0.957	0.942	0.948	0.975	0.940
X	0.977	0.981	0.976	0.988	0.976	0.994	0.994	0.992	1.007	0.987
An%	0.000	0.355	0.000	0.100	0.203	0.000	0.050	0.000	0.000	0.101
Ab%	7.686	8.723	7.833	7.478	6.163	3.722	5.205	4.455	3.240	4.683
Or%	92.314	90.922	92.167	92.422	93.634	96.278	94.745	95.545	96.760	95.216

TABLE 8: Calculated electron probe microanalysis (EPMA) data for biotites of BGN (KG) granitoids

Sample	KG	KG	KG	KG	KG	KG	KG	KG	KG	KG	KG	KG	KG	KG
SiO$_2$	38.53	38.55	38.61	38.53	38.91	38.16	38.72	39.01	39.02	38.89	38.93	38.99	39.28	38.78
Al$_2$O$_3$	12.53	12.51	12.49	12.89	12.77	12.49	12.64	12.68	12.45	12.85	12.47	12.70	12.72	12.66
TiO$_2$	2.84	3.05	2.92	3.50	3.27	3.37	3.15	3.27	2.67	3.20	2.74	2.55	2.78	2.94
Cr$_2$O$_3$	0.09	0.15	0.06	0.06	0.06	0.06	0.18	0.00	0.03	0.15	0.06	0.03	0.03	0.06
FeO	15.23	15.78	15.81	15.60	16.13	15.80	15.52	16.40	15.71	15.89	15.84	16.05	15.44	15.93
MnO	0.52	0.59	0.54	0.62	0.57	0.71	0.52	0.53	0.58	0.62	0.49	0.66	0.63	0.40
MgO	13.99	13.76	13.76	13.93	13.56	13.33	13.61	13.41	14.19	14.04	14.33	14.44	14.51	13.75
CaO	0.04	0.00	0.03	0.01	0.01	0.00	0.04	0.00	0.00	0.01	0.03	0.04	0.00	0.00
Na$_2$O	0.18	0.09	0.15	0.11	0.07	0.07	0.07	0.07	0.07	0.07	0.16	0.09	0.08	0.08
BaO	0.00	0.00	0.00	0.00	0.00	0.00	0.00	0.00	0.00	0.00	0.00	0.00	0.00	0.00

K$_2$O	9.66	9.52	9.14	9.29	9.74	9.31	9.73	9.65	9.71	9.52	9.35	9.61	9.62	9.60
Total	93.61	94.00	93.51	94.54	95.08	93.30	94.18	95.02	94.43	95.24	94.40	95.16	95.09	94.20
Structural Formulae based on 11 oxygen														
Si	2.94	2.94	2.95	2.91	2.93	2.93	2.94	2.94	2.96	2.92	2.95	2.94	2.95	2.95
Al^{IV}	1.06	1.06	1.05	1.09	1.07	1.07	1.06	1.06	1.04	1.08	1.05	1.06	1.05	1.05
$\sum$Z=4	4.00	4.00	4.00	4.00	4.00	4.00	4.00	4.00	4.00	4.00	4.00	4.00	4.00	4.00
Al^{VI}	0.07	0.06	0.08	0.06	0.07	0.06	0.07	0.07	0.07	0.06	0.06	0.06	0.07	0.08
Fe^{3+}	0.01	0.08	0.08	0.17	0.07	0.12	0.02	0.06	0.03	0.13	0.08	0.08	0.07	0.04
Ti	0.16	0.17	0.17	0.20	0.19	0.19	0.18	0.19	0.15	0.18	0.16	0.14	0.16	0.17
Mg	1.59	1.56	1.57	1.57	1.52	1.53	1.54	1.51	1.60	1.57	1.62	1.62	1.62	1.56
Fe^{2+}	0.97	0.93	0.93	0.82	0.95	0.89	0.97	0.97	0.96	0.87	0.92	0.93	0.90	0.97
Mn	0.03	0.04	0.03	0.04	0.04	0.05	0.03	0.03	0.04	0.04	0.03	0.04	0.04	0.03
$\sum$Y=3	2.83	2.84	2.86	2.86	2.84	2.79	2.81	2.83	2.85	2.85	2.87	2.87	2.86	2.85
Na	0.03	0.01	0.02	0.02	0.01	0.01	0.01	0.01	0.01	0.01	0.02	0.01	0.01	0.01
K	0.94	0.93	0.89	0.90	0.94	0.91	0.94	0.93	0.94	0.91	0.90	0.92	0.92	0.93
$\sum$X=1	0.97	0.94	0.91	0.92	0.95	0.92	0.95	0.94	0.95	0.92	0.92	0.93	0.93	0.94
Fe^t/Fe^t+Mg	0.38	0.39	0.39	0.39	0.40	0.40	0.39	0.41	0.38	0.39	0.38	0.38	0.37	0.39
Mg/Mg+Fe^t	0.62	0.61	0.61	0.61	0.60	0.60	0.61	0.59	0.62	0.61	0.62	0.62	0.63	0.61
Fe^{2+}/F^{2+}+Fe^{3+}	0.99	0.92	0.92	0.83	0.94	0.88	0.98	0.94	0.97	0.87	0.92	0.92	0.93	0.96
Fe^{3+}/F^{2+}+Fe^{3+}	0.01	0.08	0.08	0.17	0.06	0.12	0.02	0.06	0.03	0.13	0.08	0.08	0.07	0.04
FeO^t/MgO	1.09	1.15	1.15	1.12	1.19	1.19	1.14	1.22	1.11	1.13	1.11	1.11	1.06	1.16
FeO^t/FeO^t +MgO	14.99	14.76	14.76	14.93	14.56	14.33	14.61	14.41	15.19	15.04	15.33	15.44	15.51	14.75
ASI	1.16	1.19	1.24	1.25	1.2	1.23	1.19	1.2	1.17	1.24	1.21	1.2	1.2	1.2
Al^t	1.13	1.12	1.13	1.15	1.14	1.13	1.13	1.13	1.11	1.14	1.11	1.12	1.12	1.13

ASI =Molar Al$_2$O$_3$/CaO + Na$_2$O+K$_2$O; Al^t = (Al^{IV}+ Al^{VI}) pfu; FeO^t= total iron; Fe^t= total iron pfu.

TABLE 9: Calculated electron probe microanalysis (EPMA) data for biotites of BGN (LG) granitoids

Sample	LG	LG	LG	LG	LG	LG	LG	LG	LG	LG	LG
SiO$_2$	37.95	38.23	38.23	38.18	38.73	38.22	39.01	38.21	38.77	38.48	38.81
Al$_2$O$_3$	12.33	12.17	12.17	12.34	12.48	12.49	12.74	12.30	12.28	12.26	12.08
TiO$_2$	2.30	2.27	2.27	2.06	2.21	1.96	2.22	2.15	2.20	2.19	2.21
Cr$_2$O$_3$	0.00	0.03	0.03	0.00	0.00	0.03	0.08	0.04	0.00	0.03	0.00
FeO	15.05	14.18	14.18	14.69	13.71	13.05	12.02	13.80	14.26	14.61	14.15
MnO	0.69	0.70	0.70	0.68	0.60	0.84	0.74	0.59	0.68	0.74	0.80
MgO	15.38	15.39	15.39	15.21	16.00	16.44	16.46	15.92	15.64	15.52	15.61
CaO	0.02	0.00	0.00	0.00	0.02	0.00	0.00	0.04	0.03	0.02	0.00

Na_2O	0.14	0.06	0.06	0.12	0.13	0.03	0.08	0.06	0.19	0.13	0.07
BaO	0.00	0.00	0.00	0.00	0.00	0.00	0.00	0.00	0.00	0.00	0.00
K_2O	9.24	9.28	9.28	9.35	9.27	9.32	9.59	9.39	9.02	9.27	9.19
Total	93.10	92.31	92.31	92.63	93.15	92.38	92.94	92.50	93.07	93.25	92.92
Structural Formulae based on 11 oxygen											
Si	2.91	2.95	2.95	2.94	3.18	2.93	2.95	2.93	2.95	2.94	2.96
Al^{IV}	1.09	1.05	1.05	1.06	0.82	1.07	1.05	1.07	1.05	1.06	1.04
$\sum Z=4$	4.00	4.00	4.00	4.00	4.00	4.00	4.00	4.00	4.00	4.00	4.00
Al^{VI}	0.03	0.05	0.05	0.06	0.39	0.06	0.09	0.05	0.06	0.04	0.05
Fe^{3+}	0.19	0.12	0.12	0.10	0.86	0.15	0.03	0.13	0.12	0.13	0.12
Ti	0.13	0.13	0.13	0.12	0.14	0.11	0.13	0.12	0.13	0.13	0.13
Mg	1.76	1.77	1.77	1.75	1.96	1.88	1.86	1.82	1.78	1.77	1.78
Fe^{2+}	0.77	0.79	0.79	0.85	0.00	0.69	0.73	0.76	0.79	0.80	0.79
Mn	0.04	0.05	0.05	0.04	0.04	0.05	0.05	0.04	0.04	0.05	0.05
$\sum Y=3$	2.92	2.91	2.91	2.92	3.39	2.94	2.89	2.92	2.92	2.92	2.92
Na	0.02	0.01	0.01	0.02	0.02	0.00	0.01	0.01	0.03	0.02	0.01
K	0.90	0.91	0.91	0.92	0.97	0.91	0.93	0.92	0.88	0.90	0.90
$\sum X=1$	0.92	0.92	0.92	0.94	0.99	0.91	0.94	0.93	0.91	0.92	0.91
Fe^t/Fe^t+Mg	0.35	0.34	0.34	0.35	0.31	0.31	0.29	0.33	0.34	0.35	0.34
$Mg/Mg+Fe^t$	0.65	0.66	0.66	0.65	0.69	0.69	0.71	0.67	0.66	0.65	0.66
$Fe^{2+}/F^{2+}+Fe^{3+}$	0.80	0.87	0.87	0.90	0.00	0.82	0.96	0.86	0.87	0.86	0.87
$Fe^{3+}/F^{2+}+Fe^{3+}$	0.20	0.13	0.13	0.10	1.00	0.18	0.04	0.14	0.13	0.14	0.13
FeO^t/MgO	0.98	0.92	0.92	0.97	0.04	0.79	0.73	0.87	0.91	0.94	0.91
FeO^t/FeO^t+MgO	16.38	16.39	16.39	16.21	17	17.44	17.46	16.92	16.64	16.52	16.61
ASI	1.22	1.2	1.2	1.2	1.22	1.24	1.21	1.2	1.22	1.2	1.2
Al^t	1.12	1.1	1.1	1.12	1.21	1.13	1.14	1.12	1.11	1.1	1.09

ASI = Molar $Al_2O_3/CaO + Na_2O+K_2O$; $Al^t = (Al^{IV}+ Al^{VI})$ pfu; FeO^t= total iron; Fe^t= total iron pfu.

TABLE 10: Calculated electron probe microanalysis (EPMA) data for biotites of GGN (GG) granitoids

Sample	GG	GG	GG	GG	GG	GG	GG	GG	GG	GG	GG	GG	GG	GG
SiO_2	36.09	36.09	36.55	36.07	36.02	35.80	36.45	36.72	36.05	36.20	36.92	37.17	36.18	35.62
Al_2O_3	13.16	13.65	13.36	13.35	13.44	12.95	13.41	13.36	13.32	13.48	13.55	13.52	13.48	13.64
TiO_2	2.12	2.34	2.11	2.41	2.21	2.06	2.11	2.01	2.23	2.19	2.30	2.20	2.05	2.23
Cr_2O_3	0.00	0.03	0.04	0.00	0.00	0.00	0.00	0.00	0.00	0.06	0.06	0.00	0.02	0.00
FeO	22.98	22.18	22.59	23.39	22.23	23.38	22.69	21.67	22.56	22.26	21.53	22.88	22.20	22.58
MnO	0.71	0.68	0.65	0.65	0.58	0.70	0.75	0.75	0.8	0.81	0.76	0.72	0.70	0.76
MgO	7.44	7.00	7.27	6.51	6.99	7.03	7.13	7.79	6.86	7.31	8.16	7.64	7.32	6.77
CaO	0.02	0.03	0.03	0.03	0.04	0.01	0.00	0.03	0.01	0.05	0.01	0.02	0.00	0.04
Na_2O	0.15	0.16	0.12	0.10	0.17	0.15	0.10	0.11	0.10	0.10	0.16	0.13	0.11	0.12
BaO	0.00	0.00	0.00	0.00	0.00	0.00	0.00	0.00	0.00	0.00	0.00	0.00	0.00	0.00
K_2O	8.98	9.15	9.02	9.04	8.72	9.02	9.28	9.38	9.11	9.21	9.19	9.32	9.20	8.88
Total	91.65	91.31	91.74	91.55	90.40	91.10	91.92	91.82	90.32	91.67	92.64	93.60	91.26	90.64
Structural Formulae based on 11 oxygen														
Si	2.93	2.93	2.95	2.94	2.95	2.94	2.95	2.96	2.96	2.93	2.94	2.95	2.94	3.34
Al^{IV}	1.07	1.07	1.05	1.06	1.05	1.06	1.05	1.04	1.04	1.07	1.06	1.05	1.06	0.66
$\sum Z=4$	4.00	4.00	4.00	4.00	4.00	4.00	4.00	4.00	4.00	4.00	4.00	4.00	4.00	4.00
Al^{VI}	0.19	0.24	0.23	0.22	0.24	0.19	0.23	0.23	0.25	0.22	0.21	0.21	0.23	0.84
Fe^{3+}	0.12	0.22	0.20	0.17	0.21	0.14	0.22	0.25	0.26	0.20	0.17	0.18	0.22	1.91
Ti	0.13	0.14	0.13	0.15	0.14	0.13	0.13	0.12	0.14	0.13	0.14	0.13	0.13	0.16
Mg	0.90	0.85	0.88	0.79	0.85	0.86	0.86	0.94	0.84	0.88	0.97	0.90	0.89	0.95
Fe^{2+}	1.44	1.28	1.32	1.42	1.32	1.46	1.32	1.21	1.29	1.31	1.26	1.33	1.29	0.00
Mn	0.05	0.05	0.04	0.04	0.04	0.05	0.05	0.05	0.01	0.06	0.05	0.05	0.05	0.06
$\sum Y=3$	2.83	2.78	2.8	2.79	2.8	2.83	2.81	2.8	2.79	2.8	2.8	2.8	2.81	3.92
Na	0.02	0.03	0.02	0.02	0.03	0.02	0.02	0.02	0.02	0.02	0.02	0.02	0.02	0.02
K	0.93	0.95	0.93	0.94	0.91	0.94	0.96	0.96	0.95	0.95	0.93	0.94	0.95	1.06
$\sum X=1$	0.95	0.98	0.95	0.96	0.94	0.96	0.98	0.98	0.97	0.97	0.95	0.96	0.97	1.08
Fe^t/Fe^t+Mg	0.63	0.64	0.64	0.67	0.64	0.65	0.64	0.61	0.65	0.63	0.60	0.63	0.63	0.67
$Mg/Mg+Fe^t$	0.37	0.36	0.36	0.33	0.36	0.35	0.36	0.39	0.35	0.37	0.40	0.37	0.37	0.33
$Fe^{2+}/F^{2+}+Fe^{3+}$	0.92	0.85	0.87	0.89	0.86	0.91	0.86	0.83	0.83	0.87	0.88	0.88	0.86	0.00
$Fe^{3+}/F^{2+}+Fe^{3+}$	0.08	0.15	0.13	0.11	0.14	0.09	0.14	0.17	0.17	0.13	0.12	0.12	0.14	1.00
FeO^t/MgO	3.09	3.17	3.11	3.59	3.18	3.33	3.18	2.78	3.29	3.05	2.64	3.00	3.03	0.38
$FeO^t/FeO^t +MgO$	8.44	8	8.27	7.51	7.99	8.03	8.13	8.79	7.86	8.31	9.16	8.64	8.32	7.77
ASI	1.33	1.34	1.35	1.33	1.37	1.3	1.31	1.3	1.33	1.33	1.34	1.31	1.33	1.39
Al^t	1.26	1.31	1.28	1.28	1.29	1.25	1.28	1.27	1.29	1.29	1.27	1.26	1.29	1.5

ASI =Molar $Al_2O_3/CaO + Na_2O+K_2O$; $Al^t = (Al^{IV}+ Al^{VI})$ pfu; FeO^t= total iron; Fe^t= total iron pfu.

TABLE 11: Calculated electron probe microanalysis (EPMA) data for biotites of PGN (KZ-33) granitoids

ASI =Molar Al_2O_3/CaO + Na_2O+K_2O; Al^t = (Al^{IV}+ Al^{VI}) pfu; FeO^t= total iron; Fe^t= total iron pfu.

Sample	KZ-33	KZ-33	KZ-33	KZ-33	KZ-33	KZ-33	KZ-33	KZ-33	KZ-33	KZ-33	KZ-33	KZ-33	KZ-33	KZ-33
SiO_2	36.60	35.18	36.70	36.77	36.92	36.22	36.09	36.46	36.58	36.68	36.20	36.56	36.86	36.43
Al_2O_3	15.66	15.18	15.84	15.66	15.42	15.72	15.21	15.22	14.37	15.97	15.29	15.66	15.34	15.55
TiO_2	2.68	1.84	2.86	2.71	2.50	2.58	2.55	2.51	2.61	2.72	2.56	2.25	2.83	2.54
Cr_2O_3	0.08	0.01	0.10	0.00	0.00	0.06	0.00	0.02	0.11	0.05	0.00	0.00	0.00	0.02
FeO	22.88	23.84	22.43	22.35	22.44	22.87	23.68	22.64	23.51	21.78	23.53	22.74	22.53	22.95
MnO	0.62	0.50	0.56	0.58	0.51	0.53	0.63	0.62	0.77	0.64	0.73	0.60	0.53	0.65
MgO	6.10	6.70	5.79	6.03	6.22	5.57	6.25	6.52	6.97	6.62	6.11	6.69	6.10	6.06
CaO	0.00	0.02	0.00	0.08	0.02	0.04	0.00	0.00	0.00	0.02	0.00	0.03	0.00	0.03
Na_2O	0.06	0.05	0.03	0.04	0.06	0.12	0.07	0.04	0.03	0.07	0.08	0.05	0.05	0.06
BaO	0.00	0.00	0.00	0.00	0.00	0.00	0.00	0.00	0.00	0.00	0.00	0.00	0.00	0.00
K_2O	9.45	8.58	9.43	9.63	9.72	9.03	9.34	9.45	9.48	9.48	9.31	9.12	9.54	9.44
Total	94.13	91.90	93.74	93.85	93.81	93.74	93.82	93.48	94.43	94.03	93.81	93.70	93.78	93.73
Structural Formulae based on 11 oxygen														
Si	2.88	2.85	2.89	2.89	2.91	2.89	2.86	2.89	2.89	2.87	2.87	2.88	2.90	2.88
Al^{IV}	1.12	1.15	1.11	1.11	1.09	1.11	1.14	1.11	1.11	1.13	1.13	1.12	1.10	1.12
$\sum Z=4$	4.00	4.00	4.00	4.00	4.00	4.00	4.00	4.00	4.00	4.00	4.00	4.00	4.00	4.00
Al^{VI}	0.33	0.30	0.36	0.35	0.34	0.36	0.29	0.31	0.22	0.35	0.30	0.34	0.33	0.33
Fe^{3+}	0.26	0.06	0.31	0.34	0.36	0.30	0.16	0.24	0.11	0.27	0.19	0.22	0.30	0.27
Ti	0.16	0.11	0.17	0.16	0.15	0.15	0.15	0.15	0.15	0.16	0.15	0.13	0.17	0.15
Mg	0.72	0.81	0.68	0.71	0.73	0.66	0.74	0.77	0.82	0.77	0.72	0.79	0.72	0.71
Fe^{2+}	1.25	1.55	1.17	1.13	1.12	1.22	1.41	1.26	1.44	1.15	1.37	1.28	1.19	1.25
Mn	0.04	0.03	0.04	0.04	0.03	0.04	0.04	0.04	0.05	0.04	0.05	0.04	0.04	0.04
$\sum Y=3$	2.76	2.86	2.73	2.73	2.73	2.73	2.79	2.77	2.79	2.74	2.78	2.8	2.75	2.75
Na	0.01	0.01	0.00	0.01	0.01	0.02	0.01	0.01	0.00	0.01	0.01	0.01	0.01	0.01
K	0.95	0.89	0.95	0.97	0.98	0.92	0.95	0.95	0.95	0.95	0.94	0.92	0.96	0.95
$\sum X=1$	0.96	0.90	0.95	0.98	0.99	0.94	0.96	0.96	0.95	0.96	0.95	0.93	0.97	0.96
$Fe^t$$Fe^t$+Mg	0.68	0.67	0.68	0.68	0.67	0.70	0.68	0.66	0.65	0.65	0.68	0.66	0.67	0.68
Mg/Mg+Fe^t	0.32	0.33	0.32	0.32	0.33	0.30	0.32	0.34	0.35	0.35	0.32	0.34	0.33	0.32
$Fe^{2+}/F^{2+}+Fe^{3+}$	0.83	0.96	0.79	0.77	0.76	0.80	0.90	0.84	0.93	0.81	0.88	0.85	0.80	0.82
$Fe^{3+}/F^{2+}+Fe^{3+}$	0.17	0.04	0.21	0.23	0.24	0.20	0.10	0.16	0.07	0.19	0.12	0.15	0.20	0.18
FeO^t/MgO	3.75	3.56	3.87	3.71	3.61	4.11	3.79	3.47	3.37	3.29	3.85	3.40	3.69	3.79
FeO^t/FeO^t +MgO	7.1	7.7	6.79	7.03	7.22	6.57	7.25	7.52	7.97	7.62	7.11	7.69	7.1	7.06
ASI	1.51	1.61	1.55	1.49	1.44	1.56	1.49	1.48	1.4	1.54	1.51	1.57	1.47	1.51
Al^t	1.45	1.45	1.47	1.46	1.43	1.47	1.43	1.42	1.33	1.48	1.43	1.46	1.43	1.45

TABLE 12: Calculated electron probe microanalysis (EPMA) data for biotites of NPG (KH-7A) granitoids
ASI =Molar Al_2O_3/CaO + Na_2O+K_2O; Al^t = (Al^{IV}+ Al^{VI}) pfu; FeO^t= total iron; Fe^t= total iron pfu.

Sample	KH-7A	KH-7A	KH-7A	KH-7A	KH-7A	KH-7A	KH-7A	KH-7A	KH-7A	KH-7A	KH-7A	KH-7A
SiO_2	36.37	36.62	36.4	36.45	36.13	36.43	36.47	36.19	36.51	36.6	36.17	36.33
Al_2O_3	14.52	14.79	13.99	14.22	14.07	14.24	14.14	15.03	14.47	14.34	14.41	14.9
TiO_2	2.54	3.03	2.84	2.91	2.95	2.96	2.8	2.65	2.86	2.88	3	2.44
Cr_2O_3	0.06	0.00	0.06	0.00	0.00	0.00	0.03	0.00	0.03	0.02	0.00	0.00
FeO	22.67	22.43	22.97	22.26	23.61	23.45	23.15	21.9	22.97	23.32	22.71	22.37
MnO	0.62	0.46	0.57	0.58	0.46	0.5	0.56	0.4	0.48	0.56	0.55	0.5
MgO	7.48	7.67	8.1	7.89	7.68	7.67	7.63	7.16	7.5	7.67	7.96	7.46
CaO	0.06	0.01	0.00	0.00	0.00	0.01	0.00	0.00	0.00	0.00	0.00	0.00
Na_2O	0.05	0.03	0.09	0.07	0.07	0.07	0.07	0.1	0.12	0.08	0.07	0.09
BaO	0.00	0.00	0.00	0.00	0.00	0.00	0.00	0.00	0.00	0.00	0.00	0.00
K_2O	9.71	9.57	9.5	9.73	9.49	9.64	9.59	9.65	9.59	9.63	9.7	9.76
Total	94.08	94.61	94.52	94.11	94.46	94.97	94.44	93.08	94.53	95.10	94.57	93.85
Structural Formulae based on 11 oxygen												
Si	2.87	2.86	2.86	2.87	2.85	2.86	2.87	2.87	2.87	2.86	2.84	2.87
Al^{IV}	1.13	1.14	1.14	1.13	1.15	1.14	1.13	1.13	1.13	1.14	1.16	1.13
$\sum Z=4$	4.00	4.00	4.00	4.00	4.00	4.00	4.00	4.00	4.00	4.00	4.00	4.00
Al^{VI}	0.23	0.23	0.16	0.19	0.16	0.18	0.19	0.28	0.21	0.19	0.18	0.26
Fe^{3+}	0.15	0.08	0.00	0.08	0.02	0.02	0.06	0.22	0.09	0.04	0.01	0.19
Ti	0.15	0.18	0.17	0.17	0.18	0.17	0.17	0.16	0.17	0.17	0.18	0.14
Mg	0.88	0.89	0.95	0.93	0.90	0.90	0.90	0.85	0.88	0.89	0.93	0.88
Fe^{2+}	1.35	1.39	1.51	1.38	1.54	1.52	1.47	1.23	1.42	1.49	1.48	1.29
Mn	0.04	0.03	0.04	0.04	0.03	0.03	0.04	0.03	0.03	0.04	0.04	0.03
$\sum Y=3$	2.80	2.80	2.83	2.80	2.83	2.82	2.81	2.77	2.80	2.82	2.82	2.79
Na	0.01	0.00	0.01	0.01	0.01	0.01	0.01	0.02	0.02	0.01	0.01	0.01
K	0.98	0.95	0.95	0.98	0.96	0.96	0.96	0.98	0.96	0.96	0.97	0.98
$\sum X=1$	0.99	0.95	0.96	0.99	0.97	0.97	0.97	1.00	0.98	0.97	0.98	0.99
Fe^t/Fe^t+Mg	0.63	0.62	0.61	0.61	0.63	0.63	0.63	0.63	0.63	0.63	0.62	0.63
$Mg/Mg+Fe^t$	0.37	0.38	0.39	0.39	0.37	0.37	0.37	0.37	0.37	0.37	0.38	0.37
$Fe^{2+}/F^{2+}+Fe^{3+}$	0.90	0.95	1.00	0.94	0.98	0.99	0.96	0.85	0.94	0.97	0.99	0.87
$Fe^{3+}/F^{2+}+Fe^{3+}$	0.10	0.05	0.00	0.06	0.02	0.01	0.04	0.15	0.06	0.03	0.01	0.13
FeO^t/MgO	3.03	2.92	2.84	2.82	3.07	3.06	3.03	3.06	3.06	3.04	2.85	3
FeO^t/FeO^t+MgO	0.75	0.75	0.74	0.74	0.75	0.75	0.75	0.75	0.75	0.75	0.74	0.75
ASI	1.36	1.42	1.34	1.34	1.35	1.35	1.35	1.42	1.37	1.36	1.36	1.39
Al^t	1.36	1.37	1.3	1.32	1.31	1.32	1.32	1.41	1.34	1.33	1.34	1.39

TABLE 12 Continued

ASI =Molar Al_2O_3/CaO + Na_2O+K_2O; Al^t = (Al^{IV}+ Al^{VI}) pfu; FeO^t= total iron; Fe^t= total iron pfu.

Sample	KH-7A	KH-7A	KH-7A	KH-7A	KH-7A	KH-7A	KH-7A	KH-7A	KH-7A	KH-7A	KH-7A	KH-7A
SiO_2	36.11	36.28	36.51	36.5	36.91	36.36	36.74	36.17	36.15	36.57	36.73	36.66
Al_2O_3	14.9	14.75	14.51	14.61	15.36	14.9	15.10	14.5	14.72	15.2	15.24	14.89
TiO_2	2.69	2.48	2.8	2.67	2.93	2.72	2.98	2.59	2.78	2.85	2.76	2.65
Cr_2O_3	0.00	0.00	0.00	0.1	0.06	0.03	0.00	0.05	0.03	0.05	0.00	0.00
FeO	22.75	22.69	23.3	23.13	21.57	22.49	21.99	22.68	22.73	22.58	23.01	22.89
MnO	0.57	0.42	0.35	0.41	0.41	0.39	0.44	0.53	0.59	0.47	0.36	0.51
MgO	7.33	7.59	7.68	7.74	7.73	7.65	7.47	7.47	7.54	7.01	7.17	7.12
CaO	0.00	0.00	0.01	0.00	0.00	0.00	0.01	0.07	0.00	0.01	0.00	0.00
Na_2O	0.11	0.1	0.06	0.05	0.05	0.08	0.07	0.05	0.06	0.08	0.07	0.06
BaO	0.00	0.00	0.00	0.00	0.00	0.00	0.00	0.00	0.00	0.00	0.00	0.00
K_2O	9.63	9.9	9.56	9.51	9.62	9.67	9.49	9.65	9.66	9.78	9.64	9.69
Total	94.09	94.21	94.78	94.72	94.64	94.29	94.29	93.76	94.26	94.60	94.98	94.47
Structural Formulae based on 11 oxygen												
Si	2.85	2.86	2.86	2.86	2.87	2.86	2.87	2.87	2.85	2.87	2.87	2.88
Al^{IV}	1.15	1.14	1.14	1.14	1.13	1.14	1.13	1.13	1.15	1.13	1.13	1.12
$\sum Z$=4	4.00	4.00	4.00	4.00	4.00	4.00	4.00	4.00	4.00	4.00	4.00	4.00
Al^{VI}	0.24	0.23	0.20	0.21	0.28	0.24	0.26	0.22	0.22	0.27	0.27	0.26
Fe^{3+}	0.12	0.16	0.05	0.06	0.16	0.12	0.14	0.13	0.08	0.19	0.15	0.18
Ti	0.16	0.15	0.17	0.16	0.17	0.16	0.18	0.15	0.16	0.17	0.16	0.16
Mg	0.86	0.89	0.90	0.90	0.90	0.90	0.87	0.88	0.89	0.82	0.83	0.83
Fe^{2+}	1.39	1.33	1.48	1.46	1.24	1.36	1.29	1.37	1.42	1.29	1.35	1.33
Mn	0.04	0.03	0.02	0.03	0.03	0.03	0.03	0.04	0.04	0.03	0.02	0.03
$\sum Y$=3	2.80	2.80	2.82	2.82	2.77	2.80	2.78	2.80	2.81	2.77	2.79	2.78
Na	0.02	0.02	0.01	0.01	0.01	0.01	0.01	0.01	0.01	0.01	0.01	0.01
K	0.97	1.00	0.96	0.95	0.95	0.97	0.95	0.98	0.97	0.98	0.96	0.97
$\sum X$=1	0.99	1.02	0.97	0.96	0.96	0.98	0.96	0.99	0.98	0.99	0.97	0.98
Fe^t/Fe^t+Mg	0.64	0.63	0.63	0.63	0.61	0.62	0.62	0.63	0.63	0.64	0.64	0.64
Mg/Mg+Fe^t	0.36	0.37	0.37	0.37	0.39	0.38	0.38	0.37	0.37	0.36	0.36	0.36
Fe^{2+}/F^{2+}+Fe^{3+}	0.92	0.89	0.97	0.96	0.88	0.92	0.90	0.91	0.95	0.87	0.90	0.88
Fe^{3+}/F^{2+}+Fe^{3+}	0.08	0.11	0.03	0.04	0.12	0.08	0.10	0.09	0.05	0.13	0.10	0.12
FeO^t/MgO	3.1	2.99	3.03	2.99	2.79	2.94	2.94	3.04	3.01	3.22	3.21	3.21
FeO^t/FeO^t +MgO	0.76	0.75	0.75	0.75	0.74	0.75	0.75	0.75	0.75	0.76	0.76	0.76
ASI	1.41	1.36	1.39	1.41	1.46	1.41	1.45	1.36	1.39	1.42	1.44	1.41
Al^t	1.39	1.37	1.34	1.35	1.41	1.38	1.39	1.35	1.37	1.4	1.4	1.38

TABLE 13: Calculated electron probe microanalysis (EPMA) data for biotites of NPG (KH-8A) granitoids
ASI =Molar Al_2O_3/CaO + Na_2O+K_2O; Al^t = (Al^{IV}+ Al^{VI}) pfu; FeO^t= total iron; Fe^t= total iron pfu.

Sample	KH-8A	KH-8A	KH-8A	KH-8A	KH-8A	KH-8A	KH-8A	KH-8A	KH-8A	KH-8A	KH-8A	KH-8A
SiO_2	36.72	36.55	36.64	36.79	36.62	36.87	36.77	36.66	36.79	37.08	36.69	36.52
Al_2O_3	13.96	14.20	14.07	14.75	14.67	14.47	14.19	14.32	14.42	14.46	14.25	14.33
TiO_2	1.90	1.96	1.87	2.01	2.00	1.55	2.17	2.11	2.01	2.14	1.95	1.93
Cr_2O_3	0.00	0.06	0.04	0.05	0.01	0.00	0.00	0.04	0.00	0.01	0.00	0.03
FeO	22.41	22.63	23.44	22.40	22.49	22.82	22.09	22.26	21.96	22.06	22.68	22.46
MnO	0.00	0.53	0.66	0.54	0.47	0.51	0.67	0.51	0.58	0.54	0.61	0.74
MgO	8.95	8.97	8.94	8.51	8.63	8.90	8.99	8.91	8.64	8.88	8.88	8.59
CaO	0.00	0.02	0.00	0.04	0.00	0.03	0.04	0.00	0.00	0.01	0.02	0.03
Na_2O	0.07	0.05	0.05	0.02	0.02	0.05	0.07	0.09	0.08	0.10	0.09	0.09
BaO	0.00	0.00	0.00	0.00	0.00	0.00	0.00	0.00	0.00	0.00	0.00	0.00
K_2O	9.49	9.56	9.63	9.50	9.63	9.57	9.49	9.63	9.48	9.58	9.56	9.55
Total	94.10	94.53	95.34	94.61	94.54	94.77	94.48	94.53	93.96	94.86	94.73	94.27
Structural Formulae based on 11 oxygen												
Si	2.89	2.87	2.86	2.88	2.87	2.88	2.88	2.87	2.89	2.89	2.87	2.87
Al^{IV}	1.11	1.13	1.14	1.12	1.13	1.12	1.12	1.13	1.11	1.11	1.13	1.13
$\sum Z=4$	4.00	4.00	4.00	4.00	4.00	4.00	4.00	4.00	4.00	4.00	4.00	4.00
Al^{VI}	0.19	0.18	0.16	0.23	0.22	0.22	0.19	0.19	0.23	0.21	0.19	0.20
Fe^{3+}	0.07	0.04	0.01	0.11	0.09	0.11	0.05	0.07	0.12	0.10	0.05	0.09
Ti	0.11	0.12	0.11	0.12	0.12	0.09	0.13	0.12	0.12	0.13	0.11	0.11
Mg	1.05	1.05	1.04	0.99	1.01	1.04	1.05	1.04	1.01	1.03	1.04	1.01
Fe^{2+}	1.41	1.45	1.53	1.36	1.39	1.39	1.40	1.39	1.32	1.33	1.43	1.39
Mn	0.04	0.04	0.04	0.04	0.03	0.03	0.04	0.03	0.04	0.04	0.04	0.05
$\sum Y=3$	2.86	2.87	2.89	2.05	2.85	2.87	2.86	2.85	2.84	2.84	2.87	2.86
Na	0.01	0.01	0.01	0.00	0.00	0.01	0.01	0.01	0.01	0.02	0.01	0.01
K	0.95	0.96	0.96	0.95	0.96	0.95	0.95	0.96	0.95	0.95	0.96	0.96
$\sum X=1$	0.96	0.97	0.97	0.95	0.96	0.96	0.96	0.97	0.96	0.97	0.97	0.97
Fe^t/Fe^t+Mg	0.58	0.59	0.60	0.60	0.59	0.59	0.58	0.58	0.59	0.58	0.59	0.59
$Mg/Mg+Fe^t$	0.42	0.41	0.40	0.40	0.41	0.41	0.42	0.42	0.41	0.42	0.41	0.41
$Fe^{2+}/F^{2+}+Fe^{3+}$	0.95	0.98	1.00	0.93	0.94	0.93	0.97	0.95	0.91	0.93	0.96	0.94
$Fe^{3+}/F^{2+}+Fe^{3+}$	0.05	0.02	0.00	0.07	0.06	0.07	0.03	0.05	0.09	0.07	0.04	0.06
FeO^t/MgO	2.5	2.52	2.62	2.63	2.61	2.56	2.46	2.5	2.54	2.48	2.55	2.61
$FeO^t/FeO^t +MgO$	0.71	0.72	0.72	0.72	0.72	0.72	0.71	0.71	0.72	0.71	0.72	0.72
ASI	1.34	1.36	1.34	1.42	1.40	1.38	1.36	1.35	1.39	1.37	1.35	1.36
Al^t	1.3	1.31	1.3	1.35	1.35	1.34	1.31	1.32	1.34	1.32	1.32	1.33

TABLE 13 Continued

ASI =Molar Al_2O_3/CaO + Na_2O+K_2O; Al^t = (Al^{IV}+ Al^{VI}) pfu; FeO^t= total iron; Fe^t= total iron pfu.

Sample	KH-8A	KH-8A	KH-8A	KH-8A	KH-8A	KH-8A	KH-8A	KH-8A	KH-8A	KH-8A	KH-8A	KH-8A
SiO_2	36.65	36.34	36.65	36.66	36.95	37.06	37.01	36.61	36.79	36.86	36.77	36.77
Al_2O_3	14.04	14.12	14.12	14.34	14.45	14.70	14.37	14.43	13.91	14.15	14.50	14.81
TiO_2	2.25	2.34	2.22	2.29	2.30	2.45	1.85	1.83	1.71	2.06	1.98	1.98
Cr_2O_3	0.04	0.05	0.00	0.04	0.01	0.00	0.00	0.01	0.04	0.09	0.06	0.05
FeO	22.58	22.86	22.28	22.90	22.84	22.50	22.55	22.25	22.73	22.48	22.53	22.59
MnO	0.47	0.48	0.46	0.37	0.56	0.46	0.49	0.46	0.47	0.44	0.51	0.52
MgO	8.74	8.43	8.89	8.42	8.59	8.23	8.88	8.84	9.06	8.78	8.82	8.40
CaO	0.00	0.00	0.06	0.02	0.02	0.01	0.00	0.02	0.05	0.00	0.01	0.01
Na_2O	0.08	0.08	0.07	0.11	0.10	0.06	0.09	0.05	0.08	0.07	0.07	0.08
BaO	0.00	0.00	0.00	0.00	0.00	0.00	0.00	0.00	0.00	0.00	0.00	0.00
K_2O	9.64	9.44	9.55	9.48	9.25	9.54	9.39	9.40	9.32	9.55	9.30	9.34
Total	94.49	94.14	94.30	94.63	95.07	95.01	94.63	93.90	94.16	94.48	94.55	94.55
Structural Formulae based on 11 oxygen												
Si	2.88	2.87	2.88	2.87	2.88	2.88	2.89	2.88	2.90	2.89	2.88	2.88
Al^{IV}	1.12	1.13	1.12	1.13	1.12	1.12	1.11	1.12	1.10	1.11	1.12	1.12
$\sum Z$=4	4.00	4.00	4.00	4.00	4.00	4.00	4.00	4.00	4.00	4.00	4.00	4.00
Al^{VI}	0.18	0.18	0.18	0.20	0.20	0.23	0.21	0.22	0.19	0.20	0.21	0.24
Fe^{3+}	0.05	0.02	0.06	0.06	0.02	0.11	0.08	0.09	0.06	0.08	0.05	0.10
Ti	0.13	0.14	0.13	0.13	0.13	0.14	0.11	0.11	0.10	0.12	0.12	0.12
Mg	1.02	0.99	1.04	0.98	1.00	0.95	1.03	1.04	1.06	1.03	1.03	0.98
Fe^{2+}	1.43	1.49	1.40	1.44	1.46	1.36	1.39	1.38	1.44	1.39	1.43	1.38
Mn	0.03	0.03	0.03	0.02	0.04	0.03	0.03	0.03	0.03	0.03	0.03	0.03
$\sum Y$=3	2.85	2.85	2.85	2.84	2.86	2.82	2.86	2.86	2.88	2.85	2.87	2.85
Na	0.01	0.01	0.01	0.02	0.02	0.01	0.01	0.01	0.01	0.01	0.01	0.01
K	0.97	0.95	0.96	0.95	0.92	0.95	0.94	0.94	0.94	0.95	0.93	0.93
$\sum X$=1	0.98	0.96	0.97	0.97	0.94	0.96	0.95	0.95	0.95	0.96	0.94	0.94
$Fe^t$$Fe^t$+Mg	0.59	0.60	0.58	0.60	0.60	0.61	0.59	0.59	0.58	0.59	0.59	0.60
Mg/Mg+Fe^t	0.41	0.40	0.42	0.40	0.40	0.39	0.41	0.41	0.42	0.41	0.41	0.40
Fe^{2+}/F^{2+}+Fe^{3+}	0.96	0.99	0.96	0.96	0.98	0.93	0.94	0.94	0.96	0.94	0.97	0.93
Fe^{3+}/F^{2+}+Fe^{3+}	0.04	0.01	0.04	0.04	0.02	0.07	0.06	0.06	0.04	0.06	0.03	0.07
FeO^t/MgO	2.58	2.71	2.51	2.72	2.66	2.73	2.54	2.52	2.51	2.56	2.55	2.69
FeO^t/FeO^t +MgO	0.72	0.73	0.71	0.73	0.73	0.73	0.72	0.72	0.72	0.72	0.72	0.73
ASI	1.33	1.36	1.34	1.37	1.41	1.41	1.39	1.40	1.35	1.35	1.42	1.44
Al^t	1.3	1.31	1.3	1.33	1.32	1.35	1.32	1.34	1.29	1.31	1.33	1.36

TABLE 14: Calculated electron probe microanalysis (EPMA) data for biotites of PGN (KZ-15) Granitoids

Sample	KZ-15	KZ-15	KZ-15	KZ-15	KZ-15	KZ-15	KZ-15	KZ-15
SiO_2	35.41	35.73	36.42	36.07	36.32	34.46	35.98	35.70
Al_2O_3	16.86	16.76	15.43	15.33	15.43	16.47	15.88	15.90
TiO_2	2.40	2.33	2.64	2.56	2.87	2.24	2.25	2.06
Cr_2O_3	0.00	0.00	0.04	0.00	0.01	0.00	0.01	0.00
FeO	19.48	19.39	19.43	19.47	19.37	19.63	19.05	19.60
MnO	0.37	0.48	0.34	0.38	0.40	0.40	0.37	0.47
MgO	9.62	9.74	9.88	9.81	9.36	10.01	10.12	9.97
CaO	0.00	0.00	0.00	0.00	0.00	0.01	0.00	0.00
Na_2O	0.08	0.03	0.07	0.06	0.09	0.09	0.07	0.06
BaO	0.00	0.00	0.00	0.00	0.00	0.00	0.00	0.00
K_2O	9.79	9.65	9.78	9.94	9.81	9.88	9.77	9.84
Total	94.01	94.11	94.03	93.62	93.66	94.19	93.50	93.60
Structural Formulae based on 11 oxygen								
Si	2.75	2.77	2.83	2.82	2.83	2.76	2.81	2.79
Al^{IV}	1.25	1.23	1.17	1.18	1.17	1.24	1.19	1.21
$\sum Z=4$	4.00	4.00	4.00	4.00	4.00	4.00	4.00	4.00
Al^{VI}	0.30	0.30	0.24	0.23	0.25	0.27	0.27	0.26
Fe^{3+}	0.05	0.04	0.07	0.08	0.11	0.03	0.08	0.07
Ti	0.14	0.14	0.15	0.15	0.17	0.13	0.13	0.12
Mg	1.11	1.13	1.14	1.14	1.09	1.16	1.18	1.16
Fe^{2+}	1.22	1.21	1.19	1.19	1.16	1.25	1.16	1.22
Mn	0.02	0.03	0.02	0.03	0.03	0.03	0.02	0.03
$\sum Y=3$	2.84	2.85	2.82	2.82	2.80	2.86	2.84	2.86
Na	0.01	0.00	0.01	0.01	0.01	0.01	0.01	0.01
K	0.97	0.95	0.97	0.99	0.98	0.98	0.97	0.98
$\sum X=1$	0.98	0.95	0.98	1.00	0.99	0.99	0.98	0.99
Fe^t/Fe^t+Mg	0.53	0.53	0.52	0.53	0.54	0.52	0.51	0.52
$Mg/Mg+Fe^t$	0.47	0.47	0.48	0.47	0.46	0.48	0.49	0.48
$Fe^{2+}/F^{2+}+Fe^{3+}$	0.96	0.97	0.94	0.94	0.91	0.98	0.93	0.95
$Fe^{3+}/F^{2+}+Fe^{3+}$	0.04	0.03	0.06	0.06	0.09	0.02	0.07	0.05
FeO^t/MgO	2.02	1.99	1.97	1.98	2.07	1.96	1.88	1.97
FeO^t/FeO^t+MgO	0.67	0.67	0.66	0.66	0.67	0.66	0.65	0.66
ASI	1.57	1.60	1.44	1.41	1.43	1.52	1.49	1.48
Al^t	1.55	1.53	1.41	1.41	1.42	1.51	1.46	1.47

ASI =Molar A l_2O_3/CaO + Na_2O+K_2O; Al^t = (Al^{IV}+ Al^{VI}) pfu; FeO^t= total iron; Fe^t= total iron pfu.

TABLE 14 Continued

Sample	KZ-15	KZ-15	KZ-15	KZ-15	KZ-15	KZ-15	KZ-15	KZ-15	KZ-15
SiO_2	36.21	36.16	35.97	37.29	37.64	35.54	35.48	35.96	35.54
Al_2O_3	16.24	16.22	16.05	14.95	14.69	16.33	15.90	15.78	16.03
TiO_2	1.85	2.13	2.33	2.69	2.77	2.56	2.69	2.25	2.25
Cr_2O_3	0.00	0.03	0.00	0.00	0.00	0.01	0.01	0.01	0.00
FeO	19.21	19.16	19.41	17.16	16.88	19.31	19.38	19.00	19.53
MnO	0.39	0.45	0.40	0.31	0.26	0.49	0.51	0.42	0.50
MgO	10.15	10.28	9.85	11.15	11.45	9.36	9.29	9.90	9.53
CaO	0.00	0.00	0.00	0.03	0.00	0.00	0.01	0.02	0.02
Na_2O	0.08	0.06	0.08	0.09	0.09	0.07	0.04	0.07	0.06
BaO	0.00	0.00	0.00	0.00	0.00	0.00	0.00	0.00	0.00
K_2O	9.98	9.65	9.77	9.97	9.80	9.73	9.73	9.85	9.65
Total	94.11	94.14	93.86	93.64	93.58	93.40	93.04	93.26	93.11
Structural Formulae based on 11 oxygen									
Si	2.81	2.80	2.80	2.87	2.89	2.78	2.79	2.81	2.79
Al^{IV}	1.19	1.20	1.20	1.13	1.11	1.22	1.21	1.19	1.21
$\sum Z=4$	4.00	4.00	4.00	4.00	4.00	4.00	4.00	4.00	4.00
Al^{VI}	0.29	0.28	0.27	0.23	0.22	0.29	0.26	0.27	0.28
Fe^{3+}	0.15	0.06	0.08	0.15	0.13	0.07	0.06	0.12	0.07
Ti	0.11	0.12	0.14	0.16	0.16	0.15	0.16	0.13	0.13
Mg	1.17	1.19	1.14	1.28	1.31	1.09	1.09	1.15	1.12
Fe^{2+}	1.10	1.18	1.19	0.95	0.95	1.19	1.22	1.12	1.21
Mn	0.03	0.03	0.03	0.02	0.02	0.03	0.03	0.03	0.03
$\sum Y=3$	2.84	2.86	2.84	2.79	2.80	2.82	2.82	2.83	2.84
Na	0.01	0.01	0.01	0.01	0.01	0.01	0.01	0.01	0.01
K	0.99	0.95	0.97	0.98	0.96	0.97	0.98	0.98	0.97
$\sum X=1$	1.00	0.96	0.98	0.99	0.97	0.98	0.99	0.99	0.98
Fe^t/Fe^t+Mg	0.51	0.51	0.53	0.46	0.45	0.54	0.54	0.52	0.53
$Mg/Mg+Fe^t$	0.49	0.49	0.47	0.54	0.55	0.46	0.46	0.48	0.47
$Fe^{2+}/F^{2+}+Fe^{3+}$	0.88	0.95	0.94	0.86	0.88	0.94	0.95	0.90	0.94
$Fe^{3+}/F^{2+}+Fe^{3+}$	0.12	0.05	0.06	0.14	0.12	0.06	0.05	0.10	0.06
FeO^t/MgO	1.89	1.86	1.97	1.54	1.47	2.06	2.09	1.92	2.05
FeO^t/FeO^t+MgO	0.65	0.65	0.66	0.61	0.6	0.67	0.68	0.66	0.67
ASI	1.49	1.54	1.50	1.36	1.37	1.53	1.50	1.46	1.52
Al^t	1.48	1.48	1.47	1.36	1.33	1.51	1.47	1.46	1.49

ASI $=$Molar A l_2O_3/CaO $+$ Na_2O+K_2O; $Al^t = (Al^{IV}+ Al^{VI})$ pfu; $FeO^t=$ total iron; $Fe^t=$ total iron pfu.

Table 15: Calculated electron probe microanalysis (EPMA) data for biotites of PGN (KZ-17) granitoids

ASI =Molar $Al_2O_3/CaO + Na_2O+K_2O$; $Al^t = (Al^{IV}+ Al^{VI})$ pfu; FeO^t= total iron; Fe^t= total iron pfu.

Sample	KZ-17	KZ-17	KZ-17	KZ-17	KZ-17	KZ-17	KZ-17	KZ-17	KZ-17	KZ-17	KZ-17	KZ-17
SiO_2	37.82	37.61	37.89	38.22	38.05	37.60	37.61	37.61	37.19	37.65	37.78	39.29
Al_2O_3	14.14	14.31	14.50	14.85	14.77	14.52	14.71	14.91	14.64	15.03	14.07	16.01
TiO_2	1.81	1.76	1.84	1.76	1.67	1.77	1.63	1.62	1.61	1.36	1.55	1.31
Cr_2O_3	0.00	0.00	0.03	0.02	0.00	0.04	0.06	0.09	0.03	0.00	0.11	0.06
FeO	19.06	19.38	19.05	18.51	18.60	18.26	18.57	19.04	19.09	19.44	18.96	17.94
MnO	0.75	0.65	0.72	0.60	0.82	0.82	0.62	0.66	0.63	0.68	0.62	0.47
MgO	10.53	10.71	10.82	10.73	10.58	10.18	10.21	10.12	10.29	10.17	10.19	8.83
CaO	0.00	0.02	0.00	0.02	0.00	0.01	0.00	0.01	0.00	0.00	0.00	0.01
Na_2O	0.07	0.05	0.06	0.07	0.07	0.04	0.05	0.04	0.08	0.04	0.08	0.07
BaO	0.00	0.00	0.00	0.00	0.00	0.00	0.00	0.00	0.00	0.00	0.00	0.00
K_2O	9.79	9.71	9.64	9.75	9.78	10.01	9.79	9.90	9.72	9.80	9.75	9.57
Total	93.97	94.20	94.55	94.53	94.34	93.25	93.25	94.00	93.28	94.17	93.11	93.56
Structural Formulae based on 11 oxygen												
Si	2.93	2.91	2.91	2.93	2.93	2.93	2.93	2.91	2.90	2.91	2.95	3.01
Al^{IV}	1.07	1.09	1.09	1.07	1.07	1.07	1.07	1.09	1.10	1.09	1.05	0.99
$\sum Z=4$	4.00	4.00	4.00	4.00	4.00	4.00	4.00	4.00	4.00	4.00	4.00	4.00
Al^{VI}	0.22	0.22	0.23	0.27	0.26	0.26	0.28	0.27	0.25	0.28	0.25	0.45
Fe^{3+}	0.20	0.14	0.14	0.24	0.24	0.30	0.28	0.27	0.21	0.25	0.29	0.62
Ti	0.11	0.10	0.11	0.10	0.10	0.10	0.10	0.09	0.09	0.08	0.09	0.08
Mg	1.22	1.24	1.24	1.22	1.21	1.18	1.18	1.17	1.20	1.17	1.19	1.01
Fe^{2+}	1.04	1.11	1.08	0.94	0.96	0.89	0.93	0.97	1.04	1.00	0.95	0.53
Mn	0.05	0.04	0.05	0.04	0.05	0.05	0.04	0.04	0.04	0.04	0.04	0.03
$\sum Y=3$	2.83	2.85	2.85	2.82	2.82	2.80	2.81	2.82	2.84	2.84	2.81	2.72
Na	0.01	0.01	0.01	0.01	0.01	0.01	0.01	0.01	0.01	0.01	0.01	0.01
K	0.97	0.96	0.95	0.95	0.96	1.00	0.97	0.98	0.97	0.97	0.97	0.93
$\sum X=1$	0.98	0.97	0.95	0.96	0.97	1.00	0.98	0.98	0.98	0.97	0.98	0.92
Fe^t/Fe^t+Mg	0.50	0.50	0.50	0.49	0.50	0.50	0.51	0.51	0.51	0.52	0.51	0.53
$Mg/Mg+Fe^t$	0.50	0.50	0.50	0.51	0.50	0.50	0.49	0.49	0.49	0.48	0.49	0.47
$Fe^{2+}/F^{2+}+Fe^{3+}$	0.84	0.89	0.88	0.80	0.80	0.75	0.77	0.78	0.83	0.80	0.77	0.46
$Fe^{3+}/F^{2+}+Fe^{3+}$	0.16	0.11	0.12	0.20	0.20	0.25	0.23	0.22	0.17	0.20	0.23	0.54
FeO^t/MgO	1.81	1.81	1.76	1.73	1.76	1.79	1.82	1.88	1.86	1.91	1.86	2.03
$FeO^t/FeO^t +MgO$	0.64	0.64	0.64	0.63	0.64	0.64	0.65	0.65	0.65	0.66	0.65	0.67
ASI	1.32	1.35	1.38	1.39	1.38	1.33	1.38	1.38	1.37	1.41	1.32	1.53
Al^t	1.29	1.31	1.32	1.34	1.33	1.33	1.35	1.36	1.35	1.37	1.3	1.44

TABLE 15 Continued

ASI =Molar Al_2O_3/CaO + Na_2O+K_2O; Al^t = (Al^{IV}+ Al^{VI}) pfu; FeO^t= total iron; Fe^t= total iron pfu.

Sample	KZ-17	KZ-17	KZ-17	KZ-17	KZ-17	KZ-17	KZ-17	KZ-17	KZ-17	KZ-17	KZ-17	KZ-17
SiO_2	37.33	38.08	37.77	37.97	37.96	37.66	37.96	37.56	38.56	38.03	37.64	38.18
Al_2O_3	14.65	14.64	14.98	15.05	14.86	14.75	14.19	14.26	14.56	14.89	13.61	14.44
TiO_2	1.30	1.15	1.22	1.10	1.10	1	1.04	1.05	0.95	1.25	1.16	1.01
Cr_2O_3	0.00	0.06	0.00	0.00	0.00	0.00	0.15	0.14	0.00	0.03	0.10	0.08
FeO	18.96	18.84	19.09	18.64	18.39	19.73	20.06	19.63	18.61	19.54	19.56	19.68
MnO	0.70	0.63	0.72	0.64	0.63	0.67	0.65	0.63	0.70	0.71	0.68	0.79
MgO	10.14	10.57	10.38	10.54	10.66	10.39	10.48	10.37	10.49	9.99	10.23	10.36
CaO	0.00	0.00	0.00	0.00	0.00	0.00	0.03	0.00	0.01	0.02	0.02	0.05
Na_2O	0.02	0.03	0.05	0.04	0.05	0.03	0.10	0.10	0.10	0.13	0.09	0.12
BaO	0.00	0.00	0.00	0.00	0.00	0.00	0.00	0.00	0.00	0.00	0.00	0.00
K_2O	9.97	9.48	9.70	9.90	9.73	9.39	9.34	9.48	9.46	9.69	9.86	9.27
Total	93.87	93.48	93.91	93.88	93.38	93.62	94.00	93.22	93.44	94.28	92.95	93.98
Structural Formulae based on 11 oxygen												
Si	2.92	2.95	2.92	2.93	2.94	2.93	2.95	2.94	2.98	2.94	2.96	2.95
Al^{IV}	1.08	1.05	1.08	1.07	1.06	1.07	1.05	1.06	1.02	1.06	1.04	1.05
$\sum Z$=4	4.00	4.00	4.00	4.00	4.00	4.00	4.00	4.00	4.00	4.00	4.00	4.00
Al^{VI}	0.28	0.29	0.29	0.30	0.30	0.28	0.24	0.25	0.31	0.29	0.22	0.27
Fe^{3+}	0.30	0.28	0.27	0.33	0.32	0.22	0.21	0.24	0.36	0.31	0.30	0.26
Ti	0.08	0.07	0.07	0.06	0.06	0.06	0.06	0.06	0.06	0.07	0.07	0.06
Mg	1.18	1.22	1.20	1.21	1.23	1.20	1.21	1.21	1.21	1.15	1.20	1.19
Fe^{2+}	0.94	0.95	0.97	0.88	0.87	1.07	1.09	1.04	0.84	0.95	0.99	1.02
Mn	0.05	0.04	0.05	0.04	0.04	0.04	0.04	0.04	0.05	0.05	0.05	0.05
$\sum Y$=3	2.82	2.84	2.84	2.83	2.83	2.87	2.87	2.86	2.82	2.82	2.83	2.86
Na	0.00	0.00	0.01	0.01	0.01	0.00	0.02	0.02	0.01	0.02	0.01	0.02
K	1.00	0.94	0.96	0.98	0.96	0.93	0.92	0.95	0.93	0.95	0.99	0.92
$\sum X$=1	1.00	0.94	0.97	0.99	0.97	0.93	0.94	0.97	0.94	0.97	1.00	0.94
Fe^t/Fe^t+Mg	0.51	0.50	0.51	0.50	0.49	0.52	0.52	0.52	0.50	0.52	0.52	0.52
Mg/Mg+Fe^t	0.49	0.50	0.49	0.50	0.51	0.48	0.48	0.48	0.50	0.48	0.48	0.48
Fe^{2+}/F^{2+}+Fe^{3+}	0.76	0.77	0.78	0.73	0.73	0.83	0.04	0.81	0.70	0.75	0.77	0.80
Fe^{3+}/F^{2+}+Fe^{3+}	0.24	0.23	0.22	0.27	0.27	0.17	0.16	0.19	0.30	0.25	0.23	0.20
FeO^t/MgO	1.87	1.78	1.84	1.77	1.73	1.9	1.91	1.89	1.77	1.96	1.91	1.9
FeO^t/FeO^t +MgO	0.65	0.64	0.65	0.64	0.63	0.66	0.66	0.65	0.64	0.66	0.66	0.66
ASI	1.35	1.42	1.42	1.40	1.40	1.44	1.37	1.37	1.40	1.39	1.25	0.93
Al^t	1.36	1.34	1.37	1.37	1.36	1.35	1.29	1.31	1.33	1.35	1.26	1.32

TABLE 16: Calculated electron probe microanalysis (EPMA) data for biotites of NPG (NL) granitoids
ASI =Molar Al_2O_3/CaO + Na_2O+K_2O; Al^t = (Al^{IV}+ Al^{VI}) pfu; FeO^t= total iron; Fe^t= total iron pfu.

Sample	NL-22	NL -22	NL -22	NL -22	NL -22	NL-22	NL-22	NL-22	NL-22	NL-22	NL-22	NL-22
SiO_2	37.54	37.56	37.95	38.18	38.2	38.22	37.39	37.49	37.57	37.41	37.27	37.66
Al_2O_3	15.19	15.24	15.23	15.1	15.17	2.89	14.55	14.58	14.86	14.9	14.82	15.15
TiO_2	2.52	2.42	2.47	2.44	2.56	15.92	2.51	2.55	2.45	2.6	2.58	2.76
Cr_2O_3	0.01	0.04	0.00	0.00	0.02	0.04	0.06	0.00	0.04	0.00	0.00	0.03
FeO	17.11	17.63	17.32	17.39	17.14	16.78	18.81	18.39	18.27	17.75	18.25	17.13
MnO	0.57	0.61	0.64	0.59	0.56	0.72	0.53	0.7	0.63	0.66	0.64	0.59
MgO	10.83	10.84	10.84	10.93	10.9	10.02	10.61	10.58	10.50	10.68	10.46	10.37
CaO	0.00	0.00	0.00	0.02	0.01	0.02	0.00	0.03	0.00	0.01	0.08	0.00
Na_2O	0.07	0.09	0.05	0.1	0.09	0.08	0.09	0.12	0.08	0.05	0.08	0.09
BaO	0.00	0.00	0.00	0.00	0.00	0.00	0.00	0.00	0.00	0.00	0.00	0.00
K_2O	9.72	9.85	9.84	9.55	9.78	10.01	9.80	9.64	9.71	9.81	9.87	9.83
Total	93.58	94.29	94.39	94.31	94.5	94.70	94.35	94.08	94.11	93.87	93.97	93.61
Structural Formulae based on 11 oxygen												
Si	2.89	2.88	2.90	2.91	2.91	2.90	2.88	2.89	2.89	2.88	2.88	2.90
Al^{IV}	1.11	1.12	1.10	1.09	1.09	1.10	1.12	1.11	1.11	1.12	1.12	1.10
$\sum Z=4$	4.00	4.00	4.00	4.00	4.00	4.00	4.00	4.00	4.00	4.00	4.00	4.00
Al^{VI}	0.27	0.25	0.27	0.27	0.27	0.32	0.20	0.22	0.24	0.24	0.23	0.27
Fe^{3+}	0.18	0.17	0.20	0.19	0.22	0.31	0.10	0.12	0.15	0.14	0.14	0.23
Ti	0.15	0.14	0.14	0.14	0.15	0.16	0.15	0.15	0.14	0.15	0.15	0.16
Mg	1.24	1.24	1.23	1.24	1.24	1.13	1.22	1.22	1.20	1.23	1.20	1.19
Fe^{2+}	0.92	0.96	0.91	0.92	0.88	0.75	1.11	1.07	1.02	1.00	1.04	0.88
Mn	0.04	0.04	0.04	0.04	0.04	0.05	0.03	0.05	0.04	0.04	0.04	0.04
$\sum Y=3$	2.79	2.80	2.79	2.80	2.78	2.73	2.82	2.81	2.81	2.80	2.80	2.76
Na	0.01	0.01	0.01	0.01	0.01	0.01	0.01	0.02	0.01	0.01	0.01	0.01
K	0.95	0.96	0.96	0.93	0.95	0.97	0.96	0.95	0.95	0.96	0.97	0.97
$\sum X=1$	0.96	0.97	0.97	0.95	0.96	0.98	0.98	0.97	0.97	0.97	0.98	0.98
$Fe^t$$Fe^t$+Mg	0.47	0.48	0.47	0.47	0.47	0.48	0.50	0.49	0.49	0.48	0.49	0.48
Mg/Mg+Fe^t	0.53	0.52	0.53	0.53	0.53	0.52	0.50	0.51	0.51	0.52	0.51	0.52
Fe^{2+}/F^{2+}+Fe^{3+}	0.84	0.85	0.82	0.83	0.80	0.71	0.92	0.90	0.87	0.88	0.88	0.79
Fe^{3+}/F^{2+}+Fe^{3+}	0.16	0.15	0.18	0.17	0.20	0.29	0.08	0.10	0.13	0.12	0.12	0.21
FeO^t/MgO	1.58	1.63	1.6	1.59	1.57	1.67	1.77	1.74	1.74	1.66	1.74	1.65
FeO^t/FeO^t +MgO	0.61	0.62	0.62	0.61	0.61	0.63	0.64	0.63	0.64	0.62	0.64	0.62
ASI	1.43	1.41	1.42	1.43	1.41	1.45	1.35	1.36	1.40	1.39	1.37	1.40
Al^t	1.38	1.37	1.37	1.36	1.36	1.42	1.32	1.33	1.35	1.36	1.35	1.37

TABLE 16 Continued

ASI=Molar Al_2O_3/CaO + Na_2O+K_2O; $Al^t = (Al^{IV}+ Al^{VI})$ pfu; FeO^t= total iron; Fe^t= total iron pfu.

Sample	NL-22	NL-22	NL-22	NL-22	NL-22	NL-22	NL-22	NL-22	NL-22	NL-22	NL-22
SiO_2	37.84	37.63	37.44	36.68	37.15	37.16	37.26	37.3	37.33	37.34	37.26
Al_2O_3	15.04	15.23	15.14	14.8	15.01	15.24	15.25	15.33	15.12	15.26	15.52
TiO_2	2.53	2.59	2.51	2.49	2.42	2.42	2.7	2.47	2.46	2.51	2.46
Cr_2O_3	0.00	0.01	0.05	0.02	0.02	0.11	0.00	0.04	0.03	0.00	0.00
FeO	17.70	17.10	17.58	18.03	18.11	17.72	17.60	17.85	17.15	17.15	17.24
MnO	0.68	0.61	0.48	0.61	0.48	0.63	0.55	0.49	0.62	0.56	0.64
MgO	10.51	10.82	10.64	10.49	10.71	10.53	10.47	10.52	10.44	10.47	10.35
CaO	0.02	0.01	0.00	0.00	0.00	0.02	0.02	0.03	0.00	0.00	0.00
Na_2O	0.08	0.06	0.10	0.07	0.09	0.07	0.08	0.08	0.06	0.05	0.05
BaO	0.00	0.00	0.00	0.00	0.00	0.00	0.00	0.00	0.00	0.00	0.00
K_2O	9.71	9.96	9.95	9.79	9.43	9.28	9.53	9.42	9.95	9.96	9.95
Total	94.1	94.05	93.89	92.98	93.42	93.18	93.46	93.53	93.16	93.30	93.47
Structural Formulae based on 11 oxygen											
Si	2.90	2.89	2.88	2.86	2.88	2.88	2.88	2.88	2.89	2.89	2.88
Al^{IV}	1.10	1.11	1.12	1.14	1.12	1.12	1.12	1.12	1.11	1.11	1.12
$\sum Z=4$	4.00	4.00	4.00	4.00	4.00	4.00	4.00	4.00	4.00	4.00	4.00
Al^{VI}	0.26	0.26	0.26	0.23	0.24	0.27	0.26	0.27	0.27	0.28	0.29
Fe^{3+}	0.19	0.20	0.20	0.12	0.10	0.12	0.14	0.14	0.24	0.23	0.23
Ti	0.15	0.15	0.15	0.15	0.14	0.14	0.16	0.14	0.14	0.15	0.14
Mg	1.20	1.24	1.22	1.22	1.24	1.22	1.20	1.21	1.21	1.21	1.19
Fe^{2+}	0.94	0.90	0.93	1.06	1.07	1.03	1.00	1.01	0.87	0.88	0.88
Mn	0.04	0.04	0.03	0.04	0.03	0.04	0.04	0.03	0.04	0.04	0.04
$\sum Y=3$	2.79	2.78	2.79	2.81	2.83	2.82	2.80	2.81	2.78	2.78	2.78
Na	0.01	0.01	0.01	0.01	0.01	0.01	0.01	0.01	0.01	0.01	0.01
K	0.95	0.97	0.98	0.98	0.93	0.92	0.94	0.93	0.98	0.98	0.98
$\sum X=1$	0.96	0.98	0.99	0.99	0.94	0.93	0.95	0.94	0.99	0.99	0.99
Fe^t/Fe^t+Mg	0.49	0.47	0.48	0.49	0.49	0.49	0.49	0.49	0.48	0.48	0.48
$Mg/Mg+Fe^t$	0.51	0.53	0.52	0.51	0.51	0.51	0.51	0.51	0.52	0.52	0.52
$Fe^{2+}/F^{2+}+Fe^{3+}$	0.83	0.82	0.82	0.90	0.92	0.89	0.88	0.88	0.78	0.79	0.79
$Fe^{3+}/F^{2+}+Fe^{3+}$	0.17	0.18	0.18	0.10	0.08	0.11	0.12	0.12	0.22	0.21	0.21
FeO^t/MgO	1.68	1.58	1.65	1.72	1.69	1.68	1.68	1.7	1.64	1.64	1.67
FeO^t/FeO^t +MgO	0.63	0.61	0.62	0.63	0.63	0.63	0.63	0.63	0.62	0.62	0.62
ASI	1.41	1.40	1.38	1.38	1.45	1.49	1.45	1.48	1.39	1.40	1.43
Al^t	1.36	1.37	1.38	1.37	1.36	1.39	1.38	1.39	1.38	1.39	1.41

TABLE 17: Calculated electron probe microanalysis (EPMA) data for biotites of NPG (AR) granitoids

Sample	AR	AR	AR	AR	AR	AR	AR	AR	AR	AR
SiO_2	38.6	38.24	38.78	39.07	38.75	38.9	39.31	39.12	38.81	39.02
Al_2O_3	13.54	13.41	13.48	14.19	13.38	14.13	14.11	13.77	13.7	13.24
TiO_2	2.01	2.07	2.01	2.28	1.88	2.13	2.34	2.27	2.12	2.19
Cr_2O_3	0.04	0.05	0	0	0.02	0	0	0.02	0	0
FeO	15.78	17.82	16.71	16.96	16.1	16.9	16.57	15.89	16.5	15.86
MnO	0.73	0.59	0.74	0.56	0.54	0.75	0.68	0.57	0.72	0.51
MgO	11.83	11.6	11.66	10.67	12.29	10.71	11.16	11.84	12.04	12.42
CaO	0	0.01	0.03	0.03	0.03	0.01	0.02	0.02	0.01	0.04
Na_2O	0.08	0.07	0.06	0.06	0.07	0.05	0.06	0.06	0.04	0.08
BaO	0	0	0	0	0	0	0	0	0	0
K_2O	9.89	9.03	9.66	9.61	9.7	9.71	9.31	9.78	9.75	9.75
Total	92.5	92.89	93.13	93.43	92.76	93.29	93.56	93.34	93.69	93.11
Structural Formulae based on 11 oxygen										
Si	2.99	2.96	2.99	3	2.99	2.99	3	2.99	2.97	3
Al^{IV}	1.01	1.04	1.01	1	1.01	1.01	1	1.01	1.03	1
$\sum Z=4$	4	4	4	4	4	4	4	4	4	4
Al^{VI}	0.23	0.19	0.22	0.28	0.21	0.27	0.27	0.24	0.21	0.19
Fe^{3+}	0.31	0.09	0.26	0.34	0.25	0.34	0.28	0.3	0.21	0.24
Ti	0.12	0.12	0.12	0.13	0.11	0.12	0.13	0.13	0.12	0.13
Mg	1.37	1.34	1.34	1.22	1.41	1.23	1.27	1.35	1.37	1.42
Fe^{2+}	0.71	1.06	0.82	0.74	0.78	0.74	0.78	0.72	0.85	0.77
Mn	0.05	0.04	0.05	0.04	0.04	0.05	0.04	0.04	0.05	0.03
$\sum Y=3$	2.78	2.85	2.8	2.75	2.81	2.76	2.77	2.77	2.81	2.79
Na	0.01	0.01	0.01	0.01	0.01	0.01	0.01	0.01	0.01	0.01
K	0.98	0.89	0.95	0.94	0.95	0.95	0.91	0.95	0.95	0.95
$\sum X=1$	0.99	0.9	0.96	0.95	0.97	0.96	0.92	0.97	0.96	0.97
Fe^t/Fe^t+Mg	0.43	0.46	0.45	0.47	0.42	0.47	0.45	0.43	0.43	0.42
$Mg/Mg+Fe^t$	0.57	0.54	0.55	0.53	0.58	0.53	0.55	0.57	0.57	0.58
$Fe^{2+}/F^{2+}+Fe^{3+}$	0.7	0.92	0.76	0.68	0.75	0.68	0.74	0.71	0.8	0.76
$Fe^{3+}/F^{2+}+Fe^{3+}$	0.3	0.08	0.24	0.32	0.25	0.32	0.26	0.29	0.2	0.24
FeO^t/MgO	1.33	1.54	1.43	1.59	1.31	1.58	1.48	1.34	1.37	1.28
FeO^t/FeO^t+MgO	0.57	0.61	0.59	0.61	0.57	0.61	0.60	0.57	0.58	0.56
A/CNK	1.36	1.47	1.38	1.46	1.37	1.45	1.50	1.40	1.40	1.34
Al^t	1.24	1.23	1.23	1.28	1.22	1.28	1.27	1.25	1.24	1.19

ASI=Molar $Al_2O_3/CaO + Na_2O+K_2O$; $Al^t = (Al^{IV}+ Al^{VI})$ pfu; FeO^t= total iron; Fe^t= total iron pfu.

TABLE 18: RANGE OF CRYSTALLIZATION TEMPERATURE ESTIMATES FOR KAHG BIOTITE
(LUHR *et al.*, 1984)

Sample No		Temperature (°C)	
		Maximum	Minimum
BGN	KG	1061.03	948.86
	LG	979.41	938.91
GGN	GG	908.31	887.09
PGN	KZ-33	979.41	870.44
	KZ-15	968.47	895.93
	KZ-17	949.30	856.28
NPG	KH-7A	937.19	905.78
	KH-8A	900.34	864.85
	NL	1021.49	932.60
	AR	982.25	910.38

CHAPTER VI

GEOCHEMISTRY

6.1   MAJOR ELEMENT GEOCHEMISTRY

6.1.1   INTRODUCTION

Whole- rock geochemistry is an efficient tool to unravel the evidence about the petrogenesis of granitoids and related igneous rocks. Geochemical studies aid in identification of the processes of partial melting, fractional crystallization, magma mixing and assimilation or a dynamic mixture of these processes and for that it remained an indispensable instrument kindling interest among the igneous petrologists.

The geochemical character profoundly impacts the nature of the rock and reflect about the source and processes which acted on the melt, thus aids in approximating the tectonic discrimination and protolith evolution. Major element data can be principally employed for classifying the individual rock and rock associations along with construction of variation diagrams, also to use as an agent in comparing with experimentally determined rock compositions whose conditions of formations are recognized. The main intention of the current geochemical review is to understand the behaviour and association of major elements between the different variety of Karbi Anglong Hill granitoids and to draw light on their petrogenesis and evaluate their tectonic setup.

Twenty-seven representative samples of the Karbi Anglong Hills Granitoids have been analyzed, whole-rock major oxide (wt%), trace element (ppm) and rare earth element concentrations of KAHG represented by five porphyritic granitoids (PGN), 10 non-porphyritic granitoids (NPG), 5 granite gneiss (GGN) and 7 basement granite gneiss (BGN) samples have been studied. The analytical results for whole rocks are presented in Table 19-21. For convenience, the major, trace, rare earth element geochemistry of the studied rocks are labelled separately.

6.1.2   MAJOR OXIDES AND CIPW NORM

The KAHG are alkali rich granites with high SiO_2 values (64.80- 76.49 wt. %). Al_2O_3 values are moderate (11.37–15.34 wt. %), K_2O fluctuates between 4.7–6.43 wt. % and is higher than Na_2O which ranges from 2.10–3.73 wt. %. The ratio of K_2O/Na_2O ranges from 1.47- 3.06 reflecting the potash-rich character of the granitoids. Granitoids in general display high total alkalis ($K_2O + Na_2O$) contents 7.68-9.29 wt. % and comparatively low TiO_2 (0.05–0.87 wt. %), CaO (0.53–3.08 wt. %), MgO (0.06–1.53 wt. %), Fe_2O_3 (0.57–5.44 wt. %). The Alumina Saturation Index (ASI = $Al_2O_3/(CaO + Na_2O + K_2O)$) of the KAHG varies from 0.93-1.12 (average =1.02).

According to CIPW norm scheme (Janousek et al., 2006) the KAHG are quartz normative ranging from (21.26-38.44%) along with corundum (0.1-1.53%). Orthoclase exhibits a greater profusion among the normative minerals (range 28.25-37.99 %). Lone sample KJ (nPG) shows a meagre normative wollastonite (0.01%) and diopside (0.32%). The KAHG samples fall within the domain of 'quartz monzonite and granite' in the normative An- Ab- Or diagram (after O' Connor, 1965) (Fig. 6.1). CIPW normative compositions of KAHG samples are given in Table 19. The Mg# (Mg#= 100(Mg/Mg +Fe_{Total}) of KAHG is moderately low and varies within a constant range from 0.08 - 0.27.

Non- porphyritic granitoids (NPG)

The NPG record the most variance in silica content SiO_2 (64.80-76.44 wt %). AR recorded the highest SiO_2 values (76.44 wt. %) while KH recorded the lowest values (64.80 wt. %). Major oxides Al_2O_3 (11.87-15.34 wt %), CaO (0.53-3.08 wt %) also show varied range compared to the rest of samples. K_2O varies from (5.00-6.01 wt %), Na_2O (2.52-3.73 wt %). NPG has less amount of MnO (0.02-0.08 wt %); When co related with the rest of samples Fe_2O_3 and MgO contents of NPG are highest and most variable ranging from (0.57-5.44 wt % and 0.06-1.53 wt % respectively). K_2O/Na_2O ratio vary from 1.47-2.31. ASI values range from 0.97-1.12. CIPW values in order of abundance of normative minerals are quartz 21.26- 38.11, orthoclase 29.55-35.51, albite 21.32-31.56.

Porphyritic granitoid (PGN)

Porphyritic granitoids (PGN) samples have the most evolved compositions, being more acidic compared to the other varieties with silica content (71.48-74.49 wt%) and lowest in ferromagnesian elements (Fe_2O_3=1.93 to 2.53 wt. %, MgO=0.29 to 0.56 wt. %). Al_2O_3 (13.14-

13.95 wt %), low content of CaO (1.17 to 1.57 wt. **%)**, TiO_2 (0.29 to 0.31 wt. %), P_2O_5 (0.07 to 0.11 wt. %) and MnO (0.05 to 0.08 wt. %). K_2O/Na_2O ratio ranges from 1.68-2.00. Except for one sample (KZ17: A/CNK=0.99), the PGN are weakly peraluminous (1.06-1.1). In CIPW norm, quartz ranges from 29.61-35.61 %, orthoclase ranges between 29.84-33.45%. Quartz exhibits a greater profusion among the normative minerals.

Granite Gneiss (GGN)

The granite gneiss (GGN) samples are moderately acidic (SiO_2=66-71.89 wt%) and highly potassic (K_2O=4.78-5.82 wt%). K_2O/Na_2O ratios range from 1.59-1.93. The moderate concentration of Al_2O_3 (13.28-15.11 wt. %), Na_2O (2.1-03.34 wt. %), CaO (0.53-2.42 wt. %) and low TiO_2 (0.43-0.83 wt. %), MgO (0.52-1.44 wt. %) in GGN are almost identical to those of NPG samples. Fe_2O_3 ranges from (2.64-5.29 wt. %) The ASI in GGN ranges from 0.99-1.07.

The GGN are categorized by the presence of normative minerals orthoclase, quartz, albite, anorthite, hematite, hypersthene, rutile, apatite, corundum, and ilmenite in the order of abundance. CIPW normative minerals orthoclase (28.25-34.39%), quartz (24.41-29.27%) and albite 24.54-28.26% are dominant, the rest are present in minor amounts. Diopside and wollastonite are characteristically absent in all samples.

Basement Granite Gneiss (BGN)

The Basement granite gneiss (BGN) samples are also acidic (SiO_2=69.73-76.49 wt%) and highly potassic (K_2O=4.7-6.43 wt%). Ratio of K_2O/Na_2O=1.473.06, Howraghat area of BGN exhibit the most potash- rich (K_2O/Na_2O=3.06) character of the studied granitoid samples. When co related with the rest of the samples BGN has lesser MnO (0.02-0.07 wt %) also the ASI is least in BGN ranging from 0.93-1.02. Moderate concentration of Al_2O_3 (11.37-14.27 wt.%). MgO (0.08-0.86 wt. %), LG-1 and LG-2 are the only samples showing Titanite 0.86 and 0.48 respectively. Orthoclase (27.77-37.99%), quartz (26.06-38.44%); albite (17.77-27.66%).

6.1.3   CLASSIFICATION

The ternary Na_2O+ K_2O- FeO^t - MgO (AFM) diagram after Irvine and Baragar (1971) has been employed to infer the calc-alkaline and tholeiite magma series. Tholeiite magma series indicate a stronger enrichment of iron at the initial part of magmatic differentiation, while a progressive suppression of iron by the early crystallization of oxides of Fe-Ti will produce an alkalic trend in

the calc-alkaline series. The KAHG follows a comparable calc-alkaline trend in the AFM plot (Fig. 6.2 a) corresponding to the AF side of the plot indicating moderate oxidizing conditions.

According to the Shand's index (1943) in terms of molar A/NK–A/CNK, the granitoids are dominantly metaluminous to mildly peraluminous (Fig. 6.2b) which is distinctive of I-type granitoids (Chappell & White 1992). BGN sample LG-1 exhibit the most metaluminous (A/CNK-0.93) character.

Considering the compositions of SiO_2 vs K_2O, the KAHG in general occupy the fields of shoshonite series to high K-calc alkaline series in Le Maitre et al., (1989) diagram (Fig. 6.2c). The melt derived from source appears to have subsequently experienced fractional crystallization evolving from shoshonite (high-K) to a high-K calc- alkaline field. However, the gneissic rocks appear to have evolved from a single field shoshonite (high-K) fields. Except for Kathalguri (NPG) and Dolomara (GGN) samples which show composition affinity of quartz monzonite the bulk of PGN and BGN and majority of NPG fall in the granitic composition. (Fig. 6.2d).

Cationic classification of De la Roche et al. (1980) (Fig. 6.3) indicates that KAHG occupy the granodiorite, syeno- and monzo-granite fields. In the modified alkali lime index (MALI) diagram (Frost et al., 2001), totality of the sample plots under the alkali-calcic and calc-alkalic fields. GGN samples specifically (GG, DO) fall in the alkali-calcic field, meanwhile majority of NPG are of alkali-calcic affinity (Fig. 6.3b).

The Fe# (FeO^t /FeO^t+ MgO) of KAHG ranges from 0.86 to 0.80 for the PGN, 0.89 to 0.73 for the BGN, 0.83-0.77 for the GGN and NPG having the highest value 0.92 to 0.76. The (FeO^t/ (FeO^t + MgO) against SiO_2 diagram (Fig. 6.3c) classification after Frost et al. (2001) illustrates distinct trend characterizing the fields of iron-rich and magnesian-rich granites. The samples plot in both the magnesian and ferroan field. However, the BGN samples predominantly falls in the magnesian Field. Except for the KH which falls under magnesian, NPG varieties cluster close to the junction of ferroan and magnesian field, majority of NPG samples and PGN are indicative of iron- enriched granite. The data tally with the inference from Wones and Eugster (1965) ternary plot, where the KAHG biotites broadly expressed a trend of iron enrichment (Chapter-5; section 5.3.1).

Magnesian granitoids are presumed to have crystallized under high fO_2 condition, while a lower fugacity condition prevailed during the crystallization of ferroan granitoids. (Albuquerque et al., 2020).

Experimental results documented that if melting happens in a shallower crust, a dehydration melting of magnesian calc-alkalic granitoids will yield ferroan granites (Patiño Douce, 1997, and Skjerlie & Johnston, 1993). It is suggested that the partially melted ferroan granitoids tend to be silica- rich, calc- alkalic, while higher degrees of partial melting will alter the melt to an alkali-calcic composition.

Following the A versus B plot (A = Al - (K + Na + 2Ca) vs. B = (Fe + Mg + Ti), a subdivision by Villaseca et al., (1998) whereby peraluminous domain is further subdivided as low, moderate, high and felsic peraluminous suites. Metaluminous field is occupied by BGN and GGN (LG& GG) and a lone NPG Fig. 6.4. The metaluminous state (some less fractionated members) can arise from the occurrence of titanite and apatite which are ca-rich minerals. GGN samples of DO and Panbari Quarry falls in the medium peraluminous field, PGN belong to weakly peraluminous granite. Highly fractionated NPG and BGN variety (CB, KG and HW) falls within the felsic-peraluminous field. Some degree of fractionation trailed by hydrothermal or supra- crustal assimilation may have given rise to the moderately peraluminous nature (Yang et al., 2008).

Classification of the KAHG granitoids in the molar ratio Al_2O_3/ (CaO + Na_2O+K_2O) vs SiO_2 diagram, where the fields of I (igneous origin) and S (sedimentary origin) granitoids are after White and Chappell (1977). Majority of the rocks are in the I-type granite field Fig. 6.5a. I-type geochemical signature of KAHG is supported by the mineralogy (predominance of biotite as mafic silicate minerals, and the abundance of sphene and magnetite as accessory phases). Correspondingly, the magmatic origin is predictable in the P_2O_5/ TiO_2 vs MgO/ CaO diagram for discrimination of ortho- para felsic rocks after Werner (1987), the KAHG cluster at the field of magmatic rocks. (P. Masberg et al., 2005) Fig. 6.5b.

Harker Diagram (Harker, 1909) which is an extensively employed variation diagram of the constituent oxide in weight percentages, is plotted against SiO_2 wt%. SiO_2 has been preferably selected as abscissa since it shows a wide range of variation in comparison to other differentiation Index (D.I) like MgO, MgO/FeO etc. All the samples exhibit a general scattered, near linear,

negative correlation trends in the TiO_2, Fe_2O_3, MnO, MgO, and CaO against SiO_2 (Fig. 6.6). The porphyritic granitoid plot towards the silica-saturated end, within narrow ranges SiO_2 (71.48–74.49 wt.%). Al_2O_3 also have a data scatter with some of the samples plotting off the observed evolutionary trend for most of the major oxides. Na_2O and K_2O exhibit a more data scatter, lacking a systematic correlation, shifts in a positive trend with increasing SiO_2, thus the alkali oxides get enriched through the melt fractionation, especially the non-porphyritic varieties. Also, depleting Fe_2O_3 and TiO_2 with increase in SiO_2 content could be a probable result of the fractionation of biotite mineral through the magma differentiation and mixing processes.

Hassan and Hashad, (1990) ternary diagram of major oxide $Na_2O–K_2O–CaO$ wherein the fields of calc-alkaline (CA), trondhjemitic (TR) and younger granites are divided, TR and CA trends from Barker and Arth (1976); KAHG basically cluster within the field of Egyptian Younger Granites suggesting reasonable fractionated nature (Fig. 6.7). This younger evolved inference is also supplemented by the decreased K/Rb ratio values (86.63- 225.93). K/Rb ratios according to Jelinek and Dudek (1993) ranges from (100-300) for mature continental crust, (230; Taylor, 1965) for magmatic rocks and chondritic values (242; Anders and Grevesse, 1989). The BGN exhibit the highest ratios of (167.83- 225.93), GGN comparatively exhibit a high range (123.31- 200.91) linking slightly to a mature continental crust, while the PGN (95.25- 122.05), and NPG (86.63-151.98) exhibit lower ranges (below 160) which implies the involvement of post-magmatic operations with hydrothermal fluid phase (e.g., Shaw, 1968; Shearer et al., 1985; Bau, 1997; Irber, 1999).

Karbi Hill granitoids occupy the domain of alkali-calcic (Fig. 6.3b), calc-alkaline (Fig. 6.2 (a) metaluminous to peraluminous (Fig. 6.2 (b), and $FeO^t/$ (FeO^t + MgO) vs Al_2O_3 (wt%) after Dall'Agnol & de Oliveira, 2007) maintained the inference by falling within the calc-alkaline I-type granites and oxidized A-type granites (Fig. 6.8a)

TRACE ELEMENT GEOCHEMISTRY

6.2.1 INTRODUCTION

Trace elements can be measured as those negligible concentrations occurring in rocks in the sense of quantity i.e., less than 0.1 wt%, nevertheless trace element distribution including the rare earth elements perform as a reliable indicator in understanding the original nature of the primary rocks,

in fact are considered more efficient in identifying the petrological processes compared to major elements.

Trace elements tend to be more selectively incorporated or excluded within the different minerals, and within an equilibrium melt-crystal system, elements in line with their phase- activities segregate themselves among the different melt and solid phases. The trace elements can exist in granitoids in different modes from being concentrated in the accessory minerals, to substitutes for major elements. Elements can exhibit strong partition affinity to the early crystallized minerals while some prefers the melt phase, segregating into the compatible and incompatible elements with bulk distribution coefficient $D \geq 1$ and $(D \ll 1)$ respectively.

Detailed examination of the distribution pattern of trace elements will deliver evidence about magma differentiation and partial melting which is otherwise unapproachable through the major elemental studies.

Therefore, the nature and behaviour of the major rocking minerals determine whether an element or group of it may be involved in the different modes of magmatic evolution like magma- mixing, mineral fractionation, partial melting or assimilation etc. An attempt has been made to study the nature and characteristics of trace elements including rare earth elements of the representative samples of KAHG in the following section.

Analytical results of the trace element content (ppm), including the REE, and vital elemental ratio of petrogenetic significance, such as Ga/Al, K/Rb, Rb/Sr and U/Th are given in Table 20-21 for the representative samples.

6.2.2   TRACE ELEMENT CHARACTERISTIC

Samples in general express strong negative Eu anomalies (Eu/Eu*=0.17–0.54) on the chondrite-normalized REE diagram. NPG variant plots variable negative Eu anomalies with relative enrichment of LREEs. KH samples are noticed to display the most disparity in the pattern. Comparatively steeper slopes of LREEs are noted in the PGN, GGN and BGN samples, with similar flat HREE plots and depleted Eu anomalies. The fractionation of plagioclase is credited for the depleted Eu anomaly in chondrite-normalized REE.

KAHG are showing modest concentrations of Sr (35-375 ppm) except for two samples below Sr<11ppm, moderate to high contents of Ba (64-1305 ppm) which is consistent with noted high K_2O, relatively rich Rb (197-563 ppm), Y (23-92ppm), enrichment in Th (15-170 ppm). high abundance of U (5.1-53.20 ppm) with the exception of two NPG & two GGN samples (U<4 ppm).

The KAHG are characterized by reduced Ni (1-13 ppm), Y (23-92 ppm), Zr (90-553 ppm).

Eby (1992) concept of trace elemental Y/Nb values were employed for segregating the A-type granites from a mantle source (Y/Nb < 1.2; A1 subtype) to crustal origin (Y/Nb > 1.2; A2 subtype). All samples of KAHG have Y/Nb (1.35-7.00) indicative of crustal derivation.

Porphyritic granitoid (PGN)

Porphyritic granitoids have high abundances of Th (108-166 ppm) and U (23.8-52.7 ppm). Moderate enrichment of Ba (417-573ppm), Rb (384-439ppm), Zr (240-353ppm), Ce (162.12-349.3 ppm) and La (90.39-170.99ppm) with low Ni, Sc and Cu (<8ppm). Prominent Europium anomalies (Eu/Eu* 0.20-0.39). Compared to the average REE concentration of about 250 ppm recordable in normal granites (Emmermann et al., 1975), the samples exhibit an enrichment in general (REE= 380.14-798.45ppm; av. 558.49ppm).

Non- porphyritic granitoids (NPG)

The most abundant trace elements are Ba (227-1305ppm except for a sample with 64ppm; average 592.6 ppm) and Rb (281-563ppm; average content 389.1 ppm). Zr ranges from (90-553ppm), concentrations of Sr fluctuate from 3- 275ppm. The NPG are characterised by high contents of U (6-53.2 ppm, except for two samples SE-2.6ppm, KH8- 3.8ppm) and has moderately higher concentrations of Ni(2-13ppm), Sc (2.9-9ppm). V(4-75ppm), Co(2-75.2ppm), Higher REE values (ΣREE =81.88-1303.39ppm except for KH8=36.64 ppm; av. 355.01 ppm) compared to the PGN, GGN and BGN. Variable Eu anomalies (Eu/Eu* ranges from 0.17-0.54) observed. Chondrite normalized La_N/Yb_N ratios vary from 4.76-23.18. Ga/Al ranges from 2.31 to 2.88.

Granite Gneiss (GGN)

Granite Gneiss (GGN) are characterized by reduced contents of Th and U (15-52 ppm and <9ppm respectively) compared to the PGN and NPG. The rocks have low values of Eu/Eu* (0.29-0.45). Variable range of Sr (39-163ppm), high Ba contents (467-676 ppm) and lesser abundance of Th

(15-52 ppm) and Y (37-65ppm) in comparison with the other varieties. Moderate range of Rb (197-372 ppm), Zr (208-299 ppm) and REEs (ΣREE=213.22 -399.58 ppm).

Basement Granite Gneiss (BGN)

Basement granite gneiss (BGN) show the least contents of U (3.9- 7.6ppm) and Y (23-52ppm). Low Th amount 20-76ppm and Rb (205-269 ppm); High Sr (39-375ppm) and Ba contents (467-1035 ppm). Moderate range of Zr (148-270 ppm), REEs (ΣREE=160.85- 408.84 ppm) and Eu/Eu* (0.34-0.50). Chondrite normalized La_N/Yb_N ratios vary from 6.51-18.85. Ga/Al ranges from 2.08 to 2.6.

6.2.3   BEHAVIOUR OF TRACE ELEMENTS

Ce/Pb ratios of KAHG ranges from 1.75- 4.78 (BGN), 3.91- 6.91(GGN), 2.80-6.24(PGN) and 0.36-4.60(NPG); with an abnormal value of 12.81 for one sample. Green (1995) suggested Ce/Pb ratio for Primitive mantle is Ce/Pb H"9, while that of continental crust is Ce/Pb H"4. The mentioned Ce/Pb values for KAHG are lower than that of primitive mantle, linking more to a crustal source, it is also supplemented by the (Ebby, 1992) triangular plot of Y-Nb-Ce and Y-Nb-$3\times$Ga (Fig. 6.10a&b) Crustal source melt is also documented as possibility by the metaluminous to mildly peraluminous ferroan nature of KAHG which is the result of a low degree partial melting. Moreover, Eby (1990, 1992) employed the Y/Nb parameter to classify A-type granites into mantle and crustal source. It is suggested that the Y/Nb ratio of mantle origin A_1-type granites (Y/Nb < 1.2) or crustal (Y/Nb > 1.2; A_2 subtype). All samples of the KAHG have Y/Nb (1.35-7.00) similar to the rocks of continental crust and could be originated due to subducted-related magmatism.

Moreover, in the Nb–Y–Zr/4 and Nb–Y–$3\times$Th, diagrams, the samples occupy the A_2-type granites field (Eby, 1992) (Fig. 6.10c &d), where it is understood to represent anorogenic melts derived from lower continental Crust.

Whalen et al., (1987) diagrams employed to distinguish geochemically A-type from S-, M-, and I-type granites. Majority of the samples confirm the A-type nature on the Zr+Nb+Y+Ce vs Na_2O+K_2O/ CaO plot (Fig. 6.11a). The geochemical character of porphyritic samples points to A-type granites with most silica rich and also falling under ferroan composition. On the Zr vs. 10000Ga/Al, diagram (Fig. 6.11b), the PGN, BGN samples fall under the domain of A-type granite, the remaining samples (NPG and GGN) predominantly follows the pattern with few

samples in the I & S- type field. Zr+Nb+Y+Ce values of KAHG varies from 145.91-1198.9ppm; the PGN and GGN showing values >350ppm.

In general, the Harker diagram (Fig. 6.12) demonstrate positive trend of both Rb and Y with increasing SiO_2 content however, Ba and Sr decrease. Such variations are consistent with plagioclase and K-feldspar fractionation (Clarke, 1992; Christiansen and Keith, 1996; Yang et al., 2003, 2008). The PGN samples have positive correlations of Nb, Zr and Ga elements with respect to silica.

6.3   RARE EARTH ELEMENTS

Petrogenetic studies of granitoids are reinforced by the existence of naturally occurring rare earth elements (REE) such as La, Ce, Pr, Nd, Sm, Eu, Gd, Tb, Dy, Ho, Er, Yb, Lu along with the trace component since all the REEs are comparable geochemically and are quite unaffected by hydrothermal processes. Most of the REE occur in trivalent oxidation state under most geological conditions, with the exception of Europium (Eu^{2+} or Eu^{3+}), making it a fascinating element sensible for thorough investigation of its distribution. The incidence or absence of an Eu- anomaly (Eu_N/Eu^*) mainly specify the role of feldspars, and it is possible to gather information on oxidation conditions of the magmatic region. Also, the chondrite-normalized REE patterns of primary rocks help to infer minerals that have been involved in partial melting or crystal fractionation process.

The representative analyzed whole rock rare earth elements (La to Lu) in ppm, together with the chondrite-normalized values (Sun and Mc Donough, 1989) and calculated Light REE to Heavy REE fractionation (La_N/Lu_N or Ce_N/Yb_N), Eu^* (= $Sm_N +Gd_N/2$) and Eu-anomaly (Eu_N/Eu^*) are given in tables respectively.

Studying the REE and their plots indicate features which are believed to point to an interaction with hydrothermal fluids (Bau, 1996; Jahn et al., 2001; Li et al., 2014), thus they may have the potential to indicate mineralized and unmineralized granites. Pronounced Eu anomaly, flatter or positive heavy REE slope are found to be indicative of hydrothermal alteration and mineralized granites, meanwhile shallower Europium anomaly, negatively inclined HREE are exhibited by barren granites.

The KAHG are characterized by REEs (ΣREE =81.88-1303.39ppm) except for one sample (KH8; ΣREE =36.64 ppm). The BGN show relatively least contents ΣREE =160.85- 408.84 ppm,

meanwhile higher and more variable values are noted for NPG and PGN i.e., ΣREE =81.88-1303.39 ppm and ΣREE =380.14- 798.45 ppm respectively. All the samples display moderate to well pronounced negative Europium anomalies (Eu_N /Eu* ranging from 0.17-0.54; av.=0.34) signifying a substantial role of plagioclase fractionation from the parent magma. Chondrite-normalized (Sun and Mc Donough, 1989) rare earth elements (REE) patterns of the KAHG are shown (Fig. 6.13). $(Ce/Yb)_N$ value varies between 3.34 to 18.89 advocating an intense REE fractionation, $(Ce/Pb)_N$ values show a range of 0.03 to 1.15 with an average value of 0.33.

Samples in general express a comparable and fairly high LREE, LaN= 35.12-476.82 (except for a sample 12.15) moderate fractionation trend $(La/Yb)_N$=4.76-23.18). Also, high Ba (227–1305), Sc (2–9). $(Ho/Yb)_N$ ratios ranging from 0.38 to 1.32 with an average of 0.96 is signifying a mild HREE fractionation.

Chondrite-normalized REE patterns show reasonable enrichment in LREE compared to HREE in NPG ($(La/Lu)_N$ = 4.12–25.94), PGN ($(La/Lu)_N$ = 9.65–15.60), GGN($(La/Lu)_N$ = 6.60-9.44and BGN($(La/Lu)_N$ = 7.03-18.37). Non-porphyritic KH samples show the most drastic variation. Comparatively flatter HREE patterns and steeper slopes of LREEs noted for the porphyritic and gneissic granitoids.

Primitive Mantle-normalized spidergrams of all samples indicate pronounced troughs at Ba, Nb, Sr, P, Eu and Ti suggestive of magma derived from a subduction related setting, however NPG samples with high MgO contents (e.g., KH) does not mark the negative Sr and P anomalies (Fig. 6.14). Distinguished spiked pattern for Th, U, Pb, K and Ce. Whenever positive spikes of Pb are accompanied by distinguished Nb anomalies on primitive-source spider diagrams, it is understood as magmatic rocks typical of subduction zones, thus inclusion of crustal material is anticipated (e.g., Zartman and Doe, 1981; Saunders et al., 1991).

The samples normalized to Primitive mantle (Sun & McDonough, 1989) show enrichment of LILE comparative to high-field-strength elements (HFSE). Enrichment of Rb, K and Pb is noted in most of the samples, which maybe suggestive of a parental melt of these granites from an enriched Crustal source. Poor Sr content varying from 3 to 375 ppm. Negative Sr anomalies point to a probable degree of fractionation of plagioclase to generate the KAHG.

6.4   TECTONIC ENVIRONMENT

Pearce et al., 1984 & 1996 tectonic discrimination plots Fig. 6.15 (a, b) of trace elements have been employed, Nb Vs Y depict majority of KAHG fall in the territory of Within Plate Granite (WPG) supporting an anorogenic origin. Rb Vs Y+Nb diagram indicate samples overlap close to the junction point of Syn-COLG subfields and WPG. The samples follow the Pan African granitoids of NE-Brazil (Guimarães et al., 2004), signifying their generation in an extensional setting.

Supporting inference can be noted from FeO^t/FeO^t+MgO vs SiO_2 plot Fig. 6.15(c) where samples occupy the POG (Post Orogenic Granite) range. Comparable conclusion can be grasped in the Batchelor and Bowden (1985), multicationic R1= 4Si–11(Na + K)- 2(Fe + Ti)-R2= 6Ca + 2Mg + Al) diagram (De la Roche et al., 1980) Fig. 6.15(d), where majority of samples have tectonic trends linking to post orogenic, post- collisional uplift settings and the PGN samples plot in the syn-collisional terrain.

All the KAHG cluster parallel to the Ba and Rb side while it maintains away from the Sr element. The ternary plot is employed in outlining the trends of differentiation in acid suites, it is evident from the fields of (El Bouseily and El Sokkary, 1975), the samples are strongly differentiated granites normal and anomalous granites Fig. 6.16a.

In granitoids the enrichment of U is attributed to fractional differentiation, it is also indicated by the surge in K content. Th/U ratios of KAHG are analogous and close to the upper crustal estimates of 3.8 (Taylor & McLennan, 1985).

SiO_2 vs. Zn with modified fields for several granitoids from Lentz, 1998 Fig. 6.17. The plot depicts a fractional crystallization path for generation of the I-type granites, which in turn could be indicative of derivation from a mantle or crustal source.

Debon & Le Fort, 1983 A-B multicationic classification plot is employed to direct the composition of mafic parts B (Fe, Mg and Ti), and its connection to the aluminium balance (A) and consequently the typical mineral assemblage. Samples are falling both as weakly peraluminous to metaluminous character revealing both crustal and mantle source. However, majority of samples belong to Biotite field (III), slightly in Bt>Ms (II) and Bt, Amp± Px (IV). The samples follow the trend of ACG (amphibole- bearing calc-alkaline granitoids) and ATG (Arc tholeiitic granites) Fig.

6.18a. The sample plots in the Cafemic magmatic association which is inferred to be evolutionary trend corresponding to I- types, Chappell and White (1974).

Variation of Rb/Zr ratio to Nb (Brown et al., 1984) (Jin, 1986) have been employed and it designates emplacement of the KAH granitoids in a mature continental arc Fig. 6.18b. Amount of Nb and Rb rise with increasing arc maturity meanwhile Zr demonstrates the reverse.
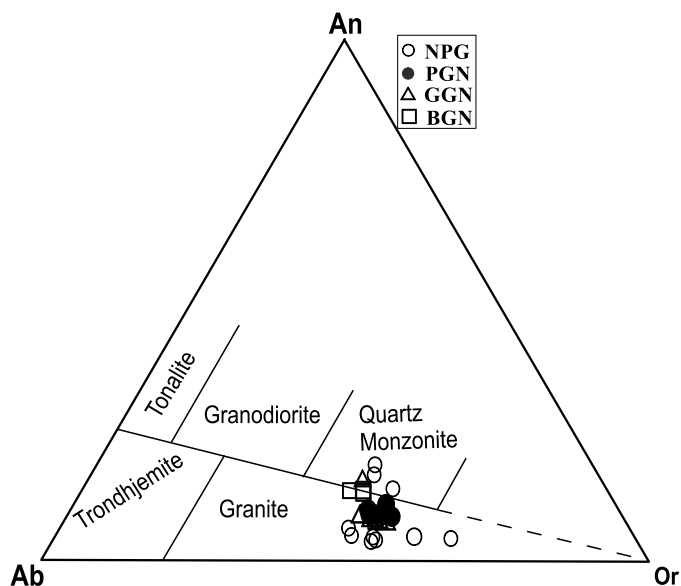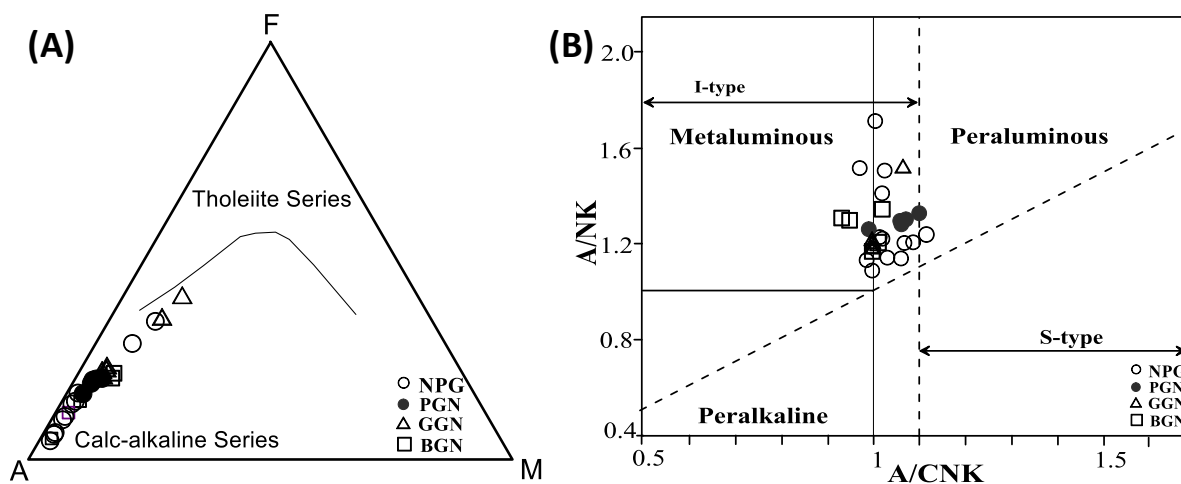
Figure 6.1: The KAHG samples fall within the domain of 'quartz monzonite and granite' in the normative An- Ab- Or diagram (after O' Connor, 1965)
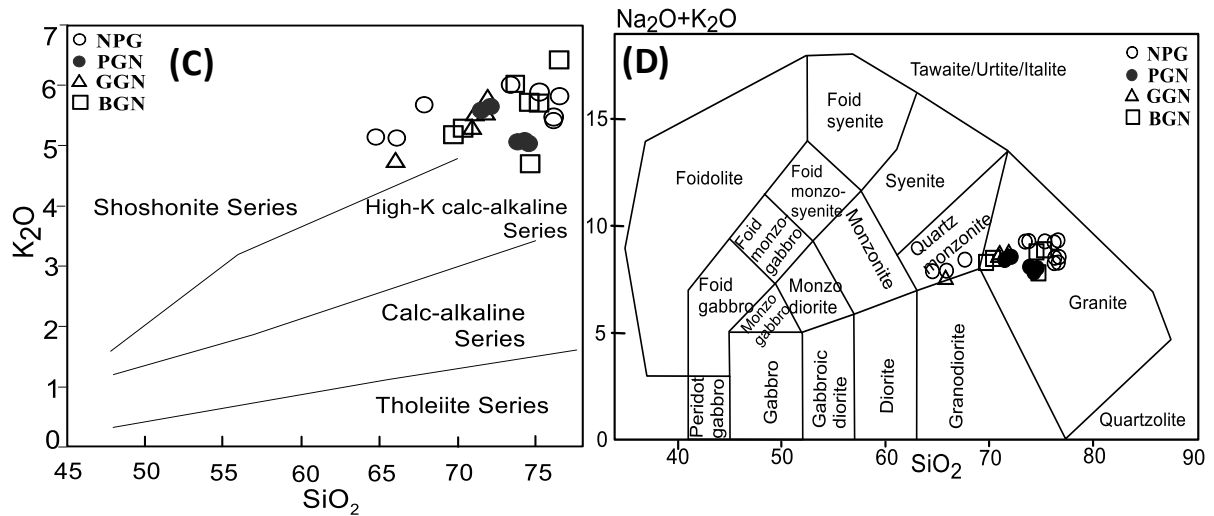
Figure 6.2 (A) $Na_2O + K_2O$-FeO^t- MgO (AFM) diagram after Irvine and Baragar (1971) (B) KAHG rocks classification according to Shand's index (1943); Boundary between the fields of I-type and S-type granite according to Maniar and Piccoli (1989) and Chappell and White (1992). (C) SiO_2 Vs KiO_2 Le Maitre et al. (1989), the KAHG occupy the fields of shoshonite series to high K-calc alkaline series. (D) $Na_2O + K_2O$ Vs SiO_2 classification diagram after Middlemost (1994). Symbols: Open Circle- NPG; Solid Circle- PGN; Triangle: GGN; Square- BGN
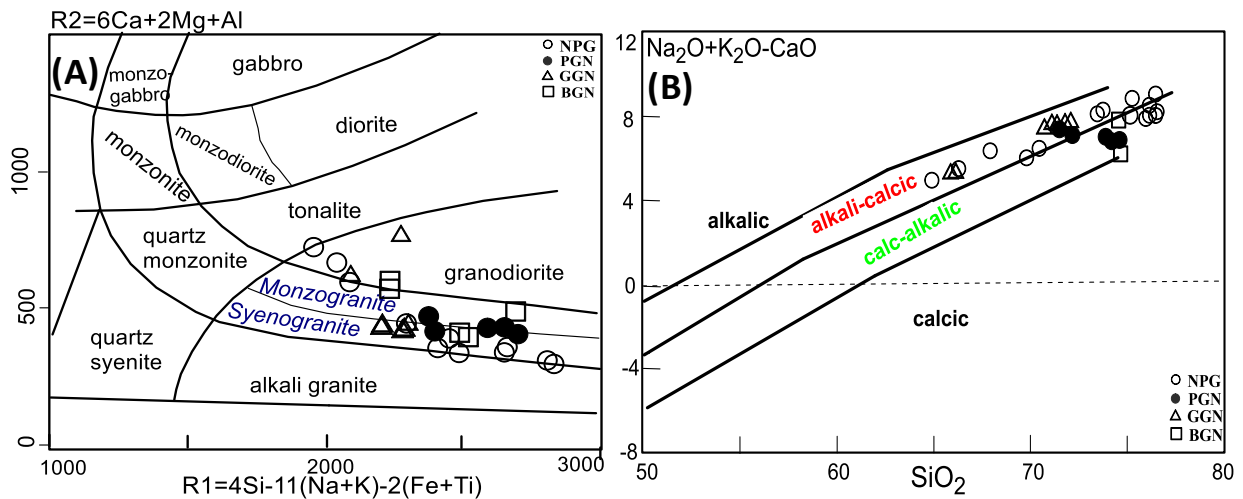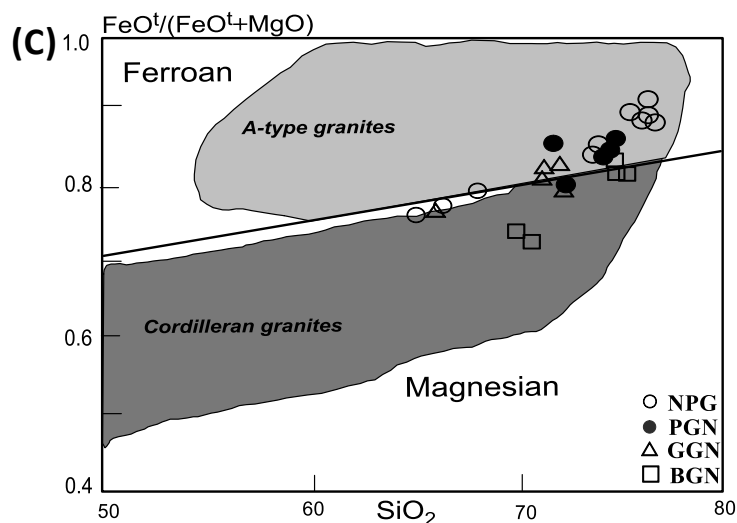
Figure 6.3 (A) R_1-R_2 cationic classification of De la Roche et al., (1980) (B) SiO_2 versus MALI (NaO + K_2O – CaO) diagram (Frost et al., 2001); (C) Whole-rock FeOt/ (FeOt + MgO) versus SiO_2 (fields of Cordilleran and A-type granites from Frost et al. 2001). Symbols: Open Circle-NPG; Solid Circle- PGN; Triangle: GGN; Square-BGN
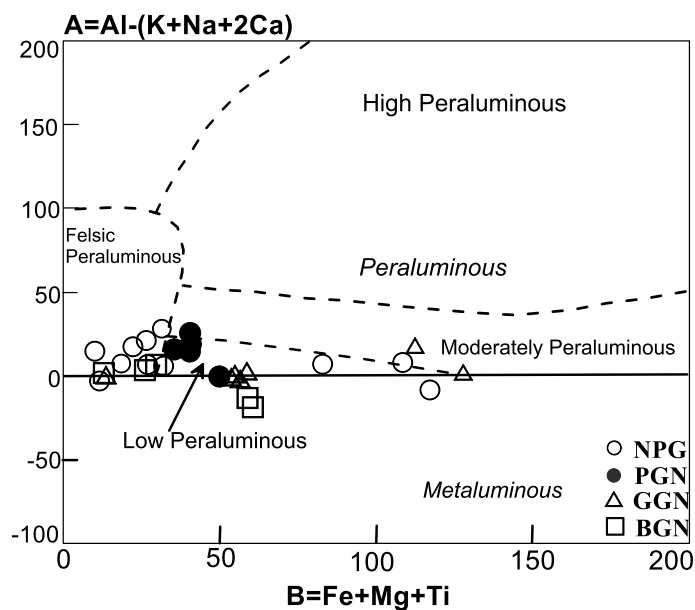

Figure 6.4 Discrimination plot of A (Al - (K + Na + 2Ca) vs. B (Fe + Mg + Ti) with field boundaries from Debon and Le Fort (1983) and modified after Villaseca et al. (1998).

Symbols: Open Circle- NPG; Solid Circle- PGN; Triangle: GGN; Square-BGN
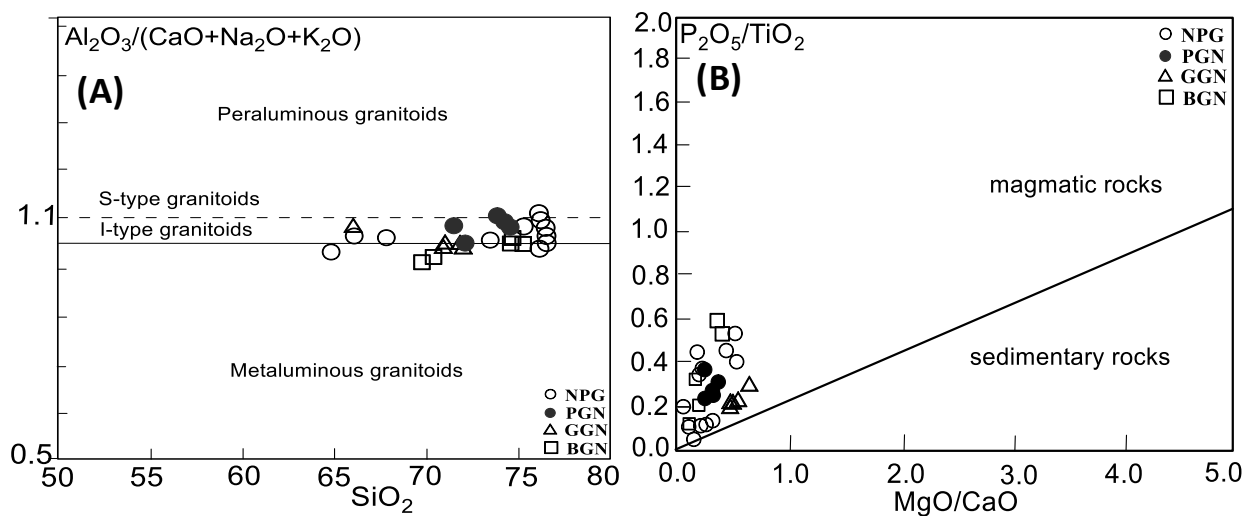
Figure 6.5: Classification scheme of (A) molar ratio $Al_2O_3/(CaO + Na_2O+K_2O)$ vs SiO_2. Peraluminous and meta-aluminous granite fields after Chappell and White (1974); I (igneous) and S(sedimentary) origin fields after White and Chappell (1977). (B) P_2O_5/TiO_2 vs MgO/ CaO discrimination diagram of Ortho-para source after Werner (1987). Symbols: Open Circle- NPG; Solid Circle- PGN; Triangle: GGN; Square-BGN
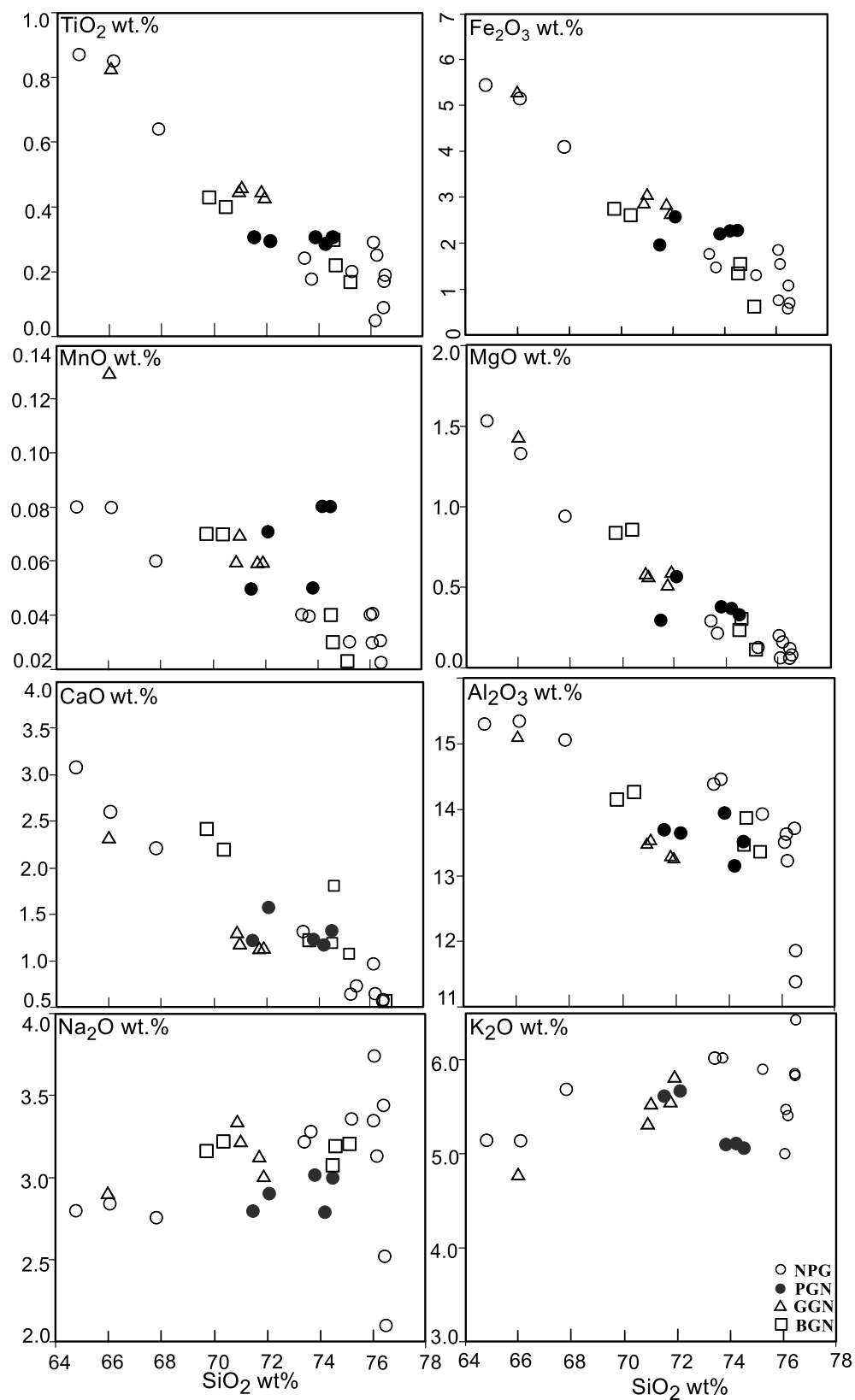
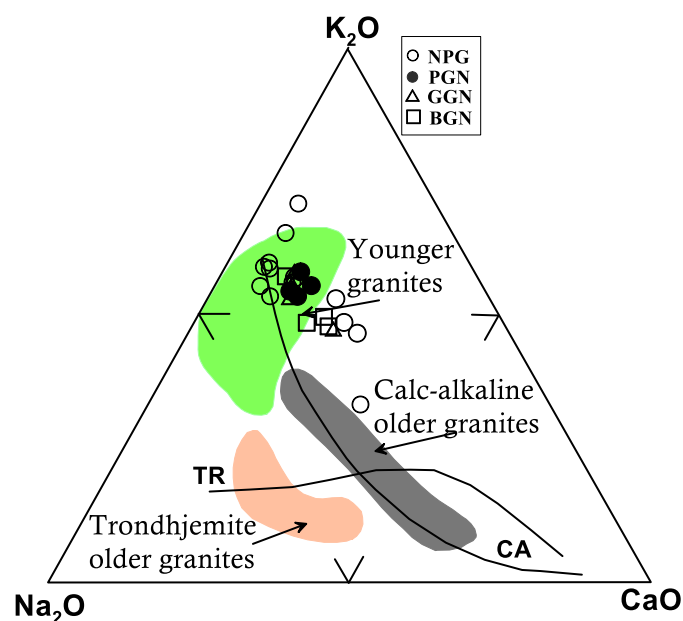Figure 6.6: Harker Diagrams (major oxides vs SiO$_2$) plotted for KAHG

Figure 6.7: Na$_2$O–K$_2$O–CaO ternary diagram showing fields of the KAHG (Hassan and Hashad, 1990). The trondhjemitic (TR) and calc-alkaline (CA) trends are from Barker and Arth (1976)
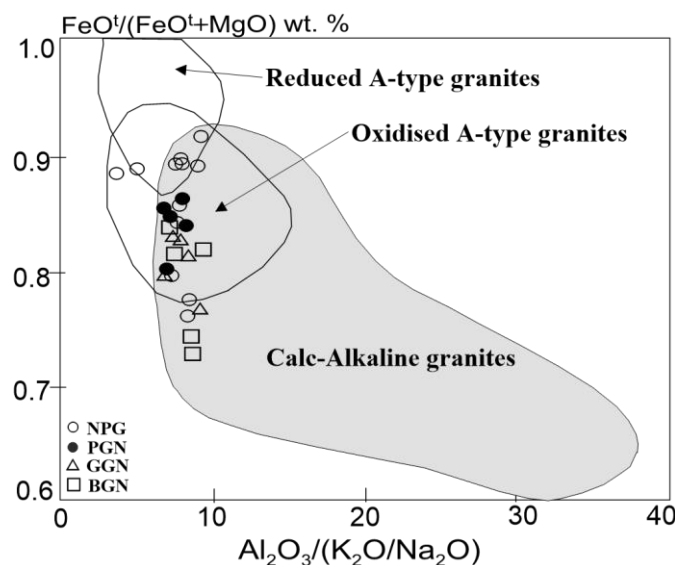Symbols: Open Circle- NPG; Solid Circle- PGN; Triangle: GGN; Square-BGN

Figure 6.8. (a) FeO^t/ (FeO^t + MgO) vs Al$_2$O$_3$ (wt%) diagram display calc-alkaline I-type, reduced A-type, and oxidized A-type granites (after Dall'Agnol & de Oliveira, 2007) (b) (Al$_2$O$_3$ + CaO)/ (FeO + Na$_2$O + K$_2$O)-100(MgO + FeO + TiO$_2$)/SiO$_2$ (after Sylvester (1989).
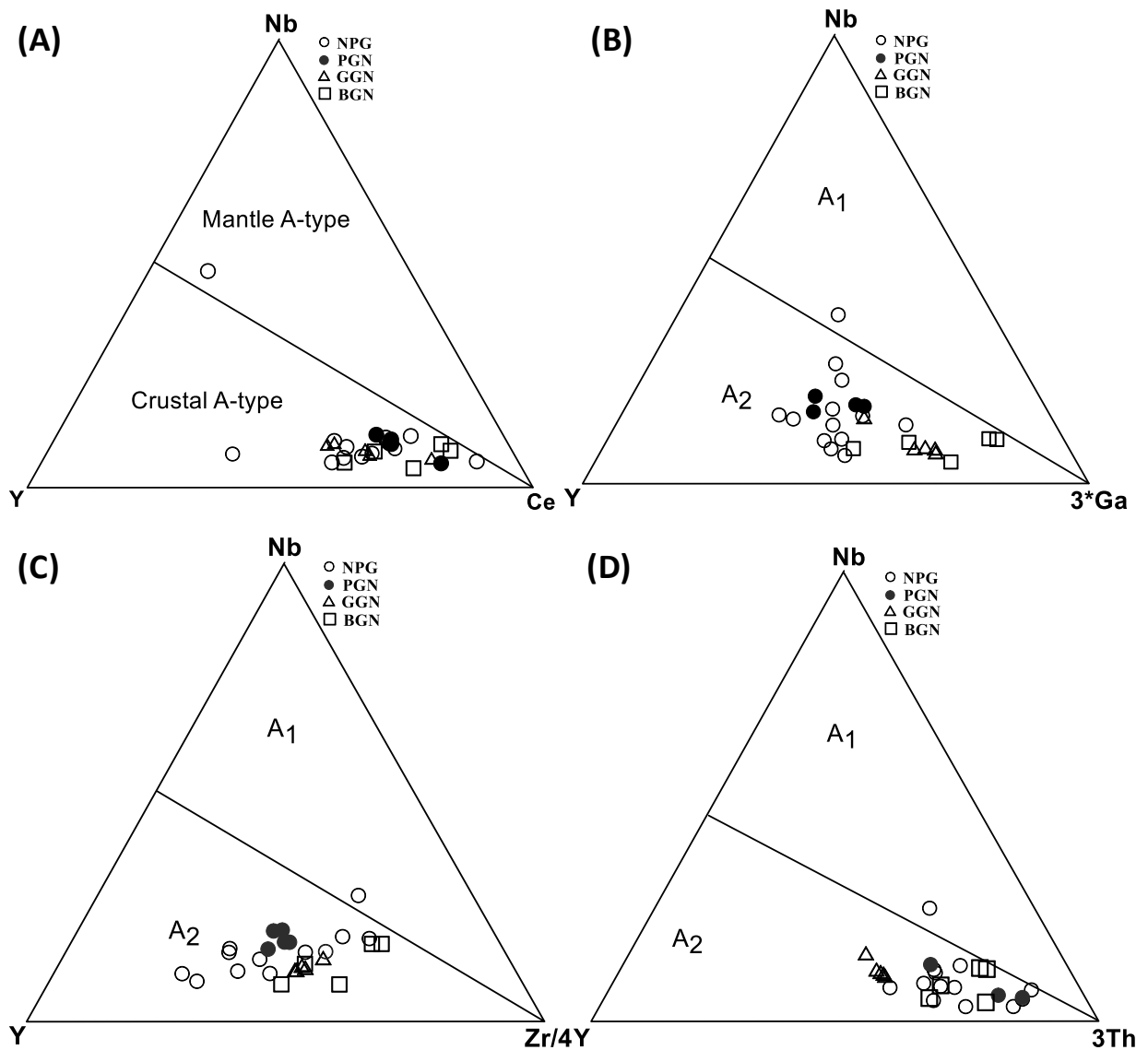Symbols: Open Circle- NPG; Solid Circle- PGN; Triangle: GGN; Square-BGN

Figure 6.10: Triangular discrimination diagram for crustal (A$_2$) versus mantle (A$_1$) derived A-type granites (Ebby, 1992). (A)Y-Nb-Ce (B) Y-Nb- 3×Ga (C) Nb–Y–Zr/4 and (D) Nb–Y–3×Th, diagrams Note that except for a sample, all samples cluster at the crustal source field.

Symbols: Open Circle- NPG; Solid Circle- PGN; Triangle: GGN; Square-BGN
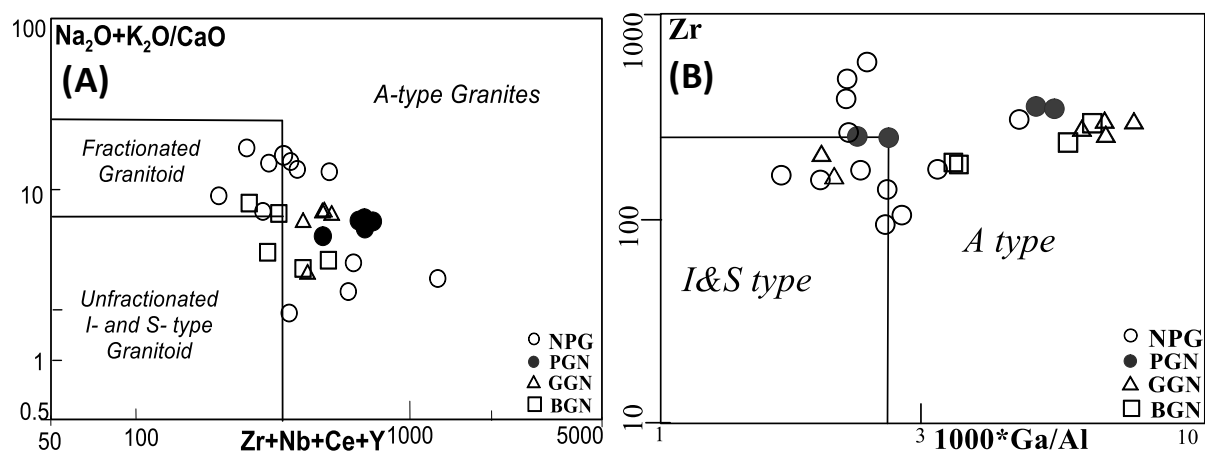
Figure 6.11 (A): Zr+Nb+Ce+Y vs Na2O +K₂O/CaO diagram. FG= Field for fractionated I-type granitoids. OGT= Field for I, S and M- type granitoids; (B) Discrimination diagram for A type granites (Whalen et al., 1987)

Symbols: Open Circle- NPG; Solid Circle- PGN; Triangle: GGN; Square-BGN
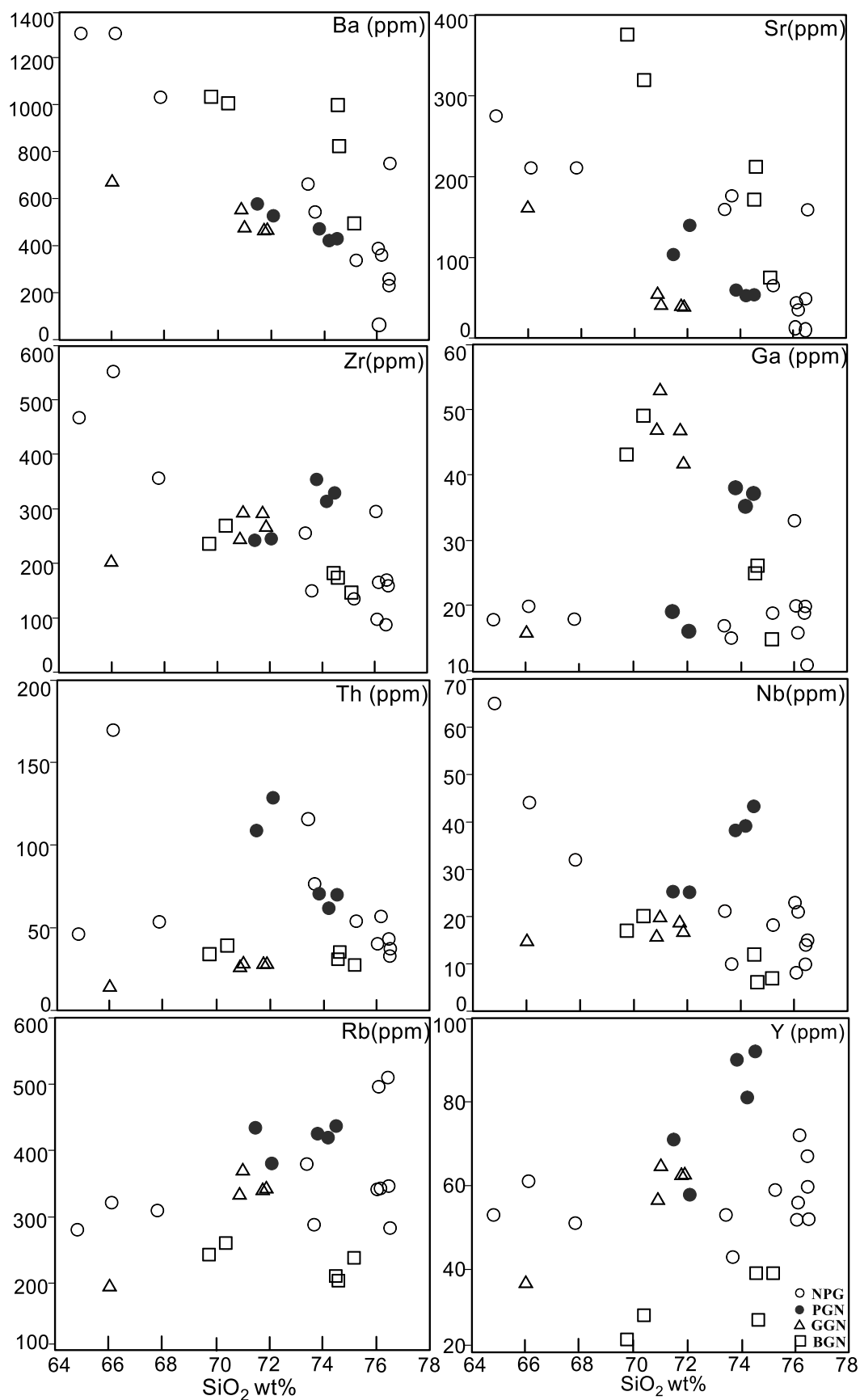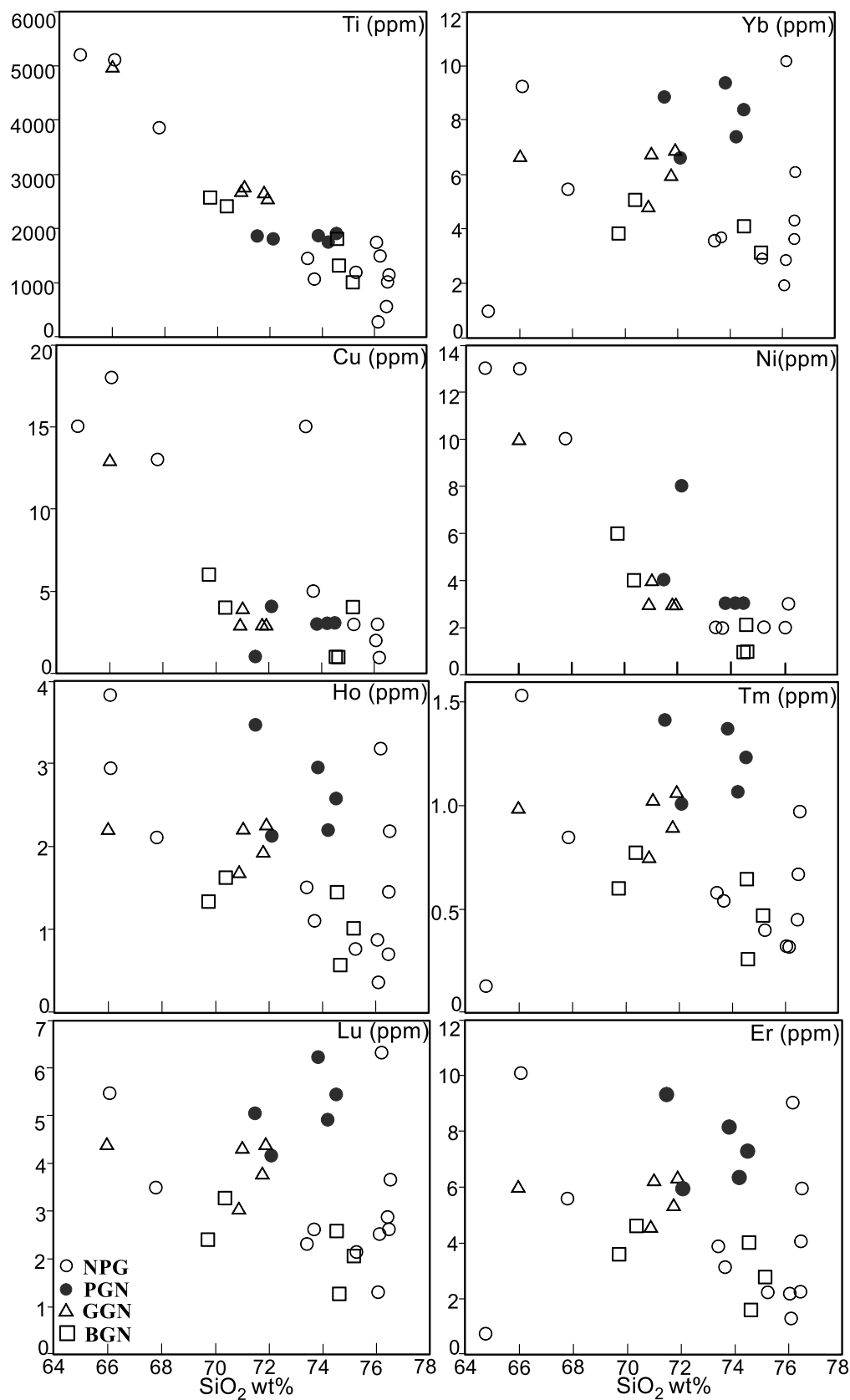
Figure 6.12: Harker variation diagram (trace elements vs SiO₂) plotted for KAHG
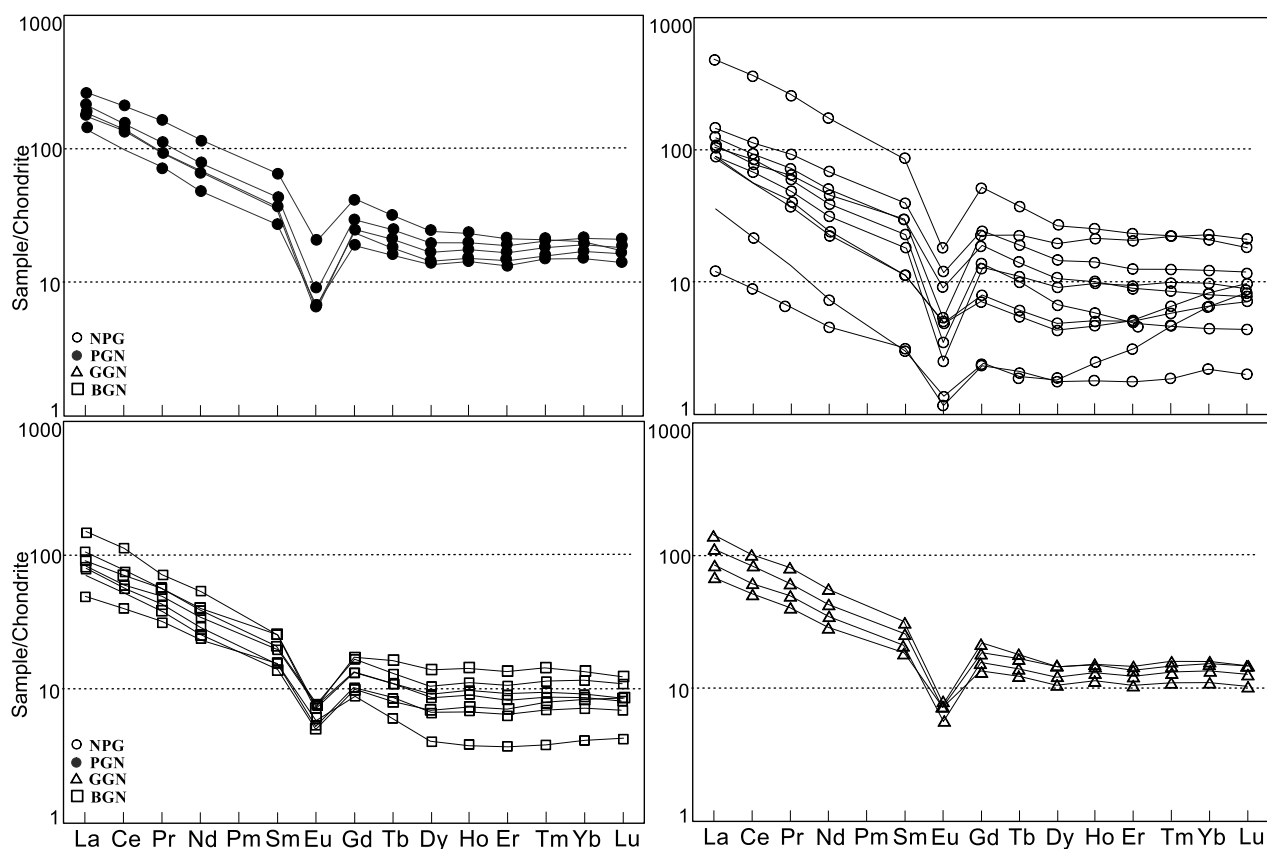
Figure 6.13: Chondrite-normalized (Sun and Mc Donough, 1989) rare earth elements (REE) patterns of the KAHG. Symbols: Open Circle- NPG; Solid Circle- PGN; Triangle: GGN; Square-BGN
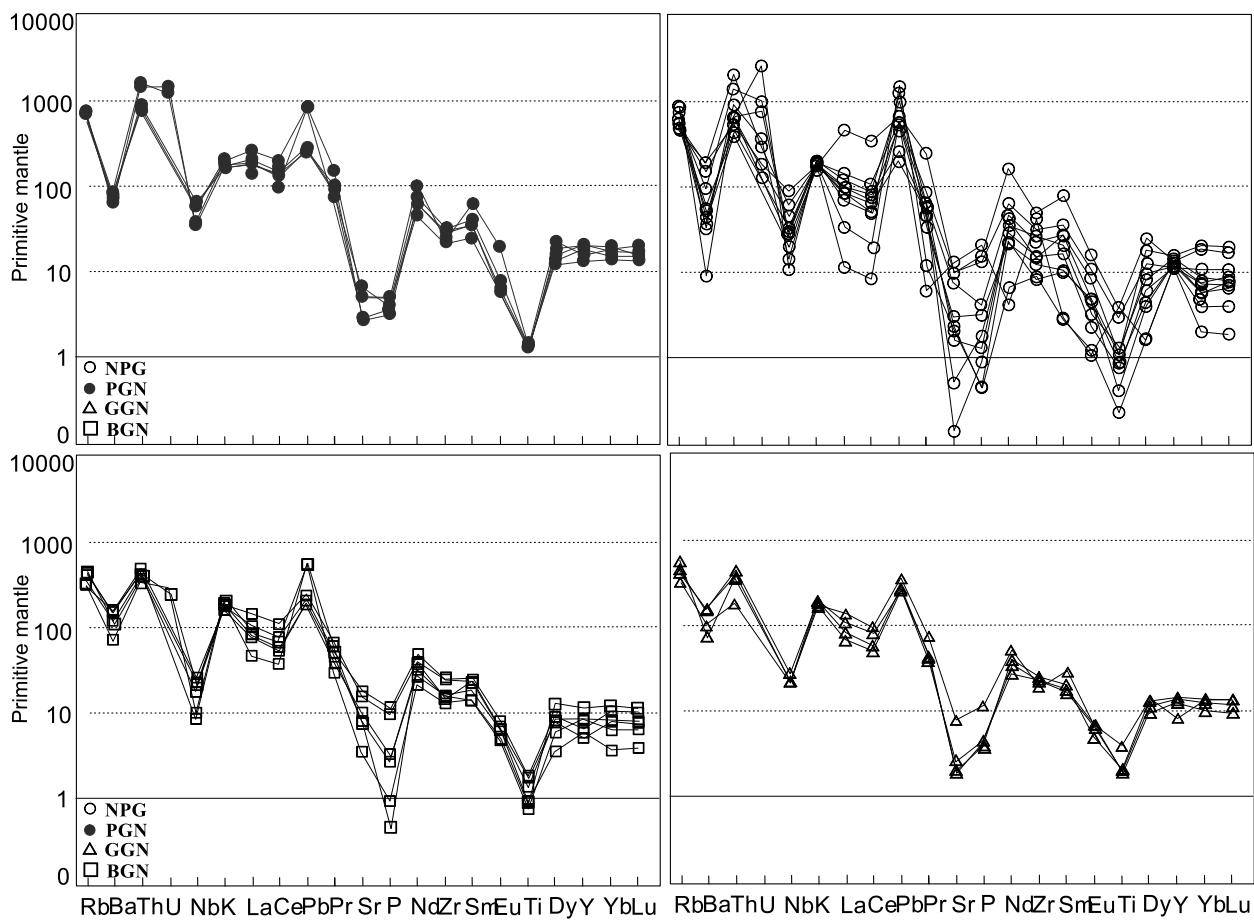
Figure 6.14: Primitive mantle-normalized diagram of trace element concentration of KAHG after (Sun and Mc Donough, 1989). Symbols: Open Circle- NPG; Solid Circle- PGN; Triangle: GGN; Square-BGN
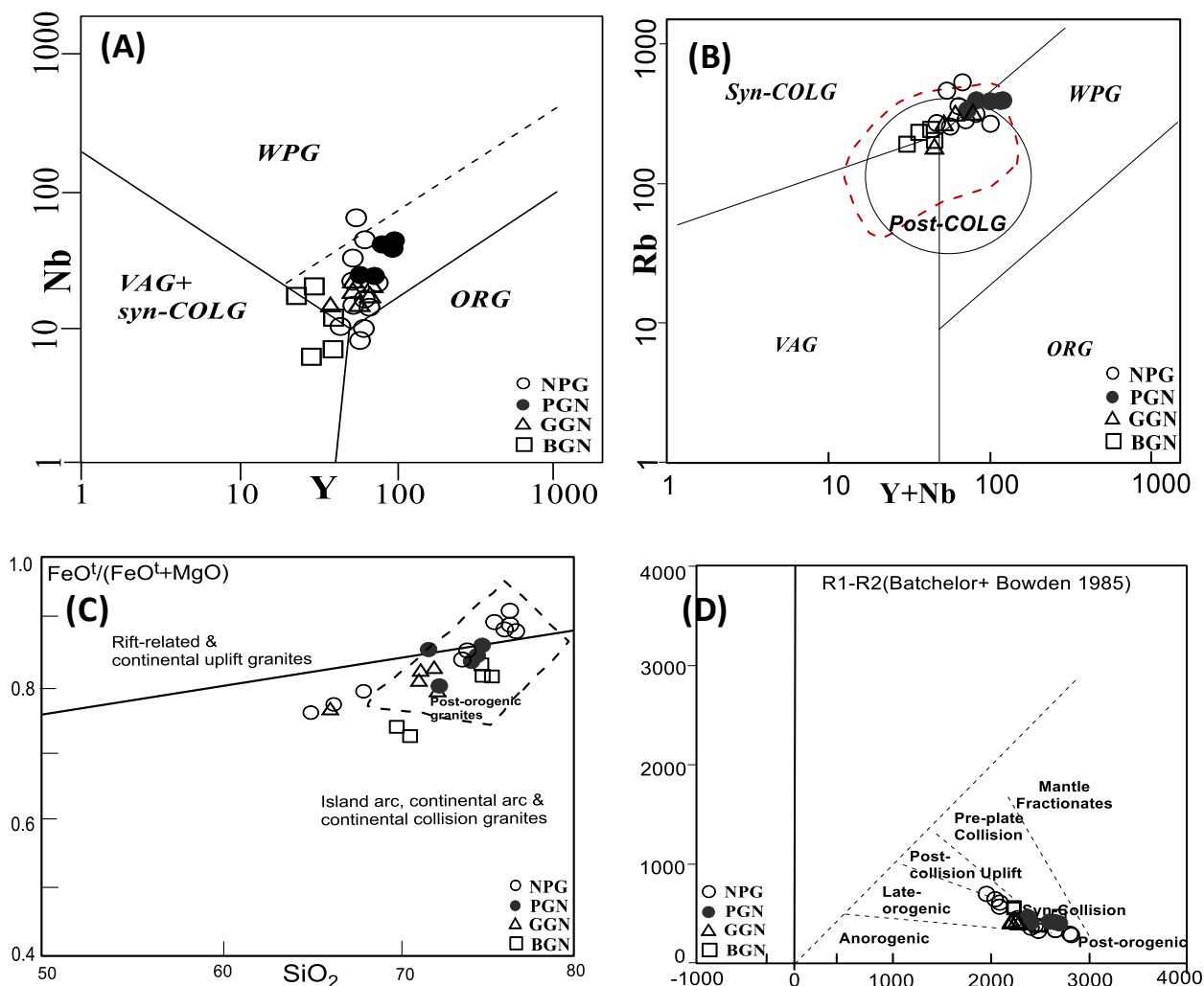
Figure 6.15: Tectonic discrimination diagram (A) Nb vs. Y (B) Rb vs. (Y + Nb) (Pearce et al., 1984). (Red dash line represents the field of Pan-African granitoids of NE-Brazil (Guimarães et al.,2004) (C) Maniar and Piccoli, 1989. (D) R1 vs R2 multicationic plot after (Batchelor & Bowden, 1985)

VAG: volcanic arc granite; WPG: within plate granite; SYN-COLG: syn-collisional.

Symbols: Open Circle- NPG; Solid Circle- PGN; Triangle: GGN; Square-BGN
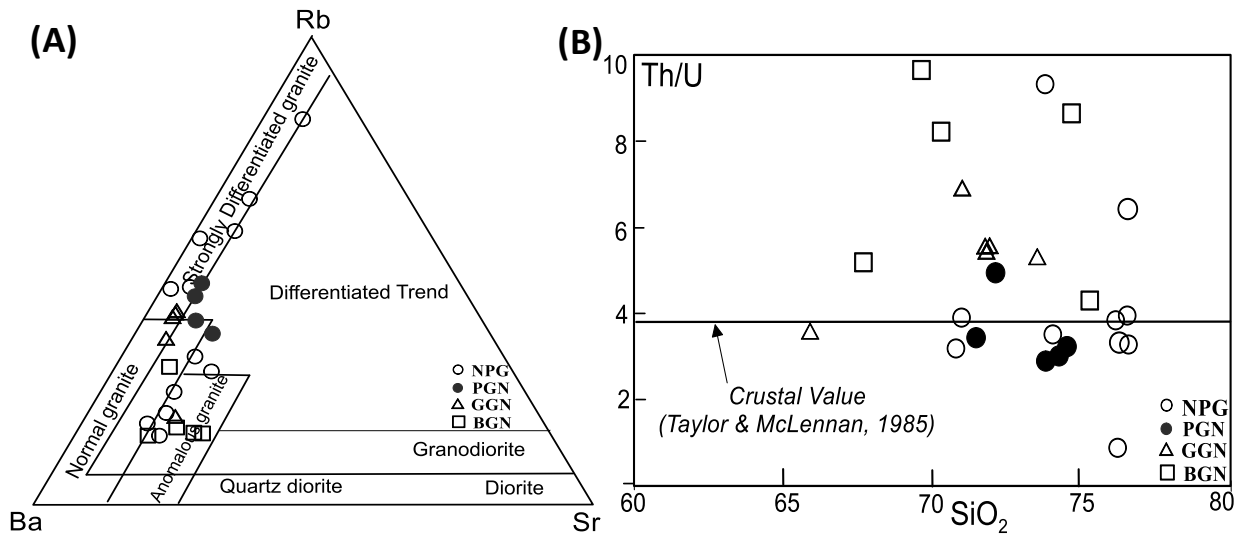
Figure 6.16 (A): Ba-Rb-Sr ternary diagram for KAH granitoid. Fields of composition and differentiation trends after El Bouseily and El Sokkary, 1975 (B) SiO_2 vs Th/U Plots with limit of crustal value (After Taylor & McLennan, 1985)

Symbols: Open Circle- NPG; Solid Circle- PGN; Triangle: GGN; Square-BGN
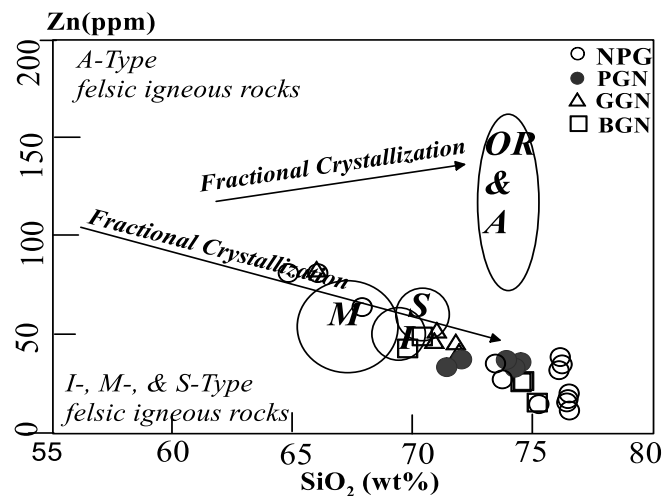
Figure 6.17 Discrimination plot of SiO_2 vs. Zn (modified from Lentz, 1998). A-type = anorogenic type (mantle or crustal); M-type = mantle depleted source; I-type = igneous source (mantle-derived or crustal); S-type = sedimentary crustal source; OR = oceanic ridge.

Symbols: Open Circle- NPG; Solid Circle- PGN; Triangle: GGN; Square-BGN
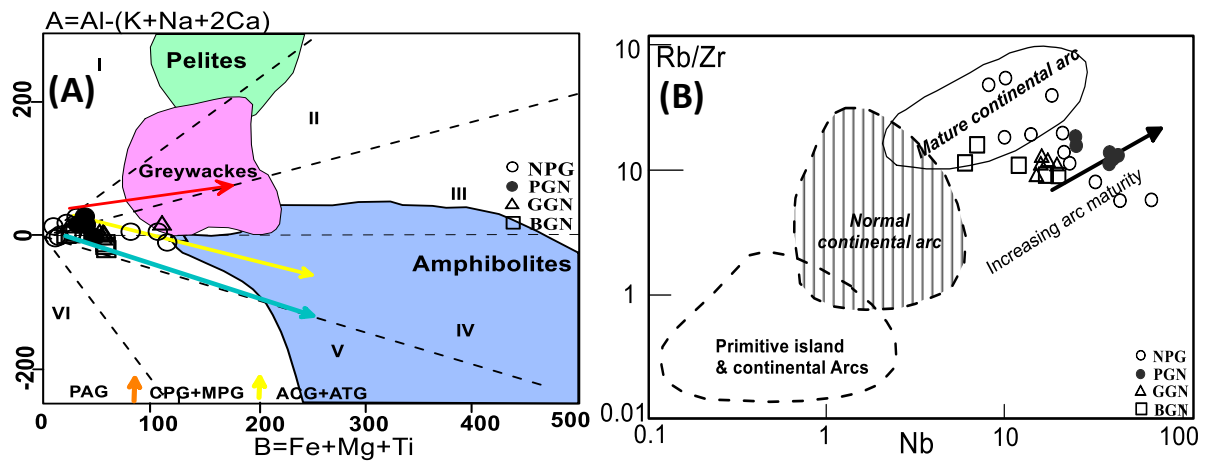
Figure 6.18 (A): A-B multicationic plot of (Debon & Le Fort 1983, 1988) of the Karbi Anglong Hills granitoids. Field I= Ms>Bt, II: Bt>Ms, and III: Bt±minor Amp characteristics of peraluminous domain; Field IV: Bt, Amp±Px, V: Cpx± Amp± Bt, and VI: Unusual associates (carbonatites) linked to Al-poor, Ca-rich metaluminous minerals (B) Nb vs. Rb/Zr diagram demonstrating tectonic setting (Brown et al.,1984) (Jin, 1986).
Symbols: Open Circle- NPG; Solid Circle- PGN; Triangle: GGN; Square-BGN

TABLE 19: MAJOR OXIDES (wt%) AND CIPW NORMATIVE (wt%) OF REPRESENTATIVE KARBI ANGLONG HILLS GRANITOIDS

Sample No	NON-PORPHYRITIC GRANITOIDS									
	NL	MH	KJ	JKL1	JKL2	SE	AR	KH-6	KH-7	KH-8
SiO$_2$	73.42	76.41	76.09	76.03	76.44	75.21	76.15	67.83	66.10	64.80
TiO$_2$	0.24	0.09	0.05	0.29	0.17	0.20	0.25	0.64	0.85	0.87
Al$_2$O$_3$	14.39	13.71	13.63	13.51	11.87	13.93	13.22	15.05	15.34	15.30
Fe$_2$O$_3$	1.75	0.57	0.75	1.85	1.08	1.30	1.53	4.10	5.14	5.44
MnO	0.04	0.03	0.03	0.04	0.02	0.03	0.04	0.06	0.08	0.08
MgO	0.29	0.06	0.06	0.2	0.12	0.13	0.16	0.94	1.33	1.53
CaO	1.31	0.53	0.98	0.65	0.58	0.64	0.64	2.22	2.60	3.08
Na$_2$O	3.21	3.44	3.73	3.35	2.52	3.35	3.13	2.76	2.84	2.80
K$_2$O	6.01	5.85	5.47	5	5.83	5.89	5.41	5.69	5.13	5.14
P$_2$O$_5$	0.09	0.01	0.01	0.04	0.02	0.07	0.03	0.29	0.34	0.46
Total	100.75	100.7	100.8	100.96	98.65	100.75	100.56	99.58	99.75	99.5
A/NK	1.22	1.14	1.13	1.24	1.14	1.17	1.20	1.41	1.50	1.50
A/CNK	1.02	1.06	0.98	1.12	1.03	1.07	1.09	1.02	1.03	0.97
CIPW NORMS										
Q	28.77	32.82	31.41	35.84	38.11	31.82	35.72	24.66	23.36	21.26
C	0.44	0.78	0	1.5	0.41	1.05	1.12	1.01	1.2	0.63
Or	35.51	34.57	32.32	29.55	34.45	34.81	31.97	33.62	30.31	30.37
Ab	27.16	29.11	31.56	28.34	21.32	28.34	26.48	23.35	24.03	23.69
An	5.91	2.56	4.29	2.96	2.75	2.72	2.98	9.12	10.68	12.28
Di	0	0	0.32	0	0	0	0	0	0	0
Wo	0	0	0.01	0	0	0	0	0	0	0
Hy	0.72	0.15	0	0.5	0.3	0.32	0.4	2.34	3.31	3.81
Il	0.09	0.06	0.06	0.09	0.04	0.06	0.09	0.13	0.17	0.17
Hm	1.75	0.57	0.75	1.85	1.08	1.3	1.53	4.1	5.14	5.44
Tn	0	0	0.04	0	0	0	0	0	0	0
Ru	0.2	0.06	0	0.25	0.15	0.17	0.21	0.57	0.76	0.78
Ap	0.21	0.02	0.02	0.09	0.05	0.17	0.07	0.69	0.81	1.09
Sum	100.76	100.7	100.78	100.97	98.66	100.76	100.57	99.59	99.77	99.52

A/CNK=molar Al$_2$O$_3$/(CaO+Na$_2$O+K$_2$O); Fe$_2$O$_3$: total iron

TABLE 19 CONTINUED

Sample No	PORPHYRITIC GRANITOIDS					GRANITE GNEISS				
	KZ15	KZ17	KZ33	KZ42	KZ46	KZ18	KZ22	KZ23	KZ27	DO
SiO2	71.48	72.08	74.49	73.82	74.2	70.88	71.89	71.74	71.01	66
TiO2	0.31	0.3	0.31	0.31	0.29	0.45	0.43	0.45	0.46	0.83
Al2O3	13.68	13.64	13.5	13.95	13.14	13.5	13.28	13.32	13.56	15.11
Fe2O3	1.93	2.53	2.26	2.18	2.25	2.88	2.64	2.85	3.07	5.29
MnO	0.05	0.07	0.08	0.05	0.08	0.06	0.06	0.06	0.07	0.13
MgO	0.29	0.56	0.32	0.37	0.36	0.59	0.6	0.52	0.57	1.44
CaO	1.21	1.57	1.31	1.22	1.17	1.31	1.15	1.15	1.2	2.33
Na2O	2.8	2.9	3	3.02	2.79	3.34	3.01	3.13	3.22	2.9
K2O	5.61	5.66	5.05	5.09	5.1	5.32	5.82	5.56	5.54	4.78
P2O5	0.11	0.09	0.07	0.08	0.07	0.1	0.1	0.09	0.1	0.25
Total	97.47	99.4	100.39	100.09	99.45	98.43	98.98	98.87	98.8	99.06
A/CNK	1.06	0.99	1.06	1.1	1.07	0.99	1	1	1.01	1.07
CIPW NORMS										
Q	31.01	29.61	34.63	33.84	35.61	27.69	29.04	29.27	27.94	24.41
C	1.06	0.1	0.88	1.45	1.07	0.1	0.18	0.28	0.32	1.53
Or	33.15	33.45	29.84	30.08	30.14	31.44	34.39	32.86	32.74	28.25
Ab	23.69	24.54	25.38	25.55	23.61	28.26	25.47	26.48	27.24	24.54
An	5.28	7.2	6.04	5.53	5.35	5.85	5.05	5.12	5.3	9.93
Di	0	0	0	0	0	0	0	0	0	0
Wo	0	0	0	0	0	0	0	0	0	0
Hy	0.72	1.4	0.8	0.92	0.9	1.47	1.49	1.3	1.42	3.59
Il	0.11	0.15	0.17	0.11	0.17	0.13	0.13	0.13	0.15	0.28
Hm	1.93	2.53	2.26	2.18	2.25	2.88	2.64	2.85	3.07	5.29
Tn	0	0	0	0	0	0	0	0	0	0
Ru	0.25	0.22	0.22	0.25	0.2	0.38	0.36	0.38	0.38	0.68
Ap	0.26	0.21	0.17	0.19	0.17	0.24	0.24	0.21	0.24	0.59
Sum	97.46	99.41	100.39	100.1	99.47	98.44	98.99	98.88	98.8	99.09

A/CNK=molar Al_2O_3/(CaO+Na_2O+K_2O); Fe_2O_3: total iron

TABLE 19 CONTINUED

| | BASEMENT GRANITE GNEISS | | | | | | |
	KG1	KG2	KG	LG1	LG2	HW	CB
SiO2	74.59	74.51	75.13	69.73	70.37	76.49	73.66
TiO2	0.22	0.3	0.17	0.43	0.4	0.19	0.18
Al2O3	13.88	13.47	13.36	14.16	14.27	11.37	14.47
Fe2O3	1.54	1.34	0.6	2.74	2.61	0.7	1.48
MnO	0.03	0.04	0.02	0.07	0.07	0.02	0.04
MgO	0.3	0.23	0.12	0.84	0.86	0.08	0.22
CaO	1.81	1.19	1.08	2.42	2.2	0.53	1.23
Na2O	3.19	3.07	3.2	3.16	3.22	2.1	3.27
K2O	4.7	5.73	5.71	5.18	5.29	6.43	6.02
P2O5	0.07	0.06	0.02	0.25	0.21	0.01	0.08
Total	100.33	99.94	99.41	98.98	99.5	97.92	100.65
A/CNK	1.02	1.00	1.00	0.93	0.95	1.00	1.02
CIPW NORMS							
Q	33.92	32	32.23	26.06	26.14	38.44	28.87
C	0.42	0.2	0	0	0	0.02	0.53
Or	27.77	33.86	33.74	30.61	31.26	37.99	35.57
Ab	26.99	25.97	27.07	26.74	27.24	17.77	27.66
An	8.52	5.51	5.22	9.15	8.86	2.56	5.58
Di	0	0	0	0	0	0	0
Wo	0	0	0	0	0	0	0
Hy	0.75	0.57	0.3	2.09	2.14	0.2	0.55
Il	0.06	0.09	0.04	0.15	0.15	0.04	0.09
Hm	1.54	1.34	0.6	2.74	2.61	0.7	1.48
Tn	0	0	0	0.86	0.48	0	0
Ru	0.19	0.26	0.15	0	0.12	0.17	0.14
Ap	0.17	0.14	0.05	0.59	0.5	0.02	0.19
Sum	100.33	99.94	99.4	98.99	99.5	97.91	100.66

A/CNK=molar Al_2O_3/(CaO+Na_2O+K_2O); Fe_2O_3: total iron

TABLE-20: TRACE ELEMENTS (ppm) AND IMPORTANT ELEMENTAL RATIO OF REPRESENTATIVE KARBI ANGLONG HILLS GRANITOIDS

Sample no	NON-PORPHYRITIC GRANITOIDS								
	NL	MH	KJ	JKL1	JKL2	SE	AR	KH-6	KH-7	KH-8
Sc	4	3	3	4.4	2.9	3	3	7	9	8
V	18	7	4	13	8	12	12	50	64	75
Cr	7	7	10	26	16	7	7	15	18	22
Co	66	47	75	2	BDL	55	50	33	30	29
Ni	2	BDL	BDL	2	BDL	2	3	10	13	13
Cu	15	BDL	3	2	5	3	1	13	18	15
Zn	36	18	39	33	20	15	35	64	82	82
Ga	17	19	20	18	14	19	16	18	20	18
Rb	379	510	496	341	346	563	343	310	322	281
Sr	159	50	44	11	3	66	35	211	211	275
Y	53	60	56	52	67	59	72	51	61	53
Zr	255	90	101	298	172	137	168	357	553	468
Nb	21	10	8	23	14	18	21	32	44	65
Ba	659	227	64	384	257	336	359	1031	1305	1304
Pb	69	86	103	40	33	48	32	41	47	40
Th	115	43	55	99	66	54	57	54	170	46
U	20.5	12.2	53.2	23.9	15.7	2.6	15.9	BDL	6.0	3.8
Ga/Al	2.32	2.72	2.88	2.61	2.31	2.67	2.37	2.35	2.56	2.31
K/Rb	131.30	94.98	91.32	121.41	139.52	86.63	130.60	151.98	131.92	151.46
Rb/Sr	2.38	10.2	11.27	31.00	115.33	8.53	9.80	1.47	1.53	1.02
U/Th	0.18	0.28	0.97	0.24	0.24	0.05	0.28	BDL	0.04	0.08
Th/U	5.61	3.52	1.03	4.14	4.20	20.77	3.58	BDL	28.33	12.11

Ga/Al = Ga x 10000/Al

TABLE-20 CONTINUED

Sample no	PORPHYRITIC GRANITOIDS					GRANITE GNEISS				
	KZ15	KZ17	KZ33	KZ42	KZ46	GG18	GG22	GG23	KZ27	DO
Sc	5	5	4.8	6.6	6.9	5.4	5.4	5.1	5.2	8
V	20	28	16	18	17	27	24	27	28	62
Cr	19	20	19	18	29	23	27	21	19	17
Co	38	46	6	5	6	7	5	6	6	20
Ni	4	8	3	3	3	3	3	3	4	10
Cu	1	4	2	2	1	12	3	3	11	13
Zn	35	39	37	38	35	47	42	47	53	84
Ga	19	16	18	19	17	17	17	17	18	16
Rb	437	384	439	428	423	336	345	343	372	197
Sr	107	142	57	62	56	56	39	40	42	163
Y	71	58	92	90	81	57	63	63	65	37
Zr	240	242	325	353	311	250	273	298	299	208
Nb	25	25	43	38	39	16	17	19	20	15
Ba	573	521	423	468	417	557	469	467	480	676
Pb	56	58	69	70	61	27	29	29	29	24
Th	108	128	155	166	152	29	52	52	48	15
U	28.9	23.8	44.8	52.7	47.8	BDL	9	8.8	6.5	BDL
Ga/Al	2.72	2.30	2.61	2.67	2.54	2.47	2.51	2.50	2.60	2.08
K/Rb	106.30	122.05	95.25	98.47	99.83	131.10	139.68	134.22	123.31	200.91
Rb/Sr	4.08	2.70	7.70	6.90	7.55	6.00	8.85	8.58	8.86	1.21
U/Th	0.27	0.19	0.29	0.32	0.31	BDL	0.17	0.17	0.14	BDL
Th/U	3.74	5.38	3.46	3.15	3.18	BD	5.78	5.91	7.38	BD

Ga/Al = Ga x 10000/Al

TABLE-20 CONTINUED

	BASMENT GRANITE GNEISS						
	KG1	KG2	KG	LG1	LG2	HW	CB
Sc	4.2	4.6	4	6.3	7.6	2	4
V	20	15	7	44	38	14	16
Cr	19	27	11	35	31	10	9
Co	1	1	41	8	7	46	65
Ni	1	1	BDL	6	4	BDL	2
Cu	7	2	4	18	16	BDL	5
Zn	26	25	15	43	49	12	27
Ga	14	13	15	15	17	10	15
Rb	205	210	239	243	261	284	289
Sr	213	170	75	375	320	159	177
Y	28	39	39	23	29	52	43
Zr	175	182	148	240	270	163	151
Nb	6	12	7	17	20	15	10
Ba	823	1000	495	1035	1007	751	547
Pb	35	31	38	34	39	42	50
Th	36	20	27	41	52	35	76
U	3.9	BDL	5.9	3.9	6	5.1	7.6
Ga/Al	1.98	1.89	2.20	2.08	2.34	1.72	2.03
K/Rb	189.84	225.93	197.83	176.51	167.83	187.47	172.48
Rb/Sr	0.96	1.24	3.19	0.65	0.82	1.79	1.63
U/Th	0.11	BDL	0.22	0.10	0.12	0.15	0.10
Th/U	9.23	0.00	4.58	10.51	8.67	6.86	10.00

Ga/Al = Ga x 10000/Al

TABLE 21: RARE EARTH ELEMENT (ppm) OF SELECTED KARBI ANGLONG HILLS GRANITOIDS

Sample No	NON-PORPHYRITIC GRANITOIDS									
	NL	MH	KJ	JKL1	JKL2	SE	AR	KH-6	KH-7	KH-8
La	80.52	59.48	22.76	67.1	57.4	56.48	70.93	96.31	308.98	7.87
Ce	154.48	91.6	36.91	142	115.2	94.18	128.72	188.57	601.9	14.93
Pr	18.09	10.5	3.38	15.2	12.4	9.31	16.35	23.55	65.84	1.66
Nd	62.68	30.19	9.04	48.9	39.3	28.19	56.95	84.98	213.41	5.7
Sm	11.9	4.55	1.25	9.2	7.44	4.65	12.15	15.81	34.42	1.31
Eu	1.4	0.75	0.21	0.55	0.39	0.76	0.85	1.83	2.74	0.18
Gd	10.25	3.89	1.35	7.54	6.96	4.3	12.4	13.47	28.15	1.28
Tb	1.41	0.55	0.19	0.99	1.09	0.61	2.21	1.92	3.7	0.21
Dy	7.18	2.96	1.26	4.53	6.15	3.33	13.28	9.8	18.32	1.2
Ho	1.5	0.7	0.37	0.88	1.45	0.76	3.18	2.11	3.81	0.27
Er	3.87	2.26	1.4	2.19	4.08	2.27	9.04	5.6	10.09	0.78
Tm	0.58	0.45	0.32	0.32	0.67	0.4	1.51	0.85	1.53	0.13
Yb	3.58	3.66	2.86	1.97	4.33	2.91	10.14	5.45	9.25	0.98
Lu	0.53	0.66	0.58	0.3	0.6	0.49	1.45	0.8	1.25	0.14
ΣREE	357.97	212.2	81.88	301.67	257.46	208.64	339.16	451.05	1303.39	36.64

Chondrite Normalized REE (after Sun & McDonough 1995)

	NL	MH	KJ	JKL1	JKL2	SE	AR	KH-6	KH-7	KH-8
LaN	124.26	91.79	35.12	103.55	88.58	87.16	109.46	148.63	476.82	12.15
CeN	92.23	54.69	22.04	84.78	68.78	56.23	76.85	112.58	359.34	8.91
PrN	71.22	41.34	13.31	59.84	48.82	36.65	64.37	92.72	259.21	6.54
NdN	50.14	24.15	7.23	39.12	31.44	22.55	45.56	67.98	170.73	4.56
SmN	29.31	11.21	3.08	22.66	18.33	11.45	29.93	38.94	84.78	3.23
EuN	9.09	4.87	1.36	3.57	2.53	4.94	5.52	11.88	17.79	1.17
GdN	18.84	7.15	2.48	13.86	12.79	7.90	22.79	24.76	51.75	2.35
TbN	14.24	5.56	1.92	10.00	11.01	6.16	22.32	19.39	37.37	2.12
DyN	10.65	4.39	1.87	6.72	9.12	4.94	19.70	14.54	27.18	1.78
HoN	10.07	4.70	2.48	5.91	9.73	5.10	21.34	14.16	25.57	1.81
ErN	8.84	5.16	3.20	5.00	9.32	5.18	20.64	12.79	23.04	1.78
TmN	8.53	6.62	4.71	4.71	9.85	5.88	22.21	12.50	22.50	1.91
YbN	8.12	8.30	6.49	4.47	9.82	6.60	22.99	12.36	20.98	2.22
LuN	7.79	9.71	8.53	4.41	8.82	7.21	21.32	11.76	18.38	2.06
(La/Lu)N	15.95	9.45	4.12	23.48	10.04	12.09	5.13	12.64	25.94	5.90
(Ce/Yb)N	11.36	6.59	3.40	18.98	7.00	8.52	3.34	9.11	17.13	4.01
Eu*	24.075	9.18	2.78	18.26	15.56	9.675	26.36	31.85	68.265	2.79
Eu/Eu*	0.39	0.54	0.49	0.20	0.17	0.52	0.21	0.38	0.27	0.42

TABLE 21 CONTINUED

Sample No	PORPHYRITIC GRANITOIDS					GRANITE GNEISS				
	KZ15	KZ17	KZ33	KZ42	KZ46	GG18	GG22	GG23	KZ27	DO
La	170.99	90.39	114	136	117	44.6	71.9	54.7	69	90.85
Ce	349.3	162.12	227	256	232	86	139	101.5	138	165.77
Pr	40.5	18.39	22.9	27.4	23.3	10.2	15.7	12.6	15.5	20.13
Nd	142.26	60.17	84	97	83	35.8	53.5	43.4	53	68.47
Sm	26.36	10.83	15	17.5	14.2	7.43	10.45	8.61	10.4	12.75
Eu	3.11	1.07	0.95	1.31	0.91	1.08	1.1	0.86	1.12	1.16
Gd	22.53	9.93	13.5	16	12.6	7.33	10.01	8.43	10.1	11.86
Tb	3.14	1.58	2.06	2.44	1.83	1.2	1.66	1.38	1.63	1.8
Dy	16.11	9.08	11.3	13.1	9.7	7.07	9.73	8.14	9.55	9.83
Ho	3.45	2.11	2.57	2.94	2.18	1.69	2.28	1.94	2.23	2.21
Er	9.28	5.91	7.26	8.13	6.3	4.61	6.39	5.39	6.28	6.04
Tm	1.41	1.01	1.23	1.37	1.07	0.75	1.07	0.9	1.03	0.99
Yb	8.86	6.6	8.36	9.35	7.36	4.86	6.92	5.99	6.79	6.71
Lu	1.15	0.95	1.24	1.42	1.12	0.7	1.01	0.87	0.99	1.01
ΣREE	798.45	380.14	511.37	589.96	512.57	213.32	330.72	254.71	325.62	399.58
Chondrite Normalized REE (after Sun & McDonough 1995)										
LaN	263.87	139.49	175.93	209.88	180.56	68.83	110.96	84.41	106.48	140.20
CeN	208.54	96.79	135.52	152.84	138.51	51.34	82.99	60.60	82.39	98.97
PrN	159.45	72.4	90.16	107.87	91.73	40.16	61.81	49.61	61.02	79.25
NdN	113.81	48.14	67.2	77.6	66.4	28.64	42.80	34.72	42.40	54.78
SmN	64.93	26.67	36.95	43.1	34.98	18.30	25.74	21.21	25.62	31.40
EuN	20.19	6.95	6.17	8.51	5.91	7.01	7.14	5.58	7.27	7.53
GdN	41.42	18.25	24.82	29.41	23.16	13.47	18.40	15.50	18.57	21.80
TbN	31.72	15.96	20.81	24.65	18.48	12.12	16.77	13.94	16.46	18.18
DyN	23.9	13.47	16.77	19.44	14.39	10.49	14.44	12.08	14.17	14.58
HoN	23.15	14.16	17.25	19.73	14.63	11.34	15.30	13.02	14.97	14.83
ErN	21.19	13.49	16.58	18.56	14.38	10.53	14.59	12.31	14.34	13.79
TmN	20.74	14.85	18.09	20.15	15.74	11.03	15.74	13.24	15.15	14.56
YbN	20.09	14.97	18.96	21.2	16.69	11.02	15.69	13.58	15.40	15.22
LuN	16.91	13.97	18.24	20.88	16.47	10.29	14.85	12.79	14.56	14.85
(La/Lu)N	15.60	9.98	9.65	10.05	10.96	6.69	7.47	6.60	7.31	9.44
(Ce/Yb)N	10.38	6.47	7.15	7.21	8.3	4.66	5.29	4.46	5.35	6.50
Eu*	53.175	22.46	30.885	36.255	29.07	15.89	22.07	18.36	22.10	26.60
Eu/Eu*	0.39	0.31	0.2	0.24	0.21	0.45	0.33	0.31	0.33	0.29

TABLE 21 CONTINUED

	BASEMENT GRANITE GNEISS						
	KG1	KG2	KG	LG1	LG2	HW	CB
La	50.7	53	31.47	68.3	97	58.1	46.16
Ce	94.7	101.3	66.65	130	186.4	117.31	88.04
Pr	10.8	12.2	8.03	14.3	17.8	14.27	9.61
Nd	35.7	42.4	28.82	48	66	50.89	31.78
Sm	6.18	7.98	6.34	8.26	10.1	10.45	5.7
Eu	0.89	1.19	0.8	1.17	1.36	1.11	0.79
Gd	4.85	7.29	5.54	7.29	9.04	9.61	5.38
Tb	0.59	1.09	0.84	1.07	1.29	1.64	0.81
Dy	2.68	6.21	4.48	5.8	6.98	9.39	4.73
Ho	0.57	1.44	1.01	1.34	1.62	2.19	1.11
Er	1.62	4.02	2.79	3.62	4.63	5.97	3.15
Tm	0.26	0.64	0.47	0.6	0.77	0.97	0.54
Yb	1.83	4.07	3.14	3.85	5.1	6.07	3.7
Lu	0.29	0.59	0.47	0.55	0.75	0.84	0.6
ΣREE	211.66	243.42	160.85	294.15	408.84	288.81	202.1
Chondrite Normalized REE (after Sun & McDonough 1995)							
LaN	78.24	81.79	48.56	105.40	149.69	89.66	71.23
CeN	56.54	60.48	39.79	77.61	111.28	70.04	52.56
PrN	42.52	48.03	31.61	56.30	70.08	56.18	37.83
NdN	28.56	33.92	23.06	38.40	52.80	40.71	25.42
SmN	15.22	19.66	15.62	20.34	24.88	25.74	14.04
EuN	5.78	7.73	5.19	7.60	8.83	7.21	5.13
GdN	8.92	13.40	10.18	13.40	16.62	17.67	9.89
TbN	5.96	11.01	8.48	10.81	13.03	16.57	8.18
DyN	3.98	9.21	6.65	8.61	10.36	13.93	7.02
HoN	3.83	9.66	6.78	8.99	10.87	14.70	7.45
ErN	3.70	9.18	6.37	8.26	10.57	13.63	7.19
TmN	3.82	9.41	6.91	8.82	11.32	14.26	7.94
YbN	4.15	9.23	7.12	8.73	11.56	13.76	8.39
LuN	4.26	8.68	6.91	8.09	11.03	12.35	8.82
(La/Lu)N	18.37	9.42	7.03	13.03	13.57	7.26	8.08
(Ce/Yb)N	13.62	6.55	5.59	8.89	9.62	5.09	6.26
Eu*	12.07	16.53	12.9	16.87	20.75	21.705	11.965
Eu/Eu*	0.50	0.48	0.41	0.46	0.43	0.34	0.44

CHAPTER VII

DISCUSSION AND CONCLUSION

7.1   INTRODUCTION

Previous chapters (1 to 6) have recounted in details about the field occurrence, magnetic susceptibility, petrography (Fig. 4.1-4.7), mineralogy (Fig. 5.1-5.12), whole- rock geochemistry (major and trace including rare-earth elements (Fig. 6.1-6.18) of representative Karbi Anglong Hill granitoids. The present chapter attempts to summarise all the acquired outcomes and advocate the involvement of most feasible processes that contributed to the formation of Karbi Anglong Hill granitoids.

7.2   FIELD PETROGRAPHY

7.2.1   TEXTURAL VARIATION

Megascopically, the studied Karbi Anglong Hills Granitoids are medium to coarse grained, leucocratic to mesocratic. Markedly porphyritic as well as gneissic. The rocks studied, in general retain enclaves of mafic rocks.

The gneissic outcrops are phenocrysts free, exhibited minor foliation with crude accumulation of mica minerals, sub-spherical or lenticular diffused rim enclaves noted. The mingled portions display extended bands and schlieren, from which presumptions can be made that differences in viscosity existed between the melts however negligible. Granites exhibiting schlieren have been recognised as the incomplete assimilation of enclaves, sedimentation or differences in flow between crystal- charged melt (e.g., Wyborn et al., 2001). The orientation of biotite grains is indicative that the rocks are faintly deformed. Presence of cross cutting intruding association of coarser grained with reduced amount of ferromagnesian minerals both along and across gneissocity could be suggestive of a younger granite activity of the former.

Massive outcrops of non-porphyritic granitoids are phenocryst free, frequently hosting quartz veins, small rounded or lenticular microgranular enclaves are hosted sparingly, larger enclaves sporadically edged by thick quartz bands. By the nature of the undeformed granitoids, it could be suggestive of no ensuing orogenic activities after their emplacement and subsequent solidification.

7.2.2   MAGNETIC SUSCEPTIBILITY (MS) AND GRANITE SERIES

From the perspective of magnetic susceptibility (MS) parameter ($\times 10^{-3}$ SI) the KAHG is categorised into the reduced-type and oxidized-type granites (Takagi and Tsukimura, 1997) linked to ilmenite series (MS$\leq 3\times 10^{-3}$ SI) granites and magnetite-series granites (MS$>3\times 10^{-3}$ SI unit) respectively (Kanaya and Ishihara, 1973; Ishihara, 1977; Ishihara et al., 2002; Takagi, 2004). Ishihara reckoned the ilmenite series to being reduced and considered identical to S-type granites of Chappell & White (1974) for the reason that integration of graphitic material occurred from the source region into the crystallizing melt. S-type granites are basically thought to be of ilmenite series yet, situations are not as simple, I-type granites may belong to either ilmenite or the magnetite series, for instance occurrence of distinct magnetite and ilmenite series granites within certain I-type domains (Cobbing et al., 1992). Despite of the moderate variation in MS values of PGN (1.684 to 10.466 $\times 10^{-3}$ SI) and NPG (0.044 to 25.734 $\times 10^{-3}$ SI unit), bulk of the granitoids can be characterized as moderately oxidized, magnetite series granitoids, which is corroborated by the presence of euhedral magnetite and ferromagnetic minerals (Anettsungla et al., 2018). The BGN recorded the highest MS value (51.182$\times 10^{-3}$ SI unit) which strongly imply prevailing oxidizing environment in its genesis. However, the mixed magnetite (metaluminous) series (78%) to ilmenite (peraluminous) series (22%) characters observed for KAHG most likely reflect the late-stage hydrothermal fluids and/or process of ductile deformation that might have obliterate the original magma-related magnetic fabric leading to alteration of magnetite to ilmenite as opined elsewhere (e.g., Gregorová et al., 2003; Kumar, 2008, Anettsungla et al., 2018).

7.2.3   MICROTEXTURAL VARIATIONS

The easily discernible petrographic features and textures observed in the studied rocks are valid attestations that point to igneous genesis (section 4.2 Chapter- 4). Typical polysynthetic twinning (plagioclase) together with the cross hatched zoning (potash- feldspars), grains of alkali -feldspar enclosing finer plagioclase crystals.

Biotite grains hosts accessory minerals like zircon, titanite, apatite and opaques. Such inclusions tend to be enriched in rare earth elements, and also impart a pleochroic halo within certain grains that may be enhanced by enrichment in elements as U and Th.

Textures observed are generally inequigranular to equigranular hypidiomorphic nature. Exsolution textures such as myrmekite, graphic and perthite are well noted. Perthitic character of alkali feldspar are suggestive of a shallow depth of emplacement which exsolves from magmatic alkali feldspar at low temperatures. The occurrence of myrmekite in deformed and gneissic granite commonly along the interface of orthoclase and plagioclase and occasionally parallel to the major foliation of the granite is highly suggestive of induced metasomatic origin during deformation. Gneissic variety exhibit moderate foliated gneissose texture with rough alignment of biotite grains.

7.3   MODAL COMPOSITION AND NOMENCLATURE

Following the IUGS scheme (Le Maitre, 2002) the KAHG show trivial variation in the modal mineralogy, the porphyritic variety correspond to monzonite, non-porphyritic granitoids falls within the same with an exception of quartz monzonite. Granite gneiss represented syenogranite and monzogranite.

7.4   VARIATION IN MINERAL COMPOSITION

Amongst the different variety of Karbi Anglong Hills granitoids the dominant mineral compositions shifts between quartz, alkali feldspar and plagioclase together with biotite. Mineral assemblages of amphibole, titanite, apatite, zircon, epidote, and iron oxides noted as accessory phase.

Magmatic hornblende is generally limited in evolved granites or if present, they tend to be altered (Anderson et al., 2008), consequently KAH granitoids hosts a very inadequate amount of the minerals, thus it is assumed that the studied rocks can be linked to an evolved nature.

7.4.1   PLAGIOCLASE COMPOSITION

The composition of plagioclases of KAHG ranges from $Ab_{70.70}$- $Ab_{97.64}$ (Albite mole %), $An_{7.17}$ (albitic) to $An_{27.50}$ (Oligoclase) was noted from all samples irrespective of the nature of granitoids. Orthoclase ranges from $Or_{0.29}$-$Or_{2.03}$. Plagioclase of porphyritic variety chiefly belong to albite; while gneissic variety is entirely of oligoclase and accounts the maximum value of anorthite within the plagioclase $An_{27.50}$.

7.4.2 BIOTITE COMPOSITION

Being a common hydrous ferromagnesian mineral present in felsic melts, biotite performs as a significant indicator of the redox conditions and nature of melts (e.g., Wones and Eugster 1965; Czamanske et al., 1981; Burkhard 1991, 1993; Kumar et al., 2005, 2006; Kumar and Singh, 2008; Kumar and Pathak, 2010, Ishihara and Imai, 2014; Bora and Kumar, 2015; Singh et al., 2016). It is employed to deduce elemental substitutions akin to the nature of host felsic magma (I-, S, and A-type) that correspondingly develops in tectonic environments as subduction-related, syn-collision and anorogenic environments (Abdel-Rahman, 1994).

Through the annite activities of magnetite in biotite, and also through the association of latter with alkali feldspar may prove valuable in calculating physical parameters such as temperature, oxygen fugacity, and water fugacity of the parental melt (e.g., Wones and Eugster, 1965; Czamanske and Wones, 1973; Czamanske et al., 1977, 1981; Speer, 1987).

7.4.2.1 NATURE OF FELSIC MAGMA AND ELEMENTAL SUBSTITUTION

Nachit et al., (2005) chemical classification of biotite demonstrated granite gneiss and basement granite gneiss evolved from primary magmatic to re-equilibrated nature which most possibly was affected by circulating late post-magmatic fluid activity. Scarce porphyritic and non-porphyritic granitoids demonstrate in these parameters to be of primary magmatic nature.

Hydrothermal biotites normally contain low Ti in contrast with magmatic biotites as Ti concentration is very sensitive to temperature (Robert, 1976). Low TiO_2 (0.95 to 3.5 wt.%) and Ti content (0.09-0.20 wt.%) within KAHG biotites supports neoformed nature of biotite (Fu, 1981).

Based on binary oxide components, BGN exhibit characteristics of an evolution related to subduction metaluminous (I-type), calc-alkaline melts with vital $Mg \rightleftharpoons Fe$ and weak $2Al \rightleftharpoons 3Fe$ and $2Al \rightleftharpoons Mg$ substitutions, meanwhile PGN, NPG and GGN varieties mostly exhibited moderate $2Al \rightleftharpoons Mg$ to weak $2Al \rightleftharpoons 3Fe$ substitutions more akin to anorogenic (A-type) alkaline melts. Biotites typical of peraluminous S-type granitoids generally exhibit $3Mg \rightleftharpoons 2Al$ substitution (Abdel-Rahman, 1994), is not perceived though slight peraluminous nature in bulk composition is observed.

Biotite compositional variation are transitional within the domain of Mg- Fe^{2+} biotites, exhibiting compositional affinity of biotites related to hornblende, pyroxene and or olivine (Albuquerque, 1973), thus it strongly advocates a contribution of mafic mantle source particularly the basement granite gneiss samples (KG&LG). Biotites of PGN, NPG, and GGN however demonstrate broader compositional affinity allied with and/or without the other ferromagnesium minerals which are features of granitoid melts formed in syn-collisional environment.

7.4.2.2 REDOX CONDITION OF FELSIC MAGMA

X_{Mg} (Mg/Mg+Fe^t) values within biotite have been considered vital for approximation about the situation during the mineral crystallization, a higher X_{Mg} value point to an oxidized condition rather than a reduced one (Ishihara et al., 2002, Kumar and Pathak, 2010, Bora and Kumar, 2015). The BGN (LG&KG) exhibiting the highest X_{Mg} (0.59-0.71) relates to oxidizing environment of crystallization, and it is consistent with the inference from MS readings (4.564-43.144 $\times 10^{-3}$ SI unit), interpreted as a moderate to strongly oxidised, magnetite-series (I-type) nature of these granitoids.

Presence of Fe-Ti oxides (magnetite ± ilmenite and titanite) co-existing with K-feldspar and biotite strongly indicate magmatic and late- to post-magmatic oxidation conditions (e.g., Wones and Eugster, 1965, Wones, 1972, 1989). Based on the studies of Wones and Eugsters (1965), biotite compositions of KAHG are plotted in terms of relative proportions of Fe^{2+}(annite)-Mg (phlogopite)-Fe^{3+}(oxyannite), to estimate relative fO_2 conditions during which biotite have crystallized. Biotite compositions (100*Fe/Fe+Mg) of KAHG projected onto an isobaric (P=2070 bars) experimental calibration of biotite equilibria carried out at various buffers (FMQ, NNO, HM) of granitoid melts (Wones and Eugster, 1965, Wones, 1972) indicate oxidising trend (fO_2:$10^{-12.5}$- $10^{-15.9}$ log unit) of biotite evolution in a felsic melt within a temperature range of 733-900°C between NNO and QFM buffers (Fig. 5.10).

7.4.2.3 TECTONIC IMPLICATION

Composition of biotite minerals is expected to be reliable in directing to origin of parental melt (e.g., Burkhard 1993; Lalonde and Bernard 1993; Aydin et al., 2003; Kumar et al., 2006; Kumar and Pathak, 2010; Machev et al., 2004; Bora and Kumar, 2015).

Grounded on (Abdel-Rahman, 1994) ternary discrimination of (MgO-FeO^t-Al$_2$O$_3$) the compositional affinity of biotites is inferred as calc-alkaline suite (mostly orogenic subduction-related) I-type granitoids.

BGN (KG&LG) is less aluminous, insignificant FeOt/MgO ratio but enhanced Mg which is considered analogous to the biotites crystallized in subduction related situations, they are calc-alkaline, metaluminous (I-type) melt (Abdel- Rahman, 1994). In the same parameters PG (KZ) and NPG (KH&NL) show characteristics between meta- and peraluminous nature. Less aluminous BGN with insignificant FeOt/MgO ratio but enhanced Mg considered analogous to the biotites crystallized in subduction related situations, are characteristic of calc-alkaline, metaluminous (I-type) melt (Abdel- Rahman, 1994). Following same parameter, GGN and NPG leans more to a peraluminous suite, more aluminous, reduced Mg, analogous to biotites crystallized in syn-collisonal tectonic setting.

7.5   GEOCHEMISTRY

7.5.1   MAJOR AND TRACE ELEMENT VARIATION AS PROCESS DIAGNOSIS

Geochemically, highly evolved signature is shown by the KAHG with SiO$_2$ (64.80- 76.49 wt. %). According to Dall'Agnol and de Oliveira (2007) partial melting under oxidizing circumstances of a lower crustal primary source or felsic granulite hold the possibility to attain alkali-calcic to calc-alkaline, metaluminous to peraluminous calc-alkaline I-type to oxidized A-type features. Molar A/NK–A/CNK also point to metaluminous to mildly peraluminous granitoids distinctive of I-type Granitoids (Chappell & White 1992). Some degree of fractionation trailed by hydrothermal or supra- crustal assimilation may have given rise to the moderately peraluminous nature (Yang et al., 2008).

Concentration of most major oxides and trace Ba and Sr in Harker variation schemes, demonstrate negatively linear with SiO$_2$ suggesting an evolution through widespread fractional crystallization from a less fractionated melt (Stern and Gottfried, 1986; Turner et al., 1992; Moghazi, 2002) more often than not the fractionating phases are feldspar, yet positive correlation of NaO$_2$ & K$_2$O could suggest chemical affinity of a blend of parent magma with additional source material. Moreover, scarce distribution of mantle derived mafic magmas in prominent dimensions as would be expected, hinder the supposition of fractional crystallization as the sole process of evolution.

Negative correlations of CaO, MgO, Fe_2O_3 and TiO_2 indicate that amphibole fractionation also played a key role in the evolution of the magma. These chemical variations are conclusive of the importance of crystal fractionation in the evolution of KAHG. Fractionating phases mainly plagioclase, k-feldspars and hornblende.

The AFM plot and the affinity of the samples in the alkaline trend indicate moderate oxidising conditions, giving clarity that the key process for extraction of the melt from the parent source is crystal fractionation. However, SiO_2 Vs KiO_2 data depicts that KAHG are closely linking both to Shoshonitic to Calc-alkaline, perhaps suggestive of potassium diffusion, to evolve into an adjacent field, process as magma mingling seems more adequate than crystal liquid separation.

Compositional variation from granite to quartz monzonite inferred from $Na_2O + K_2O$ vs SiO_2 indicate similar results from cationic classification i.e., syeno to monzo-granite and granodiorite.

Following Frost et al., (2001), the KAHG categorize both as magnesian and ferroan -rich granites. Magnesian granitoids are presumed to have crystallized under high fO_2 condition, while a lower fugacity condition prevailed during the crystallization of ferroan granitoids. (Albuquerque et al., 2020).

In terms of $CaO–SiO_2$ composition (Carroll & Wyllie, 1990; Gorring et al., 2004; Patiño Douce, 1997; Skjerlie & Johnston, 1993), majority of studied rocks have been inferred as created from fluid absent partial melts of tonalitic to granodiorite sources. Limited non-porphyritic variety (KH) are produced from mafic sources. Dehydration melting of magnesian calc-alkalic granitoids at shallower crust will yield ferroan granites (Patinõ Douce, 1997; Skjerlie & Johnston, 1993). It has been proposed that partially melted ferroan granitoids tend to be silica- rich, calc- alkalic meanwhile higher intensity melting can modify it towards an alkali-calcic composition. Low-pressure condition is vital to attain metaluminous to mild peraluminous granitic composition which is ferroan in nature, with further rise in pressure the outcome will be a strong peraluminous melt. It is implicit therefore, with the metaluminous to mildly peraluminous ferroan nature of KAHG, that the melt resulted from a partial melting situation in low-pressure condition.

The Eu anomaly generally increases from the less evolved to the more evolved facies. Generally negative Eu anomaly increases from rocks with lower silica to rocks with higher silica-SiO_2 content (which is consistent with the fractionation of feldspar).

Generation of A-type granitoids ensue globally and links to bimodal magmatic suites, i.e., anorogenic rifting and post-collision extension (Bonin, 2004; Eby, 1992). Eby (1990, 1992) classified a two-fold tectonic discrimination for A-type granitoids. A_1- type classification link to a within-plate oceanic context or adjacent to divergent limits of intracontinental systems where primary melt from mantle plumes form unobstructed at faulted area (Bonin, 2007; Collins et al., 1982; Dobrestov, 2003; Grebennikov, 2014). Meanwhile A_2- type supports a rifted origin where rising magma occupied an extension and thinning continental crust (post-collision and subduction) (Grebennikov, 2014), such granitoids are assumed as the resultants of partially melted crust which are mantle derivative (Mushkin et al., 2003; Turner et al., 1992; Eby, 1990). Partial melting of an undepleted I-type tonalitic to granodioritic source may be more suitable to generate A-type granites (Creaser et al., 1991).

Emplacement of A-type granitoids is said to be linked globally and their emplacement age is rather ordered (Bonin, 2007; Black et al., 1985). The geodynamic settings and state of lower continental crust through which the melts form ensued by its upsurge to the surface, have great impact on its compositions (trace and isotopic); continental A-type rocks depict an evolution which is rather time bound extended for million years. The granitoids represent fairly enhanced large-ion lithophile elements (LILE) like Ba, Rb, K, Th, U and REE.

However, these inferences were expected as built from bulk geochemical analyses by the earlier workers (e.g., Hussain and Ahmed, 2009; Majumdar and Dutta, 2016; Mazumdar et al., 2016), transitional nature of metaluminous (I-type) and to some extent peraluminous and magnetite bearing A-type granitoids exhibiting both I-type and S-type features are often related to the later phases of Pan-African Orogeny (e.g., Anderson and Thomas, 1985; Dall'Agnol et al., 1999; Frost et al., 2001; Eyal et al., 2004; Frost and Frost, 2011; Kumar and Vallinayagam, 2012; Scandolara et al., 2013; Mbassa et al., 2016; Kaur et al., 2017; Kumar et al., 2022).

7.5.2   RARE EARTH ELEMENT (REE)

The studied granitoids having an enhanced LREE, comparatively low HREE and depleting Eu content, have a probability to be partial melting products of an older crust. Negative Europium anomaly link to a differentiating melt undergoing plagioclase depletion from the parental melt and that the volatile rich fluids developed in oxidizing environments (Yang et al., 2012; Li et al., 2014).

Enrichment of Rare Earth elements in granitoids is reported to be a characteristic aspect of Pan-African A-type granites, crystal fractionation and differentiation of magma are the important processes for the said feature (Ukaegbu and Beka, 2008). Substantial concentrations of REE observed in the KAHG could be combined cause steered by underplated melt with some degree of chemical fractionation of the parent magma (Majumdar and Dutta, 2014; 2016).

Distinct positive spikes of Pb with Nb anomalies on the primitive source spider diagrams indicate the magma as characteristic of a subduction regime and consequently crustal contamination is predicted (e.g., Zartman and Doe, 1981; Saunders et al., 1991). Supplementary value of Th/U ratios correspond to upper crustal estimates of 3.8 (Taylor & McLennan, 1985). In granitoids the enrichment of U is attributed to fractional differentiation, it is also indicated by the surge in K content.

7.5.3 CRYSTALLIZATION TEMPERATURE OF GRANITES AND INFERRED PRESSURE CONDITIONS BASED ON WHOLE ROCK NORMS

Rb/Sr ratio which mostly increase with advanced level of fractionation was employed to trace the magmatic differentiation (after Condie, 1973), Fig. 7.1(a). infers the rocks to be consequential of highly differentiated and an evolved melt. Following the dashed contours representative of crustal thickness, it is conclusive that the melt emplacement occurred at a moderate depth >30kms, suggesting a lower crustal source.

Temperature and pressure conditions prevailing at the time of emplacement of a granitic melt are calculated in terms of water-saturated Q-Ab-Or- H_2O systems (Johannes et al., 1996). The KAHG analyses cluster rather adjacent to the compositions of minimum melt for different $P(H_2O)$. Within the experimentally calibrated isobars KAHG supports pressure fluctuations from 2-10kbars, suggestive of a low water pressure during crystallization together with crystallization temperatures fluctuating from 700-760°C Fig. 7.1b. PGN and GGN variety supports lower pressure-temperature conditions of 2-5 kbars and 700-740°C at the time of their emplacement, while NPG samples exhibit slight variation of pressure 2-10kbars and higher temperatures of 700-760°C.

7.5.4 FRACTIONAL CRYSTALLIZATION (FC): EVIDENCE FROM REE CHEMISTRY

The relationship between trace elements Ba Vs Sr and Eu Vs Sr reflects the primary melt generated by partial melting of granodioritic source, trend indicates there was subsequent fractionation of the

K-feldspar and plagioclase (Fig.7.2 a, b & c). Taking a compatible element and an incompatible trace element for a binary plot e.g., V vs Th (Fig.7.2 d). Mushkin et al., 2003 opined that two end-members plot along the straight line indicating their mixture. However, a plot of hyperbolic curve that approaches the X-axis at low concentrations of compatible element indicates products of crystal fractionation. As indicated in the plot, the KAHG rocks follows the fractional crystallization trend suggesting the intermediate products of the suite characterize halfway through the crystal fractionation.

As portrayed in the 1/Er- (Ba+Sr)/1000- Er ternary diagram Fig. 7.3 (Feio and Agnol, 2012) together with the fairly high abundance of HREE suggests absence of garnet in the residual phase (Mushkin et al.,2003). The observation depicts a dehydrated melting of hornblende and biotite bearing granitoids with plagioclase-rich residual phases may have produced the studied rocks, generating along the middle to lower crust, trailed by varying intensity of differentiation.

7.5.4 NATURE OF PROTOLITH

Low-pressure condition is vital to reach a metaluminous to mild peraluminous granitic composition which is ferroan in nature, further rise in pressure condition will result into a strong peraluminous melt. It can be assumed therefore, with the metaluminous to mildly peraluminous ferroan nature of KAHG, that the melt was produced by partial melting in a low-pressure condition. Accordingly, in the Al_2O_3/ (Fe_2O_3+MgO+ TiO_2) vs Al_2O_3+Fe_2O_3+MgO+ TiO_2 diagram Fig. 7.4 (after Patiňo Douce, 1999) which distinguishes "high pressure fields" and "low pressure fields", the entirety of the studies KAHG trend in the "low pressure" implying a lower crustal contribution (crust–mantle interaction). Further attestation of lower crust-derived melts is noted from Ce/Pb ratios, following Green (1995) parameters for primitive mantle (Ce/Pb H"9) and continental crust (Ce/Pb H"4), KAHG presented values lower than that of primitive mantle, linking more to a crustal source; furthermore, low Mg# values (<44) are considered to be typical of dehydration melting of lower crustal mafic magma (Rapp, 1995; Rapp and Watson, 1995). The inferred low Mg# values of entirety of KAHG i.e., (GGN =0.17-23; BGN=0.16-0.27; PGN=0.14-0.20; NPG=0.08-24) is consistent with the inference of lower crust-derived melts.

Normalized Y/Nb, Th/Nb and La/Nb ratios have been applied to interpret the source of magma and mechanisms of fractionation to discern OIB and subduction-related magmatic suites. According to Fig. 7.5 (a & b) the petrogenetic process related to the production of A-type granites

of KAHG is a subduction related continental crust suite. Also, A_2 granites are linked to post-collisional tectonic settings experiencing extension and are the results of partial melting of juvenile continental crust (Eby, 1990).

The studied geochemical signatures showing a general enrichment in LILE and LREE coupled with lesser contents of HREE, Nb, Sr and P are comparable to post-collisional granitoids established at orogenic belts (Majumdar and Dutta, 2016).

In terms of $CaO–SiO_2$ composition (Carroll and Wyllie, 1990; Gorring et al., 2004; Patiño Douce, 1997; Skjerlie and Johnston, 1993), all NPG samples and majority of NPG (with an exception of KH sample) and GGN except, BGG may have been constituted from fluid absent partial melts of tonalitic to granodiorite sources (Figure 7.7a). NPG variant from Kathalguri area indicate melts produced from mafic sources. Meanwhile discrimant diagrams for partial melts in terms of molar compositions (Altherr et al., 2000), depicts the studied granite suites to be originated from metagreywacke to metapelitic sources Figure 7.7(b).

KAH granitoids has moderate $Al_2O_3/(Fe_2O_3T+MgO+TiO_2)$ and $(Na_2O+K_2O)/(Fe_2O_3T+MgO+TiO_2)$ ratios (Fig. 7.7c, which present the probability of a lower crustal mafic origin (Rapp et al., 1991; Rapp and Watson, 1995).

Most of the KAH NPG samples have CaO/Na_2O ratios <0.3 (0.15-0.41) except for KH samples CaO/Na_2O (0.80-1.10), while PGN, BGN and GGN have CaO/Na_2O ratios >0.3 (0.34-0.80) except for HW sample (0.25). Sylvester (1998) verified the pelite- derived post collisional peraluminous granites shows lower CaO/Na_2O ratios (<0.3) than their psammite-derived counterparts, also supplemented by Jung and Pfander (2007) where pelite-derived granitic melts shows (CaO/Na_2O < 0.5) and melts consequent of greywackes or igneous sources (CaO/Na_2O: 0.3–1.5). The inference based on the given oxide ratios from KAHG samples is consistent with their metagreywacke source derivation.

7.5.4 GEOTECTONIC ENVIRONMENT

If the multicationic R_1- R_2 classification can be taken into account, variable tectonomagmatic trends inferred links from post- collisional uplift to post orogenic settings through syn-collision, perhaps indicative of a comparatively extensive history of the melt interaction before the final emplacement in post orogenic setting. Supplementary inference noted from the HFSE data where

samples show affinity with Syn-COLG subfields and Within Plate Granites (WPG) having a slight tendency towards the latter. The WPG maybe inherently related to their generation in an extensional post orogenic setting.

7.6   VIABLE PETROGENETIC MODEL FOR THE EVOLUTION OF KAHG

Post-collision magmatism inclines to compositionally encompass high-K calc-alkaline or alkaline to peralkaline magma types (Bonin, 2004; Liégeois, 1998). The calc-alkaline composition of a late or post- collisional could be sourced from crust and mantle while the later rocks are frequently sourced from lithospheric mantle underneath collisional regions. Mantle source due to adiabatic decompression or a crustal source due to thermal relaxation after collision (Barbarin, 1999; Harris et al., 1986); magma underplating source and thickening of continental crust involving intra-continent settings (Castro, 2014) are proposed methods accountable to develop post-collisional calc-alkaline rocks. Both adiabatic decompression melting (mantle) and thermal relaxation (crust) processes should be accountable for granitoids originated from crustal and mantle (Eby, 1990; Harris et al., 1986). Frost and Frost, (2011) estimated granites of ferroan A- type nature can be sourced through partial melting of quartzo-feldspathic rocks or magmatic differentiation of alkali or tholeiitic basalts, assimilation may or may not be involved. Moderate depleted Nb anomaly depicted by all samples is a distinct attribute common to subduction- related melts, mainly link to the retention of said element in residual titanite in the subducting plate. Such anomaly is also the outcome of contamination of mantle melts from crust (Tarney et al., 1994; Herget et al., 1989).

The inference of A-type granites of Karbi Anglong Granitoids and the calc-alkaline I-type granites links to an analogous source of evolution but probably different petrogenesis history. The petrological and geochemistry of Karbi hills granitoids point to an evolution by partial melting of mafic-magma underplating in lower crust (I-type granitoids) together with partial melting of tonalitic- granodioritic middle/lower crust. Asthenosphere upwelling may have given rise to I-type magma during the syn-collisional to post-collisional stages concurrently dehydrating the rocks at its vicinity. The resultant process may produce melt which is chemically undepleted though dehydrated which on further partial melting can give rise to the A-type granites (Anderson, 1983; Creaser et al., 1991) emplaced within plate tectonic domain. High HFSE in the given rocks advocates a dry origin (Collins et al., 1982). Accordingly, the inference of the A-type nature is signifying a less hydrous environment compared with the I-type. It can be conclusively drawn that

the Karbi Anglong Hill granitoids are resultants of anatexis of continental crust initially in a subduction-related tectonic setting which later progressed to rifting (Fig. 7.8).

7.6 CONCLUSION

Magnetic susceptibility, phase petrology and geochemical characters of the KAHG suggest the metaluminous to moderately peraluminous nature, transitional from I- type to A- type granites formed in a post-collisional tectonic regime. The KAHG felsic melts are derived from enriched mantle, generated in the subduction zone evolving under oxidising condition. The Karbi Anglong Hill Granitoids were emplaced at shallow crustal depth, and correspond to bimodal magnetite (oxidized) to ilmenite (reduced) series granites.
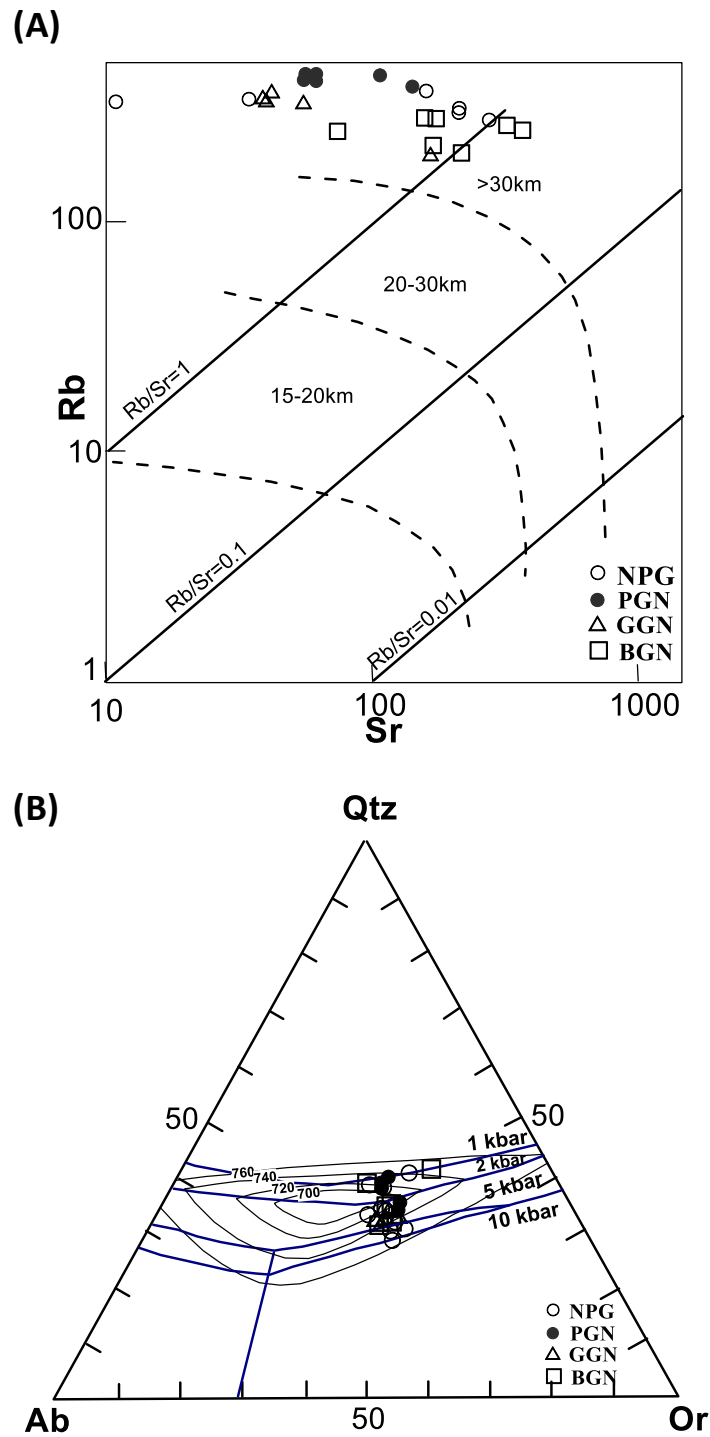
Figure 7.1 (A) Rb–Sr diagram with pressure contours after (Condie, 1973) (B) quartz–albite–orthoclase diagram showing experimentally calibrated isobars after (Johannes et al., 1996)
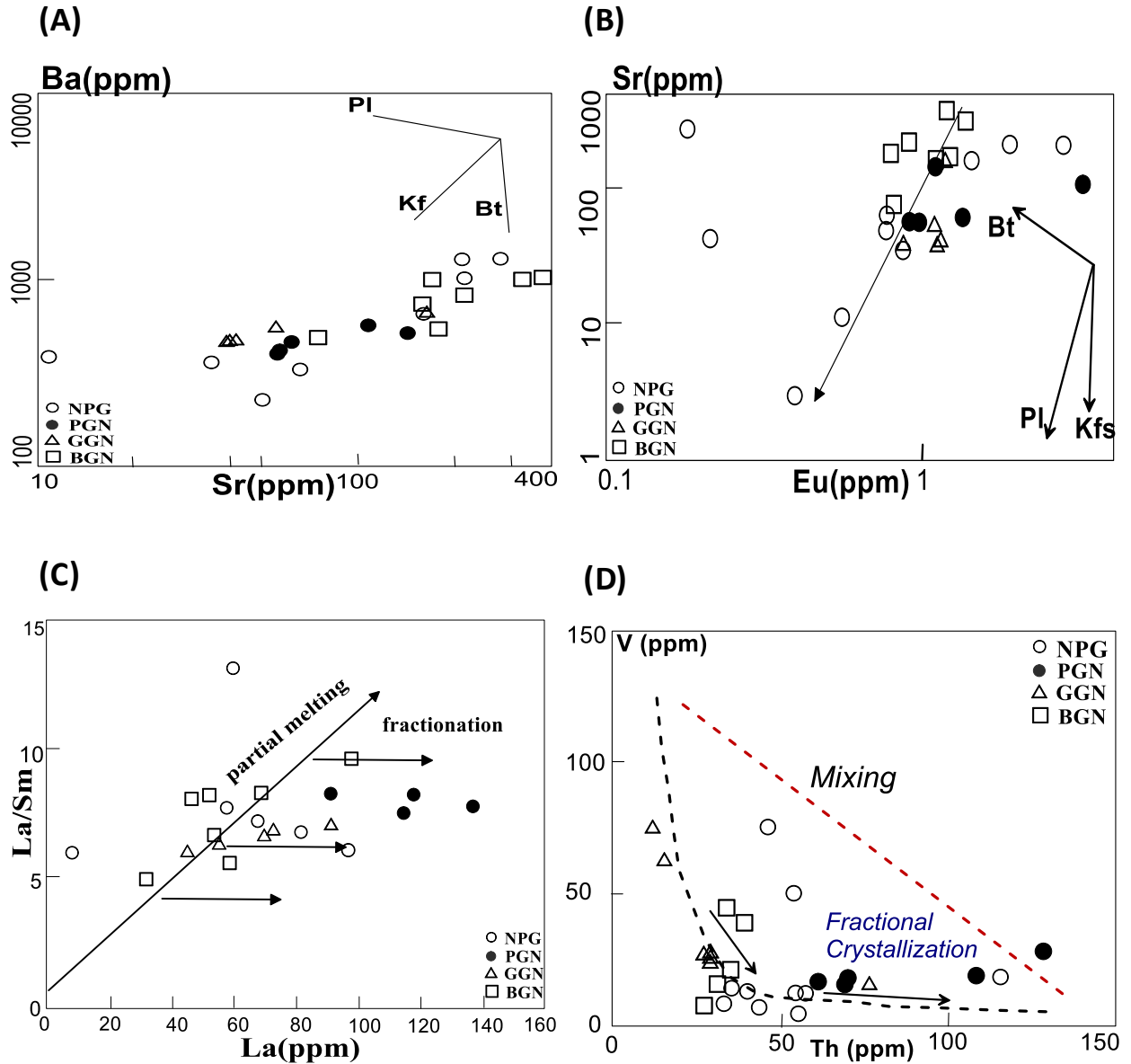
Figure 7.2: Diagrams depicting mineral fractionation (A) Sr Vs Ba (Arth, 1976); (B) Eu vs Sr (Jiang et al., 2011); (C) La/Sm vs La. Vectors depict the pattern in fractionation of minerals on the composition of residual liquids: Pl-plagioclase, Kfs- potassium-rich feldspar and Bt- biotite. Arrows depict possible pattern during crystal fractionation; (D) Th (ppm) vs V (ppm) for the KAHG. A hyperbolic curve line which approaches Th-axis represents crystallization by fractionation. The straight line indicate mixing between two magma end- members.
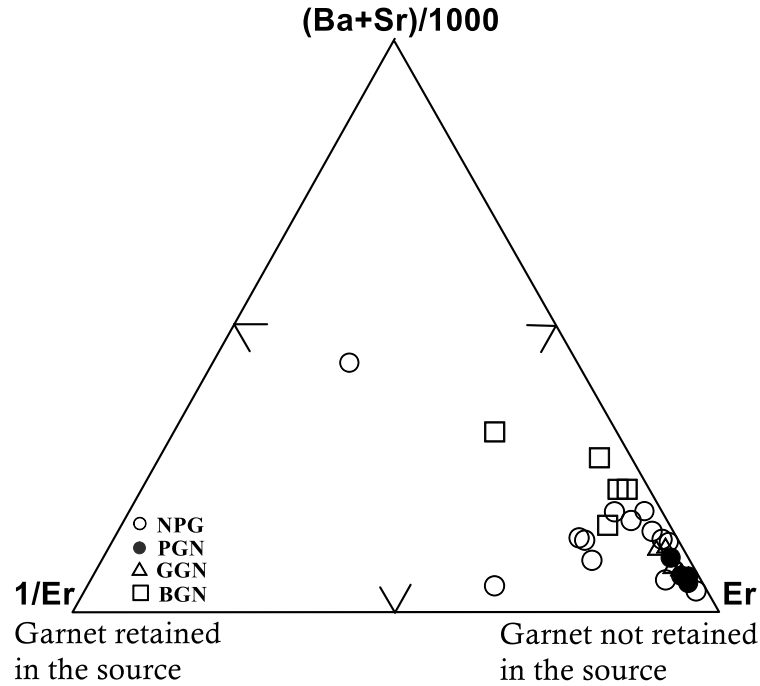
Figure 7.3: (Ba+Sr)/1000- 1/Er- Er ternary plot (Feio and Agnol, 2012) indicates that the majority of the granites had no garnet retained in the source.
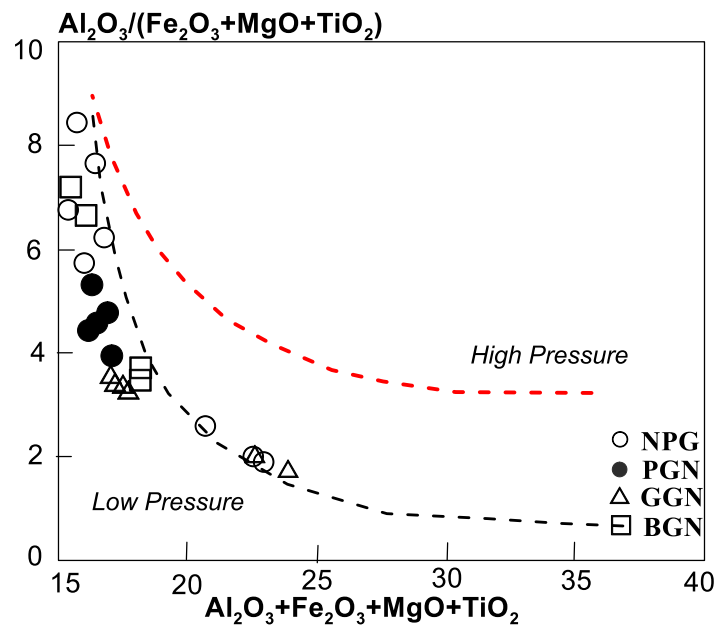
Figure 7.4: $Al_2O_3/ (Fe_2O_3+MgO+ TiO_2)$ vs $Al_2O_3+Fe_2O_3+MgO+ TiO_2$ diagram after (Patiňo Douce, 1999) which distinguishes the entirety of KAHG trend in the "low pressure"
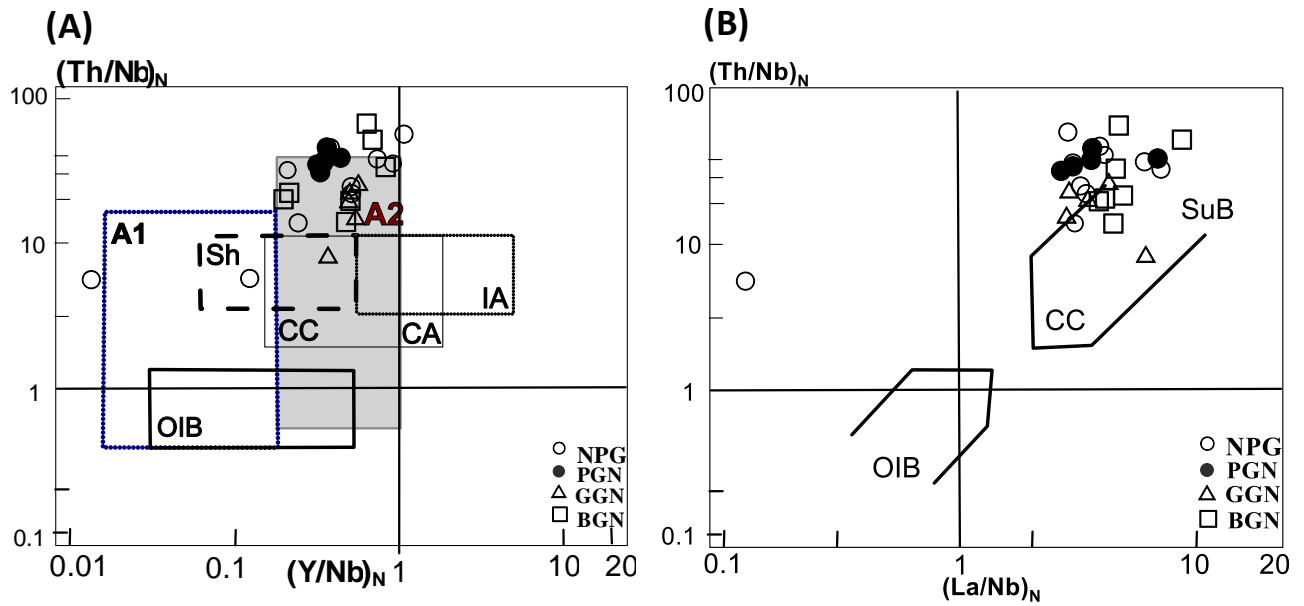
Figure 7.5: Relationships between normalized Y, Nb, Th and La. (A) $(Y/Nb)_N$ vs. $(Th/Nb)_N$ (B) $(La/Nb)_N$ vs. $(Th/Nb)_N$. Normalization standards after McDonough and Sun (1995).

Field CA-Continental Arcs; CC-Continental Crust; IA-Island Arcs; OIB- Ocean Island Basalts; Sh- Shoshonites; SuB- Subduction-related magmatic suites.
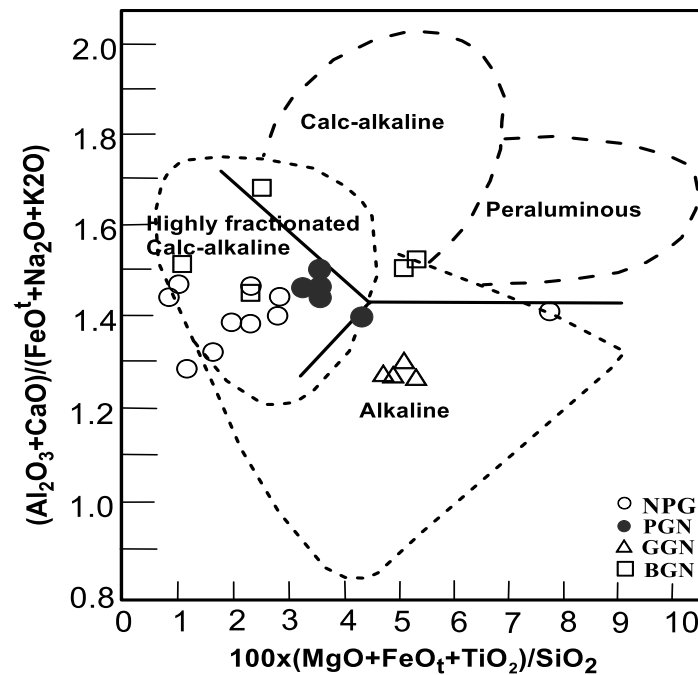
Figure 7.6 Highly fractionated calc-alkaline granites represented in $(Al_2O_3 + CaO)/(FeOt + Na_2O + K_2O)$-$100(MgO + FeO + TiO_2)/SiO_2$, plot after Sylvester, 1989.
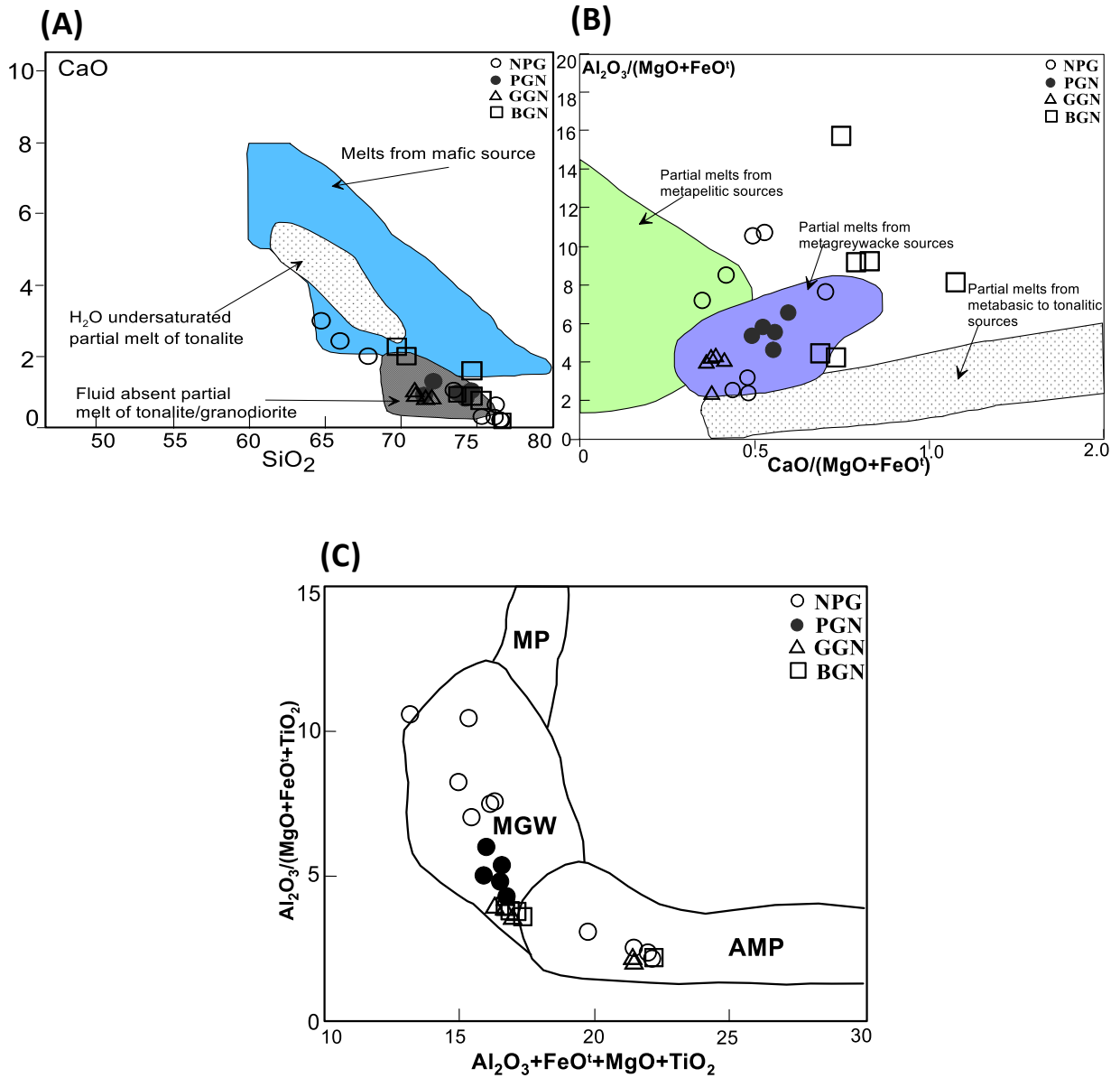
Figure 7.7: (A)Molar CaO–SiO$_2$ composition (Carroll and Wyllie, 1990; Gorring et al., 2004; Patiño Douce, 1997; Skjerlie and Johnston, 1993) (B) Discrimant diagrams for partial melts from various sources of (Altherr et al., 2000) showing plots of the KAHG. (C) Source discrimination diagrams for KAH granitoids. MGW-metagreywackes; MP-metapelites; AMP-amphibolites
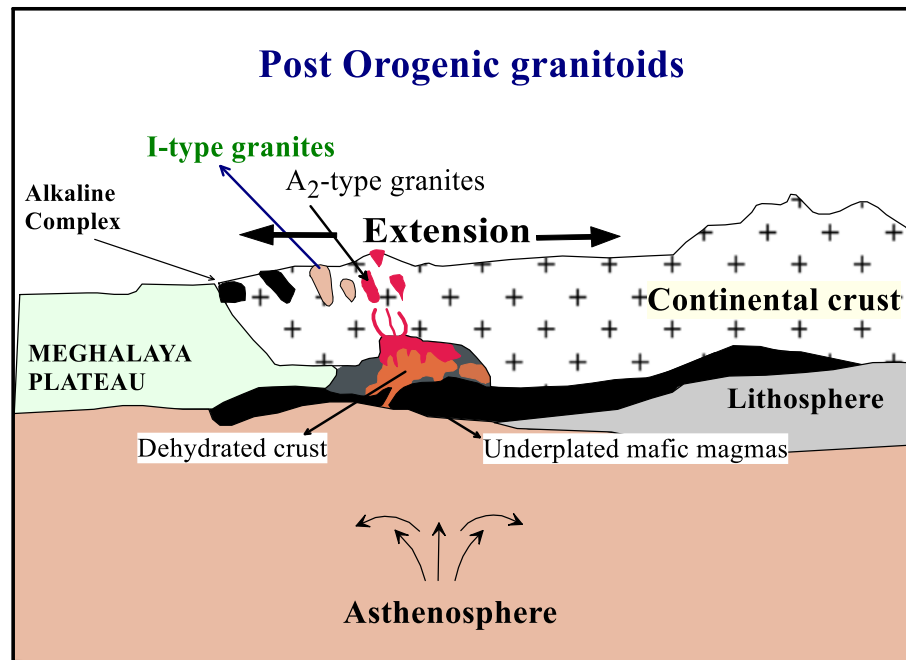
Figure 7.8: Simplified petrogenetic model for the generation of I-type and A_2- type granites in the Karbi Anglong Hills

References

Abdel-Rahman, A.M. (1994): Nature of biotites from alkaline, calc- alkaline and peraluminous magmas. *Jour. Petrol.*, v.35, pp.525-541.

Acharya, S. K. (1986): Cenozoic Plate Motions creating the eastern Himalayas and Indo-Burmese Range around the north-east corner of India. In: Ophiolite and Indian Plate Margin: (Eds. N.C, Ghose and S. Varadrajan), pp.143-161.

Acharya, S. K. and Ghosh, S. K. (1968b): Geology and Coal resources of Siju Coalfield (eastern part) Garo Hills District, Assam. Rep. F.S. 1967 - 68.

Acharyya, S. K.; Mitra, N. D. and Nandy, D. R. (1986): Regional geology and tectonic setting of northeast India and adjoining region. *Memoirs of the Geological Survey of India,* v.119, pp.6–12.

Acharyya, S. K., and Roy, A. (2000). Tectonothermal history of the Central Indian Tectonic Zone and reactivation of major faults/shear zones. *Journal of the Geological Society of India*, v.55, pp.239–256.

Acharyya, S. K. (2001): Geodynamic setting of the Central Indian Tectonic Zone in central, eastern and northeastern India. *Geological Survey of India Special Publications*, v.64, pp.17–35.

Acharyya, S. K. (2003): The nature of Mesoproterozoic Central Indian Tectonic Zone with exhumed and reworked older granulites. *Gondwana Research*, v.6(2), pp.197–214.

Ague, J.J. and Brimhall, G.H. (1988): Magmatic arc asymmetry and distribution of anomalous plutonic belts in the batholiths of California: effects of assimilation, crustal thickness, and depth of crystallization. *Geological Society of America Bulletin*, v.100, pp.912–927.

Albuquerque, C. A. R. (1973): Geochemistry of biotites from granitic rocks, Northern Portugal: Geochimica et Cosmochimica Acta., v.37, pp.1779–1802.

Anderson, J.L., and Thomas, W.M. (1985): Proterozoic anorogenic two-mica granites—Silver Plume and St. Vrain batholiths of Colorado. *Geology*, v.13(3), pp.177–180.

Anettsungla; Rino, V., and Kumar, S. (2018): Redox condition, nature and tectono-magmatic environment of granitoids and granite gneisses from the Karbi Anglong Hills, Northeast India: Constraints from magnetic susceptibility and biotite geochemistry. *Journal of the Geological Society of India*, v.91(5), pp.601–612.

Arslana, M, Z. Aslan, Z. (2006): Mineralogy, petrography and whole-rock geochemistry of the Tertiary granitic intrusions in the Eastern Pontides, Turkey. *Jour. of Asian Earth Sc.*, v.27(2), pp.177-193.

Aydin, F.; Karsli O. and Sadiklar M.B. (2003): Mineralogy and chemistry of biotites from Eastern Pontide granitoid rocks, NE-Turkey: Some petrological implications for granitoid magmas.Chem.Erde., v.63, pp.163-182.

Banerjee, M.; Mitra, P. and Chakravorty, D. K. (1977): Occurrence of lower Gondwana rocks in western Garo Hill, India. *IV Int. Gond. Symp. India.*, v.1, pp.71-75.

Barbarin, B. (1990a): Granitoids: Main petrogenetic classifications in relation to origin and tectonic setting. *Geol. Jour.*, v .25, pp.227-238.

Barbarin, B. (1990b): Plagioclase xenocrysts and mafic magmatic enclaves in some granitoids of the Sierra Nevada Batholith, California. *Jour. Geophys. Res.*, v.95, pp.17747-17756.

Barbarin, B. (1999): A review of the relationships between granitoid types, their origins and their geodynamic environments: Lithos., v.46, pp.605-626.

Baruah, J. M. M. and Ratnam, G. (1982): Variation of thickness of the sedimentary succession in the Upper Assam Valley. *Rec. Geol. Survey of India.*, v.112(4), p.26-30.

Batchelor, A. R. and Bowden, P. (1985): Petrogenetic interpretation of granitoid rock series using multicationic parameter. *Chemical Geology*, v.48, pp.43–55.

Bean, R.E. (1974): Biotite stability in the porphyry copper environment: *Eco. Geol.*, v.69, pp.241–256.

Bidyananda, M. and Deomurari, M. P. (2007): Geochronological constraints on the evolution of Meghalaya Massif, northeastern India: An ion microprobe study. *Current Science*, v.93(11), pp.1620–1623.

Biswas, B. (1961) : Geology of Bengal Basin with special reference to stratigraphy and micropalaeontology, STANVAC (Calcutta), I & II (Unpub).

Bonin B. (2007): A-type granites and related rocks: Evolution of a concept, problems and prospects. *Lithos,* v.97, pp.1–29.

Bónová, K.; Broska I. and Petrík I. (2010): Biotite from Čierna Hora Mts. granitoids (Western Carpathians, Slovakia) and estimation of water contents in granitoid melts. *Geol. Carpathica.*, 02.2010, v.61, No.1, pp. 3-17.

Bora, A. K. and Roy, G. (1999): Preliminary investigation for gold and other mineral potentialities in the area around Kaliyani and Diju Valley, Karbi Anglong District, Assam. *Rec. Geol. Soc. India* (130), 16.

Burkhard, D. J. M. (1991): Temperature and redox path of biotite-bearing intrusives: a method of estimation applied to S- and I-type granites from Australia. *Earth Planet Sci. Lett.*, v.104, pp.89- 98.

Burkhard, D. J. M. (1993): Biotite crystallization temperatures and redox states in granitic rocks as indicator for tectonic setting. *Geol. En Mijnb.*, v.71, pp.337-349.

Castro, A.; Moreno-Ventas, I. and De/La Rosa, J.D. (1991): H-type (hybrid) granitoids: A proposed revision of the granite-type classification and nomenclature: *Earth-Sci. Reviews.*, v.31, pp.237-253.

Chappell, B.W. and White, A. J. R. (1974): Two contrasting granite types. *Pacific Geol.*, v.8, pp.173-174.

Chappell, B.W.; White, A.J.R. and Wyborn, D. (1987): The importance of residual source material (restite) in granite petrogenesis. *Journal of Petrology,* v.28, pp.1111–1138.

Chappell, B.W. and White, A.J.R. (1992): I- and S-type granites in the Lachlan Fold Belt. Transactions of the Royal Society of Edinburgh. *Earth Sciences*, v.83, pp.1–26.

Chappell, B.W.; Bryant, C. J.; Wyborn, D.; White, A. J. R. and Williams, I. S. (1998): High- and low-temperature I-type granites. *Resource Geology*, v.48, pp.225–235.

Chappell, B.W. and White, A.J.R. (2001): Two contrasting granite types: 25 years later. *Aust. J. Earth Sci.*, v.48, pp.489–499.

Choudhury, J. M. and Rao, M. N.: A review of the Precambrian stratigraphy of the Assam-Meghalaya plateau. Gauhati University.

Collins, W. J.; Beams, S. D.; White, A. J. R. and Chappell, B. W. (1982): Nature and origin of A-type granites with particular reference to southeastern Australia. *Contrib. Mineral. Petrol.*, v. 80, pp.189-200.

Creaser, R. A.; Price, R. C. and Wormald, R. J. (1991): A-type granites revisited: assessment of a residual-source model. *Geology*, v.19, pp.163–166.

Czamanske, G.K. and Wones, D.R. (1973): Oxidation during magmatic differentiation, Finnmarka complex, Oslo area, Norway: Part 2, the mafic silicates: *Jour. Petrol.*, v.14, pp.349–380.

Czamanske, G. K.; Wones, D. R. and Eichelberger, J. C. (1977): Mineralogy and petrology of the intrusive complex of the Pliny Range, New Hampshire: Amer. *Jour. Sci.*, v.277, pp.1073–1123.

Dall'Agnol, R.; Scaillet, B. and Pichavant, M. (1999): An experimental study of a Lower Proterozoic A-type granite from the Eastern Amazonian Craton, Brazil. *Journal of Petrology*, v.40, pp.1673–1698.

Dall'Agnol, R.; Teixeira, N. P.; Rämö, O. T.; Moura, C. A. V.; Macambira, M. J. B. and de Oliveira, D. C. (2005): Petrogenesis of the Paleoproterozoic rapakivi A-type granites of the Archean Carajás metallogenic province, Brazil. *Lithos Ilmari Haapala*, v.80, pp.101–129.

Das Gupta, A.B. (1977): Geology of Assam Arakan region. *Quart. Jour. Geol. Min. Met. Soc. India.*, v.49, No.122, pp.1-53.

Das Gupta, S. and Nandy, D. R. (1982): Seismicity and tectonics of Meghalaya plateau, Northeastern India: *VII Symposium on Earthquake Engineering*, Univ. Roorkee., v.1, pp.19-24.

De, A. K and Boral, M. C. (1978): A note on the Singsimani (Hallidagganj) area, Garo Hills, Meghalaya, Geol. Surv. Rep.

Debon, F. and Le Fort, P. (1983): A Chemical-Mineralogical Classification of Common Plutonic Rocks and Associations. Transactions of the Royal Society of Edinburgh: *Earth Sciences*, v.73, pp.135-149.

Debon, F. and Lefort, P. (1988): A Cationic Classification of Common Plutonic Rocks and their Magmatic Associations: Principles, Method, Applications. *Bulletin de Mineralogie*, v.111, pp.493-510.

Desikachar, S. V. (1974): A review of the tectonic and geological history of Eastern India in terms of Plate Tectonics Theory. *Jour. Geol. Soc. India.*, v.15, pp.137-149.

Dymek, R. F. (1983): Titanium, aluminium and interlayer cation substitutions in biotite from high-grade gneisses, West Greenland. *Amer. Mineral.*, v.68, pp.880-889.

Eby, G. N. (1990): The A-type granitoids: a review of their occurrence and chemical characteristics and speculations on their petrogenesis. *Lithos*, v.26, pp.115–134.

Eby, G. N. (1992): Chemical subdivision of the A-type granitoids: petrogenetic and tectonic implications. *Geology*, v.20, pp.641–644.

El Bouseily, A. M. and El Sokkary, A. A. (1975): The Relation between Rb, Ba and Sr in Granitic Rocks. *Chemical Geology*, v.16, pp.207-219.

Evans, P. (1935): General Report of Geological Survey of India. *Rec. Geol. Surv. Ind*., v.69, 83p.

Evans, P. (1964): The tectonic framework of Assam. *Jour. Geol. Soc. India*., pp.580-96.

Foster, M. D. (1960): Interpretation of the composition of tri-octahedral micas. *USGS Prof. Paper* 354- B., pp.11-49.

Fox, C.S. (1934): The Lower Gondwana Coalfields of India. *Mem. Geol. Surv. Ind*., v.59, pp.1 - 386.

Frost, B.R.; Barnes, C.G.; Collins, W.J.; Arculus, R.J.; Ellis, D.J. and Frost, C.D. (2001): A geochemical classification for granitic rocks. *J. Petrol*., v.42, pp.2033–2048.

Ghosh, S.; Bhalla, J. K.; Paul, D. K.; Sarkar, A.; Bishul, P. K.; Gupta, S. N. and Chakraborty, S. (1991): Geochronology and geochemistry of granite plutons from East Khasi Hills, Meghalaya. *Journal of the Geological Society of India*, v.37(4), pp.331–342.

Ghosh, S.; Paul. D. K.; Bhalla, J. K.; Bishui P. K.; Gupta S. N. and Chakraborty, S. (1994): New Rb-Sr isotopic ages and geochemistry of granitoids from Meghalaya and their significance in middle-to late Proterozoic crustal evolution. *Indian Minerals*, v.48, pp.33–34.

Ghosh, S.; Fallick, A. E.; Paul, D. K. and Potts, P. J. (2005): Geochemistry and origin of Neoproterozoic granitoids of Meghalaya, northeast India: Implications for linkage with amalgamation of Gondwana Supercontinent. *Gondwana Research*, v.8(3), pp.421–432.

Gogoi, A.; Majumdar, D.; Cottle, J. and Dutta, P. (2019): Geochronology and geochemistry of Mesoproterozoic porphyry granitoids in the northern Karbi Hills, NE India: Implications for early tectonic evolution of the Karbi Massif. *Journal of Asian Earth Sciences*, v.179, pp.65–79.

Goswami, A.C. (1960): Geological Mapping of the Makum and Jeypore areas bordering the Lakhimpur district, Assam. rep. F.S. 1959 - 60. *Geol. Surv. of India. Progress Report* (unpublished).

Gottini, V. (1968): The TiO2 frequency in volcanic rocks. *Geologische Rundschau*, v.57, pp.930–935.

Gregorová, D., Hrouda, F. and Kohút, M. (2003) Magnetic susceptibility and geochemistry of Variscan West Carpathian granites: implications for tectonic setting. Phys. Chem. Earth., v. 28, pp. 729–734. Mem. Geol. Soc. India, no.72, pp.83-102.

Gupta, A. B. and Biswas, A. K. (2000): Geology of Assam. *Geological Soc. of India, Bangalore.,* 169p.

Hecht, L. (1994): The chemical composition of biotite as an indicator of magmatic fractionation and metasomatism in Sn-specialised granites of the Fichtelgebirge (NW Bohemian Massif,Germany).In: Seltmann R., Kämpf H. & Möller P. (Eds.): Metallogeny of collisional orogens. *Czech Geol. Surv., Praha*, pp.295-300.

Heinrich, E. W. (1946): Studies in the mica group: *Sci.*, v.244, pp.836–848.

Ishihara, S. (1971): Modal and chemical composition of the granitic rocks related to the major molybdenum and tungsten deposits in the Inner Zone of Southwest Japan. *Jour. Geol. Soc. Japan.*, v.77, pp.441-452.

Ishihara, S. (1977): The magnetite-series and ilmenite-series granitic rocks. *Min. Geol. (Tokyo).,* v.27, pp.293-305.

Ishihara, S.; Robb, L. J.; Anhaeusser, C. R. and Imai, A. (2002): Granitoid series in terms of magnetic susceptibility: A case study from the Barberton Region, South Africa. *Gond. Res.,* v.5, pp.581-589.

Jan, M. Q.; Agheem, M. H.; Khan, T.; Rehman, H. U. and Markhand, A. H. (2022): Geochemistry and Petrogenesis of theWadhrai Granite Stock of the Malani Igneous Suite in Nagar Parkar Area, SE Pakistan. *Minerals 2022*, v.12, 1240p.

Kanaya, H. and Ishihara, S. (1973): Regional variation of magnetic susceptibility of granitic rocks in Japan. *Jour. Japan Assoc., Mineral. Petrol. Econ. Geol.*, v.68. pp.219-224.

Krishnan, M.S. (1960): Geology of India and Burma, Higginbothams (Pvt.) Ltd. Mount Road, Madras., pp.151-55.

Krishnan, M.S. (1960): Geology of India and Burma Archaean Group of Peninsula, Assam, Higginbothams Pvt. Ltd., Mount Road, Madras., 151p.

Kumar, S. (1990): Petrochemistry and geochronology of pink granite from Songsak, east Garo Hills, Meghalaya. *Journal of the Geological Society of India*, v.35, pp.39–45.

Kumar, S., and Kmet, J. (1995): The calculated magma differentiation trend of the Hodruša–Štiavnica intrusive complex, western Carpathians. *Bulletin of the Czech Geological Survey*, v.70, pp.15–18.

Kumar, S. (2002): Calculated magma differentiation trends of discrete tholeiitic and alkaline magma series of Phenai Mata igneous complex, Baroda district, Gujarat, Western India. *Journal of Applied Geochemistry*, v.4(2), pp.93–102.

Kumar, S.; Pieru, T. and Rino, V. (2005): Evaluation of granitoid-series and magmatic oxidation of Neoproterozoic South Khasi Granitoids and their microgranular enclaves, Meghalaya: Constraints from magnetic susceptibility and biotite composition. *Journal of Applied Geochemistry*, v.7, pp.175–194.

Kumar, S.; Pieru, T.; Rino, V. and Lyngdoh, B. C. (2005): Microgranular enclaves in Neoproterozoic granitoids of south Khasi Hills, Meghalaya Plateau, northeast India: Field evidence of interacting coeval mafic and felsic magmas. *Journal of Geological Society of India*, v.65(5), pp.629–633.

Kumar, S. and Singh, K. M. (2008): Granite series evaluation of Early Ordovician Kyrdem granitoids and enclaves, Meghalaya Plateau, northeast India: Implication on oxidation condition of interacting mafic-felsic magma system. *Earth Science India*, v.1, pp.148–159.

Kumar, S. (2008) Magnetic susceptibility mapping of Ladakh granitoids, northwest Higher Himalaya: Implication to redox series of felsic magmatism in the subduction environments.

Kumar, S. and Pathak, M. (2010): Mineralogy and geochemistry of biotites from Proterozoic granitoids of western Arunachal Himalaya: Evidence of bimodal granitogeny and tectonic affinity: Jour. Geol. Soc.India., v.75, pp.715-730.

Kumar, S., and Pieru, T. (2010): Petrography and major elements geochemistry of microgranular enclaves and Neoproterozoic granitoids of South Khasi, Meghalaya: Evidence of magma mixing and alkali diffusion. *Journal of the Geological Society of India*, v.76(4), pp.345–360.

Kumar, S. (2014): Magmatic processes: Review of some concepts and models. In S. Kumar & R. N. Singh (Eds.), Modelling of magmatic and allied processes, *Society of Earth Scientists Series, Switzerland: Springer International Publishing*. pp.1–22.

Kumar, S.; Rino, V.; Hayasaka, Y.; Kimura, K.; Raju, S.; Terada, K. and Pathak, M. (2017): Contribution of Columbia and Gondwana Supercontinent assembly and growth-related magmatism in the evolution of Meghalaya Plateau and the Mikir Hills, Northeast India: constraints from U-Pb SHRIMP zircon geochronology and Geochemistry. *Lithos,* v.277, pp.356-377.

Kumar, S.; Pieru, T.; Rino, V. and Hayasaka, Y. (2017): Geochemistry and U– Pb SHRIMP zircon geochronology of microgranular enclaves and host granitoids from the South Khasi Hills of the Meghalaya Plateau, NE India: Evidence of synchronous mafic–felsic magma mixing– fractionation and diffusion in a post-collision tectonic environment during the Pan-African orogenic cycle. *Geological Society, London, Special Publications*, v.457(1), pp.253–289.

Kumar, S.; Pundir, S.; Rino, V.; Bora, S.; Pathak, M.; Anettsungla, Joshi, H.; Rawat, M. S.; Pieru, T. and Singh, K. M. (2021): Geochemistry of Proterozoic and Cambrian granites from Meghalaya Plateau, north-east India: Implication on petrogenesis of post-collisional, transitional from I-type to A-type felsic magmatism: *Geological Journal*, pp.1–35.

Kumar, S., Pundir, S., Vikoleno Rino, Bora, S., Pathak, M., Anettsungla, Joshi, H., Rawat, M.S., Pieru, T. and Singh, K. M (2022) Geochemistry of Proterozoic and Cambrian granites from Meghalaya Plateau, Northeast India: Implication on petrogenesis of post-collisional, transitional from I-type to A-type felsic magmatism. Geological Journal. v. 57, Issue 4, pp.1476-1510. DOI:10.1007/s11629-017-4410-3.

Lalonde, A.E. and Bernard, P. (1993): Composition and color of Biotite from granites: two useful properties in the characterization of plutonic suites from the Hepburn internal zone of Wopmay orogen, Northwest Territories. *Can. Mineral.*, v.31, pp.203-217.

Le Maitre, R.W. (1982): Numerical Petrology. Developments in Petrology. *Elsevier, Amsterdam*, v.8, 281p.

Le Maitre, R. W. (2002): A classification and glossary of terms. Recommendations of IUGS Subcommision on the Systematics of Igneous rocks.2nd Ed., *Cambridge Univ. Press, Cambridge.*, 236p.

Lentz, D.R. (1998): Petrogenetic evolution of felsic volcanic sequences associated with Phanerozoic volcanic-hosted massive sulphide systems: the role of extensional geodynamics. *Ore Geology Reviews*, v.12, pp.289–327.

Loiselle, M. C. and Wones, D. S. (1979): Characteristics and origin of anorogenic granites. *Geol. Soc. Amer. Abs.* with Progr., v.11, 468p.

Machev, P.; Klain, L. and Hecht, L. (2004): Mineralogy and geochemistry of biotites from the Belogradchik pluton – some petrological implications for granitoid magmatism in north-west Bulgaria: *Bulgarian Geol. Soc., Ann. Sci. Conf. "Geology 2004",* 16.–17.12.2004., pp.48–50.

Majumdar, D. and Dutta, S. (2006): Geochemistry and petrography of Kaziranga polyphase granitoids and their metallogeny. *J. Appl. Geochem.*, v.8, pp.25–36.

Majumdar, D. and Dutta, S. (2007): Geological investigations on sulphide ore occurrences in Magmatic Complex, Mikir Hills, Assam. *Indian Geol. Congr. Bull.*, v.1(2), pp.7–21.

Majumdar, D. (2010): Need to intensify base metal exploration activities in Mikir Hills, northeastern India. *Cur.Sci.*, 10.09.2010, v.99(5), pp.1–8.

Majumdar, D. and Dutta, P. (2014): Rare earth element abundances in some A-type Pan-African granitoids of Karbi Hills, North East India. *Curr. Sc.*, v.107 (12), pp.2023 - 2029.

Majumdar, D. and Dutta, P. (2016): Geodynamic evolution of a Pan-African granitoid of extended Dizo Valley in Karbi Hills, NE India: Evidence from Geochemistry and Isotope Geology. *Journal of Asian Earth Sciences*, v.117, pp.256–268.

Maswood, M. D. (1977): Petrology of the pink Granite around Gauhati, Assam -Jour. *Assam Sci. Soc.*, v.20, pp.72-75.

Mathur, L. P. and Evans, P. (1964): Oil in India, a brochure in 22nd I.G.C. New Delhi, 1964. 86p.

Mazumdar, S. K. (1976): A summary of the Precambrian geology of the Khasi Hills, Meghalaya. *Geological Survey of India Miscellaneous Publication*, v.23, pp.311–334.

Mazumdar, S. K. (1986): The Precambrain famework of part of the Khasi Hills, Meghalaya, *Geol. Surv. of India, Records*, v.117, part-2.

Maniar, P.D. and Piccoli, P.M. (1989): Tectonic discrimination of granitoids. *Geological Society of America, Bulletin*, v.101, pp.635–643.

Moghadama, H. S.; Li, X. H.; Ling, X.X.; Sternc, R. J.; Santos, J. F.; Meinhold, G.; Ghorbani, G. and Shahabi, S. (2015): Petrogenesis and tectonic implications of Late Carboniferous A-

type granites and gabbronorites in NW Iran: Geochronological and geochemical constraints. *Lithos*, v.212-215, pp.266-279.

Moghazi, A. M. and Kanisawa, S. (1999): Geochemical and petrological evidence of calc-alkaline and A-type magmatism in the Homrit Waggat and El-Yatima areas of eastern Eqypt. *Jour. of African Earth Sc.,* v.29(3), pp.535-549.

Murlidharan, P. K. and Raj, D. (1983): Systematic geological mapping and detailed investigation around ultra-basic occurrences in the central and northern parts of 'Karbi Anglong' (Mikir Hills) District, Assam. *Rec. Geol. Surv. India*, v.111 (part 1).

Nachit, H.; Ibhi, A.; Abia, El. H. and Ohoud, M. B. (2005): Discrimination between primary magmatic biotites, reequilibrated biotites and neoformed biotites. *C. R. Geosci.*, v.337(2005), pp.1415–1420.

Nandy, D. R. (1980): Tectonic Pattern in NE India: *Ind. Jour. Earth. Sci.*, v.7(1), pp.103-107.

Nandy, D. R. (1986a): Geology and tectonics of Arakan Yoma- a reappraisal GEOSEA V. proc. Vol.II. Bull. *Geol. Soc. Malaysia.*, v.20, pp.137-148.

Nandy, D. R. (1986b): Tectonics, seismicity and gravity of Northeastern India and adjoining region: *Mem. Geol. Surv. India.*, v.119, pp.13-16.

Nandy, D. R. (2001): Geodynamics of northeastern India and the adjoining region. *Abc publication, Kolkata* 209.

Pascoe, E. (1962): A manual of geology of India and Burma. III, pp.1345 – 2130.

Patiño Douce, A.E. (1991): Experimental generation of hybrid silicic melts by reaction of high-Al basalt with metamorphic rocks. *Journal of Geophysical Research*, v.100(15), pp.623–639.

Patiño Douce, A.E. (1997): Generation of metaluminous A-type granitoids by low-pressure melting of calc-alkaline granitoids. *Geology*, v.25, pp.743–746.

Patiño Douce, A.E. (1999): What do experiments tell us about the relative contributions of crust and mantle to the origin of granitic magmas? In: Castro, A., Fernández, C., Vigneresse, J.L. (Eds.), Understanding Granites. *Geological Society, London, Special Publications*, v.168, pp. 55–75.

Pearce, J. A.; Harris, N. B. W. and Tindle, A. G. (1984): Trace element discrimination diagrams for the tectonic interpretation of granitic rocks. *J. Petrol.*, v.25, pp.956–983.

Pitcher, W. S. (1983): Granite type and tectonic environment, in Hsu, K. Ed., Mountain building processes*: London, Acad. Press.*, pp.19-40.

Rittmann, A. (1973): Stable mineral assemblages of igneous rocks. *Springer-Verlag, Berlin*. 262p.

Rollinson, H.R. (1993): Using geochemical data: evaluation, presentation, interpretation. *Longman Scientific & Technical, London*, 352p.

Sah, S. C. D (1974): Palaeogene biostratigrapohy of the Shillong Plateau. In aspects and appraisal of Indian Palaeobotany (Ed. K. R. Surangs, R. N. Lakhanpal and Dr. Bharadwaj) Bidwal Sahni Institute of Palaeobotany, pp.525-533.

Saha, A.; Ganguly, S.; Ray, J. and Dhang, A. (2010): Vanadium bearing titaniferous magnetite ore bodies of Ganjang, Karbi-Anglong district, NE India. *Journal of the Geological Society of India*, v.76, pp.26–32.

Saha, A.; Ganguly, S.; Ray, J.; Koeberl, C.; Thöni, M.; Sarbajna, C. and Sawant, S. S. (2017): Petrogenetic evolution of Cretaceous Samchampi-Samteran Alkaline Complex, Mikir Hills, Northeastern India: Implications on multiple melting events of heterogeneous plume and metasomatized sub-continental lithospheric mantle. *Gondwana Research*, v.48, pp.237–256.

Sarma, K.P. and Dey Tulika (1996): Re-look on Shillong Plateau. *Bull. Pure and Applied Sci.*, 15F (2), pp.51-54.

Speer, J.A. (1984): Micas in igneous rocks. In Micas (S.W. Bailey, ed). *Rev. Mineral.*, v.13, pp.299-356.

Speer, J. A. (1987): Evolution of magmatic AFM mineral assemblages in granitoid rocks: The hornblende+melt=biotite reaction in the Liberty Hill pluton, South Carolina: *Amer. Min.*, v.72, pp.863–878.

Streckeisen, A. (1973): Classification and Nomenclature of Plutonic Rocks Recommendations by the IUGS Subcomission on the Systematics of Igneous Rocks. N. *Jahrburchfür Mineralogie, Monatshefre*, pp.149-164.

Takagi, T. and Tsukimura, K. (1997): Genesis of oxidized- and reduced- type granites. *Econ. Geol.*, v.92, pp.81-86

Takagi, T. (2004): Origin of magnetite- and ilmenite-series granitic rocks in the Japan arc. *Amer. Jour. Sci.*, v. 304, pp.169-202.

Taylor, S.R. and Mclennan, S.M. (1985): The continental crust: its composition and evolution. *Blackwell, Oxford*. 312p.

Whalen, J.B.; Curry, K.L. and Chappell, B.W. (1987): A-type granites: Geochemical characteristics, discrimination and petrogenesis. *Contrib. Mineral. Petrol.*, v.95, pp.407–419.

Wones, D. R. and Eugster, H. P. (1965): Stability of biotite: Experiment, theory and application: *Amer. Min.*, v.50, pp.1228–1272.

Wones, D. R. (1972): Stability of biotite: A reply: *Amer. Min.*, v.57, pp.316–317.

Wones, D. R. (1981): Mafic silicates as indicators of intrusive variables in granitic magmas: *Min. Geol.*, v.31, pp.191–212.

Wones, D. R. (1989): Significance of the assemblage titanite+magnetite+quartz in granitic rocks: *Amer. Min.*, v.74, pp.744–749.

Yang, X.M. (2007): Using the Rittmann Serial Index to define the alkalinity of igneous rocks. *Neues Jahrbuch fur Mineralogie*, v.184, pp.95–103.

Yang, X. M.; Lentz, D. R.; Chi, G.; Kathleen and Thorne, G. (2008): Geochemical characteristics of gold-related granitoids in southwestern New Brunswick, Canada. *Lithos,* v.104, pp.355–377.

Yang, J.-H.; Peng, J.-T.; Zheng, Y.-F.; Hu, R.-Z.; Bi, X.-W.; Zhao, J.-H.; Huang, J.-C.; Zhang, B.-L. (2016): Petrogenesis of the Mesozoic Shuikoushan per-aluminous I-type granodioritic intrusion in Hunan Province, South China: Middle-lower crustal reworking in an extensional tectonic setting. *Jour. Asian Earth Sci.*, v.123, pp.224–242.

Yavuz, F. and Öztaş, T. (1997): BIOTERM- a program for evaluating and plotting microprobe analyses of biotite from barren and mineralized magmatic suites*: Comput. Geosci.*, v.23, pp.897-907.

Yin, J.; Chen, W.; Xiao, W.; Yuan, C.; Windley, B.F.; Yu, S. and Cai, K. (2017): Late Silurian-early Devonian adakitic granodiorite, A-type and I-type granites in NW Junggar, NW China: Partial melting of mafic lower crust and implications for slab roll-back. *Gondwana Res.*, v.43, pp.55–73.

Zen, E. (1988): Phase relations of peraluminous granitic rocks and their petrogenetic implications. *Ann. Rev. Earth Planet. Sc*i., v.16, pp.21-51.

APPENDIX -1

LOCATION COORDINATES	LOCATION NAME
26°34'41.5" -- 93°24'26.4"	Kaziranga
26°34'40.6" -- 93°24'26.4"	Kaziranga
26°34'40.6" -- 93°24'26.6"	Kaziranga
26°34'24.1" -- 93°24'09.0"	Kaziranga
26°34'24.1" -- 93°24'09.5"	Kaziranga
26°34'26.0" -- 93°24'16.1"	Kaziranga
26°34'28.5" -- 93°24'18.3"	Kaziranga
26°34'31.5" -- 93°24'21.0"	Kaziranga
26°34'37.9" -- 93°24'24.6"	Kaziranga
26°34'42.4" -- 93°24'25.9"	Kaziranga
26°34'47.2" -- 93°24'57.5"	Kaziranga
26°34'18.4" -- 93°23'45.0"	Kaziranga
26°34'22.0" -- 93°24'00.8"	Kaziranga
26°34'42.2" -- 93°24'26.6"	Kaziranga
26°35'01.8" -- 93°24'21.8"	Kaziranga
26°35'06.9" -- 93°19'07.9"	Near Bagoria
26°35'06.9" -- 93°19'08.5"	Near Bagoria
26°35'06.9" -- 93°19'07.9"	Near Bagoria
26°35'70.0" -- 93°19'09.7"	Near Bagoria
26°35'06.5" -- 93°19'07.7"	Near Bagoria
26°35'07.0" -- 93°19'07.9"	Near Bagoria
26°35'06.06" -- 93°19'07.9"	Near Bagoria
26°35'06.0" -- 93°19'09.8"	Near Bagoria
26°35'06.7" -- 93°19'10.2"	Near Bagoria
26°22'19.8" -- 93°53'01.9"	Kathalguri
26°22'17.1" -- 93°53'01.4"	Kathalguri
26°22'44.5" -- 93°52'58.5"	Kathalguri
26°12'50.0" -- 93°03'42.9"	Krist Jyoti
26°32'48.11" -- 93°00'46.6"	Seconee Tea Estate
26°35'32.4" -- 93°43'58.4"	Numaligarh Tea Garden
26°35'35.5" -- 93°43'57.6"	Numaligarh Tea Garden
26°11'59.5" -- 93°04'17.0"	Mahamaya
26°12'01.4" -- 93°04'09.5"	Mahamaya
26°12'00.7" -- 93°04'00.2"	Mahamaya
26°12'28.4" -- 93°04'12.8"	Mahamaya Sing Teron village
26°34'03.9" -- 93°03'51.1"	Amguri
26°34'03.9" -- 93°03'51.4"	Amguri
26°34'03.9" -- 93°03'51.6"	Amguri
26°34'03.9" -- 93°03'51.8"	Amguri
26°34'07.1" -- 93°04'13.8"	Amguri
26°34'8.2" -- 93°04'13.9"	Amguri
26°34'26.2" -- 93°06'16.1"	Amguri

26°34'26.9" -- 93°06'15.0"	Amguri
26°34'26.4" -- 93°06'15.1"	Amguri
26°33'41.8" -- 93°03'29.0"	Amguri
26°05'20.6" -- 93°08'59.3"	Howraghat
26°05'20.9" -- 93°08'59.3"	Howraghat
26°34'57.6" -- 93°33'01.8"	Dolomara
25°59'51.7" -- 93°18'33.7"	Karkok
25°59'51.1" -- 93°18'33.9"	Karkok
26°05'32.7" -- 93°08'24.2"	Karkok
26°05'32.6" -- 93°08'24.1"	Karkok
26°05'33.9" -- 93°08'24.5"	Karkok
26°05'32.3" -- 93°08'24.9"	Karkok
26°05'32.2" -- 93°08'24.8"	Karkok
26°05'31.3" -- 93°08'18.3"	Karkok
26°07'05.7" -- 93°08'41.7"	Loringthepi
26°07'04.9" -- 93°08'41.8"	Loringthepi
26°07'06.1" -- 93°08'42.8"	Loringthepi
26°07'05.6" -- 93°08'42.8"	Loringthepi
26°07'05.3" -- 93°08'43.0"	Loringthepi
26°07'05.2" -- 93°08'43.1"	Loringthepi
26°07'04.1" -- 93°08'41.0"	Loringthepi
26°07'04.9" -- 93°08'43.7"	Loringthepi
26°36'13.5" -- 93°29'40.7"	Panbari
26°36'11.1" -- 93°29'42.0"	Panbari
26°36'13.1" -- 93°29'36.0"	Panbari
26°34'28.3" -- 93°06'40.8"	Gajraj
26°34'28.5" -- 93°06'41.3"	Gajraj
26°34'28.6" -- 93°06'41.3"	Gajraj
26°34'28.7" -- 93°06'42.3"	Gajraj
26°34'28.8" -- 93°06'42.3"	Gajraj
26°34'27.4" -- 93°06'42.1"	Gajraj
26°34'27.6" -- 93°06'43.4"	Gajraj
26°34'29.1" -- 93°06'44.5"	Gajraj
26°34'29.2" -- 93°06'46.4"	Gajraj
26°34'29.5" -- 93°06'38.6"	Gajraj

Ouriginal
by Turnitin

Document Information

Analyzed document	Anett Plagiarism check.docx (D154664710)
Submitted	2022-12-30 17:15:00
Submitted by	Temsulemba Walling
Submitter email	tem_wall@yahoo.com
Similarity	1%
Analysis address	tem_wall.naga@analysis.urkund.com

Sources included in the report

W	URL: https://link.springer.com/article/10.1007/s12594-018-0911-0 Fetched: 2021-02-13 07:02:12		1
SA	**Final Thesis of Pankhi Dutta50.docx** Document Final Thesis of Pankhi Dutta50.docx (D40776559)		3
SA	**AbhijitGogoi_PhDThesis_DU.docx** Document AbhijitGogoi_PhDThesis_DU.docx (D141368893)		1
SA	**Ph D_Plagiarism.docx** Document Ph D_Plagiarism.docx (D98741200)		2
SA	**R.ANSHU.pdf** Document R.ANSHU.pdf (D113147471)		2
SA	**Chapter3_FIELD RELATIONS AND PETROGRAPHY.pdf** Document Chapter3_FIELD RELATIONS AND PETROGRAPHY.pdf (D116499910)		1
SA	**Dimple_Doley_CompleteThesis_plagiarism.docx** Document Dimple_Doley_CompleteThesis_plagiarism.docx (D117290538)		1
SA	**plagarisam-b.docx** Document plagarisam-b.docx (D148491522)		1
SA	**Ph.D. Thesis_Susmita Das_all Chapters.doc** Document Ph.D. Thesis_Susmita Das_all Chapters.doc (D149950983)		1

Entire Document